

Integration of solar energy with industrial processes

THÈSE N° 8635 (2018)

PRÉSENTÉE LE 27 JUILLET 2018

À LA FACULTÉ DES SCIENCES ET TECHNIQUES DE L'INGÉNIEUR

GROUPE SCI STI FM

PROGRAMME DOCTORAL EN ENERGIE

ÉCOLE POLYTECHNIQUE FÉDÉRALE DE LAUSANNE

POUR L'OBTENTION DU GRADE DE DOCTEUR ÈS SCIENCES

PAR

Anna Sophia WALLERAND

acceptée sur proposition du jury:

Dr J. Van Herle, président du jury
Prof. F. Maréchal, Prof. S. Haussener, directeurs de thèse
Prof. P. Radgen, rapporteur
Prof. C. Markides, rapporteur
Prof. C. Ludwig, rapporteur



ÉCOLE POLYTECHNIQUE
FÉDÉRALE DE LAUSANNE

Suisse
2018

To both my grandmas

“Have no fear of perfection; you’ll never reach it.”

Marie Curie



Integration of solar energy with industrial processes



Acknowledgments

Foremost, I would like to express my gratitude to my Professor, François Maréchal, for the opportunity and the trust given to me. You are not only a great person and musician, but an even greater scientist and a true inspiration. Thank you.

A great thank also goes to my co-supervisor, Sophia Haussener, for your availability whenever it was needed and very motivating support. I admire you highly. I am sincerely honored by the participation of Peter Radgen, Christos Markides, Christian Ludwig in my thesis jury. I would like to express my deep gratitude for the time, effort and devotion spent on the review of this work. I have greatly learned from your detailed insight and careful revision.

All this would have never been realised, if it was not for Gianluca Ambrosetti, who introduced me to the laboratory and created the contact to Airlight Energy SA, who financed the first part of this PhD. Gianluca, you are a visionary, a great person and an inspiration. I would like to extend my gratitude to Carina Alles and the BFE for supporting our research and giving us the chance to participate in the IEA Heat Pump Annex 48. This thank is further extended to Carmen Stadtländer and Dr. Reiner Jakobs representative for all participants in the Annex and the incredible work they are doing. Mathias Blaser, du hast mir nicht nur eine wunderbare Zeit auf der Heat Pump Summit beschert, sondern auch mit grosser Hingabe die wirklich wichtigen Fragen beantwortet, und damit einen kleinen Einblick in die Industrie bereitet.

Non of this would have been possible without the dedication of talented students. Thank you, Angelos Selviaridis, for being a great person and teaching me many things including TRNSYS. Régis Voillat, it was a pleasure working with you. Your grit, wit and talent in this initially unknown territory impressed me.

Maziar. You are clearly the most gifted person I know. I do not know how to thank you for being the most inspiring, fair, and ethical working colleague anyone could ask for. For being an advisor, a teacher, and most of all being a friend. I hope you will fly.

Ivan, thanks a lot! May I say that once? It fits perfectly. I would like to express my gratitude

Acknowledgments

for many *fruitful* discussions, for a lot of fun while dealing with difficult projects and foremost for your reading and re-reading of every single document I authored and improving it in any possible way. You are awesome.

The laboratory has been a great social environment and going to work was a pleasure. Many colleagues became close friends. Stefano, I cannot really express how much our friendship means to me, it makes me tearful. Only so much: it is a lot. Victor, your blissful non-caring caring-ness makes me care about you, you are great. Raman, you are the only poet I know, thank you for being you. Stéphane, you are the coolest person I know, and you have a great heart.

Emma, you were a great flatmate and friend, thanks. Katie & Guillaume, I would love to make another attempt at your lives, in the meantime: stay awesome! Thank you, Dilan and Raluca for taking care of me during ECOS 2016, the great time in Venice, and being generally nice people. Hür, you are the kindest person I know, and I love watching you suffer (in crossfit). Nils, I want to harvest your genes; and I admire you. Elfie, while speaking of people I admire... I might also add TiVi, Nicolas, and Jean-Loup. Samira, thank you for being my first office mate and a mentor. Manu, thank you for our shared love of Kim, Patrick and Priscilla, who is such a kick-ass woman. Francesco, for offering yourself *voluntarily* to a great party joke and for being kind. Francesca, for never giving up. Luise, for being the future and so lovely German. A great thank you to all the other great colleagues, it was an amazing time.

Rike and Wiebke, thanks for being such important friends and sharing the path and the pain.

Marion, Birthe, Anna danke für viele schöne Urlaube und die Erinnerung an die wirklich wichtigen Dinge. Anja, danke für die Zeichnung, du bist super. An alle Konstanzer Mädels: Ihr seid geil.

Danke an meine furchtbar fabelhafte Familie. Misi, André, Enno, Sari, ihr seid grossartig. Opa, ich bewundere dich, und Jutta, ich bin dankbar, dass es dich gibt. Mama, manchmal hasse ich, wie sehr ich dich liebe. Papa, danke für alles, immer. Felix, ich hab dich sehr lieb.

Riccardo, I am lacking words and will therefore refer to the words of a friend: If nothing would have come out of these past years than meeting you, it would have been worth it all.

Lausanne, 31 May 2018

Abstract

Solar energy offers a great potential for integration with industrial processes, which conventionally rely on fossil fuels to provide energy [1]. The seasonal, daily, and regional dependence of solar energy alongside the scarcity of space or financial resources in many territories constitute great challenges. These may be overcome by efficient solar energy use through optimal integration methods. Such methods should address multiple aspects including accurate solar technology models and identification of the "true" process requirements. Beyond that, optimal design of the integrated systems and quantification of the added value of solar integration, particularly with regard to competing technologies, is crucial. This thesis explores this multi-dimensional problem formulation through elaboration of methodologies tailored to the low-temperature processing industries.

The intricacies behind this goal are addressed in four main chapters. (a) Chapter 2 examines options for solar technology modeling in view of industrial integration. A design approach is developed which allows estimation of solar system performance at sufficient precision and constrained computational effort. (b) In Chapter 3, a comprehensive method is proposed which addresses simultaneous optimization of the process heat recovery, the conventional utilities, and the renewable utility system (including thermal storage) using ε -constrained parametric optimization. (c) The promising results from the third chapter motivate a more thorough analysis of industrial heat pump systems, which is addressed in Chapter 4 presenting a novel generic heat pump superstructure-based synthesis method for industrial applications based on mathematical programming. (d) The subsequent two chapters address generalization of the derived methods to estimate potentials of relevant technologies at national and international scale from the perspective of multiple stakeholders. The derived method generates a database of solutions by applying generalized optimization techniques.

The proposed methods are applied to the dairy industry and results reveal that solar energy should be considered as part of a series of efficiency measures. It is shown that in many cases heat pumping or mechanical vapor re-compression lead to more efficient and less costly solutions, which may be extended with solar thermal energy or complemented with solar electricity.

Keywords

solar thermal collectors; high concentration photovoltaic and thermal system (HCPVT); photovoltaic panels; industrial refrigeration; mathematical programming; heat pump superstructure; dairy industry; waste heat recovery and reuse;

Zusammenfassung

Die Integration von Solarenergie in industrielle Prozesse, die normalerweise mit fossilen Brennstoffen versorgt werden, hat grosses Potential. Doch die saisonale, tägliche und regionale Abhängigkeit von Sonnenstrahlung zusammen mit einer Knappheit an Platz und finanziellen Mitteln stellen in vielen Gebieten grosse Herausforderungen dar. Mit effizienter Solarenergienutzung durch optimale Integrationsmethoden können diese jedoch überwunden werden. Solche Methoden sollten verschiedene Blickpunkte berücksichtigen einschliesslich akkurater Modellierung der Solartechnologien und Identifizierung des wahren Prozesswärmebedarfs. Darüber hinaus muss das integrierte System optimal geplant und der Mehrwert der Solarenergie gegenüber anderen Technologien genau bestimmt werden. Diese Doktorarbeit beschäftigt mit dieser mehrdimensionalen Problemstellung indem Methoden, die besonders auf Niedertemperatur-Prozesse ausgerichtet sind, in vier Kapiteln entwickelt werden.

(a) Im ersten Kapitel werden verschiedene Möglichkeiten für Modellierung von Solartechnologien vor dem Hintergrund der Prozessintegration diskutiert. Der entwickelte Ansatz erlaubt es den Ertrag von Solaranlagen mit minimalem Rechenaufwand und genügender Präzision zu bestimmen. (b) Im zweiten Kapitel wird eine umfassende Methode vorgestellt, die eine gleichzeitige Optimierung der Wärmerückgewinnung, Wärmepumpen und des erneuerbaren Energiesystems (mit thermischen Speichern) unter Verwendung von ϵ -Bedingungen ermöglicht. (c) Die Ergebnisse des zweiten Kapitels motivieren eine genauere Analyse von industriellen Wärmepumpen, worauf die im dritten Kapitel vorgestellte neuartige Methode zur generischen Wärmepumpensynthese abzielt. (d) Die letzten beiden Kapitel dienen der Verallgemeinerung der entwickelten Methoden, um internationale Potentiale für die relevanten Technologien aus der Perspektive von verschiedenen Akteuren zu bestimmen. Die Methode entwickelt Lösungen durch verallgemeinerte Optimierungsverfahren. Die vorgestellten Methoden werden in der Milchindustrie angewendet und die Ergebnisse decken einen Zusammenhang zwischen solarer Energieintegration und einer Reihe anderer Effizienzmassnahmen auf. Die Ergebnisse zeigen, dass in vielen Fällen Wärmepumpen oder Dampfverdichtung zu effizienteren Systemen mit niedrigeren Kosten führen, was mit solarthermischen Technologien erweitert oder mit solarelektrischen Systemen komplementiert werden kann.

Schlüsselwörter

solarthermische Kollektoren; hochkonzentrierte photovoltaisch und thermische Systeme; photovoltaische Kollektoren; industrielle Wärmepumpen; mathematische Programmierung; Milchindustrie; Restwärmeverwertung und -nutzung;

Contents

Acknowledgments	i
Abstract (English/Deutsch)	iii
Table of content	vii
List of figures	xiii
List of tables	xvii
Acronyms and abbreviations	xix
List of Symbols	xxiii
Introduction	1
Focus and goal of this thesis	2
State-of-the-art: methods for solar energy for industrial processes (SEIP) applications . . .	3
Solar modeling and design	3
"Integration" with industrial processes	5
Extrapolation of solar potential	6
Synthesis and scope	7
Contribution and outline of the thesis	8
Terminology, conventions	10
Mathematical conventions	10
Cost conversion and currencies	10
1 Context and motivation	11
1.1 Energy requirements in industry	11
1.2 Solar energy conversion	12
1.3 Industrial heat pumping	14
1.4 Heat recovery potential in a process: pinch analysis	15
1.4.1 Minimum approach temperature ΔT_{\min}	15
1.4.2 Graphical representation, pinch point, and pinch rules	17

Contents

1.4.3	Implications for solar energy for industrial processes (SEIP)	18
1.4.4	Implications for industrial heat pumps	18
1.4.5	The use of pinch analysis (PA) throughout the thesis	20
1.5	Integrated solar and heat pump systems	20
2	Solar modeling and design	23
2.1	State-of-the-art	23
2.1.1	Solar collector modeling	24
2.1.2	Design of solar systems	24
2.1.3	Discussion and contribution	26
2.2	Problem statement	26
2.3	Modeling	27
2.3.1	Solar technologies	27
2.3.2	Meteorological data clustering	32
2.4	System design and integration	33
2.4.1	Objective function	33
2.4.2	Constraints	34
2.5	Results and discussion	37
2.5.1	Solar technologies	37
2.5.2	System design: Sensitivity to data clustering	39
2.6	Conclusions	40
3	Comprehensive integration method	41
3.1	State-of-the-art	42
3.1.1	Solar design and system integration	42
3.1.2	Industrial heat pumping	44
3.1.3	Discussion and contribution	44
3.2	Methodology	45
3.2.1	Problem statement	45
3.2.2	Overview	45
3.2.3	Data collection & clustering (A)	46
3.2.4	System resolution (B)	51
3.2.5	Performance calculation (C)	53
3.3	Results and discussion	55
3.3.1	Scenario definition	55
3.3.2	Daytime operation of the process (Δ)	55
3.3.3	Continuous process operation (O)	63
3.4	Conclusions	66

4	Generic heat pump superstructure	67
4.1	State-of-the-art	68
4.1.1	Conceptual methods	68
4.1.2	Mathematical methods	69
4.1.3	Discussion and contribution	71
4.2	Methodology	72
4.2.1	Problem statement	72
4.2.2	Superstructure synthesis	73
4.2.3	Mathematical formulation	73
4.2.4	Fluid selection	79
4.3	Results and discussion	79
4.3.1	Benchmarking analysis	80
4.3.2	Optimization	82
4.3.3	Extended analysis	86
4.4	Conclusions	90
5	Generalization (A): heat pumping and co-generation	91
5.1	State-of-the-art	92
5.1.1	Design studies	92
5.1.2	Potential studies	94
5.1.3	Discussion and contribution	94
5.2	Methodology	95
5.2.1	Problem statement	95
5.2.2	Overview	96
5.2.3	Comprehensive solution space generation	97
5.2.4	Results retrieval	102
5.3	Application	102
5.3.1	Modular dairy plant	102
5.3.2	Scope definition	104
5.3.3	Solution generation	106
5.4	Results and discussion	109
5.4.1	Comprehensive solution space generation	109
5.4.2	Results retrieval	112
5.5	Conclusions	120
6	Generalization (B): addition of solar utilities	123
6.1	State-of-the-art	124
6.1.1	Top-down	124
6.1.2	Bottom-up	124

Contents

6.1.3 Discussion and contribution	126
6.2 Methodology	126
6.2.1 Problem statement	126
6.2.2 Derivation	127
6.2.3 Approach	130
6.3 Results and discussion	132
6.4 Conclusions	136
Conclusions	137
Main results summary	137
Significance of the work	140
Recommendations and guidance	141
Future perspectives	142
Appendix	143
A General data	145
A.1 Introduction	145
B Comprehensive integration method (Chapter 3)	147
B.1 Additional results	147
B.2 Performance parameters and cost functions	148
B.2.1 Heat exchanger network (HEN) cost estimation	148
B.2.2 Non-renewable technologies	148
B.2.3 Solar technologies	151
B.3 Weather data & clustering	156
B.4 Dairy process	157
C Generic heat pump superstructure (Chapter 4)	159
C.1 General	159
C.1.1 MOGA input parameters	159
C.1.2 MILP input parameters	160
C.2 Benchmark analysis	160
C.2.1 Benchmark cases	160
C.2.2 Extended case <i>E2</i>	163
C.3 Heat pump superstructure	165
C.3.1 Heat pump parameters in targeting problem (MILP)	165
C.3.2 Heat pump specific constraints	167

D Generalization (A) - heat pumping and co-generation (Chapter 5)	171
D.1 General	171
D.1.1 MOGA input parameters	171
D.1.2 MILP input parameters	172
D.2 Additional results	172
D.2.1 Sampling in detail	172
D.2.2 Solution generation & pruning: remaining plants	173
D.2.3 Results retrieval: remaining plants	176
D.2.4 Database of solutions	176
D.3 Industrial case study	184
D.3.1 Dairy process	184
D.3.2 Utilities	186
Curriculum Vitae	213

List of Figures

1	Global availability of fossil reserves, and renewable energy supplied to Earth's surface within a year.	2
2	Focus in literature on "integration" of solar energy with industrial processes.	5
3	Bottom-up, top-down approaches for solar potential studies.	6
4	Graphical overview of thesis structure.	9
1.1	Industrial thermal energy requirements and respective temperature levels.	12
1.2	Solar energy conversion routes tree diagram.	13
1.3	Web of science, key words: <i>waste heat recovery</i> , top cited papers of last 10 years.	16
1.4	Heat pumping technology tree diagram.	16
1.5	Temperature enthalpy profile of a counter current heat exchanger to illustrate the ΔT_{\min} . 16	
1.6	(a) Individual hot streams, (b) hot composite curve (CC) in temperature enthalpy diagram.	17
1.7	(a) Hot and cold CCs, (b) grand composite curve (GCC) in temperature enthalpy diagram. 17	
1.8	Heat pump integration to process GCC.	19
1.9	Comparison of overall sun-to-thermal conversion efficiency.	20
1.10	Solar and heat pump integration to process GCC.	21
2.1	Angles of the sun towards earth normal and inclined surface.	28
2.2	Transient System Simulation Tool [2] (TRNSYS) flowchart of flat plate collector model. 38	
3.1	Methodology proposed in Chapter 3.	46
3.2	Dairy process flowsheet including utility system.	47
3.3	Hot and cold CCs and GCC of dairy process.	48
3.4	Heat pump superstructure model. (a) Ammonia liquid-vapor saturation curve with isobars, (b) flowchart of heat pump superstructure.	50
3.5	Load duration curve of DNI in Sion, Switzerland (CH), of original data and 8 typical plus 2 extreme days.	51
3.6	Integrated composite curves (ICCs) of the dairy process and respective utility system. 57	
3.7	Illustration of the conversion cycles involved in the respective scenarios.	57
3.8	Process operation scheme and solar radiation during typical periods.	59

List of Figures

3.9	Results from ϵ -constraint optimization of different solar options for daytime only process operation.	60
3.10	(a) Optimal active solar area, from ϵ -constraint optimization (ϵ between 95 and 60%), (b) ICC of the dairy process and respective utility system.	62
3.11	Solar integration, (a) hot utility streams heat load vs time, (b) multi-period ICCs of the dairy process and respective utility system.	62
3.12	Results of ϵ -constraint optimization of different solar options for continuous process operation.	65
3.13	(a) Optimal active solar area, from ϵ -constraint optimization (ϵ between 95 and 70%), (b) ICCs of the dairy process and respective utility system.	65
4.1	Flowsheet and temperature-entropy diagram of the heat pump superstructure (HPS) with sample cycles.	73
4.2	Method proposed in Chapter 4.	74
4.3	GCCs from process thermal streams of three benchmark cases.	81
4.4	<i>E2</i> . (a) Multi-objective results, (b) utility ICCs of <i>Reference</i> and <i>min(HPS)</i>	83
4.5	<i>Ethylene</i> . (a) Multi-objective results, (b) utility ICCs.	83
4.6	<i>Cold Tray</i> . (a) Multi-objective results, (b) utility ICCs.	83
4.7	Flowchart of <i>min(HPS)</i> solutions heat pump designs.	85
4.8	(a) Fluid set and (b) multi-objective optimization results. In black: multi-fluid solution.	87
4.9	Performance of compressor between saturation levels T_1 (32.5°C) and T_2 (-17°C).	88
4.10	Overall non-dominated frontier of MOGA results from master level fluid selection.	89
5.1	Standard deterministic multi-objective optimization problem statement.	96
5.2	Method proposed in Chapter 5.	97
5.3	Relations between input data and desired output.	98
5.4	Generalized multi-objective optimization strategy.	99
5.5	Flowsheet of the pruning step.	102
5.6	Flowsheet of the modular dairy plant.	105
5.7	Dairy plants' utility ICCs.	105
5.8	Resource prices, commercial bank lending rates, annualization factor, low voltage electricity grid emissions of various OECD countries.	106
5.9	ϵ -constraint case: results from multi-objective optimization of plant 2.	109
5.10	Weighted sum of objectives: results from multi-objective optimization of plant 2.	110
5.11	Occurrence of minimum TAC solutions during the sampling of plant 2.	110
5.12	Exergy efficiency and utility selection of selected plants.	111
5.13	Pruned solution characteristics, plant 2.	112
5.14	Cost data, CO ₂ equivalent emissions, plant 2.	114
5.15	Plant 2, utility maps.	114

5.16 Plant 2, $\Delta T_{\min}/2=5K$ fixed HEN, utility maps.	114
5.17 Most recurring solution of ε -constrained objective of plant 2, $\Delta T_{\min}/2=5K$ fixed HEN.	116
5.18 On-line decision making platform.	117
5.19 Minimum TAC solutions and respective payback time. Influence of political actions on economically viable solutions.	118
5.20 Detailed cost data versus CO ₂ equivalent emissions for min(TAC) points.	119
5.21 Boiler, co-generation engine and cooling water loads versus CO ₂ equivalent emissions for min(TAC) points.	119
5.22 Electrical power loads (and heat pump data) versus CO ₂ equivalent emissions for min(TAC) points.	119
6.1 Results from MILP in Chapter 3, flat plate collector area for different process operating times.	129
6.2 Thermal utility operation for flat plate collector integration, from Chapter 3, non-stop operation, solar fraction of 0.3.	129
6.3 Thermal utility operation for flat plate collector integration, from Chapter 3, non-stop operation, solar fraction of 0.5.	129
6.4 Methodology proposed in Chapter 6.	131
6.5 Database enhanced with solar data, results of statistical analysis, and break-even collector cost.	133
6.6 TAC versus emissions of solar enhanced database.	133
6.7 Cost analysis of min(TAC) points of solar enhanced database, 2500 h.	133
6.8 Cost analysis of min(TAC) points of solar enhanced database, 2500 h, break-even cost.	135
6.9 Cost analysis of min(TAC) points of solar enhanced database, 8000 h, break-even cost.	135
6.10 Thermal units of min(TAC) points of solar enhanced database, 2500 h, break-even cost.	135
A.1 Global availability of DNI and GHI.	145
B.1 Primary energy, fuel, electricity, and CO ₂ emission savings of non-stop operation solutions.	147
B.2 Thermal conversion efficiency of flat plate (FP) solar thermal collectors.	151
B.3 Electrical conversion efficiency of photovoltaic modules (PVs).	153
B.4 Comparison of TRNSYS results and static model for HCPVT.	154
B.5 Thermal storage volume and temperature distribution.	155
C.1 Analysis of multi-objective genetic algorithm (MOGA) propagation of extended case E2.160	
C.2 Set of selected fluids considered during multi-objective optimization.	163
C.3 Extended case E2 minimum total annualized costs (TAC) solution.	164
C.4 Heat exchanger network design of extended case E2 with Aspen Energy Analyzer.	165
C.5 Temperature-entropy diagram with mass and energy balances of the HPS.	167

List of Figures

D.1	Analysis of MOGA propagation of plant $x = 2$.	172
D.2	Selection of solutions with different sampling algorithms.	173
D.3	Histogram and cumulative sum of occurrences.	173
D.4	Solution generation.	174
D.5	Solution pruning.	174
D.6	Pruned solution characteristics.	175
D.7	Solution indexes.	176
D.8	Cost data.	177
D.9	ICCs selected during data retrieval of plant 2.	178
D.10	ICCs selected during data retrieval of plant 2, $\Delta T_{\min}/2=5K$.	181
D.11	Compressor cost functions, installed cost.	186

List of Tables

2.1	State-of-the-art summary of solar modeling and design studies for SEIP applications.	25
2.2	Different numbers of typical days and influence on results of mixed integer linear programming (MILP) case study.	40
3.1	State-of-the-art summary of solar modeling and integration studies for SEIP applications.	43
3.2	Data related to emissions, primary energy consumption and operating cost in Switzerland (CH).	53
3.3	Investigated utility technology integration scenarios.	55
3.4	Utility integration scenarios as described in Section 3.3.1.	57
4.1	Heat pump features considered in this work.	69
4.2	State-of-the-art summary of synthesis methods for heat pump design and integration with industrial processes.	70
4.3	Variables and objective function at master level.	76
4.4	Variables and objective function at slave level.	80
4.5	Comparison of original data and data reproduced (<i>Reference</i>) in this work with the HPS.	82
4.6	Optimization results. Data shown as <i>Reference</i> was generated with HPS based on the respective literature input data (Section 4.3.1).	85
5.1	State-of-the-art summary of synthesis methods and potential studies for heat pump integration with industrial processes.	93
5.2	Key performance indicators (KPI) calculated during post-computational analysis. . .	103
5.3	Product mass flow rates and reference resource consumption of examined dairy plants.	105
5.4	Free and fixed input parameter set to optimization problem.	107
5.5	Variables and objective function of the problem.	108
6.1	State-of-the-art summary of potential estimation studies for SEIP applications. . . .	125
6.2	General solar data assumed.	134
6.3	Data ranges of free parameters as derived in Chapter 5.	134
B.1	Heat exchanger network (HEN) cost estimation parameters.	148
B.2	Boiler (BOI) parameters.	149

List of Tables

B.3	Heat pump parameters.	150
B.4	Flat plate solar collector (FP) parameters.	152
B.5	Photovoltaic module (PV) parameters.	154
B.6	High concentration photovoltaic and thermal system (HCPVT) parameters.	155
B.7	Mean data and performance indicators of typical days compared to original.	156
B.8	Hot and cold streams of the dairy process.	157
C.1	Input parameters for MOGA method.	159
C.2	Input parameters for CPLEX.	160
C.3	Streams data of the three benchmark cases.	161
C.4	Benchmark case data.	162
C.5	Optimization problem description: extended case <i>E2</i>	164
C.6	Data of streams of the heat pump superstructure (HPS).	167
D.1	Input parameters for MOGA method.	171
D.2	Input parameters for CPLEX.	172
D.3	Database of solutions for plant 2 (I).	179
D.4	Database of solutions for plant 2 (II).	180
D.5	Database of solutions for plant 2, $\Delta T_{\min}/2=5K$ (I).	182
D.6	Database of solutions for plant 2, $\Delta T_{\min}/2=5K$ (II).	183
D.7	Hot and cold streams of the generalized dairy process.	185
D.8	Utility thermal and resource stream data.	185

Acronyms and abbreviations

<i>SP-A</i>	solar system and industrial process analysis
<i>SP-I</i>	solar system and industrial process integration and optimization
<i>SP</i>	solar systems analysis for industrial process applications
AHP	absorption heat pump
AMPL	A Mathematical Programming Language [3]
CA	Canada
capex	annualized capital expenses
CC	composite curve
CDC	load duration curve of the average
CEPCI	Chemical Engineering Plant Cost Index [4]
CH	Switzerland
CHP	combined heat and power
CO ₂	carbon dioxide
COGEN	co-generation engine
COP	coefficient of performance
CPC	concentrating parabolic collector
CPLEX	IBM ILOG CPLEX Optimization Studio [5]
CPV	concentrating photovoltaic system
CSE	concentrated solar energy
CST	concentrated solar thermal system
DE	Germany
DNI	direct normal irradiation
environomic	environmental and economic
ES	Spain
ETC	evacuated tube collector
FP	flat plate thermal collector
GA	genetic algorithm
GCC	grand composite curve
GHI	global horizontal irradiation
GWP	global warming potential

Acronyms and abbreviations

HCPVT	high concentration photovoltaic and thermal system
HEN	heat exchanger network
HEX	heat exchanger
HF	heliostat field
HFC	Hydrofluorocarbons
HP	heat pump
HPS	heat pump superstructure
ICC	integrated composite curve
ICC	Intergovernmental Panel on Climate Change
KPI	key performance indicators
LDC	load duration curve
LHV	lower heating value
LP	linear programming
mELDC	mean error of the load duration curve
mELDC ²	mean squared error of the load duration curve
MER	minimum energy requirement
MILP	mixed integer linear programming
MINLP	mixed integer nonlinear programming
MIP	mixed integer programming
MOGA	multi-objective genetic algorithm
MSI	Marshall and Swift Index [6]
MVR	mechanical vapor re-compression
NLP	nonlinear programming
NOCT	nominal cell operating temperature
OECD	Organization for Economic Co-operation and Development
opex	yearly operating expenses
ORC	organic rankine cycle
PA	pinch analysis
PAM	partitioning around medoids
PSO	particle swarm optimization
PT	Portugal
PTC	parabolic trough collector
PV	photovoltaic module
PVT	(non-concentrating) photovoltaic and thermal system
SEIP	solar energy for industrial processes
SHIP	solar heat for industrial processes
ST	solar (non-concentrating) thermal system
STC	standard testing conditions

TAC	total annualized costs
thermo- economic	thermodynamic and economic
thermo- environmental	thermodynamic and environmental
TMY	typical meteorological year
TPES	total primary energy supply
TRNSYS	Transient System Simulation Tool [2]
TSA	total site analysis
US	United States of America

List of Symbols

Variables (MILP)

A^{HEN}	heat exchanger network (HEN) area	[m ²]
C^{capex}	annualized capital expenses	[currency/y]
C^{HEN}	investment cost of heat exchanger network (HEN)	[currency]
C^{INV}	total (installed) investment cost	[currency]
C^{opex}	total annual operating expenses	[currency/y]
C^{TAC}	total annual cost	[currency/y]
C^w	updated investment cost of utility technology w	[currency]
$CO_{2,tot}$	system overall resource CO ₂ equivalent emissions	[kgCO ₂]
$f_p^{g,COMP\ i \rightarrow j}$	compressor sizing factor from level $i \rightarrow j$ of heat pump g in period p	[-]
$f_p^{g,COND\ i}$	condenser sizing factor on level i of heat pump g in period p	[-]
$f_p^{g,DE-SUP\ i}$	de-superheating through mixing unit sizing factor from level i of heat pump g in period p	[-]
$f_p^{g,EVAP\ i}$	evaporator sizing factor on level i of heat pump g in period p	[-]
$f_p^{g,GAS-COOL\ i}$	gas-cooling heat exchanger sizing factor from level i of heat pump g in period p	[-]
$f_p^{g,MIX\ i}$	mixer sizing factor on level i of heat pump g in period p	[-]
$f_p^{g,PRESAT\ j \rightarrow i}$	presaturator sizing factor from level $j \rightarrow i$ of heat pump g in period p	[-]
f_{loss}^{st}	loss factor of storage unit st	[-]
$f_p^{st,in}$	inlet unit sizing factor during period p of storage unit st	[-]
$f_p^{st,out}$	outlet unit sizing factor during period p of storage unit st	[-]
f_p^{st}	sizing factor during period p of storage unit st	[-]
f_p^w	sizing factor of technology w during period p , [$f^{w,max}$, $f^{w,min}$]	[-]
f^w	maximum size of technology w	
N_{min}^{HEN}	minimum number of HEXs	[#]
y_p^w	existence of technology w in period p , {0,1}	[-]
y^w	maximum existence of technology w , {0,1}	
wC^{TAC}	weighted total annual cost function	[currency/y]
$x_V^{g,j \rightarrow i}$	vapor fraction after expansion from level j to i of heat pump g	[-]

List of Symbols

$y_p^{g,COMP\ i \rightarrow j}$	compressor existence from level $i \rightarrow j$ of heat pump g in period p	[-]
$y_p^{st,in}$	inlet unit existence during period p of storage unit st , {0,1}	[-]
$y_p^{st,out}$	outlet unit existence during period p of storage unit st , {0,1}	[-]
$\dot{E}^{g,COMP\ i \rightarrow j}$	maximum (electrical) power consumption of compressor $i \rightarrow j$ in heat pump g	[kW]
\dot{E}^w	maximum (electrical) power consumption of utility technology w	[kW]
\dot{E}^r	energetic consumption of resource r	[kW]
\dot{Q}^{st}	thermal flow during charge and discharge of storage unit st	[kJ/period]
$\dot{R}_{p,k}$	residual heat in period p transferred from interval $k - 1$ to interval k	[kW]
V_p^{st}	volume of storage material in unit st during p , which is at hot temperature T_h^{st}	[m ³]

Variables (nonlinear constraints)

$\Delta T_{i,DSH}$	superheated temperature difference after compression on level i	[K]
$\Delta T_{i,PRE}$	preheating temperature difference before compression on level i	[K]
$\Delta T_{i,SC}$	subcooling temperature difference before expansion on level i	[K]
T_i	saturation temperature on level i	[K]
ϵ^r	epsilon constraint on the resource consumption	[-]
ξ	slave function weighting factor	[-]

Greek Letters

α	thermal stream heat transfer coefficient	[W/m ² K]
η_0	reference efficiency of solar systems	[-]
η_{el}	electrical efficiency	[-]
$\eta_{isentropic}$	isentropic compressor efficiency of heat pump	[kg/s]
η_{el}^{ws}	average solar utility electricity efficiency	[-]
η_{th}^{ws}	average solar utility thermal efficiency	[-]
η^{ws}	average solar utility efficiency	[-]
η_{th}	thermal efficiency	[-]
γ_i	surface, i , azimuth angle	[°]
γ_s	solar azimuth angle (vector)	[°]
λ_{is}	solar beam incidence angle with respect to an inclined surface, i (vector)	[°]
Ω	storage cycle length (in number of periods)	[#]
ρ_g	ground reflectivity	[-]
ρ^{st}	density of fluid in storage unit st	[kg/m ³]
$\tau\alpha$	effective transmittance-absorptance product	[-]
τ	investment cost annualization factor	[1/y]
θ_i	surface inclination angle	[°]

θ_s	solar zenith angle (vector)	[°]
Parameters (heat pump)		
$\dot{E}^{g,COMP\ i \rightarrow j}$	electricity consumption of compressor between temperature level $i \rightarrow j$ of heat pump g	[kW]
$\dot{Q}^{g,COND\ i}$	heat release in condenser on level i of heat pump g	[kW]
$\dot{Q}^{g,EVAP\ i}$	heat consumption on level i in evaporator of heat pump g	[kW]
$\dot{Q}^{g,GAS-COOL\ i}$	heat release during gas-cooling at compressor outlet on level i of heat pump g	[kW]
$\dot{Q}^{g,PRESAT\ i}$	heat release during subcooling at outlet of presaturator on level i of heat pump g	[kW]
$T_{log,c}$	logarithmic temperature (cold streams)	[K]
$T_{log,h}$	logarithmic temperature (hot streams)	[K]
$T_{i,DSH}$	superheated temperature after compression on level i	[K]
$T_{i,PRE}$	preheated temperature before compression on level i	[K]
$T_{i,SC}$	subcooled temperature before expansion on level i	[K]
T_i	saturation temperature on level i	[K]
ε^r	epsilon constraint on the resource consumption	[-]
f_p^r	sizing factor of resource r during period p	[-]
$h_{out}^{g,COMP\ k \rightarrow i}$	outlet enthalpy of compressor from level $k \rightarrow i$ of heat pump g	[kJ/kg]
$h_{DSH}^{g,i}$	superheated enthalpy after compression on level i of heat pump g	[kJ/kg]
h_{DSH}	superheated enthalpy after compression stage of heat pump	[kJ/kg]
$h_{isentropic,i}$	isentropic enthalpy after compression from level i of heat pump g	[kJ/kg]
h_L	liquid saturation enthalpy	[kJ/kg]
$h_{PRE}^{g,i}$	preheated enthalpy before compression on level i of heat pump g	[kJ/kg]
h_{PRE}	preheated enthalpy before compression stage of heat pump	[kJ/kg]
$h_{SC}^{g,i}$	subcooled enthalpy before expansion on level i of heat pump g	[kJ/kg]
h_{SC}	subcooled enthalpy before expansion	[kJ/kg]
h_V	vapor saturation enthalpy	[kJ/kg]
n_g^{max}	maximum number of stages in heat pump g	[-]
p	pressure level	[bar]
Parameters (MILP)		
\dot{E}^{GRID}	reference grid electricity inlet/outlet	[kW]
\dot{E}^w	(electrical) power reference consumption of utility technology w	[kW]
\dot{E}	(electrical) power	[kW]
F_{BM}	bare module factor to account for installation, material, freight, and taxes	[-]
\dot{Q}_{ng}	natural gas consumption	[kW]

List of Symbols

$\dot{Q}_{p,k}^s$	thermal power of process streams s in period p and temperature interval k	[kW]
$\dot{Q}_{p,k}^w$	thermal power of utility w in period p and temperature interval k	[kW]
$\dot{Q}_{p,k}^{ws}$	thermal power of solar utility ws in period p and temperature interval k	[kW]
\dot{Q}	thermal power	[kW]
T_c^{st}	cold temperature of storage of storage unit st	[°C]
T_h^{st}	hot temperature of storage of storage unit st	[°C]
$\dot{V}^{\text{ref},st}$	reference volume flow rate of storage unit st	[m ³ /period]
$V^{\text{ref},st}$	reference volume of storage unit st , l	[m ³]
CI^{ref}	cost index in reference year of cost function	[-]
CI	cost index in current year	[-]
$CO_{2,\text{el}}$	life cycle emissions related to electricity from the grid	[kgCO ₂ /kWh _{el}]
$CO_{2,\text{ng}}$	life cycle emissions related to natural gas from the grid	[kgCO ₂ /kWh _{ng}]
$CO_{2,\text{tot}}^{\text{ref}}$	reference case resource CO ₂ equivalent emissions	[kgCO ₂]
c_p^{st}	specific heat capacity of fluid in storage unit st	[kJ/kgK]
ΔT_{min}	minimum temperature difference in the heat exchanger	[K]
Δt_p	operating time of period p	[h]
\dot{E}_{CO_2}	total emissions	[t CO ₂ eq]
ε	fractional constraining of a second objective in a single-objective MILP problem	[-]
IV_1^w	fixed (installed) investment cost factor of technology w	
IV_2^w	area specific proportional (installed) investment cost factor of technology w	
IV_A^w	proportional (installed) investment cost factor of technology w	
\dot{m}^{ref}	reference mass flow rate	[kg/s]
$f^{w,\text{max}}$	maximum size parameter of technology w	-
$f^{w,\text{min}}$	minimum size parameter of technology w	-
m	maintenance cost fraction of investment cost	[1/y]
n	equipment life time	[y]
occ_p	occurrence of period p	[1/y]
$OP_{1,p}^w$	fixed operating cost for using technology w during period p	[currency/h]
$OP_{2,p}^{\text{el}}$	electricity price during period p	[currency/kWh _{el}]
$OP_{2,p}^{\text{ng}}$	natural gas price during period p	[currency/kWh _{ng}]
$OP_{2,p}$	proportional operating cost during period p	[currency/h]
$OP_{2,p}^w$	proportional operating cost using technology w during period p , scaled with the multiplication factor	[currency/h]

Parameters (Solar)

A^{ws}	solar utility area	$[m^2]$
A	surface area	$[m^2]$
\dot{E}_{el}^{GRID}	average grid electricity requirement	$[kW]$
\dot{E}_{ng}^{GRID}	average grid natural gas requirement	$[kW]$
\dot{E}^{PROC}	average process requirements	$[kW]$
\dot{E}_{el}^{ws}	average solar utility electricity production	$[kW]$
\dot{E}^{ws}	average solar energy production over the year	$[kW]$
\dot{Q}_{th}^{ws}	average solar utility thermal energy production	$[kW]$
\dot{Q}_{th}^w	average process thermal energy requirements	$[kW]$
$T_{a,NOCT}$	ambient temperature during NOCT conditions, 20	$[^\circ C]$
T_{NOCT}	nominal cell operating temperature (measured)	$[^\circ C]$
T_{STC}	standard testing conditions temperature, 25	$[^\circ C]$
$T_{a,p}$	ambient temperature during period p	$[^\circ C]$
T_a	ambient temperature	$[^\circ C]$
$T_{c,p}$	cell temperature during period p	$[^\circ C]$
T_{in}	inlet temperature	$[^\circ C]$
T_m	mean temperature	$[^\circ C]$
T_{out}	outlet temperature	$[^\circ C]$
a_1	experimental performance parameter	$[W/m^2K]$
a_2	experimental performance parameter	$[W/m^2K^2]$
$b_{i,p}$	direct radiation present on inclined surface i during period p	$[W/m^2]$
$b_{n,p}$	direct normal radiation during period p	$[W/m^2]$
\mathbf{b}_h	direct horizontal radiation (vector)	$[W/m^2]$
\mathbf{b}_i	direct radiation present on inclined surface i (vector)	$[W/m^2]$
\mathbf{b}_n	direct normal radiation (vector)	$[W/m^2]$
$d_{i,p}$	diffuse radiation present on inclined surface i during period p	$[W/m^2]$
\mathbf{d}_h	diffuse horizontal radiation (vector)	$[W/m^2]$
\mathbf{d}_i	diffuse radiation present on inclined surface i (vector)	$[W/m^2]$
Δt^{PROC}	process operating time	$[h/y]$
f_T	temperature reduction factor	$[-]$
f_{field}	field loss factor	$[-]$
f_{gen}	generator electrical conversion efficiency factor	$[-]$
$f_{g,p}$	radiation dependent factor	$[-]$
f_{IAM}	incidence angle modifier	$[-]$
f_{inst}	cost installation factor	$[-]$
f^{ws}	solar fraction	$[-]$
g_{200}	solar global radiation of 200	$[W/m^2]$
g_{NOCT}	radiation during NOCT conditions, 800	$[W/m^2]$

List of Symbols

g_{STC}	radiation during STC conditions, 1000	$[W/m^2]$
$g_{h,p}$	global horizontal radiation during period p	$[W/m^2]$
$g_{i,p}$	global radiation present on inclined surface i during period p	$[W/m^2]$
$g_{gr,i}$	ground reflected radiation present on inclined surface i (vector)	$[W/m^2]$
g_h	global horizontal radiation (vector)	$[W/m^2]$
g_i	global radiation present on inclined surface i (vector)	$[W/m^2]$
$v_{a,p}$	ambient wind speed during period p	$[m/s]$
z	Earth surface normal, zenith	$[^\circ]$

Sets

F	set of fluids
P	set of time periods $p \{1,2,3, \dots, n_p\}$
STO	set of storage units $\subset \mathbf{W}$ (a subset of the utility set \mathbf{W})
S	set of streams (heating and cooling requirements)
\mathbf{W}_s	set of solar utility technologies $ws \in \mathbf{Ws} \subset \mathbf{W}, \{FP, PV, HCPVT\}$
W	set of utility technologies w
K	set of temperature intervals $\{1,2,3, \dots, n_k\}$
R	set of resources {electricity, natural gas, etc. }

Indexes

BOI	boiler
COGEN	co-generation engine
COMP	compressor unit of heat pump or refrigeration cycle
COND	condenser unit of heat pump or refrigeration cycle
CW	cooling water
DE-SUP	de-superheating through mixing unit of heat pump or refrigeration cycle
d	fluid index
EVAP	evaporator unit of heat pump or refrigeration cycle
field	field performance index
GAS-COOL	gas-cooling unit of heat pump or refrigeration cycle
GRID	electricity grid
g	heat pump
ref	reference case
k	temperature interval
MIX	mixer unit between liquid and vapor of refrigeration cycle, this unit is not physically built in the HP, the function will in reality be covered by the presaturator, it rather serves as supporting units for closing the energy balances

<i>obj</i>	objective function
PRESAT	presaturator of heat pump or refrigeration cycle
PROC	process specific property
<i>p</i>	period
REF	refrigeration cycle
<i>r</i>	resource
STO	thermal storage tank
<i>s</i>	stream (heating or cooling requirement)
<i>ws</i>	solar utility technology
FP	flat plate thermal collector
HCPVT	high concentration photovoltaic and thermal system
PV	photovoltaic module
<i>st</i>	storage unit
*	new system consumption
<i>w</i>	utility technology

Introduction

"Solar energy is the last energy resource that isn't owned yet - nobody taxes the sun yet."

Bonnie Raitt

Overview

- What are the advantages and challenges of solar energy?
- Motivation and scope of the work.
- Contributions and novelty of this thesis.
- Thesis structure overview.
- Notations and conventions.

Solar energy is free of charge, carbon neutral¹, and it is the largest energy resource on the planet [1, 7, 8]. The solar radiation reaching Earth's surface within 90 minutes would suffice to fulfill our population's entire yearly energy demand², if it could be fully converted and stored. Figure 1 shows the yearly incoming solar radiation on the earth surface in comparison to other (fossil and renewable) primary energy resources available on the planet based on two different origins [1, 7]. Even though the estimation of the potential of all resources (especially wind, uranium, and geothermal) is not consistently estimated, the exhaustive solar potential generally agreed upon [1, 7, 8] is clearly highlighted.

In tandem with an extensive potential, there are also great challenges to face. The greatest challenge is the intermittent availability of solar energy which exhibits large temporal (daily and seasonal) and spatial variations. Furthermore, solar energy is dilute: The maximum horizontal solar irradiance measurable at the Earth's surface during solar noon and clear sky conditions approximates 1000 W/m² [10]. In comparison, fueling a car transfers 20 MJ of energy (in the form of fuel) per second of refueling³. This power requirement is equivalent to the amount of solar radiation which insulates on a clear day (at noon) a surface area spanning three football fields⁴.

The aforementioned challenges highlight the need for efficient solar energy conversion routes and adequate tools to derive these.

¹ Life-cycle emissions from conversion equipment are neglected in this statement.

² Incoming yearly radiation 3.19×10^9 PJ [1], TPES of the population (2015) 5.71×10^5 PJ [9].

³ Car fueling requires 20 MJ/s of diesel with diesel energy density 35.8 MJ/l [11], refueling pump flow rate 35l/min [12].

⁴ Surface of 20×10^3 m², with solar energy to fuel conversion efficiency assumed to be 100% for this comparison.

Introduction

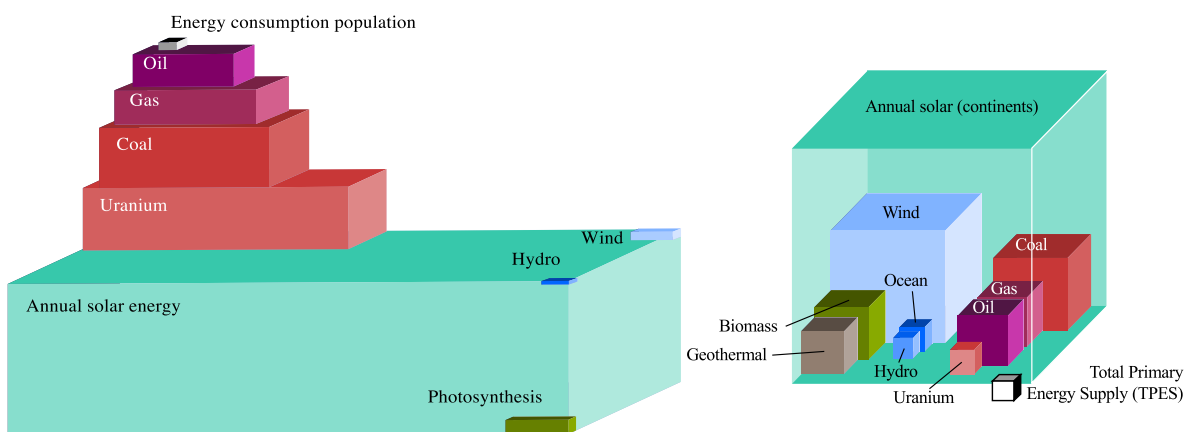


Figure 1 – Global availability of fossil reserves, and renewable energy supplied to Earth’s surface within a year. [left] Philibert [1], original from Craig et al. [8]; [right] European Photovoltaic Industry Association (EPIA) [7].

In the past, solar energy has been widely associated with electrical power generation [13]. More recently, applications and research have been extended to such domains as urban energy systems [14, 15], production of solar fuel [1, 16, 17], and industrial process heat applications [13, 18]. The latter being of great interest, since industrial sites is often positioned at the periphery of urban centers where cost of land is comparatively small.

Solar heat for industrial processes (SHIP), or more generally referred to as solar energy for industrial processes (SEIP) is an emerging field which is driven by the high carbon footprint of industrial processes [13]. Employment of solar installations in industry are estimated to grow continuously over the coming decades. Currently, SEIP installations account for less than 0.1% of total industrial energy requirements⁵ indicating the immense opportunities for improvement. To identify the barriers and enablers for more wide-spread use of solar energy in the industry is the general goal of this thesis.

This chapter serves as an introduction to the goal, motivation, and contributions of this thesis. The *focus and goal of this thesis* is presented in the following section before providing a general *state-of-the-art* review of relevant work and the identified gaps in this field. This is followed by the detailed *outline* of the thesis together with the main *contributions* of each chapter. The final part of this chapter addresses *notations and conventions* used throughout this thesis.

Focus and goal of this thesis

The specific goal of this thesis is the development of methods that aid in planning, design, and potential assessment of solar-assisted industrial processes to ultimately achieve cost-effective emission reductions in the industrial sector.

Industrial energy requirements can be generally distinguished between thermal and electrical

⁵OECD total industry requirement (2015) 7.92×10^5 ktoe, geothermal/solar etc. 4.53×10^2 ktoe [19].

demands. Thermal demands usually need to be produced on site⁶ and adequately fit to the process temperature levels, while electrical demands can be balanced through the electricity network. Due to these characteristics, a more detailed analysis of *thermal* process requirements is conducted in this thesis. Nevertheless, it is assured that *all* energy and material balances (including electricity and natural gas) are closed at all times within each problem formulation presented in this thesis.

For illustration, the methods are applied to an industrial case study from a low-temperature industry. The choice is motivated in the context and motivation section (Section 1.1). Integration measures are presented and discussed to investigate the inherent trade-offs between specific technology options. In particular, the competition and synergy of solar technologies with compression heat pump options is studied. The environmental benefits of the renewable options in comparison to conventional measures, such as improved heat recovery and heat pump systems is carefully weighed and rigorous methods for such analysis are derived.

It has to be noted that the goal of this work is not a complete analysis of all available solar and heat pump energy conversion routes, but rather a validation of the developed methodologies with adequate case studies and an in-depth analysis of some specific technologies. The motivation for the choice of the solar and heat pump equipment is provided in Sections 1.2 and 1.3.

State-of-the-art: methods for SEIP applications

A large body of work has been conducted on various aspects of integration of solar energy with industrial processes. A detailed state-of-the-art analysis of the specific field addressed in each chapter of the thesis will be provided at the introduction to the respective chapter. The following paragraphs provide a general overview of the topics relevant to SEIP and the identified gaps that motivate the work conducted in this thesis.

Solar modeling and design

Solar collector and field performance modeling in the wider context of SEIP encompasses a wide range of topics which are introduced in some key points below.

Solar collector modeling Quantification of incoming solar radiation (direct and diffuse) on inclined surfaces as well as identification of the angle of incidence and its influence on collector performance have been subject to numerous studies, especially prior to the 1980s [18, 20–26]. The steady-state performance estimation of solar (non-concentrating) thermal systems (STs) carried out by Hottel and Whillier [27] and transient modeling by Klein et al. [28] are still the most applied methods today [18] and led to the development of the widely-used proprietary software Transient System Simulation Tool [2] (TRNSYS). Modeling of photovoltaic modules (PVs) has focused on derivation of the operating cell temperature which is the main factor influencing PV performance [26, 29, 30].

⁶Industrial symbiosis and district heating can avoid on site production of thermal energy requirements.

Introduction

Concentrated solar energy (CSE) performance was originally derived from Monte-Carlo ray-tracing [16, 31, 32]; however, static (empirical) correlations have been developed based on polynomial functions [33, 34], typically of Hottel and Whillier-type [18].

Solar field modeling and system design A central research focus in SEIP applications is adequate performance estimation and design⁷ of the solar collector field. The methods presented in this section focus on the solar system while the industrial process is modeled simply as a constant or intermittent load. Interactions between the solar systems and process were disregarded.

Dynamic modeling provides the most detailed insights to solar (thermal) systems and their transient behavior and was regularly applied to analyze a fixed design [31, 35, 36]. However, computational burden is high and evaluating enough design points to identify favorable configurations, let alone application of more rigorous optimization strategies, often exceeds the computational capacity. Silva et al. [33] presented a rare example in which a transient collector field and storage model was optimized with respect to thermodynamic and economic (thermo-economic) objectives using a memetic genetic algorithm (GA) (though the collector performance is approximated with polynomial regression).

To overcome computational limitations, a large number of studies presented correlations (mostly based on regression of results from transient analysis) to estimate annual [37–39] or monthly [40–42] solar system performance. These were then used to derive optimal designs using analytical [43] and brute-forcing [44] methods, or mathematical programming (GA) [39]. The most applied brute-force method is the ϕ -f-chart method [40, 41], providing the monthly solar fraction of a SHIP system based on solar collector area, storage fraction, and constant industrial load. It is also available as a proprietary software [45]⁸. Another approach is presented by Kulkarni et al. [46, 47], who based their design strategy on one annual average day. Further contributions include collector tilt angle optimization [48, 49], and field design optimization (with respect to shading, losses etc.) [31, 50–53], and optimal temperature control [54], which are not the focus of this thesis.

Synthesis Summarizing, it can be seen that static or dynamic solar system performance estimation at hourly or minutely timescales are well explored, however, are rarely employed for optimal design purposes due to the computational effort. Monthly or annual regression models provide good estimates at reduced computational cost; however, the derived correlations are limited in applicability to the range of operating conditions and control strategies they were designed for. The f-chart method, for example, was derived from solar water and air heating systems with storage (double-pass) and a constant load profile, assuming a pre-set control strategy and specific storage sizes [44]. Apart from few exceptions, rigorous design strategies employing mathematical programming are not commonly applied in the literature discussed here.

⁷ *Design* refers here to the sizing and layout of the solar collector field.

⁸ The regression functions were derived from various TRNSYS simulations.

"Integration" of solar energy with industrial processes

"Integration" is highlighted in the title of this subsection, since it is a fuzzy notion which was interpreted broadly in scientific literature. Three types of *integration* studies were identified and are depicted in Figure 2.

Solar systems analysis for industrial process applications (SP) The first type, "SP", has been addressed in the previous section and refers to studies which focused on modeling and design of solar systems considering a constant or intermittent industrial load, with little focus on the interactions between the solar system, process and potential process improvement measures.

Solar system and industrial process analysis (SP-A) The second type, "SP-A", refers to studies which analyzed the solar and process system as a whole, addressing not only solar modeling, but also identification of the relevant process or utility streams suited to solar integration [55–58], heat exchanger network design [55, 58], and/or technical constraints related to this integration [36]. Alteration in the process design or process improvement measures were not considered.

Solar system and industrial process integration and optimization (SP-I) The third type, "SP-I", refers to studies which considered the solar and process as a whole and, additionally, addressed process improvement measures including internal heat recovery through pinch analysis (PA), and possibly competing technologies. Schnitzer et al. [59] and Atkins et al. [60] analyzed the thermodynamic and environmental (thermo-environmental) benefits of solar heat integration in the dairy industry, considering PA to identify the target solar temperatures for a fixed number of collectors. A complete utility integration, such as by modeling refrigeration of the sub-ambient streams, was not considered. Integration of a mechanical vapor re-compression (MVR) system was considered in the study presented by Eiholzer et al. [61], though the refrigeration of the sub-ambient process streams and the condenser hot stream were not modeled, which were in direct competition to the solar heat at 60°C. The solar sizing was based on brute-force generation of design points, though the time horizon and meteorological data were not specified. Perry et al. [62] presented a general approach of integrating renewable energy to industrial clusters with aid of total site analysis (TSA) but without elaborating on the specific design and modeling approach. Varbanov and Klemeš [63] extended the

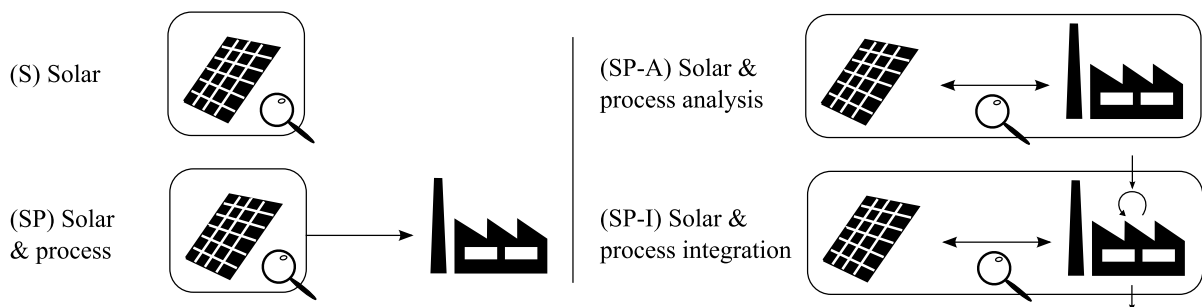


Figure 2 – Focus in literature on "integration" of solar energy with industrial processes.

Introduction

approach presented by Perry et al. [62] to account for time-slices and storage, focusing on graphical derivation of the utility system. Bühler et al. [64] presented a rigorous nonlinear programming (NLP) approach using particle swarm optimization (PSO) and pattern search to identify the optimal solar collector and storage sizes considering one year of hourly meteorological data. The sub-ambient process side and refrigeration was not included. Mian [65] proposed a solar sizing and heat exchanger network (HEN) design method for the high-temperature hydrothermal gasification based on four average seasonal days considering co-generation formulated as a mixed integer nonlinear programming (MINLP) problem.

Synthesis In summary, analysis of solar energy integration in industrial processes led to derivation of three types of studies. The most comprehensive type of studies "SP-I" considered the solar and process system as a whole, addressed process improvement measures including internal heat recovery through PA, and in rare cases, competing technologies.

A research gap was identified which pertains to comprehensive methods which provide rigorous sizing of the solar system and consider competing technologies. Particularly relevant technologies such as heat pumping, refrigeration, and MVR have been disregarded. This is especially relevant in one of the target industry for these methods: the dairy industry. Recurrently, the concept of formulating average/typical days was presented, though verification of the selection of typical days and effect on the sizing has not been addressed.

Extrapolation of solar potential

Solar potential studies form a body of work which aims at identification of the total energetic potential for solar installations in specific sectors or industries at a regional, national, or global level. As depicted in Figure 3, these studies are generally distinguished between *bottom-up* and *top-down* approaches.

Classical *top-down* approaches are presented by Brown et al. [66], Beath [67], and Lauterbach et al. [68], in which the total energy demands of different industrial sectors at the national level were estimated, categorized by temperature levels, and matched with solar technologies. Some go as far

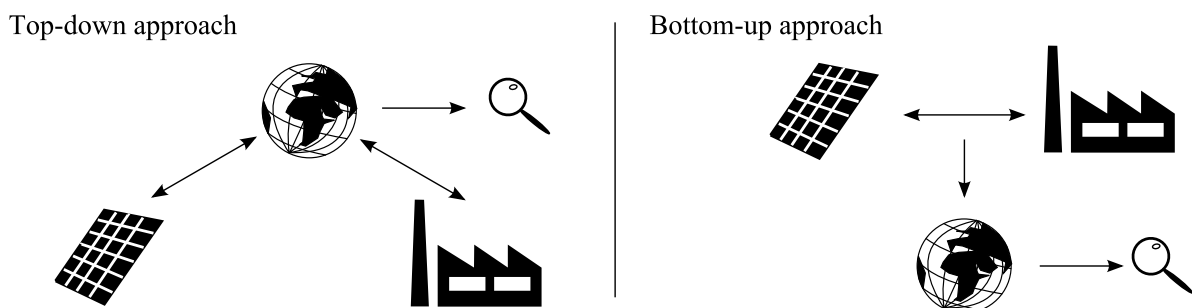


Figure 3 – Bottom-up, top-down approaches for solar potential studies.

as identifying industrial clusters in specific regions and matching those with the annual irradiation [66, 67]. Sharma et al. [69–71] presented a more detailed methodology in which the plants associated with certain sectors were individually identified and classified by their hot utility type (boiler or co-generation). The solar systems were then sized by plant capacity and the annual CO₂ emission mitigation potentials were derived.

A *bottom-up* approach was presented by Calderoni et al. [72] presenting three textile plants and estimating the economic feasibility of solar integration. The solar modeling approach was unfortunately not specified. Meyers et al. [73] compared ST systems for a fixed process load to PV systems combined with resistance heating, which is an exergetically inefficient way to provide heating. Based on a regression model, the results were extrapolated to various meteorological conditions to derive the turn-key cost based on assumed current and future specific project investment costs.

Synthesis *Top-down* and *bottom-up* approaches for solar potential estimation were presented. *Top-down* approaches provide powerful tools to identify relevant regions, industrial sectors, and possibly political measures to increase profitability of carbon emission reduction measures. However, the results are coarse and some options may be completely overlooked. *Bottom-up* approaches can also provide estimations for profitability of carbon emission reduction measures, though usually for specific sectors and regions. The studies presented in the literature either focus on the solar system or on the industrial process but do not consider them in a combined framework.

A gap was identified for a *bottom-up* rigorous approach which considers both the process and solar system, as well as a wider set of utilities and integration options, to identify relationships between energy prices and utility selection at a national or international level.

Synthesis and scope

The gaps in this state-of-the-art analysis can be summarized in three main points.

1. A lack of rigorous solar design methods is identified which provide precision at reasonable computational cost.
2. A lack for comprehensive integration methods, especially in the low-temperature sectors considering competing technologies, process improvements, and rigorous solar design.
3. A gap for bottom-up potential analyses which comprehensively address solar and process analysis, competing technologies, and allow extrapolation of results to the (inter)national level in a systematic manner.

Based on the identified gaps, this thesis addresses development of methods for solar energy for industrial processes (SEIP) (including electrical and thermal technologies) with focus on the low temperature sectors, considering competing technologies specifically heat pumps (HPs), refrigeration, and mechanical vapor re-compression (MVR).

Contribution and outline of the thesis

The chapters are presented below with the associated contributions alongside four central research questions. The main contributions are found in Chapters 3 to 6.

Context of the thesis (Chapter 1): Chapter 1 provides the wider context of the topics discussed in this thesis. It motivates the case study selection and technologies studied, and introduces concepts and nomenclature used throughout the work.

How can solar system design be accurately and rigorously addressed?

Solar modeling and design (Chapter 2): A rigorous solar system modeling and design approach is presented which allows to estimate collector and storage performance at sufficient precision and constrains the computational effort. The model performance is compared to dynamic results from TRNSYS. A clustering algorithm [74] is applied to select typical operating periods and results are compared for different sets of periods. The chapter addresses the gaps identified in point (1) in the synthesis and scope section. It contributes by adaptation of the multi-period mixed integer linear programming (MILP) approach from Maréchal and Kalitventzeff [75] to SEIP applications.

What problem formulation is required for a comprehensive design method for solar-assisted low-temperature processes?

Comprehensive integration method (Chapter 3): A comprehensive method is proposed which addresses simultaneous optimization of the process heat recovery, the conventional utilities, and the renewable utility system (including thermal storage) using ϵ -constrained parametric optimization. The method, tailored for the low-temperature industry, is based on multi-period utility targeting, including process heat recovery through pinch analysis (PA) and re-use through heat pumping, and identifies the optimal design and operation of the utility and storage system. The proposed methodology is illustrated on the basis of a dairy plant for which the different utility technologies are compared and evaluated based on economic and environmental criteria. This chapter addresses the shortcomings mentioned in point (2). The main contribution is the development of a comprehensive approach for solving the problem.

How can design of an optimal industrial heat pump system be conducted?

Generic heat pump superstructure synthesis and integration method (Chapter 4): Based on the promising results from Chapter 3, a novel, generic heat pump synthesis method for industrial applications is presented. The superstructure-based approach is solved with a decomposition solution strategy based on mathematical programming. Heat pump features are incorporated in a comprehensive way while considering technical limitations and providing a solution set to allow

expert-based decision-making at the final stage. The main contributions are found in the comprehensive superstructure, addressing fluid selection, component sizing, heat exchanger network (HEN) cost estimations, operating condition selection, and technical constraints.

How can the results be extrapolated to a wider scope?

Extrapolating impact: environomic potential (Chapter 5 and 6): A method for estimating the environmental and economic (environomic) potential of various emission reduction measures and technologies in industrial process applications is derived, generalizing the methodologies developed in the previous chapters. This includes generalized optimization techniques and generation of a publicly available database⁹ of solutions based on a wide range of possible economic and environmental conditions. By fixing the conditions (e.g. considering a particular country), the optimal solutions for these conditions can be drawn from the database. This allows identification of environmental and economic (environomic)ally optimal solutions in different countries and under different political boundary conditions, and hence, brings a twofold advantage: (1) process engineers can use the results from the generic plants to conduct pre-feasibility assessment, (2) policy-makers and equipment manufacturers can identify favorable conditions for installation of the technologies under scrutiny. The method is applied to a modularized dairy plant considering heat pumping and co-generation utilities, and generalized conclusions are drawn.

In a subsequent step, the methodology is extended to include solar utilities. The results from Chapter 3 are used for deriving a correlation to predict the annual solar collector and storage performance under optimal control. The chapter addresses the shortcomings mentioned in point (3). The method, though simple in application, displays a contribution to the field of potential analysis, offering a novel, detail-oriented, bottom-up approach.

A graphical overview of the presented chapters is depicted in Figure 4.

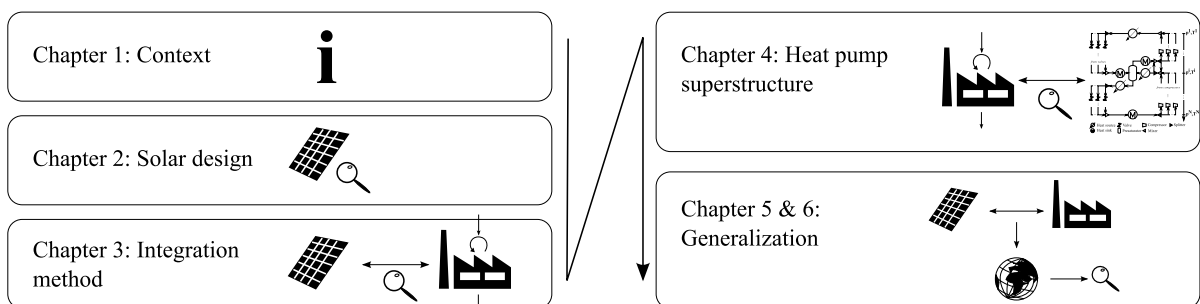


Figure 4 – Graphical overview of thesis structure.

⁹ The data can be accessed via an on-line parallel coordinate [76] decision-making platform.

Terminology, conventions

Mathematical conventions

The conventions in the equations presented throughout the thesis are that scalar decision variables are represented by *italics*, scalar parameters by roman text, vectors are always represented in **bold** (*italic* for variables, **roman** for parameters), and sets are represented in roman bold **Uppercase**.

Cost conversion and currencies

The equipment cost estimation follows common literature conventions as originally presented by Guthrie [77], expanded by Ulrich [78], and summarized by Turton et al. [79].

Bare module cost The bare module cost (also here referred to as installed cost) describes the direct and indirect expenses related to the unit including: material, construction, freight, taxes, and installation. Thereby the purchase price of the unit is corrected with various factors accounting for the material (if not carbon steel CS), operating pressures, piping, and the installation. These factors can be summarized in the bare module factor, F_{BM} [-]. In this work, all cost functions, C^w , of technology w as well as their linearized cost factors, IV_1^w and IV_2^w , refer to their bare module (installed) costs.

Effect of time: inflation Cost functions which date back to a reference year before the current year are corrected with cost indexes, CI, to account for inflation. Thereby, the out-dated cost function is multiplied with the fraction between the current and the reference cost index, as depicted in Equation 1. Common indexes used in chemical engineering practice and in this thesis are the Chemical Engineering Plant Cost Index [4] (CEPCI) and the Marshall and Swift Index [6] (MSI).

$$C^w = \frac{CI}{CI^{\text{ref}}} \cdot C^{w,\text{ref}} \quad (1)$$

Currencies and conversion The cost functions used throughout the thesis are represented in different units depending on the context of the study. The studies conducted in Europe are based on Euros [€] (Chapter 3), while international studies with extra-European references are conducted in US Dollars [\$] (Chapter 4-6). Since most chapters are based on published work, the currencies were not altered in this thesis so as to retain consistency with the publications. Most cost indexes are valid for US Dollars only. Therefore, if an original cost functions was provided in Euros (and was needed in US Dollars), it was converted to Dollars with the currency conversion rate of the reference year and subsequently updated.

Context and motivation 1

Overview

- Quantification and characterization of process energy requirements
- Classification of solar energy conversion technologies and identification of relevant ones
- Introduction to and identification of relevant heat pumping technologies
- Role of pinch analysis and implications for heat pumping and solar energy

Chapter 1: Context



This chapter provides a wider context of the topics discussed in this thesis. It motivates the choice of the analyzed case study and technologies, and introduces concepts and nomenclature used throughout the work.

1.1 Energy requirements in industry

Analysis of energy intensity in industry aids in identifying the most impacting industries and, therewith, candidates for emission reduction measures. As shown in Figure 1.1a, the most energy-consumptive industrial sectors in Switzerland (CH) are identified as the chemical (22%), mineral (12%), food (12%), paper (10%), and metal (8%) industry. While the absolute demand is important, temperature levels of the thermal requirements have a great influence on the feasibility of solar process *heat* applications.

Figure 1.1b shows the estimated thermal requirements and related temperature levels of these sectors from a study in Germany (DE). It reveals that the overall thermal demand of the food, textile, and paper sector is well below 300 °C, which constitutes a good match with the operating ranges of most solar thermal systems [13, 18, 68]. The other sectors each display heat requirements above 1000 °C and, hence, are seen to have less potential for solar integration [68].

The *dairy industry* in CH represents about 15% of the food sector¹, and is identified as an ideal candidate for the application of the methodologies derived in this thesis, due to its favorable temperature ranges (below 150 °C) and potentially large impact.

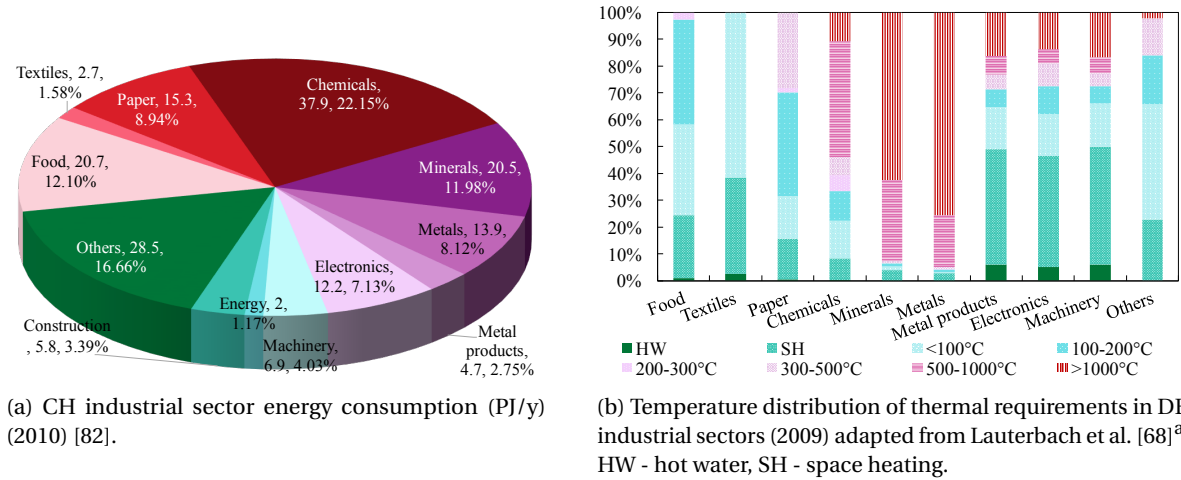


Figure 1.1 – Industrial thermal energy requirements and respective temperature levels.

^a Sectors from [68] were consolidated to match sectors depicted in Figure 1.11.1a: food: 12,12 (NACE Rev. 2 Code), textiles: 13-15, paper: 17,18, chemicals: 20,22, minerals: 23, metal products: 25, electronics: 27, machinery: 28-30.

1.2 Solar energy conversion

Figure 1.2 provides a summary of common solar energy conversion routes excluding natural conversion pathways such as photosynthesis or wind current generation. Three main products are identified: electricity, fuel, and heat. The conversion systems are differentiated between active and passive.

Passive systems describe structural elements or modifications (windows, walls, etc.) in buildings which are designed with the purpose of specifically harvesting solar energy, for example, as a heat source during cold seasons and rejecting heat during hot ones [1]. One example is provided by Čongradac et al. [49] who presented an algorithm for automatic control of window blinders based on the incident solar radiation. Agricultural greenhouses are possibly the oldest passive solar systems.

Active systems can be divided into non-concentrating and concentrating systems, while concentrating systems can be further distinguished between self-tracking and active tracking technologies. Concentrating technologies rely on redirection of the incoming light through reflectors (mirrors) or refractors (lenses) to increase the energy density in the focus thereby leading to reduced thermal losses due to reduced collector surface area [26]. This leads to increased temperatures in the receiver, which is advantageous in thermal systems to achieve higher operating temperatures, either for high-temperature industrial process use, or for thermo-mechanical (solar Rankine cycles) or thermo-chemical (solar gasification) applications, inducing higher conversion efficiencies. Reducing the active area allows utilization of higher efficiency receivers at similar investment cost, therefore motivating the use of concentrating photovoltaic systems (CPVs). CPVs require active cooling, which enables co-generation of heat and electricity.

¹ Raw milk treated in CH: 3.49×10^6 t (2015) [80], average energy requirement of raw milk treatment to various products: 0.9 GJ/t [81].

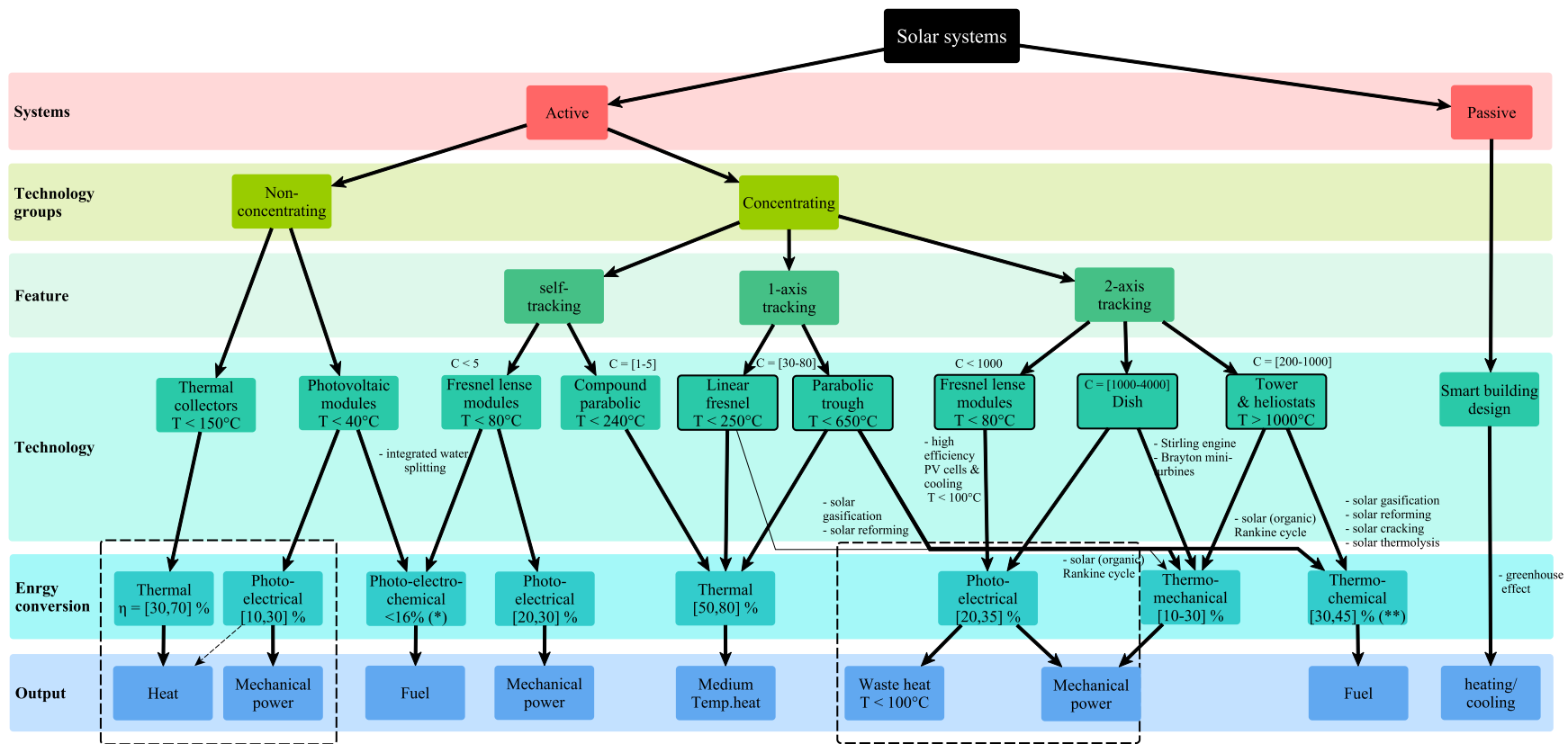


Figure 1.2 – Solar energy conversion routes tree diagram [10, 15, 17, 18, 26, 83, 84], excluding natural routes such as photosynthesis during biomass growth or wind current. (Framed) high concentrating technologies can solely harvest the direct portion of the incoming solar irradiance (DNI), while the other can harvest also the diffuse part of the irradiance (GHI). Conversion efficiencies given as ranges of yearly averages. (*) Photo-electro-chemical devices at experimental stage [17], efficiency given as fraction between thermodynamic potential, current density and irradiance, (**) thermo-chemical conversion at pilot stage [85], efficiency given by exergy efficiency of solar to electricity [83].

With increasing concentration ratios (> 10 [15, 18]), technologies require active tracking and cannot accept the diffuse fraction of solar irradiance. These concentrating systems are framed in Figure 1.2 and their efficiencies are usually expressed with respect to the direct normal irradiation (DNI), while non- and low-concentrating systems accept both types of solar irradiance (diffuse and direct) and their efficiency is reported with respect to the global horizontal irradiation (GHI).

Figure A.1 (in Appendix A.1) depicts the global yearly availability of the DNI and GHI indicating that the GHI varies between 900 and 2700 kWh/m²y in different regions, while the DNI ranges from 600 to more than 3000 kWh/m²y. Concentrated solar energy (CSE) is usually installed in regions with DNI above 2000 kWh/m²y, while non-concentrating solar technologies are considered even for regions with a GHI of 1000 kWh/m²y [73].

Since most heat demand in the dairy industry is below 130 °C [81], the focus in this thesis is placed on low-temperature *solar (non-concentrating) thermal systems (STs)*. *Photovoltaic modules (PVs)* are also investigated for fulfilling the electricity requirements of the system. Specifically, *(non-concentrating) photovoltaic and thermal systems (PVTs)* are not modeled assuming that a combination of photovoltaic module (PV) and solar (non-concentrating) thermal system (ST) could represent this type of system. In addition, a novel high concentration photovoltaic and thermal system (HCPVT) system [86–88] which co-generates electricity and low-temperature heat (<100 °C) is also compared to ST and PV. Other solar systems produces either higher temperature heat, or fuels, which is not the focus of this thesis.

1.3 Industrial heat pumping

Heat pumping has gained increasing attention during the past decades, not only for household applications but also for improving energy efficiency of industrial processes through waste heat recovery and valorization at elevated temperatures [89, 90].

However, analysis of the most cited publications during the past decades related to the keywords *waste heat recovery* shows different results. Figure 1.3 illustrates the distribution of the most cited publications within the last 10 years having average citations greater than or equal to five per year, resulting in 158 publications. Results show that research in the field of (industrial) *waste heat recovery* is largely dominated by organic Rankine cycles (ORC) [91, 92] and thermoelectric devices [93]. This may stem from a fully explored state-of-the-art of industrial heat pumps; however, the marginal penetration of industrial heat pump systems (apart from basic refrigeration and air-conditioning) [90, 94] contradicts this notion. The main barriers for broad usage in industry were identified as lack of knowledge and of comprehensive heat pump integration methods to provide improvement potentials [90, 94]. Figure 1.4 depicts a technology tree of heat pump concepts distinguished between open and closed systems, and further between sorption and mechanically driven systems.

This work addresses open- and closed-cycle, mechanically driven heat pumps with a focus on latent, single fluid systems, the reasoning for this is introduced in Section 1.4. Improving industrial resource efficiency through heat pumping is achieved by recovering waste heat at low temperature levels and returning it at higher temperatures as useful heat to the process. The temperature lift is achieved through mechanical compression of a working fluid which requires electricity. Before the concept of heat pumping in industrial processes can be discussed at greater depth, the concept of "waste heat" must be introduced, and with it, pinch analysis (PA).

1.4 Heat recovery potential in a process: pinch analysis

Pinch analysis is a methodology developed in the 1970s by Linnhoff and Flower [97, 98] and extensively discussed by Kemp [99], which allows estimation of the maximum energy recovery potential of industrial processes. This requires decomposition of an industrial site into its thermodynamic requirements. The result is a set of hot (net cooling requirement) and cold (net heating requirement) thermal streams.

The second principle of thermodynamics states that heat can only flow from a source at higher temperature to a sink at lower temperature. Ensuring thermodynamic feasibility, the heat cascade² is derived which allows estimation of the maximum energy recovery potential of an industrial process and the temperature ranges in which external heating and cooling are required.

1.4.1 Minimum approach temperature ΔT_{\min}

An ideal heat exchanger is an adiabatic device in which a hot stream transfers heat to a cold stream at lower temperatures as depicted in Figure 1.5. The second law of thermodynamics dictates that a temperature gradient between the hot and the cold stream is required to provide a driving force for heat to flow.

From the principles of pinch analysis (PA), a minimum approach temperature, ΔT_{\min} , defines the point in a heat exchanger where the hot and the cold streams exhibit the smallest temperature difference. The position of ΔT_{\min} depends on the inclination of the temperature-enthalpy profiles of the hot and cold streams, which are proportional to the inverse product of heat capacity and mass flowrate (mc_p). The optimal minimum temperature difference is conventionally found by optimization which considers the balance between operating and investment cost for heat exchangers. A smaller approach temperature reduces the operating cost due to higher heat recovery while increasing investment cost related to larger heat exchange area.

In general practice, engineering estimate values of the minimum approach temperature difference are assumed and to ensure thermodynamic feasibility, the hot (cold) streams are shifted downwards (upwards) by half of this difference, resulting in what are referred to as *corrected temperatures*.

² The heat cascade refers to the theoretical concept of successively transferring thermal energy from high to low temperature levels within a process.

Chapter 1. Context and motivation

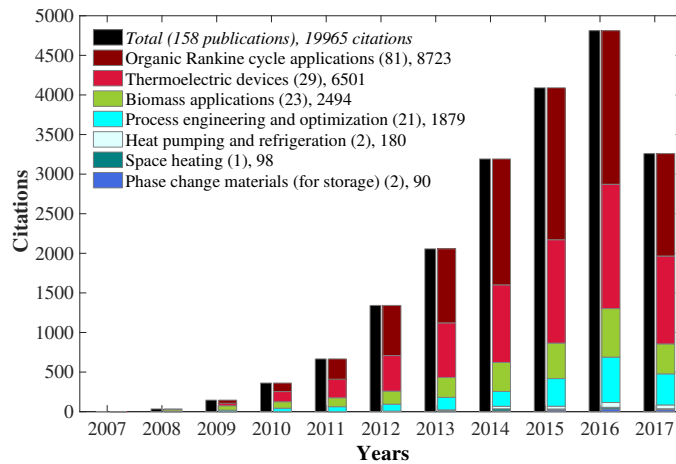


Figure 1.3 – Web of science [95], key words: *waste heat recovery*, top cited papers of last 10 years (≥ 5 citations/year), accessed 11.08.2017.

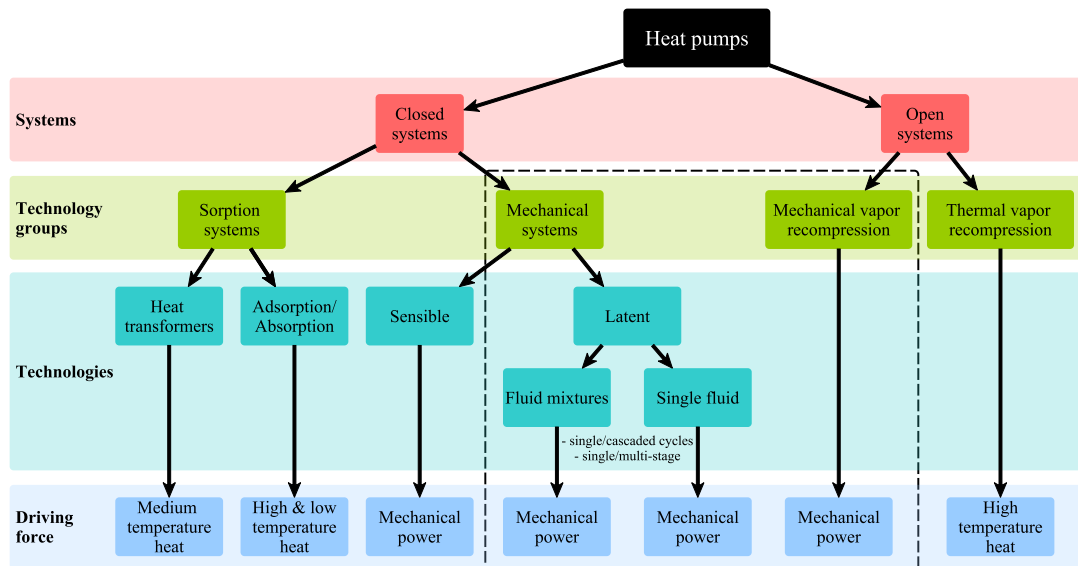


Figure 1.4 – Heat pumping technology tree diagram, adapted and extended based on Nellissen and Wolf [96].

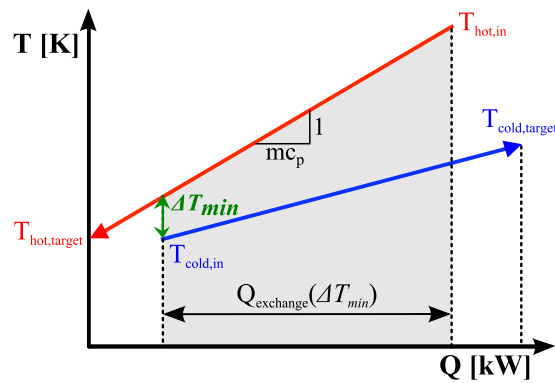


Figure 1.5 – Temperature enthalpy profile of a counter current heat exchanger to illustrate the ΔT_{min} .

1.4.2 Graphical representation, pinch point, and pinch rules

An example of a hot composite curve (CC) generated from the process thermal requirements is illustrated in Figure 1.6 (b). It is constructed by vectorial addition of all individual hot stream contributions (shown in Figure 1.6 (a)) in each temperature interval. The cold CC is constructed likewise. The hot and cold process CCs represent the process total heating and cooling demand. The vertical overlap between the two curves marks the maximum possible heat recovery potential of the industrial process.

The grand composite curve (GCC), depicted in Figure 1.7 (b), is derived by subtraction of the thermal load of the cold from the hot CC in each temperature interval. The GCC monitors the net heating and cooling loads and their temperature levels under the assumption of maximum heat recovery or minimum energy requirement (MER). The pinch point is marked by the impingement of the GCC on the temperature axis. Above, the process exhibits a net heating requirement (heat sink), and below, a net cooling requirement (heat source).

The distance from the temperature axis at the highest and lowest temperature represents the

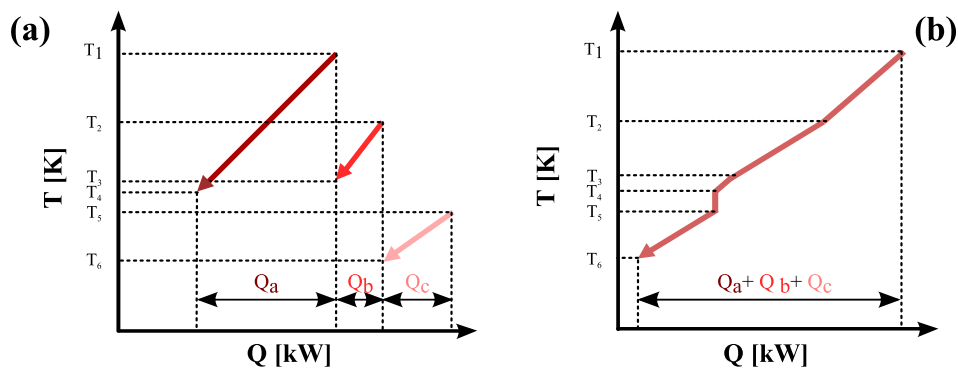


Figure 1.6 – (a) Individual hot streams, (b) hot CC in temperature enthalpy diagram [99].

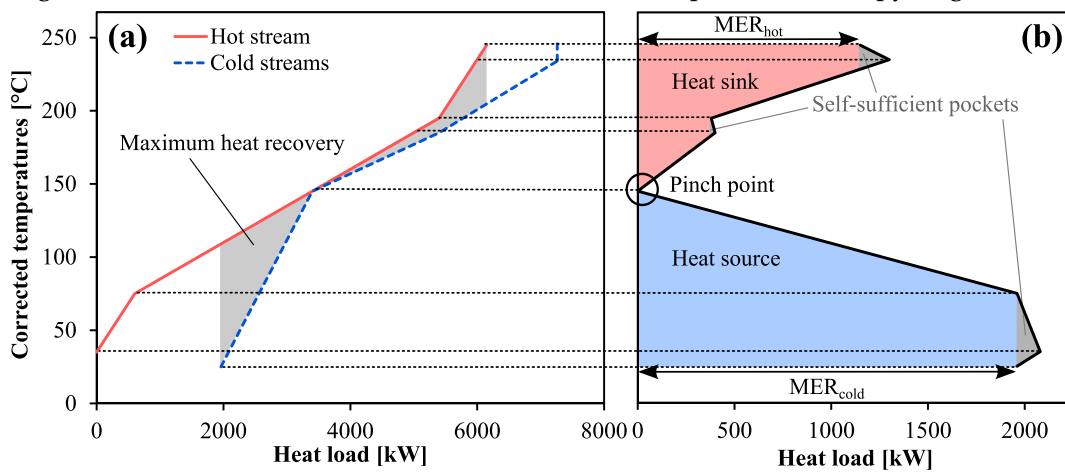


Figure 1.7 – (a) Hot and cold CCs, (b) GCC in temperature enthalpy diagram.

minimum hot (MER_{hot}) and cold (MER_{cold}) energy requirements, respectively.

The pinch point or pinch temperature induces three thermodynamics-based, so-called, *pinch rules* [97, 98]:

1. *Hot utilities* should only be installed at temperatures *above* the pinch (point),
2. *Cold utilities* should only be placed *below* the pinch (point), and
3. *No heat exchange* should occur *across* the pinch (point).

Violating any of these rules results in an increase of the utility requirements and, hence, a reduction of the process exergy efficiency. In the context of pinch analysis, "waste heat" is referred to as the heat available below the process pinch point which represents the process' net cooling demand.

1.4.3 Implications for solar energy for industrial processes (SEIP)

Solar thermal systems constitute classic hot utilities. The pinch rules presented in Section 1.4 clearly state that a hot utility is only beneficial to the process energy requirements if it is installed above the pinch temperature. This leaves a simple design guideline for solar heat for industrial processes (SHIP) applications. The pinch rules do not leave any guidelines for other solar energy systems which provide electricity or fuel.

1.4.4 Implications for industrial heat pumps

This section addresses mechanically driven heat pumps (HPs) due to their widespread application [94]; however, it should be noted that sorption systems present different and interesting integration options but are not within the scope of this work.

Townsend and Linnhoff [100] derived the theoretical foundation for optimal placement of heat pumps in an industrial process based on pinch analysis: heat pumps should always be placed across the process pinch point if energy savings are desired. In essence, energy savings are achieved by recovering waste heat from below the pinch and, after upgrading it through application of mechanical work, to supply it back to the process above the pinch temperature, which is hence referred to as *waste heat valorization* or *re-use*.

There is one crucial factor which influences the efficiency of heat pump cycles: the required temperature lift and thus the compression ratio. In the context of industrial waste heat valorization, the temperature lift is directly linked to the "sharpness" of the pinch, meaning the shape of the process grand composite curve close to the pinch point.

Figure 1.8 shows the temperature enthalpy diagrams of processes (A) and (B). Process (A) has sharp pinch point with a small temperature lift. While process (B) shows a smooth pinch point with heating and cooling requirements spanning over a range of temperatures. Integration of different mechanical heat pump systems are illustrated, starting from a single-stage, single fluid (inverted

1.4. Heat recovery potential in a process: pinch analysis

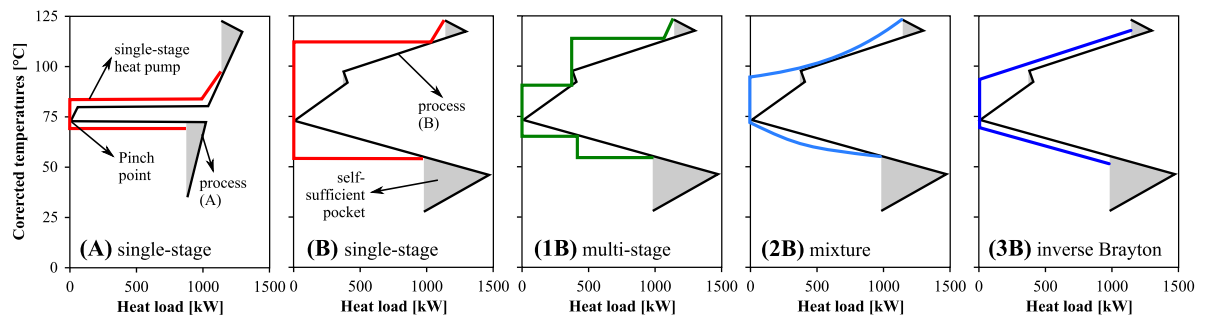


Figure 1.8 – Heat pump integration to process GCC. (A) GCC with "sharp" pinch point & single-stage heat pump (HP), (B) "smooth" pinch point & single-stage HP, (1B) "smooth" pinch point & multi-stage HP, (2B) mixture HP, (3B) inverse Brayton HP.

Rankine cycle) heat pump in Figure 1.8 (A) and (B). If a high temperature lift is required as illustrated in Figure 1.8 (B), the efficiency of standard (single-stage, single fluid) heat pump cycles is drastically compromised.

Three options to overcome this issue are discussed in the literature which are depicted in Figure 1.8 (1B-3B).

- (1B) **Multi-stage or cascaded heat pump cycles** based on latent heat release/ consumption in condenser/ evaporator with multi-stage compression and/or expansion [101–104], potentially a cascade of cycles
- (2B) **Zetropic mixture cycles** based on latent heat release of mixtures where the difference in fluid boiling points is expressed in a temperature glide and liquid/ vapor composition shift during evaporation and condensation [105, 106]
- (3B) **Inverse Brayton cycle** heat pumps based on sensible heat release and consumption in the condenser and evaporator, respectively [107]

Single fluid (inverse Rankine) heat pumps can satisfy constant temperature thermal requirements (single-stage) as well as continuous temperature ranges with help of multi-stage cycles at a reasonable coefficient of performance (COP) (above 2). In generating a temperature glide, zeotropic mixtures [105, 106] or heat pumps relying on the inverse Brayton cycle [107] may be advantageous for demands spanning wide temperature ranges, but less flexible relative to constant temperature requirements.

This thesis focuses on *mechanically driven, single fluid, multi stage (inverse Rankine) heat pumps* (depicted in the first three diagrams in Figure 1.8 (A-B-1B)), due to their operational flexibility, wide-spread application, and the technical realization being mostly dependent on mature technologies [94].

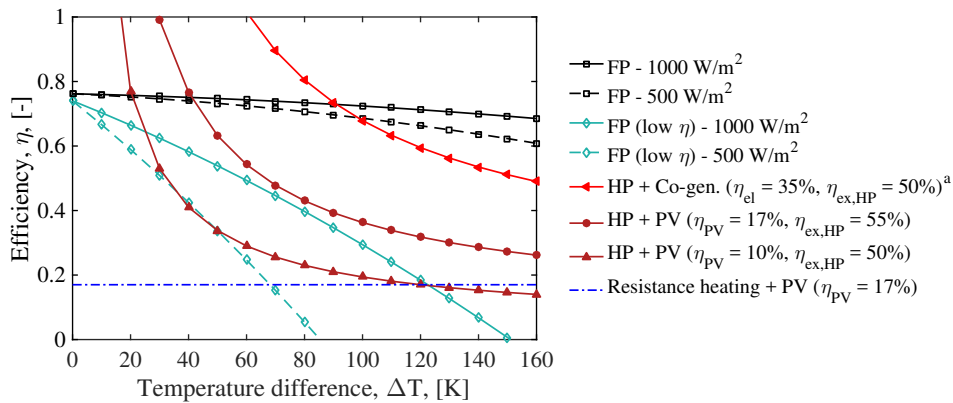
1.4.5 The use of PA throughout the thesis

The principles of PA are considered throughout the thesis. Therefore, a heat cascade formulation from the literature [75] is adopted which is presented in Equations 2.14-2.15 of Chapter 2. The formulation realizes heat recovery assessment in the process by imposing the second law of thermodynamics to assure that heat is only transferred from higher to lower temperatures. This formulation is the foundation of all methods developed in the main chapters (3-6) of the thesis, which are solved with optimization techniques aiming at minimizing the total system cost.

It has to be noted that the *pinch rules* presented in Section 1.4.2, are thermodynamically driven, while the objective functions of most optimization problems presented in the thesis are economically driven, which may lead to solutions that do not comply with the *pinch rules*. Whenever the utility temperature levels are, however, manually selected (as presented in Chapter 3) the *pinch rules* are respected.

1.5 Integrated solar and heat pump systems

Before discussing the implications of PA on combined solar and heat pump placement in industrial processes, a conceptual comparison between ST, PV, and HP systems is conducted. The sun-to-thermal efficiency³ is presented in Figure 1.9 for two types of flat plate ST collectors (high- and low-efficiency) and heat pumping driven by co-generation and two different PV systems. These are further compared to PV with resistance heating.



^a HP + Co-gen: natural gas-to-thermal efficiency is shown.
^b $\eta_{FP} [108, 109] \eta_{FP} = 0.74 - 3.5940 \cdot \frac{\Delta T}{G} - 0.00864 \cdot \left(\frac{\Delta T}{G}\right)^2$, [18](Eq. 76); HP based on COP with exergy efficiency as specified. $\Delta T = T - T_a$, $T_a = 20^\circ\text{C}$.

Figure 1.9 – Comparison of overall sun-to-heat conversion efficiency^a, ST, PV and heat pump or resistance heating^b.

It is observed that increasing temperature increment yields the best performance with high-efficiency flat plate collectors. However, it should be noted that the applied efficiency correlation of Hottel and Whillier [27]-type does not include an incidence angle modification (due to the sun inclination),

³ For HP with co-generation: natural gas-to-thermal efficiency.

1.5. Integrated solar and heat pump systems

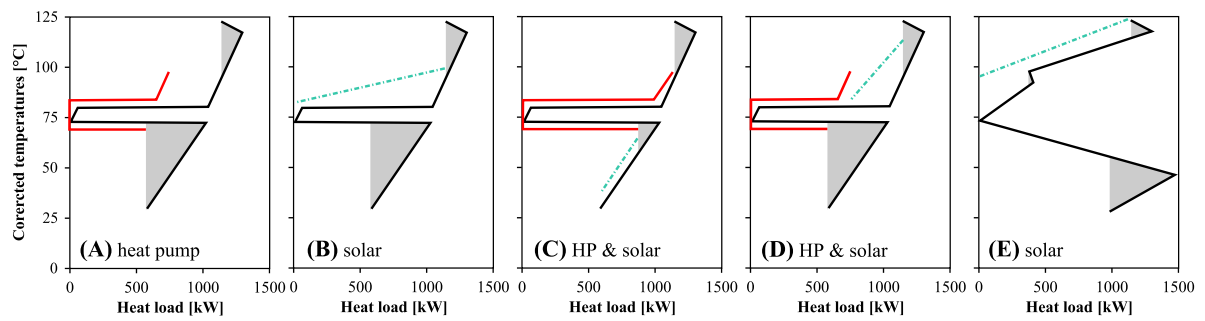


Figure 1.10 – Solar and heat pump integration into process GCC. (A) & single-stage HP, (B) ST, (C) synergetic ST and HP, (D) complementary ST and HP, (E) ST.

which, if applied, would yield lower average efficiencies. Heat pumping with co-generation generates similar (gas-to-thermal) efficiencies as the flat plate collectors even for a high temperature increments. High efficiency PV with an exergetically well designed HP (e.g. with liquid subcooling before expansion) shows better efficiencies than the resistance heating case even for high temperature lifts.

The above presented analysis provides indications for the advantages of the different heating systems not considering integration with an industrial process. Figure 1.10 depicts different options for beneficial integration of solar thermal systems and heat pumping in an industrial process. *Beneficial* refers to reducing the hot and/or cold conventional utility (boiler and cooling water) consumption.

Figure 1.10 (A) and (B,E) show the classical integration of a heat pump across the process pinch temperature and a solar thermal system providing heat above the pinch, respectively. Two options of combined solar and heat pump integration are shown in Figure 1.10 (C) and (D). Figure 1.10 (C) presents an example of synergistic integration of both solar and heat pump systems. Providing solar heat below the pinch to the self-sufficient pocket allows for a larger installation of the heat pump and a drastic reduction in hot and cold utility requirements. Figure 1.10 (D) presents an example of complementary installation of solar and heat pump system, where the solar energy satisfies the heat requirement that is not provided by the heat pump.

This analysis exemplifies the need for systematic integration methods, in providing beneficial solutions which do not necessarily comply with the classical pinch rules (section 1.4). Comprehensive derivation of a range of options for a multitude of different process profiles cannot be manually achieved which necessitates the use and derivation of systematic, mathematical programming approaches presented in this thesis.

Solar modeling and design 2

Overview

- Presentation of solar technologies and respective modeling approaches
- Introduction to typical period clustering and testing
- Introduction of multi-period MILP sizing method

Chapter 2: Solar design



This chapter is a summary of the work presented in Wallerand et al. [110], Wallerand et al. [111], and Selviaridis et al. [112]

This chapter aims at introducing the solar modeling and sizing approach applied in this thesis. The goal of this chapter is to derive models for estimation of collector and storage performance at sufficient precision while constraining the computational effort. The model performance is compared to transient results (TRNSYS). A clustering algorithm [74] is applied to select typical operating periods and several sets of typical days are compared. The sensitivity of the optimal sizing towards the typical days selection is, further, analyzed.

After a state-of-the-art analysis, the different (static, dynamic) modeling approaches are presented, followed by an introduction to the typical periods selection algorithm. In the subsequent section, the system design and integration method considered in this work is discussed. In the results and discussion section, the solar modeling approaches are compared to transient results and the typical period selection criteria are elaborated.

2.1 State-of-the-art

The studies discussed in this section are compared in various aspects in Table 2.1. The solar modeling and design approaches have already been discussed in the introduction of this thesis. Here, a few further points are highlighted, which were not mentioned before in order to increase conciseness.

2.1.1 Solar collector modeling

Early work by Liu and Jordan [20], Perez et al.[21, 22] and others [18, 23–26] dealt with proper assessment of incident direct and diffuse radiation on (inclined) surfaces.

This development went in parallel with the derivation of models for performance estimation of solar (non-concentrating) thermal systems (STs) at steady-state by Hottel and Whillier [27] and by Klein et al. [28] considering transience. The Hottel and Whillier equations augmented by incidence angle modifiers [18, 26] are still the basis for performance calculation of solar thermal systems (ST and CST) today.

2.1.2 Design of solar systems

This section addresses solar system design in the context of solar energy for industrial processes (SEIP). As derived in the introduction section, three levels for solar integration to industrial processes are treated in the literature ranging from solar systems analysis for industrial process applications (*SP*) with focus on the solar system to studies addressing solar system and industrial process integration and optimization (*SP-I*). The literature presented in this section is focused on the aspects of solar modeling and design with weaker focus on the industrial processes. Studies from any of the three categories (*SP*, *SP-A*, *SP-I*) are hence considered as long as the solar design is treated in a systematic manner.

As mentioned before, dynamic modeling provides the most detailed insights to solar (thermal) systems and their transient behavior and was regularly applied to analyze a fixed design [31, 35, 36]. However, computational burden is high and evaluating enough design points to identify favorable configurations, let alone application of more rigorous optimization strategies, often exceeds the computational capacity. To overcome computational limitations, a large number of studies presented correlations (mostly based on regression of results from transient analysis) to estimate annual [37–39] or monthly [40–42] solar system performance.

Not based on dynamic modeling, however, based on a typical meteorological year (TMY) of hourly data, Ashouri et al. [113] presented a mixed integer linear programming (MILP) approach for optimal design and operation in urban districts. The computational effort is low, since integration with an industrial process and its heat recovery system is not treated. Also Bühler et al. [64] presented a nonlinear programming (NLP) approach using particle swarm optimization (PSO) and pattern search to identify the optimal solar collector and storage sizing and operation considering a TMY of hourly meteorological data. The model is sequentially solved, identifying the relevant heat exchangers (HEXs) prior to sizing the solar system. The sub-ambient process side and refrigeration was not included.

Another approach was presented by Kulkarni et al.[46, 47] as well as Quijera et al. [114, 115], who based their conceptual design strategy on one annual average day.

Table 2.1 – State-of-the-art summary of solar modeling and design studies for SEIP applications.

Author	Year	Foc	Appr	Obj	Vars	Siz.	Ec.	Solar modeling				Proc. m.		SC	Process	Description.
								M	dT	Tool	Stor.	PA	HEN			
Hottel and Whillier [27]	1955	S	M	TP	T,IRR	F	X	S	hour	MEB	X	X	X	ST	-	Commonly used approximation of ST performance.
Liu and Jordan [20]	1960	S	M	TP	IRR	F	X	S	-	MEB	X	X	X	various	-	Determination of diffuse radiation on a horizontal surface.
Collares-Pereira and Rabl [23, 24]	1979	S	M	TP	T,IRR	B	X	S	hour	MEB	X	X	X	ST	-	Long term performance modelling of solar collector output.
Suehrcke and McCormick [25]	1988	S	M	TP	air mass	F	X	S	inst.	MEB	X	X	X	ST	-	Method for instantaneous determination of diffuse fraction.
Dudley et al. [34]	1995	S	E	TP	T,IRR	PR	X	D	sec	R,MEA	X	X	X	acrshortptc	-	Experimental results of PTC and polyn. regression.
Weinstock and Appelbaum [50]	2004	S	D	TP	FD	M-SQP(NLP)	X	S	hour	Matlab	X	X	X	FP,PV	-	NLP model of stationary field shading & optimal configuration.
Skoplaki and Palyvos [29]	2009	S	R	TP	IRR	F	X	S	hour	-	X	X	X	PV	-	Review of correlations for PV cell temperature derivation.
Talebizadeh et al. [48]	2011	S	D	TP	FD	M-GA (NLP)	X	S	hour	MEB	X	X	X	ST	-	Use of genetic algorithm for tilt and azimuth angle optimization for maximal energy efficiency, considering static equations of [116].
Tiwari et al. [30]	2011	S	R	TP	T,IRR	F	✓	S	hour	-	X	X	X	PV	-	Review of PV modeling, efficiencies and cost.
Yadav and Chandel [117]	2013	S	R	TP	FD	-	X	-	-	-	X	X	X	ST	-	Review of tilt angle optimization studies, methods, and correlations.
Klein et al. [118], [28]	1975	SP	M	TP	-	F	X	D	hour,min	TRNSYS	✓	X	✓	various	generic	Work presenting the dynamic modeling tool TRNSYS.
Beckman et al. [40, 41, 119]	1977	SP	D,M	TP	C,S,L	B	X	D	month	φf-Chart	✓	X	X	various	generic	Modeling approach based on fitting functions from TRNSYS results.
Clark [120]	1982	SP	A	E	cost	F	✓	S	year	MEB	-	X	X	acrshortptc	-	Break-even cost analysis of parabolic troughs in US.
Gordon and Rabl [37],[38]	1982	SP	D,M	E	C	R	✓	S	year,	MEB	X	X	X	FP	textile	Optimal collector sizing based on economic analytical optimization, based on polyn. regression of hourly static calculations [38].
Duffie and Mitchell [119]	1983	SP	M,E	TP	C,S,L	F	X	S	month	f-Chart	✓	X	X	ST	-	Testing of f-chart method with performance measurements.
Collares-Pereira et al. [43]	1984	SP	D	E	C,S	A	✓	S	year	MEB	✓	X	X	various	generic	Analytical storage and collector sizing method (incl. weekend storage).
Suehrcke and McCormick [42]	1992	SP	D,M,E	TP	C,L	F	X	S	month	MEB	✓	X	X	ST	-	Yearly fraction estimation method considering a bi-modal control strategy validated with experiments.
Kalogirou [35]	2003	SP	A	TP	-	F	✓	D	hour	TRNSYS	✓	X	X	ST	-	Comparison of the performance of various flat plate collectors for SHIP applications in Cyprus.
Kalogirou [39]	2004	SP	D,M	E	C,S	M-GA (NLP)	✓	D	year	ANN,GA	✓	X	X	various	food	Train ANN from TRNSYS data, use GA to optimize fitted functions.
Kalogirou et al. [121]	2007	SP	A	TP	-	F	✓	D	hour	TRNSYS	✓	X	X	PV/T	-	Economic and energetic comparison between various PV/T systems.
Kulkarni et al. [46],[47]	2009	SP	D,M	E	C,S	B	✓	S	hour,	DSM	✓	X	X	various	milk	Design space method for solar collector and storage sizing, however, based on an average day.
Silva et al. [31]	2013	SP	M,E	TP	FD	F	X	D	hour	TRNSYS,	✓	X	X	acrshortptc	generic	Dynamic modeling including ray tracing of parabolic troughs for industrial process heat applications.
Silva et al. [33]	2014	SP	D	TEP	FD,S	M-GA (NLP)	✓	D	VST	R,Modelica	✓	X	X	acrshortptc	generic	Memetic GA applied to optimize various design variables in CSE plants with fixed process load. Collector performance polynomially fitted.
Baniassadi et al. [122]	2016	SP	D	TP	SF	R	✓	S	year	MEB	✓	(✓)	X	HF	generic	R-curve method to add renewables to a co-generation system.
Meyers et al. [73]	2018	SP	M,Pb	E	C	B	✓	D,S	year,	R,TRNSYS	✓	X	X	various	-	Method for cost comparison between solar thermal and photovoltaics via resistance heating based on regression model.
Ashouri et al. [113]	2013	SU	D,O	E	C,control	M-BC(MILP)	✓	S	hour	MEB	✓	X	X	ST,PV	urban	Optimal design and control of urban district for a TMY.
Fazlollahi et al. [123, 124]	2014	SU	D,O	TEP	C,control	M-GA(MINLP)	✓	S	hour	MEB	✓	✓	✓	ST,PV	urban	Multi-period MINLP design of urban energy systems (based on decomposition strategy [125]) based on typical days.
Quijera et al. [114, 115]	2011	SP-I	D	TP	SF	C	X	S	hour	MEB	✓	✓	X	ETC	various	Solar system design based on desired solar fraction and av. annual day.
Míán [65]	2016	SP-I	D,O	TEP	C,control,	M-PGSCOM	✓	S	hour,	MEB	✓	✓	✓	CSE,PV	fuel	Multi-period HEN design and solar sizing based on four av. seasonal days applied to hydrothermal gasification.
Bühler et al. [64]	2016	SP-I	D,O	E	HEX, C	M-PSO	✓	S	hour	MEB	✓	✓	✓	FP	dairy	Process integration, HEN synthesis and solar sizing (sequentially solved) in a dairy case study (considering process hot side).

Focus: Solar (S), Solar integration to urban system (SU), SP, SP-A, SP-I based on notation presented in the introduction Section, Figure 2

Approach: Design (D), operation (O), modeling (M), analysis (A), potential (P), review (R), empirical (E)

Objective: Thermodynamic principles (TP), economic (E), thermo-economic (TEP), technical (T)

Variables: temperature (T), collector area (C), storage size (S), load (L), irradiation (IRR), field design (FD), solar fraction (SF), location (LOC)

Sizing: Fixed (F), brute forcing (variation of parameters, identification of maxima) (B), mathematical programming (M - genetic algorithm (GA) - sequential quadratic programming (SQP) - branch and cut (BC)), conceptual methods (C), R-curve analysis (R), analytical (A), polynomial regression (PR)

Economic (Ec.): economics considered in study (✓, X)

Modeling (M): (Quasi-) static (S), dynamic (D)

Time discretization (dT): instantaneous (ins.), variable time step (VST); horizon: unless stated differently: yearly analysis; unless specified differently (the discretization is usually applied to the scope of one year)

Tool: Mass and energy balances (MEB), design space method (DSM), regression (R), measurements (MEA)

heat exchanger network (HEN): ✓ - full HEN design (analysis), (✓) - focus on identification of relevant HEX for solar integration, X - no specific HEN design

Solar collector types (SC): Evacuated tube collectors (ETC), flat plate (FP), power tower heliostat field (HF), parabolic trough (PTC), flat plate photovoltaic and thermal systems (PVT), compound parabolic concentrator (CPC)

Mian [65] used four seasonal average days for their design method using a multi-period mixed integer nonlinear programming (MINLP) approach (with a sequential solution strategy) to design the solar system and HEN. Typical days (periods) were addressed in a rigorous manner by Domínguez-Muñoz et al. [126] for combined heat and power (CHP) applications, and Fazlollahi et al. [123] and Rager [127] for ST integration to urban energy systems. The methods applied rely on k-medoids or k-means clustering [74] to agglomerate meteorological or energetic data into smaller sets demonstrating that data clustering reduces the computational effort while maintaining a desired accuracy. Domínguez-Muñoz et al. [126] did not consider solar technologies, while Fazlollahi et al. [123] did not focus on the solar system accuracy and neither on the aspect of components sizing, addressing optimal operation instead.

2.1.3 Discussion and contribution

The state-of-the-art analysis can be summarized in a few main points.

1. Extensive work has been conducted to model (static and dynamic) solar performance accurately at hourly or minutely timescales.
2. Solar design were often applied with aid of monthly or annual regression models, which are limited in their applicability especially considering the storage system.
3. Rigorous design with mathematical programming has been applied in a yearly scope (TMY) of hourly time steps, if integration with the process side is not simultaneously addressed.
4. Rigorous, simultaneous solar system and industrial process design requires a reduced time horizon often resolved with typical or average days.
5. Clustering techniques for typical period selection were applied, but not comparatively studied at detail.

This chapter addresses points (3) and (4), by proposing a solar system and storage modeling approach which allows to estimate collector and storage performance at sufficient precision and constrains the computational effort. The model performance is compared to transient results from Transient System Simulation Tool [2] (TRNSYS). A clustering algorithm [74] is applied to select typical operating periods, and selection of the correct number of periods was derived. The contributions in this chapter are the adaptation of the multi-period MILP approach from Maréchal and Kalitventzeff [75] for SEIP applications and the comparative analysis of the typical period selection.

2.2 Problem statement

The goal of the research presented in this chapter can be summarized as depicted below.

Problem statement*Given*

- solar collector technology
- meteorological data

Determine

- governing performance equations as a trade-off between accuracy and computational effort
- typical days
- rigorous design approach in the context of solar process integration

2.3 Modeling

2.3.1 Solar technologies

As derived in Section 1.2, the focus in this work is placed on non-concentrating, low-temperature ST and photovoltaic module (PV) systems. A novel high concentration photovoltaic and thermal system (HCPVT) system [86–88] co-generating electricity and low-temperature heat (<100 °C) is also compared to traditional technologies. In the subsequent sections the static performance equations of the three solar systems are presented.

2.3.1.1 Solar irradiation on inclined surfaces

Global horizontal radiation The global solar radiation incident on a horizontal plane is composed partly of direct and partly of diffuse radiation reflected from the ground, clouds and the atmosphere. As mentioned in the meteorological data section, a common measurement provided by weather stations around the globe is the global horizontal irradiation (GHI, \mathbf{g}_h , [W/m²]) as well as the direct normal irradiation (DNI, \mathbf{b}_n , [W/m²]) or beam radiation. The global horizontal irradiation (GHI) is derived from the diffuse and the direct radiation incident on a plane [128].

$$\begin{aligned}\mathbf{g}_h &= \mathbf{d}_h + \mathbf{b}_h \\ &= \mathbf{d}_h + \mathbf{b}_n \cdot \cos(\theta_s)\end{aligned}\tag{2.1}$$

Where \mathbf{d}_h [W/m²] is the diffuse horizontal and \mathbf{b}_h [W/m²] is the direct horizontal radiation, θ_s [°] is the solar zenith angle indicated in Figure 2.1 (in grey) as the angle between the earth surface normal (zenith, z) and the sun.

Global radiation on inclined surface The global radiation present on an inclined surface, i , is derived from the solar beam on the slope and the present diffuse radiation. The direct beam on an inclined surface is calculated by the product of the direct horizontal radiation and the cosine of the

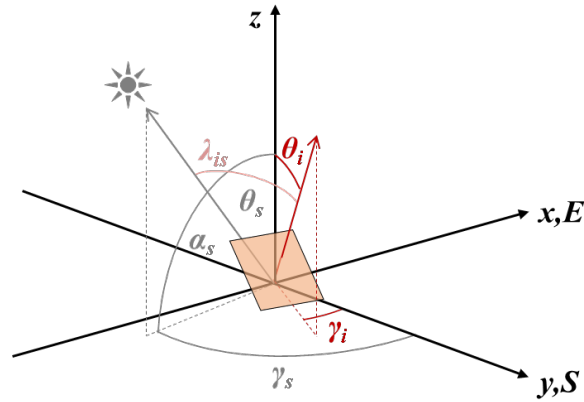


Figure 2.1 – Angles of the sun towards earth normal and inclined surface.

incidence angle between beam and slope. Calculation of the diffuse component on a slope is not trivial since the diffuse sky radiation is anisotropic meaning that it is not uniformly distributed over the hemisphere. Perez et al. [21, 22] offer correlations for modeling the anisotropic component of the diffuse radiation. In order to keep the problem at reasonable complexity the isotropic diffuse model proposed by Lui and Jordan [129], reprinted in Duffie and Beckman [26], is used in this work. It is divided into three components: the beam, isotropic diffuse, and global radiation diffusely reflected from the ground (Eq. 2.15.1 Duffie and Beckman [26]).

$$\begin{aligned} \mathbf{g}_i &= \underbrace{\mathbf{b}_n \cdot \cos(\lambda_{is})}_{\mathbf{b}_i} + \underbrace{\mathbf{d}_h \cdot \left(\frac{1 + \cos(\theta_i)}{2}\right)}_{\mathbf{d}_i} + \underbrace{\mathbf{g}_h \cdot \rho_g \cdot \left(\frac{1 - \cos(\theta_i)}{2}\right)}_{\mathbf{g}_{gr,i}} \\ &= \mathbf{b}_i + \mathbf{d}_i + \mathbf{g}_{gr,i} \end{aligned} \quad (2.2)$$

Where \mathbf{b}_i [W/m^2] is the direct beam, \mathbf{d}_i [W/m^2] is the sky diffuse and $\mathbf{g}_{gr,i}$ [W/m^2] is the ground reflected diffuse radiation present on the surface i , θ_i [$^\circ$] is the slope inclination angle. The ground reflectivity, ρ_g [-], is fixed at 0.154 as given by Ineichen et al. [130].

Under the assumption that the solar angles are known, the incidence angle of the solar beam with respect to an inclined surface, λ_{is} [$^\circ$], can be calculated (Eq. 1.6.3 Duffie and Beckman [26]) as follows.

$$\begin{aligned} \cos(\lambda_{is}) &= \cos(\theta_s) \cdot \cos(\theta_i) + \sin(\theta_s) \cdot \sin(\theta_i) \cdot \cos(\gamma_s - \gamma_i) \\ &= \sin(\alpha_s) \cdot \cos(\theta_i) + \cos(\alpha_s) \cdot \sin(\theta_i) \cdot \cos(\gamma_s - \gamma_i) \end{aligned} \quad (2.3)$$

Where θ_s [$^\circ$] is the solar zenith angle (vector), θ_i [$^\circ$] surface inclination angle, γ_s [$^\circ$] is the solar azimuth angle (vector), and γ_i [$^\circ$] is the surface, i , azimuth angle.

2.3.1.2 Solar (non-concentrating) thermal system (ST): flat plate thermal collector (FP)

The efficiency of solar thermal collectors at steady state conditions is commonly described by a quadratic performance curve that depends on the operating temperature, $T_m^{FP} = 0.5 \cdot (T_{in}^{FP} + T_{out}^{FP})$ [°C], the incoming radiation intensity during that period, $g_{i,p}$ [W/m²], the ambient temperature during period p , $T_{a,p}$ [°C], the conversion factor, η_0^{FP} [-], and two experimental parameters accounting for convection and radiation heat losses, a_1^{FP} [W/Km²] and a_2^{FP} [W/K²m²].

The general conversion factor, η_0 [-], is defined by the absorber material, thickness, and heat transfer fluid flow characteristics. The first experimental coefficient is usually related to the collector convective heat losses, and the latter is influenced by the collector re-radiation losses. The temperature dependent efficiency Equation 2.4 is then written as follows (Duffie and Beckman [26] Eq. 6.17.7, [60]).

$$\eta_{th,p}^{FP} = \eta_0^{FP} - a_1^{FP} \cdot \frac{T_m^{FP} - T_{a,p}}{g_{i,p}} - a_2^{FP} \cdot g_{i,p} \cdot \left(\frac{T_m^{FP} - T_{a,p}}{g_{i,p}} \right)^2 \quad \forall p \in \mathbf{P} \quad (2.4)$$

The formula accounts for a reduction in efficiency for operating temperatures higher than the ambient (due to thermal losses) and for reduction in efficiency due to reduced radiation intensities at normal incidence. However, since panels are installed at a fixed position, an incidence angle modifier, f_{IAM} [-], is introduced in order to account for optical losses related to the angle of the incident radiation. By definition, it is set to one at 0° incidence and is usually provided at 50°. In order to find other data points a cosine law is traditionally suggested (e.g. 6.17.10 [26] also in ASHRAE 93-2003), which however cannot be evaluated for angles close to 90°. Therefore an Ambrosetti-type equation [131] is used here which can be evaluated up to 90°.

$$f_{IAM}^{FP}(\lambda) = 1 - \tan^a \left(\frac{\lambda}{2} \right) \quad (2.5)$$

Where the coefficient a is usually derived from known data at a certain inclination (e.g. 50°); For beam radiation, the incidence angle, λ [°], is equivalent to the solar angle of incidence on the slope, λ_{is} [°]. For the diffuse and ground reflected component, the incidence angle is found from Equation 2.6 based on the slope inclination angle, θ_i^{FP} [°], (Duffie and Beckman [26], Figure 5.4.1, Eq. 5.4.1, 5.4.2).

$$\begin{aligned} \lambda_{id} &= 90 - 0.5788 \cdot \theta_i^{FP} + 0.002693 \cdot (\theta_i^{FP})^2 \\ \lambda_{igr} &= 59.7 - 0.1388 \cdot \theta_i^{FP} + 0.001497 \cdot (\theta_i^{FP})^2 \end{aligned} \quad (2.6)$$

Chapter 2. Solar modeling and design

With this, the time-dependent thermal energy production, \dot{Q}_p^{FP} [kW], of the solar flat plate collectors FP can be formulated.

$$\dot{Q}_p^{\text{FP}} = \eta_{\text{th},p}^{\text{FP}} \cdot f_{\text{field}}^{\text{FP}} \cdot \left(b_{i,p} \cdot f_{\text{IAM,ib},p}^{\text{FP}} + d_{i,p} \cdot f_{\text{IAM,id}}^{\text{FP}} + g_{\text{gr},i,p} \cdot f_{\text{IAM,ir}}^{\text{FP}} \right) \cdot A^{\text{FP}} \quad \forall p \in \mathbf{P} \quad (2.7)$$

Where each type of radiation (direct beam, $b_{p,i}$ [W/m²], sky diffuse, $d_{p,i}$ [W/m²], ground reflected diffuse, $g_{p,\text{gr},i}$ [W/m²]) is multiplied with the respective incidence angle modifier from Equation 2.5 and Equation 2.6, the collector area, A^{FP} [m²], the thermal field loss factor, $f_{\text{field}}^{\text{FP}}$ [-], and the efficiency from Equation 2.4.

2.3.1.3 Photovoltaic module (PV)

As mentioned before, the two main parameters influencing the PV performance is the cell temperature and the irradiation intensity. The cell temperature can be determined by correlations found in the literature (Eq. 23.3.4 Duffie and Beckman [26]).

$$T_{c,p}^{\text{PV}} = T_{a,p} + \frac{g_{i,p}}{g_{\text{NOCT}}} \cdot \frac{9.5}{5.7 + 3.8 \cdot v_{a,p}} \cdot \left[1 - \frac{\eta_{\text{el}}^{\text{PV}}}{(\tau\alpha)} \right] \cdot (T_{\text{NOCT}}^{\text{PV}} - T_{a,\text{NOCT}}) \quad \forall p \in \mathbf{P} \quad (2.8)$$

where $T_{a,p}$ [°C] is the (time dependent) ambient temperature during period p , $v_{a,p}$ [m/s] is the ambient wind speed during period p , and $g_{i,p}$ is the global incident radiation on an inclined surface during period p (see 2.3.1.1). The irradiation, g_{NOCT} , of 800 W/m² and ambient temperature, $T_{a,\text{NOCT}}$, of 20 °C during nominal cell operating temperature (NOCT) conditions are pre-set parameters. The nominal cell operating temperature, $T_{\text{NOCT}}^{\text{PV}}$ [°C], is a parameter measured and provided by the module manufacturer. The ambient temperature and wind speed are provided from the meteorological data described in Section 3.2.3.2.

A factor accounting for the influence of the incident radiation intensity is calculated by linear interpolation between the standard testing conditions (STC), defined at a radiation, g_{STC} , of 1000 W/m² and a cell temperature, T_{STC} , of 25 °C, and the certified indication at g_{200} 200 W/m².

$$f_{g,p}^{\text{PV}} = f_{200} + \left(g_{i,p} - g_{200} \right) \cdot \frac{1 - f_{200}}{g_{\text{STC}} - g_{200}} \quad \forall p \in \mathbf{P} \quad (2.9)$$

The time-dependent electricity production \dot{E}_p^{PV} [kW] is then written according to the following (Eq.

23.2.16 [26]).

$$\dot{E}_p^{\text{PV}} = \eta_{\text{el}}^{\text{PV}} \cdot f_{\text{gen}}^{\text{PV}} \cdot f_{\text{g},p}^{\text{PV}} \cdot [1 - f_{\text{T}}^{\text{PV}} \cdot (T_{\text{c},p}^{\text{PV}} - T_{\text{STC}})] \cdot g_{\text{i},p} \cdot A^{\text{PV}} \quad \forall p \in \mathbf{P} \quad (2.10)$$

where A^{PV} [m²] is the module area, $\eta_{\text{el}}^{\text{PV}}$ [-] is the module reference electrical efficiency, f_{T}^{PV} [-] is the temperature reduction factor, $f_{\text{gen}}^{\text{PV}}$ [-] is the generator electrical conversion efficiency factor.

2.3.1.4 Photovoltaic and thermal (HCPVT)

The high concentration photovoltaic and thermal system (HCPVT) system is novel technology under development by Airlight Energy Holding SA [86, 87, 132]. It consists of a multi-facet concentrating dish (reaching concentrations up to 2000).

High concentration devices only convert direct beam radiation. In the focal point, a multi-cell receiver is placed, which is equipped with PV cells, efficiently cooled by a micro-channel cooling system. A secondary concentrator is placed around the receiver which also needs to be cooled. Thermal energy is harvested from the micro-channel (primary cooling), and the secondary concentrator (secondary cooling). Due to the high concentration ratio, and based on the results from dynamic modeling [112], the efficiency is assumed to be independent of the incident radiation intensity and due to the two axis tracking the angle of incidence is always zero. The time-dependent electricity, \dot{E}_p^{HCPVT} [kW], and thermal energy production, \dot{Q}_p^{HCPVT} [kW], is formulated according to the following.

$$\begin{aligned} \dot{E}_p^{\text{HCPVT}} &= f_{\text{gen}}^{\text{HCPVT}} \cdot \eta_{\text{el}}^{\text{HCPVT}} \cdot b_{\text{n},p} \cdot A^{\text{HCPVT}} \quad \forall p \in \mathbf{P} \\ \dot{Q}_p^{\text{HCPVT}} &= Q_{\text{prim},p}^{\text{HCPVT}} \Big|_{T_{\text{in,prim}}^{\text{HCPVT}}}^{T_{\text{out,prim}}^{\text{HCPVT}}} + Q_{\text{sec},p}^{\text{HCPVT}} \Big|_{T_{\text{out,prim}}^{\text{HCPVT}}}^{T_{\text{out,sec}}^{\text{HCPVT}}} \\ &= f_{\text{field}}^{\text{HCPVT}} \cdot (\eta_{\text{th,prim}}^{\text{HCPVT}} + \eta_{\text{th,sec}}^{\text{HCPVT}}) \cdot b_{\text{n},p} \cdot A^{\text{HCPVT}} \quad \forall p \in \mathbf{P} \end{aligned} \quad (2.11)$$

where $b_{p,n}$ is the direct beam normal radiation in period p and $\eta_{\text{el}}^{\text{HCPVT}}$ is the PV electrical conversion efficiency, and $f_{\text{field}}^{\text{HCPVT}}$ is the thermal field loss factor. The primary efficiency, $\eta_{\text{th,prim}}^{\text{HCPVT}}$ [-], stems from the PV cell cooling while the secondary efficiency, $\eta_{\text{th,sec}}^{\text{HCPVT}}$ [-], is derived from the cooling of the secondary concentrators positioned immediately prior to the receiver. The PV cell cooling is constrained by the cell temperature which should not exceed 100°C; and assuming a minimum temperature difference in the heat exchanger of ΔT_{min} of 5K, the cooling stream cannot reach temperatures higher than 95°C. The secondary cooling, contrary to the restriction imposed for the primary PV cooling, can reach any temperature. Therefore, two thermal streams are produced which are between the three temperatures $T_{\text{in,prim}}^{\text{HCPVT}}$, $T_{\text{out,prim}}^{\text{HCPVT}}$, and $T_{\text{out,sec}}^{\text{HCPVT}}$.

2.3.2 Meteorological data clustering

2.3.2.1 Meteorological data

Due to the non-surprising difficulty of predicting future weather data, a common approach is the use of weather data from a typical meteorological year (TMY) [133]¹. A TMY is derived based on hourly historical data from a minimum period of ten years, in which each monthly profile is selected from an individual year selected by statistical indicators.

Weather data of locations which do not possess historical measurements are usually interpolated. The interpolation of weather data obviously leads to errors which cannot be avoided. In tandem with planning solar installations, reliable meteorological data should hence be acquired. Meteornorm7.0 [134] and SolarGIS [135] are standard (proprietary) softwares, which provide such (interpolated) data. Most transient modeling tools provide TMY data [2, 136]. If higher data resolution is desired (e.g. minute-by-minute) Meteornorm7.0 applies noise on the hourly averages. The meteorological data usually contained in a TMY are: direct normal irradiation (DNI), global horizontal irradiation (GHI), dry bulb temperature, humidity ratio, wind velocity, and the solar angles. Throughout this work, an hourly and minutely TMY [134] for the city of Sion, Switzerland (CH), is considered.

2.3.2.2 Typical periods selection

The MILP presented in the subsequent section relies on typical operating periods. This section presents a strategy for selecting those periods in a systematic manner.

k-means or *k*-medoids clustering is usually applied when robustness to outliers is required, or when the mean or median do not have a clear meaning. Weather data for optimal design of solar systems naturally falls into both categories. *k*-medoids clustering was selected since the resulting set is always a subset of the original data. A Matlab [137] function, which is based on the widely employed partitioning around medoids (PAM) algorithm [74], was used in order to reduce the problem size from 8760 points of hourly weather data to below 500 points. In Appendix B.3 the data and parameters are described in more detail. Following the indications of Domínguez-Muñoz et al. [126], the typical days were built from *n* clusters with and without 2 extreme days.

If extreme days are desired, then they are removed from the data set in advance and the clustering is applied on the remaining data. For clustering, three weather data were chosen which influence the solar performance the most: direct normal irradiation (DNI), GHI, and the ambient temperature. Since the DNI fluctuates the most on an hourly, daily, and monthly basis with a high influence on the solar output, it was chosen as the main reference for determination of the performance indicators. Also the extreme days were determined based on the DNI.

¹ There are various developments related to TMYs, which are distinguished by TMY, TMY-2, TMY-3

The procedure for finding the optimal number of clusters is divided into three steps:

1. Data normalization: The data are scaled such that all values are represented between zero and one [0,1]. Additionally, they are sub-divided into 365 data knots, each containing 24 hours of data.
2. k -medoids clustering: Data clustering is performed, increasing the number of clusters after each iteration until the stopping criterion is met. Since the clustering is a heuristic approach, for each number of clusters a set of iterations is conducted, and only the best ones are kept for further analysis.
3. Stopping criterion: The mean squared error of the normalized load duration curve (LDC) of the DNI is used as stopping criterion, as it is found that the LDC is best representing the data characteristics.

$$\text{mELDC}^2 = \frac{\sum_{t=1}^{8760} (\text{LDC}_{\text{original}}(t) - \text{LDC}_{\text{typical days}}(t))^2}{8760} \quad (2.12)$$

2.4 System design and integration

The solar sizing approach was based on utility targeting constraints [138, 139] which are commonly used for optimization of industrial process heat recovery and utility systems considering pinch analysis (PA). The rigorous MILP formulation can be extended to address multi-period problems [75]. This forms an excellent basis for a comprehensive approach which addresses optimal integration of solar energy in industrial processes. In the following paragraphs, the targeting constraints, which will be the basis for most of the developments presented in this thesis, are described in detail together with the modeling of the solar utilities.

2.4.1 Objective function

The objective function can be adapted to the respective needs. It needs to be formulated from linear dependencies of the decision variables in order to remain in the linear domain. Below, an exemplary objective function (as used in Chapter 3) is presented. Scalar decision variables are represented by italic letters and parameters by standard text; vectors and sets are represented in bold. In this case, the objective is the minimization of the total annualized cost (TAC, depicted in Equation 2.13) which is composed of the operating cost of each utility technology w during period p and the annualized investment that is found with aid of the maximum size of each technology.

$$\min_{y_p^w, f_p^w, y^w, f^w} \sum_{p \in \mathbf{P}} \underbrace{\left(\sum_{w \in \mathbf{W}} \text{OP}_{1,p}^w \cdot y_p^w + \text{OP}_{2,p}^w \cdot f_p^w \right)}_{\text{Operating cost}} \cdot \Delta t_p \cdot \text{occ}_p + \underbrace{\sum_{w \in \mathbf{W}} (\text{IV}_1^w \cdot y^w + \text{IV}_2^w \cdot f^w)}_{\text{Investment cost}} \quad (2.13)$$

Where

P	set of periods $\{1,2,3, \dots, n_p\}$
W	set of utility technologies w
$f_p^w \in \mathbf{R}^+$	continuous variable for sizing technology w during period p
$y_p^w \in \{0, 1\}$	binary variable related to existence of technology w during p
f^w	maximum size of technology w
y^w	overall existence of technology w
$OP_{1,p}^w$	[€/h] fixed operating cost for using the technology w during period p
$OP_{2,p}^w$	[€/h] proportional operating cost for using technology w during period p and is scaled with the multiplication factor
IV_1^w	[€/y] annualized, actualized fixed cost related to the investment of technology w
IV_2^w	[€/y] annualized, actualized proportional cost related to the investment of technology w
Δt_p	[h] operating time of period p
occ_p	[1/y] the occurrence of period p

2.4.2 Constraints

Heat cascade constraints The second law of thermodynamics states that heat can only flow from a source at higher temperature to a sink at colder temperature and is expressed in the heat cascade constraints in Equation 2.14-2.15. These constraints ensure maximum heat recovery in the system, which refers back to the principles of PA presented in Section 1.4.

$$\sum_{w \in \mathbf{W}} f_p^w \cdot \dot{Q}_{p,k}^w + \sum_{s \in \mathbf{S}} \dot{Q}_{p,k}^s + \dot{R}_{p,k+1} - \dot{R}_{p,k} = 0 \quad \forall p \in \mathbf{P}, k \in \mathbf{K} \quad (2.14)$$

Where

P	set of time periods $\{1,2,3, \dots, n_p\}$
K	set of temperature intervals $\{1,2,3, \dots, n_k\}$
S	set of process streams
$\dot{Q}_{p,k}^w$	[kW] reference heat release or demand of a utility technology w during period p in the temperature interval k
$\dot{Q}_{p,k}^s$	[kW] heat release or demand of process stream s during period p in the temperature interval k
$\dot{R}_{p,k}$	[kW] residual heat of temperature interval $k-1$ that is cascaded to interval k during period p

Thermodynamic feasibility The thermodynamic feasibility ensures a closed energy balance, as shown in Equation 2.15.

$$\dot{R}_{p,k} \geq 0, \quad \dot{R}_{p,1} = 0, \quad \dot{R}_{p,n_k+1} = 0 \quad \forall p \in \mathbf{P}, k \in \mathbf{K} \quad (2.15)$$

Existence of a technology The maximum size of operation and existence of technology w is given by Equation 2.16.

$$\begin{aligned} f^w - f_p^w &\geq 0 && \forall w \in \mathbf{W}, p \in \mathbf{P} \\ y^w - y_p^w &\geq 0 && \forall w \in \mathbf{W}, p \in \mathbf{P} \\ f^{w,\min} \cdot y_p^w &\leq u_p^w \leq f^{w,\max} \cdot y_p^w && \forall w \in \mathbf{W}, p \in \mathbf{P} \end{aligned} \quad (2.16)$$

where $f^{w,\min}$ [-] is the minimum size parameter of technology w and $f^{w,\max}$ [-] is the maximum size parameter of technology w .

Electricity balance The electricity balance in Equation 2.17 is closed by considering the electricity input and output of all utility technologies w .

$$\sum_{w \in \mathbf{W}} f_p^w \cdot \dot{E}^w = 0 \quad \forall p \in \mathbf{P} \quad (2.17)$$

Where \dot{E}^w is the reference electricity consumption (positive) or production (negative) of a utility technology w during period p .

Natural gas balance The natural gas balance in Equation 2.18 is closed by considering the natural gas input and output of all utility technologies w .

$$\sum_{w \in \mathbf{W}} f_p^w \cdot \dot{Q}_{\text{ng}}^w = 0 \quad \forall p \in \mathbf{P} \quad (2.18)$$

Where \dot{Q}_{ng}^w is the reference natural gas thermal input (positive) or output (negative) of utility technology w during period p .

Solar equation An additional equation for the solar utilities is introduced, since their utilization (multiplication factor), which is equivalent to the installed capacity of collectors or panels, cannot vary over different time steps. Here the intention is not to waste solar energy and, therefore, always to operate the solar field at full capacity rather than actively shading parts of the collector field or defocussing the trackers if less capacity is needed. Hence, the multiplication factor in period p needs to be equal to the maximum multiplication factor. This implies that if the solar system is delivering more heat than the amount needed by the process, cooling water will be consumed to evacuate the surplus heat.

$$f^{ws} - f_p^{ws} = 0 \quad \forall ws \in \mathbf{W}_s \subset \mathbf{W}, p \in \mathbf{P} \quad (2.19)$$

Where \mathbf{W}_s is the set of solar utility technologies which is a subset (\subset) of the set of all utility technologies \mathbf{W} . The solar radiation input and therefore the output does change with time, but that is accounted for in the constant solar heat release $\dot{Q}_{p,k}^{ws}$ [kW] of solar technology ws during period p in temperature interval k . The solar heat release is defined in Equation 2.7 for flat plate thermal collectors (FPs), in Equation 2.10 for PVs, and in Equation 2.11 for HCPVTs.

Thermal storage constraints The thermal storage model presented by Becker [140] was adapted to fulfill the imposed requirements of accuracy and reasonable computational effort. The model of Becker [140] assumes several isothermal tanks which are connected, and between which mass is transferred when the storage is charged or discharged. A higher number of isothermal storage tanks may increase the discretization and with that the precision, however preliminary results have shown that this occurs at high computational costs. Therefore, the mass storage presented by Moret et al. [141] was further developed to represent a thermal storage tank assuming a fully stratified tank between two temperature levels and proportional losses. The respective constraints are presented in Equation 2.20 - 2.24.

The energy balance of the storage is formulated in Equation 2.20.

$$f_p^{st} = \begin{cases} f_{p-1}^{st} \cdot f_{\text{loss}}^{st} + (f_p^{st,in} - f_p^{st,out}) \cdot \Delta t_p, & p \in \mathbf{P} \setminus \{1\} \\ f_{|\mathbf{P}|}^{st} \cdot f_{\text{loss}}^{st} + (f_p^{st,in} - f_p^{st,out}) \cdot \Delta t_p, & p = 1 \end{cases} \quad \forall st \in \mathbf{STO} \quad (2.20)$$

Where f_p^{st} [-] is the sizing factor during period p of storage unit st , $f_p^{st,in}$ [-] is the inlet unit sizing factor during period p of storage unit st , $f_p^{st,out}$ [-] is the outlet unit sizing factor during period p of storage unit st , f_{loss}^{st} [-] is the loss factor of storage unit st , $f_{|\mathbf{P}|}^{st}$ is the sizing factor at the end of the set of periods $|\mathbf{P}|$, and Δt_p [h] is the operating time of period p . The cyclic constraint depicted in Equation 2.21 ensures that the storage content is the same at the end of each cycle.

$$f_{|\mathbf{P}|}^{st} = f_{\omega}^{st} \quad \forall \omega = \Omega \cdot l, \quad l \in \{1, 2, \dots, |\mathbf{P}|/\Omega\} \quad \forall st \in \mathbf{STO} \quad (2.21)$$

Where Ω is the storage cycle length (in number of periods) and is usually 24 periods and l is the cycle index. The charging constraint depicted in Equation 2.22 ensures that storage charge and discharge do not happen at the same time.

$$y_p^{st,in} + y_p^{st,out} \leq 1 \quad \forall st \in \mathbf{STO} \quad (2.22)$$

Where $y_p^{st,in}$ [-] is the inlet unit existence during period p of storage unit st , $\{0,1\}$ and $y_p^{st,out}$ [-] is the outlet unit existence during period p of storage unit st , $\{0,1\}$. The heat which is transferred to the storage tank, \dot{Q}^{st} [kJ/period], during the charge and discharge mode is depicted in Equation 2.23.

$$\dot{Q}^{st,in/out} = f_p^{st,in/out} \cdot c_p^{st} \cdot \dot{V}^{\text{ref},st} \cdot \rho^{st} \cdot (T_h^{st} - T_c^{st}) \quad \forall st \in \mathbf{STO} \quad (2.23)$$

Where c_p^{st} [kJ/kgK] is the specific heat capacity of fluid in storage unit st , $\dot{V}^{ref,st}$ [m³/period] is the reference volume flow rate of storage unit st , ρ^{st} [kg/m³] is the density of fluid in storage unit st , T_h^{st} [°C] is the hot temperature of storage of storage unit st , and T_c^{st} [°C] is the cold temperature of storage of storage unit st . The volume of storage material, V_p^{st} [m³], which is at hot temperature of storage of storage unit st , T_h^{st} , is given by Equation 2.24.

$$V_p^{st} = f_p^{st} \cdot V^{ref,st} \quad \forall st \in \mathbf{STO} \quad (2.24)$$

Where $V^{ref,st}$ is the reference size of the storage, which is equal to 1 m³.

Computational environment The overall thermo-economic model is solved in Lua-based platform OSMOSE developed at École Polytechnique Fédérale de Lausanne in Switzerland [142, 143]. In the Lua-based platform, the MILP problem is converted to A Mathematical Programming Language [3] (AMPL) and then solved by IBM ILOG CPLEX Optimization Studio [5] (CPLEX).

2.5 Results and discussion

2.5.1 Solar technologies

2.5.1.1 Flat plate thermal collectors (FPs)

Flat plate thermal collectors (FPs) were modeled based on hourly static equations. The full list of equations is presented in Section 2.3.1.2. For comparison a TRNSYS model was created to quantify the difference between the static and transient performance estimation. The TRNSYS model relied on standard components, the collector was modeled with a Type 539, the pump with a Type 3b, the temperature was controlled through flow regulation with a Type 22, as depicted in Figure 2.2. The irradiation on the slope was estimated with a newly made component based on the Lui and Jordan [129] approach presented in Section 2.3.1.1. Table B.4 in Appendix B.2.3.2 shows the input data of the FP collector considered in this section and in Section 3.3. The average efficiency found by the TRNSYS model was 16.8%, while the static, hourly model yielded 17.1%, resulting in a 3 % error. It has to be noted that this efficiency is very low, which is related to the fact that the collector is operated at temperatures at the upper limit of its feasible range. The solar collector catalog [109] presented similar yearly estimations for the city of Sion. This shows on the one hand, that the modeling equations were correctly chosen, however, the collector type, or technology may in future work be reconsidered. Other non-concentrating options are evacuated tube collector (ETC) which yield higher efficiencies, at higher costs. In Chapter 3, the here presented collector is studied, while in Chapter 6 more efficient collector technologies are assumed.

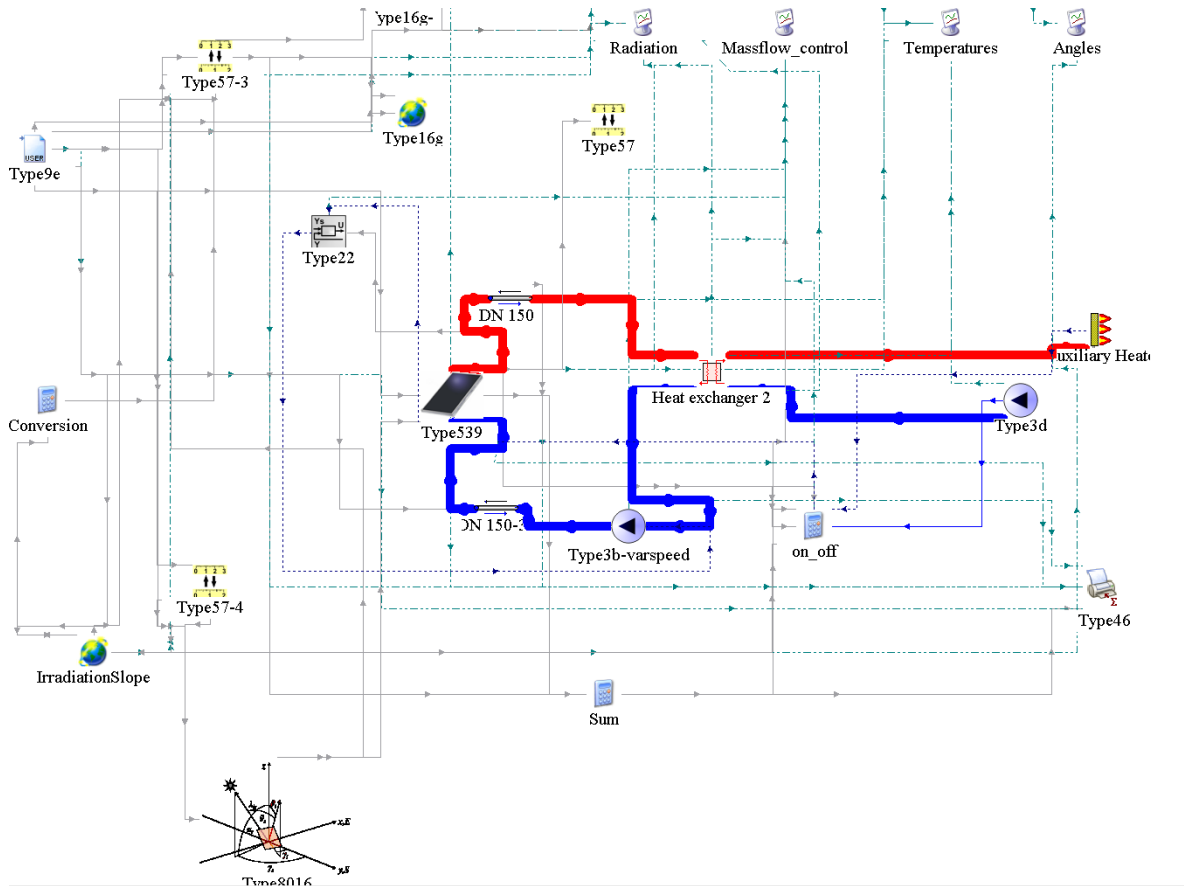


Figure 2.2 – TRNSYS flowchart of flat plate collector model.

2.5.1.2 Photovoltaic modules (PVs)

The photovoltaic modules (PVs) were modeled based on hourly static equations with the assumption that the transient behavior is negligible. A full description of the parameters used to model the photovoltaic modules (PVs) is presented in Table B.5 in Appendix B.2.3.3.

Figure B.3 shows the conversion efficiency from the global horizontal irradiance (GHI) $g_{p,i}$ in each period p to the electricity produced in the photovoltaic modules $\eta_{p,tot}^{PV} = E_p^{PV} / (g_{i,p} \cdot A^{PV})$, where E_p^{PV} is the electrical production of a PV module in period p . As discussed previously, the GHI only covers the fraction of the solar radiation that hits the earth at a perpendicular angle. This allows the conversion efficiency (if it is described in this manner) to exceed the rated efficiency of the PV modules (e.g. on day 1), since the inclined modules may capture more of the inclined sun rays than the GHI takes into account. The assessment also changes if shadowing was taken into account, though this was not considered as a factor in this study. The winter days (1, 4, and 9) show due to this peculiarity and due to lower ambient temperatures the highest efficiencies. In agreement with the observation from the plate collectors, it can be seen that higher inclinations are favored in winter days while lower inclination angles perform better during summer days. The highest overall efficiency was found for the lowest inclination angle of 30° with an average of 18.5 %. Such efficiencies may only be reached

for high performance PV modules such as the ones assumed. More detailed modeling, considering shading and conversion losses, will most likely show lower performance values.

2.5.1.3 High concentration photovoltaic and thermal system (HCPVT)

The high concentration photovoltaic and thermal system (HCPVT) system is novel technology under development by Airlight Energy Holding SA [86, 87, 132]. It consists of a multi-facet concentrating dish (reaching concentrations up to 2000), which focuses solar energy on a multi-cell receiver covered with highly efficient photovoltaic cells. The multi-cell receiver requires constant cooling, so that the photovoltaic cells do not overheat.

Since the HCPVT is still under development, no standard component in TRNSYS could be found to adequately model the transient behavior. Therefore, a dynamic model was created in C++ and linked to TRNSYS. A detailed description of the dynamic model can be found in Refs. [110, 144]. The main challenge was modeling the thermal mass of the multi-cell receiver component, as well as managing the flow control, such that the cell temperature never exceeds 100 °C. A comparison between transient and static model was conducted and it was shown that the error between static and dynamic model was approximately 5%, meaning that the static model slightly overestimated the solar production. Therefore, the parameters used in this thesis (depicted in Table B.6), were adapted to show lower efficiencies than in Wallerand et al. [110]. The details of the static model and the parameters assumed are presented in Appendix B.2.3.4.

2.5.2 System design: Sensitivity to data clustering

The clustering algorithm was applied to the data set of Sion (CH) and different numbers of typical days (clusters) were selected, as shown in Table 2.2. Several quality indicators are depicted for the various cluster sizes, including the mean error of the load duration curve (mELDC) presented by Fazlollahi et al. [123], as well as the deviation from the load duration curve of the average (CDC) [123], and the profile deviation (profile) [123], and the newly derived mean squared error of the load duration curve (mELDC²), presented in Equation 2.12.

The typical periods were applied to the case study presented in Chapter 3, and the results are shown in Table 2.2. What can be observed is that with increasing number of clusters in the typical periods, the resolution time increases. It can be further seen that the optimal collector size, together with the storage and objective function converge to similar numbers for increased number of clusters. It can be concluded that four clusters or less, as used by many studies (in the form of seasonal days), are absolutely insufficient for optimally sizing the system. Interestingly, eight typical days with two extreme days show lower resolution time than eight days without extreme days. It turns out that the CDC is not a good indicator, since the difference in the CDC between six and eight clusters was comparatively small (0.5%), even though the results are significantly different (6% difference in collector size). Likewise conclusions can be drawn for the profile deviation. Both the mELDC and

Chapter 2. Solar modeling and design

Table 2.2 – Different numbers of typical days and influence on results of MILP case study presented in Chapter 3. Indicators with respect to DNI.

Number of clusters	4	6	8	8+2 ^a	20
mELDC	0.013025	0.010251	0.0071645	0.0070295	0.005558
mELDC ²	6.147×10^{-4}	3.989×10^{-4}	1.65×10^{-4}	1.627×10^{-4}	9.717×10^{-5}
CDC	0.71387	0.49138	0.49282	0.46184	0.30262
Profile	1.0595	0.78829	0.78368	0.73987	0.57291
Resolution time [s]	56.5036	665.781	1370.73	682.021	3416.75
Collector size [-]	73.9372	46.7654	43.8621	43.5626	43.5819
Storage size [-]	1182.46	781.398	646.696	654.462	724.065
Objective [\$/y]	732219	478813	448042	432347	450952

^a Eight typical days and two extreme days (selected based on DNI)

the mELDC² show a higher sensitivity to the higher number of clusters which is in agreement with the results precision, and are, therefore, both recommended as quality indicators.

For the underlying study, eight typical days with two extreme days were selected, due to the reduced resolution time and the sufficient accuracy compared to 20 clusters. The collector efficiency was compared to the previous results and yielded consistent results. The limit was identified based on the last non-acceptable number of days to be 3.5×10^{-4} (below six typical days). In future studies, it is recommended to always test the results of the clustering on the real model, as not to improperly identify the numbers of clusters.

2.6 Conclusions

How can solar system design be accurately and rigorously addressed?

This chapter served as an introduction to the approach considered for modeling the solar technologies evaluated in this thesis. Static hourly performance equations were presented for flat plate thermal collectors (FPs), photovoltaic modules (PVs), and a high concentration photovoltaic and thermal system (HCPVT). A rigorous MILP solar system modeling and design approach was presented which allows estimation of collector and storage performance at sufficient precision and limited computational effort. The static performance models were compared to dynamic results from TRNSYS. It was found that hourly static collector performance estimations remain within a 5% error margin compared to the TRNSYS results.

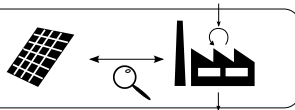
A clustering algorithm was applied to select typical operating periods, and selection of the correct number of periods was derived. Comparison of the typical period selection revealed that especially when addressing storage operation and sizing, adequate period selection is crucial. Application of a clustering approach reduced the resolution time successfully while guarding the accuracy for sufficient numbers of clusters. For low cluster numbers a deviation of the results was revealed, highlighting a need to proper investigation of the clustering results. Eight periods with two extreme days were selected as the best trade-off between accuracy and computational effort for the Swiss weather data of the city of Sion treated as a case study in this thesis.

Comprehensive integration method 3

Overview

- Method to simultaneously optimize the conventional and renewable utility system
- Based on ϵ -constrained parametric optimization
- Multi-period utility targeting, including process heat recovery through pinch analysis (PA)
- Identification of the optimal design and operation of the solar utility and storage system
- The preliminary version of a heat pump superstructure (HPS) shows great potential thus motivating more thorough analysis (as conducted in Chapter 4)

Chapter 3: Integration
method



This chapter is based on Wallerand et al. [111].

Implementation of solar energy in industrial processes is constrained by several obstacles. Identification of the best point of integration is not trivial and should comply with the process specific thermodynamic and technical constraints related to e.g. the heat exchange equipment [145, 146].

One important point which is often neglected is that integration of more efficient or less emitting heating sources (such as solar thermal) should always be compared to other process optimization measures. Process integration is a first step in capitalizing the maximum heat recovery potential together with retrofitting of the heat exchanger network. Beyond this, further measures are possible such as optimization of the operating points of the available utility equipment (e.g. the temperatures of the refrigeration system), mechanical vapor re-compression (MVR), or integration of closed cycle heat pumps (HPs) especially in the low-temperature industry. Therefore, it is advisable to use proper tools for comparison of various emission and cost reduction measures, including refrigeration cycles, heat pumping, and various heat sources which is the goal of this chapter.

After a state-of-the-art analysis of current synthesis methods, this chapter presents the applied methodology, followed by application of the method to the case study of a Swiss dairy, which is discussed in the results and discussion section.

3.1 State-of-the-art

The studies discussed in this section are compared in various aspects in Table 3.1. As derived in the introduction section, three levels for solar integration to industrial processes are treated in the literature (*SP*, *SP-A*, *SP-I*). The literature presented in this section is focused on studies which address integration between solar energy and industrial processes considering the entire system, meaning the process as well as the solar side.

3.1.1 Solar design and system integration

"*SP-A*" refers to studies which analyzed the solar and process system as a whole, addressing not only solar modeling, but also identification of the relevant process or utility streams suited to solar integration [55–58], heat exchanger network design [55, 58], and/or technical constraints related to this integration [36]. Alterations in the process design or process improvement measures were not considered.

"*SP-I*" refers to studies which considered the solar and process as a whole and, additionally, addressed process improvement measures including internal heat recovery through pinch analysis (PA), and possibly competing technologies. Schnitzer et al. [59] and Atkins et al. [60] analyzed the thermodynamic and environmental (thermo-environmental) benefits of solar heat integration in the dairy industry, considering PA to identify the target solar temperatures for a fixed number of collectors. A complete utility integration, such as by modeling refrigeration of the sub-ambient streams, was not considered. Quijera et al. [114, 115] analyzed a solar-assisted heat pump integration to a fish tinning process with aid of the time-average approach disregarding the obvious integration of mechanical vapor re-compression (MVR), and thereby missing a major process improvement opportunity.

Integration of a MVR system was considered in the study presented by Eiholzer et al. [61], though the refrigeration of the sub-ambient process streams and the condenser hot stream were not considered, which are in direct competition with the solar heat at 60°C. The solar sizing was based on brute-force generation of design points, though the time horizon and meteorological data were not specified. Perry et al. [62] presented a general approach of integrating renewable energy to industrial clusters with aid of total site analysis (TSA) but without elaborating on the specific design and modeling approach. Varbanov and Klemeš [63] extended the approach presented by [62] to account for time-slices and storage, focusing on graphical derivation of the utility system.

Bühler et al. [64] presented a rigorous nonlinear programming (NLP) approach using particle swarm optimization (PSO) and pattern search to identify the optimal solar collector and storage sizes considering one year of hourly meteorological data. The sub-ambient process side and refrigeration was not included.

Table 3.1 – State-of-the-art summary of solar modeling and integration studies for solar energy for industrial processes (SEIP) applications.

Author	Year	Foc	Appr	Obj	Vars	Siz.	Econ.	Solar modeling				Proc. m.		SC	P	Uti.	Description
								M	dT	Tool	Stor.	PA	HEN				
Niemann et al. [55]	1997	SP-A	A,D	E	C	C	✓	S	hour	MEB	X	X	✓	CPC, ET	AHP	AHP	Analysis of solar-driven AHP for ice making, sizing based on typical monthly days and baseline production volume.
Schweiger et al. [56]	2000	SP-A	Pb,D	TP	C,T	B	✓	S	year	MEB	X	X	X	various	various	-	Potential analysis and design of SHIP in ES and PT through steam production and integration with conventional utility system.
Calderoni et al. [72]	2012	SP-A	A,Pb	E	-	F	✓	S	-	-	✓	X	✓	PT	textile	-	Economic feasibility study of solar-assisted process plants in Tunisia.
Lauterbach et al. [68]	2012	SP-A	Pt	TP	L	C	X	S	-	-	X	X	X	various	various	-	Top-down analysis of industrial heat demand, temperature ranges in Germany.
Pietruschka et al. [57]	2012	SP-A	D	TP	C,control	C	X	S	year	-	X	X	✓	various	various	-	Preliminary design of multiple SHIP installations based on desired capacity and presentation of online monitoring/control.
Schmitt et al. [58, 147]	2012	SP-A	D	T	HEX	C	X	-	-	-	✓	X	✓	various	various	-	Analysis of integration options for solar process heat at the HEX technical design level.
Lauterbach et al. [36]	2014	SP-A	A	TP	control	F	X	D	-	TRNSYS	✓	X	✓	FP	brewery	-	Analysis of operational system faults with respect to model.
Müller et al. [148]	2014	SP-A	Pb	TP	FD,L	C	X	S	year	MEB	✓	X	X	various	food	-	Methodology to estimate the potential for solar heat in the liq. food industry, based on available area, and temperature levels.
Sharma et al. [69, 70]	2016	SP-A	Pt,D	TP	SF	C	X	S	year	MEB	X	X	X	PT	paper	Co-gen.	Potential analysis of solar heat for paper industry in India, considering solar sizing (by capacity), location, and co-generation.
Sharma et al. [71]	2017	SP-A	Pt,D	TP	SF	C	X	S	year	MEB	X	X	X	PT	dairy	-	Potential analysis of solar heat for dairy industry in India, considering solar sizing (by capacity) and locations of plants.
Schnitzer et al. [59]	2007	SP-I	A	E	-	F	✓	S	year	-	-	✓	X	FP	dairy	-	Analysis of environmental and economic potential for solar integration to an Austrian dairy (without process sub-ambient side).
Perry et al. [62]	2008	SP-I	D	TP	-	C	X	S	year	EMINENT[149]	X	✓	X	PV	[150]	various	TSA with EMINENT tool for urban industrial clusters design.
Varbanov and Klemeš [63]	2011	SP-I	D	TP	C,S	C	X	S	-	-	✓	✓	X	various	generic	various	TSA with time slices to conceptually design renewable utility systems for urban industrial clusters.
Atkins et al. [60]	2010	SP-I	A	TP	T	F	X	S	hour	MEB	X	✓	✓	ET	dairy	-	Solar collector size is fixed, analysis of outlet temperature on efficiency in 4 scenarios.
Quijera et al. [114, 115]	2011	SP-I	D	TP	SF	C	X	S	hour	MEB	✓	✓	X	ETC	dairy	-	Sizing solar system for desired solar fraction in dairy plant (process hot side), based on annual av. day.
Quijera et al. [151]	2013	SP-I	D	E	SF	C	✓	S	year	MEB	✓	✓	X	ETC	fish	HP	Analysis of solar-assisted heat pump integration to fish tinning process disregarding the obvious integration of MVR, time av. approach.
Quijera and Labidi [152]	2013	SP-I	D	TP	SF	C	✓	S	year	MEB	✓	✓	X	ETC	dairy	-	Exergoeconomic analysis of solar integration to dairy process (process hot side), time av. approach.
Baniassadi et al. [153]	2015	SP-I	D	TP	HEX	B,C	✓	D	min	EnergyPlusX	✓	✓	✓	FP	distillation	-	Solar fraction targeting, main goal: identify appropriate HEX.
Bühler et al. [64]	2016	SP-I	D	E	HEX, C	M-PSO (MINLP)	✓	S	hour	MEB	✓	✓	✓	FP	dairy	-	Process integration, HEN synthesis and solar sizing (sequentially solved) in a dairy case study (considering process hot side).
Mian [65]	2016	SP-I	D	E	C,control, HEX	M-PGSCOM (MINLP)	✓	S	hour	MEB	✓	✓	✓	CSE,PV	fuel	various	Multi-period HEN design and solar sizing based on four av. seasonal days applied to hydrothermal gasification.
Eiholzer et al. [61]	2017	SP-I	D	E	C,S	B	✓	S	month	MEB	✓	✓	X	ST	brewery	MVR	Multi-period and time-average analysis of brewery with solar integration disregarding heat pump integration/refrigeration.
Baniassadi et al. [154]	2018	SP-I	A,D	TP	HEX	B,C	X	S	hour	MEB	✓	✓	✓	FP	generic[99]	-	Identification of "best" HEX for varying collector number.
Becker [140]	2012	P	D	TEP	-	M-GA(MINLP)	✓	S	hour	MEB	✓	✓	X	-	dairy	HP,MVR	Design of industrial heat pump systems with MINLP (bi-level approach).

Focus: Solar (S), Solar integration to urban system (SU), SP, SP-A, SP-I based on notation presented in the introduction Section, Figure 2

Approach: Design (D), operation (O), modeling (M), analysis (A), potential (P), review (R), empirical (E)

Objective: Thermodynamic principles (TP), economic (E), thermo-economic (TEP), technical (T)

Variables: temperature (T), collector area (C), storage size (S), load (L), irradiation (IRR), field design (FD), solar fraction (SF), location (LOC)

Sizing: Fixed (F), brute forcing (variation of parameters, identification of maxima) (B), mathematical programming (M - genetic algorithm (GA) - sequential quadratic programming (SQP) - branch and cut (BC)), conceptual methods (C), R-curve analysis

(R), analytical (A), polynomial regression (PR)

Economic (Ec.): economics considered in study (✓,X)

Modeling (M): (Quasi-) static (S), dynamic (D)

Time discretization (dT): instantaneous (ins.), variable time step (VST); horizon: unless stated differently: yearly analysis; unless specified differently (the discretization is usually applied to the scope of one year)

Tool: Mass and energy balances (MEB), design space method (DSM), regression (R), measurements (MEA)

heat exchanger network (HEN): ✓ - full HEN design (analysis), (✓) - focus on identification of relevant HEX for solar integration, X - no specific HEN design

Solar collector types (SC): Evacuated tube collectors (ETC), flat plate (FP), power tower heliostat field (HF), parabolic trough (PTC), flat plate photovoltaic and thermal systems (PVT), compound parabolic concentrator (CPC)

Mian [65] proposed a solar sizing and heat exchanger network design method for the high-temperature hydrothermal gasification based on four average seasonal days considering co-generation using a bi-level solution strategy to solve the mixed integer nonlinear programming (MINLP) problem. Baniassadi et al. [154] most recently presented a conceptual method based on previous work [122, 153] for identification of good heat exchangers for variable collector area.

In all cases presented in the *SP-I* category the importance of process integration and pinch analysis for solar utility integration was considered. However, the time-variance of solar radiation and the related effect on the solar system performance as well as the influence of storage was often simplified or even neglected during the design phase. Furthermore, other process optimization techniques such as heat pumping were completely or partially disregarded. A full utility integration (including the cold process side and refrigeration, as well as MVR) was seldom conducted.

3.1.2 Industrial heat pumping

Heat pump systems (including refrigeration) allow valorization of low-temperature waste heat and thereby improve the process energy efficiency. Optimization of industrial heat pumps has been addressed by various authors. Shelton and Grossmann [101, 102] proposed a mixed integer linear programming (MILP) model for optimization of flexible heat pump superstructures which complies with the general process integration methodology presented by Papoulias and Grossmann [138, 139, 155]. They define all possible connections of refrigeration stages with the drawback of high complexity for problems with many temperature levels. Other authors based their formulation in the linear domain [103, 156–158]. More recent work dealt with exergy analysis of heat pumps and Mixed Integer Nonlinear Programming (MINLP) [159, 160]. None of these works have dealt with solar utility integration.

Optimization of a refrigeration and heat pump system for a dairy plant has been investigated by Becker et al. [140, 161] without the presentation of a flexible superstructure containing a variable number of stages, mixing, and various temperature levels.

3.1.3 Discussion and contribution

The state-of-the-art analysis can be summarized in three main points.

1. Comprehensive utility integration is seldom performed in solar integration studies.
2. The competing role of heat pumping in low temperature applications is neglected.
3. Comprehensive methods which provide rigorous sizing of the solar system and considering competing technologies are not presented for low temperature processes.

To overcome the identified gaps, a comprehensive method is proposed which addresses simultaneous optimization of the process heat recovery, the conventional utilities (including heat pumping),

and the renewable utility system (including thermal storage) using ε -constrained parametric optimization. The method is based on multi-period utility targeting, including process heat recovery through PA and re-use through heat pumping, and identifies the optimal design and operation of the utility and storage system. The innovative aspects are summarized in the following points:

- A multi-period mixed integer linear programming (MILP) approach is chosen, which has been applied by other authors [75, 124, 162], but is extended to account for the specific characteristics of solar utilities and contains ε -constraints.
- A novel heat pump superstructure is applied for optimal design of multiple stage heat pump cycles.
- The meteorological data is clustered based on common clustering algorithms [74] by proposing a new performance indicator, being the mean squared error of the load duration curve (mELDC²)
- Solar performance calculations are based on verified state-of-the-art correlations and data from independent testing facilities and producers.

This chapter bases on the mathematical models introduced in Chapter 2.

3.2 Methodology

3.2.1 Problem statement

The goal of the research presented in this chapter can be summarized as depicted below.

Problem statement

Given

- (low temperature) industrial process thermal and material demands
- meteorological data
- set of utility technologies, including solar utilities and heat pumps

Determine

- optimal utility design and scheduling including
 - solar collector area and storage sizes and operating schedules
 - heat pump size and operating conditions

3.2.2 Overview

A sketch of the applied methodology is presented in Figure 3.1. The work is employed in a computational framework which is based on the Lua [163] programming language. It is separated into three main steps: (A) data collection, (B) system resolution, and (C) performance calculation.

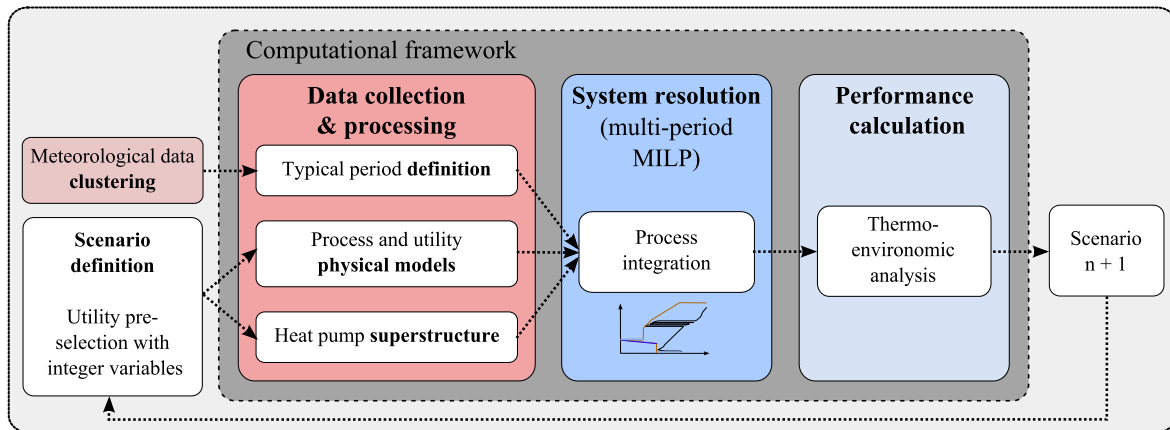


Figure 3.1 – Methodology proposed in Chapter 3.

(A) Data collection During the data collection phase, utility and process data are gathered, the energy and mass balances are formulated, and the thermodynamic models are developed. In a preliminary step the meteorological data are clustered to form a set of typical days such that the problem size can be reduced from a typical meteorological year (TMY) composed of 8760 hours to a much smaller set (of a few hundred hours). This part of the procedure is presented in Section 3.2.3.

(B) System resolution The system resolution aims at targeting different utility designs by solving the multi-period MILP for minimum total annual cost subject to the heat cascade constraints. The general formulation of the multi-period MILP can be found in Section 3.2.4. During the multi-period MILP a single-objective optimization is performed with the objective of minimizing the total annual cost. To compare the different scenarios under equal boundary conditions, an ϵ -constraint is introduced to limit the CO₂ equivalent emissions for a set of values.

(C) Performance calculation Since the results of step (B) are based on linearized equations, it is necessary to recalculate some indicators that are more realistically described by non-linear relations such as the investment cost. Other performance indicators such Carnot efficiency are derived during this step. The respective equations are presented in Section 3.2.5.

(*) Scenario definition & parameter selection Different utility scenarios are studied by activating or deactivating the respective integer variables. These scenarios are evaluated based both on cost and emissions for a continuous process operation and a daytime only scheme. The different cases are presented in Section 3.3.1.

3.2.3 Data collection & clustering (A)

This step includes utility and process data gathering, meteorological data clustering, energy and mass balances formulation, and thermodynamic model development.

3.2.3.1 Process and utility modeling

A flowsheet of the process case study and proposed utility system is presented in Figure 3.2. The units marked in black (boiler, and ammonia refrigeration cycle) are the utilities in place. Units indicated with an asterisk (*) are newly added in this study (mainly the heat pump superstructure and solar utilities).

Process The analyzed dairy plant is modeled as a retrofit problem, it transforms raw milk into concentrated milk, pasteurized milk and cream, yogurt, and dessert. Due to various outputs, specific heat requirements will always be provided with respect to the raw milk inlet of 10 kg/s. The process requires heating (up to 98 °C) and cooling (down to 4 °C), which in the original plant is provided by a boiler and an ammonia refrigeration cycle. Heating is conveyed through steam and cooling through a water glycol mixture (from the refrigeration) or cooling water. The original process energy requirements are 2.1 MW_{th} of heat and 167 kW_{el} of electricity (from the refrigeration cycle).

Figure 3.3 depicts the process composite curves. The three evaporation stages of the concentrated milk production create a clear process pinch point at 59 °C. The highest temperature heat requirement is slightly below 100 °C. The hot minimum energy requirement (MER_{hot}) is 1.6 MW_{th} and the

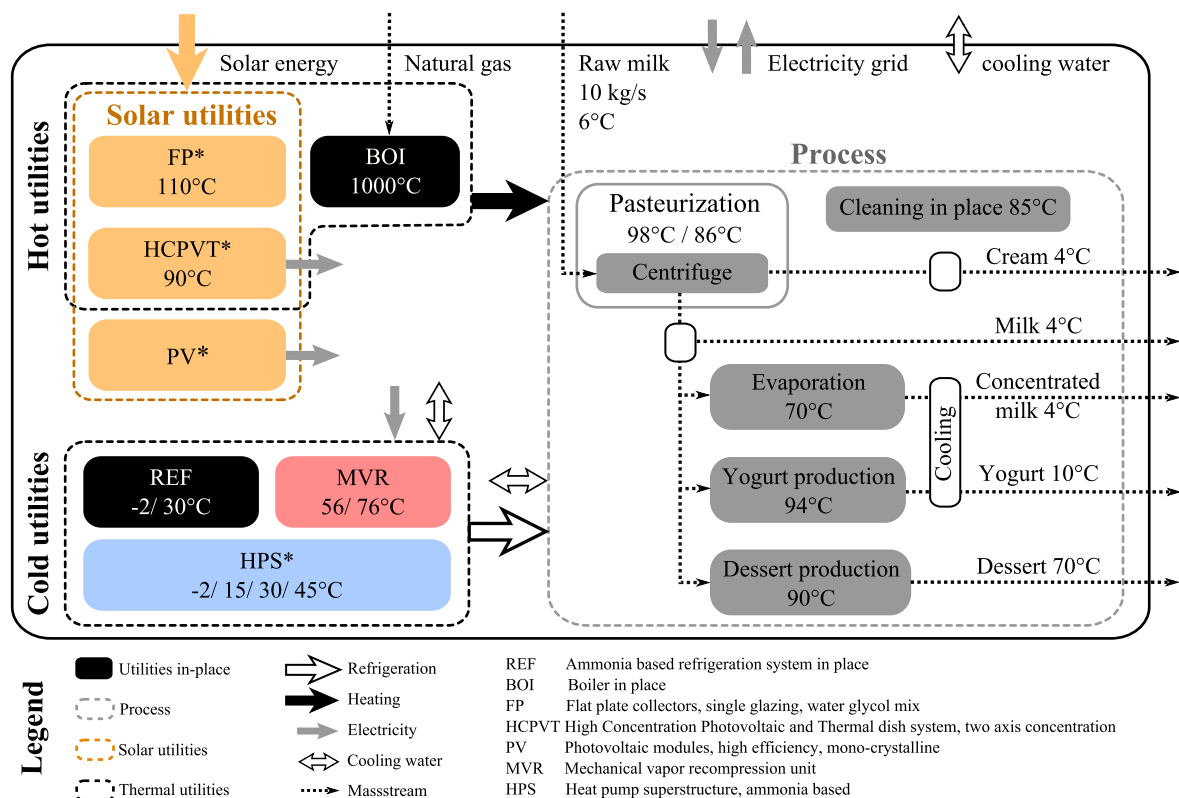


Figure 3.2 – Dairy process flowsheet including utility system. Marked in black are the utilities that are currently in place. Units marked with asterisk (*) are newly added in this thesis.

Chapter 3. Comprehensive integration method

MER_{cold} lies at 0.8 MW_{th}. Through process integration (maximum heat recovery) the hot utility requirement can be reduced by 24% (compared to 2.1 MW_{th}).

The plant is positioned in Switzerland and the process heat requirements are taken as constant during its operation. This could eventually be refined by considering shifted operation schedules of different units throughout a working day, but is currently not considered. A full list of process streams is provided in B.4. The dairy plant was originally modeled by Becker et al. [140, 161], who proposed options for reduction of CO₂-emissions with mechanical vapor re-compression and heating with a co-generation engine. In this study, the referenced work is expanded by evaluation of a flexible heat pump superstructure comprising various pressure levels which allows to optimize the refrigeration system, in addition to analysis of the potential for time-variant solar utility integration. Two process operating schedules are investigated:

- daytime only operation (7h/day, 2625h/year), Δ
- continuous (8760h/year), O

Boiler (BOI) It is assumed that the boiler is already installed in the industrial retrofit problem. Therefore, there is no capital cost associated with the use of the boiler. The boiler is activated in all scenarios as back-up hot utility. It relies on natural gas combustion and therefore generates CO₂-emissions when in operation. Part-load performance is neglected. All respective modeling equations and input data are specified in Appendix B.2.2.2.

Flat plate thermal collectors (FPs) Single glazing flat plate thermal collectors are modeled according to available performance data of independent testing facilities (such as the Institut für

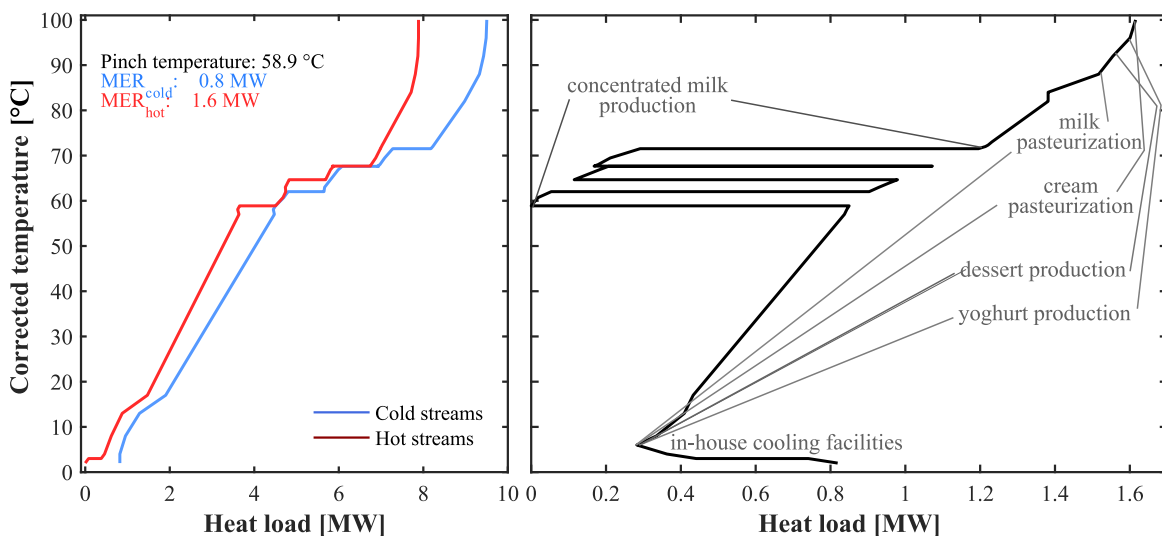


Figure 3.3 – Hot and cold composite curves (CCs) and grand composite curve (GCC) of dairy process reproduced from Becker [140] for raw milk inlet of 10 kg/s.

Solartechnik, (SPF) [164]) with solar keymark [165] status. The provided test parameters comply with the European norm for efficiency measurements of thermal collectors EN-12975. Flat plate thermal collectors produce heat up to approximately 130°C. However, efficiency decreases with higher operating temperatures due to heat losses.

Therefore, the operating temperature range is fit to the dairy process demand which is between 80 and 105°C. The collector working fluid is a water glycol mixture. The efficiency is further dependent on the intensity of the incoming radiation and its direction. All respective performance equations are presented in Section 2.3.1.2. The input data for the considered collector is shown in Table B.4 in Appendix B.2.3.2.

Photovoltaic modules (PVs) High efficiency mono-crystalline photovoltaic modules were considered during the calculation. The modeled energetic output was based on certified producer data (IEC 61215, IEC 61730, [166]) taken from the 10th year of operation. The two main parameters influencing the PV performance are the cell temperature (dependent on the ambient temperature, the incident radiation, and the wind speed) and the irradiation intensity. All relevant performance equations are presented in Section 2.3.1.3. The input data for the considered collector is shown in Table B.5 in Appendix B.2.3.3.

High concentration photovoltaic and thermal system (HCPVT) The high concentration photovoltaic and thermal system is a concentrating dish (with concentrations of up to 2000 at the focal point) with two axis tracking of the sun which is mounted on a tower. Electricity is generated with photovoltaic cells in the receiver positioned in the focal point. Highly efficient cooling prevents receiver and photovoltaic cell overheating and provides useful heat around 100°C. Thereby the exergetic losses of the photovoltaic conversion are recovered. High concentration devices can only convert direct beam radiation. Performance indicators are retrieved from producer data [32, 86, 112, 132]. All modeling equations are depicted in Section 2.3.1.4. All respective performance equations are presented in Section 2.3.1.4. The input data for the considered collector is shown in Table B.6 in Appendix B.2.3.4.

Thermal storage tank (S) The thermal storage mass and energy balances are formulated based on the assumption of sensible heat storage at different temperature levels modeled as one tank operating between two temperatures. An intra-cyclic constraint is introduced, which ensures that the storage is always at initial conditions at the end of each day. Furthermore, it is defined (in agreement with a storage tank with two outlets) that the fluid leaving the storage tank is always at the lowest temperature (bottom) during charge periods or highest temperature (top) during discharge periods. More information on the considered storage tank can be found in Section 2.4.2 and in Appendix B.2.3.5.

Limitations The performance of the three respective solar systems is modeled for one piece of equipment. Industrial applications require large collector fields and, therefore, a constant loss factor

Chapter 3. Comprehensive integration method

is introduced in this work to account for thermal and transmission losses in the field. This factor, in reality, scales with the field size and follows certain power laws. Additionally, the impact of shading on the overall output is non-negligible especially for the tracking systems considering the space is usually limited which is not accounted for either. It is planned to explore the validity of these simplifications by further in-depth analysis in future work.

Heat pump superstructure (REF, MVR, HPS) A superstructure is employed which permits investigation of possible combinations between different heat pump components: compressors, evaporators, condensers, and presaturators [167].

For selecting the optimal heat pump structure, a set of pressure levels must be defined. The active levels are selected during the system resolution with help of integer variables. The choices are only constrained by the fact that the highest pressure level must be a condenser and the lowest level needs to be an evaporator. Since the pressures and respective temperature levels are chosen in advance, the sizing of the components can be formulated by linear constraints as part of the MILP. Figure 3.4(a) presents a temperature entropy diagram to illustrate the problem definition, formulating all generic heat pump cycles once the pressure levels are selected. Figure 3.4(b) shows a flow chart of the superstructure. Connections between all pressure levels are defined as well as potential presaturation, evaporation, and condensation units on every level.

This permits the generation of all possible single and multi-stage cycles between a predefined set of pressure levels. The one-stage refrigeration cycle in place, the vapor re-compression system as well as the improved multi-stage heat pump cycle are modeled with this superstructure. The performance equations as well as all investigated specifications are presented in Appendix B.2.2.3.

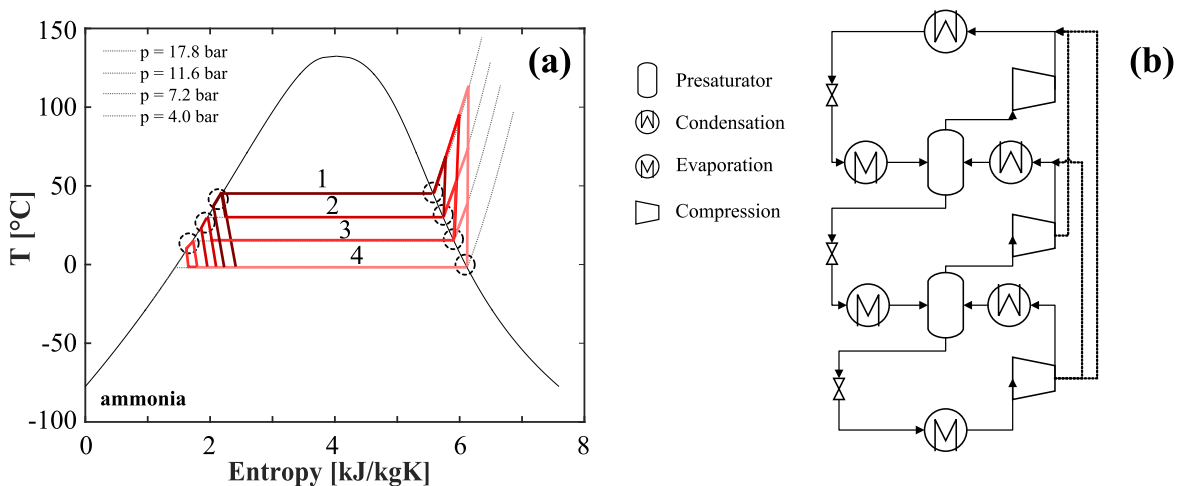


Figure 3.4 – Heat pump superstructure model. (a) Ammonia liquid-vapor saturation curve with isobars (marked in gray in descending order) and potential heat pump cycles (isentropic compressor efficiency $\eta_{\text{isentropic}} = 1$), (b) flowchart of heat pump superstructure.

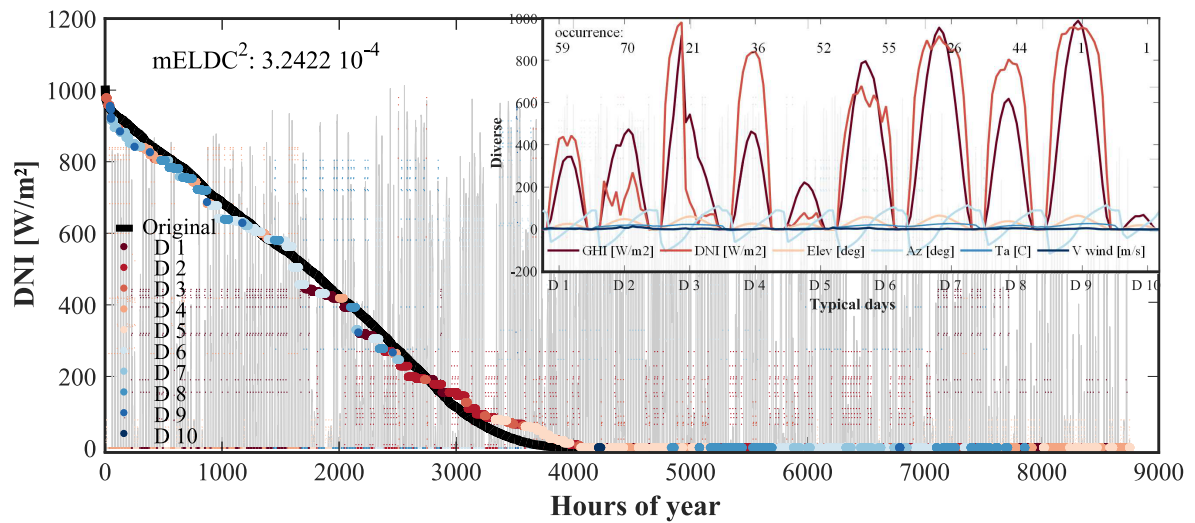


Figure 3.5 – Load duration curve of DNI in Sion, Switzerland (CH), of original data and 8 typical plus 2 extreme days. In background yearly distribution of DNI of original and typical days.

3.2.3.2 Meteorological data clustering

Meteorological data Weather data including the solar angles (azimuth and elevation), wind speed, ambient temperature, and global horizontal (GHI) and direct normal (DNI) irradiance of hourly time resolution is retrieved from a commercial software (Meteonorm 7.0 [134]). The analysis is carried out for the Swiss city of Sion, having comparably high yearly solar irradiance (global horizontal irradiation (GHI) 1430, direct normal irradiation (DNI) 1690 kWh/m²) relative to the rest of the country (1200 kWh/m²) due to a favorable micro-climate.

Data clustering Figure 3.5 presents the results from the clustering algorithm presented in Chapter 2.3.2.2. The load duration curve of the DNI is displayed for the original data and the typical days. In the background, the hourly data is displayed showing that high values can also be reached during winter. This is particular for the DNI as it is not reduced by cosine losses in contrast to the GHI. The $mELDC^2$ is below the limit of 3.5×10^{-4} (as derived in Section 2.3.2.2) and is also visibly acceptable. In the upper right corner the resulting typical days and their occurrence are illustrated. The two extreme days are represented only once. It can be seen that there are few days with very low DNI.

3.2.4 System resolution (B)

This section presents the optimization problem formulation and the respective constraints. The sets presented in the following Section 3.2.4.1 are specified in this case study in the following manner. The set of utility technologies \mathbf{W} refers to Section 3.2.3.1. $\mathbf{W} = \{\text{boiler (BOI), refrigeration (REF), mechanical vapor re-compression (MVR), heat pump superstructure (HPS), flat plate thermal collectors (FPs), photovoltaic modules (PVs), high concentration photovoltaic and thermal system (HCPVT), thermal storage (STO), cooling water (CW), electricity grid (GRID)}\}$. The set of periods \mathbf{P}

Chapter 3. Comprehensive integration method

stems from Section 3.2.3.2.

3.2.4.1 MILP utility targeting formulation

The problem is formulated as a multi-period MILP that solves the heat cascade and finds optimal utility integration [75, 138, 139, 155].

Objective function The problem objective is the minimization of the total annualized costs (TAC) is depicted in Equation 3.1. It is composed of the yearly operating expenses (opex) of each utility technology w during period p and the annualized capital expenses (capex) that is found with aid of the maximum size of each technology w .

$$\min_{y_p^w, f_p^w, y^w, f^w} \underbrace{\sum_{p \in \mathbf{P}} \left(\sum_{w \in \mathbf{W}} \text{OP}_{1,p}^w \cdot y_p^w + \text{OP}_{2,p}^w \cdot f_p^w \right) \cdot \Delta t_p \cdot \text{occ}_p}_{\text{Operating cost}} + \underbrace{\sum_{w \in \mathbf{W}} (\text{IV}_1^w \cdot y^w + \text{IV}_2^w \cdot f^w)}_{\text{Investment cost}} \quad (3.1)$$

Where

\mathbf{P}	set of periods {1,2,3, ...,n _p }
\mathbf{W}	set of utility technologies w
$f_p^w \in \mathbf{R}^+$	continuous variable for sizing technology w during period p
$y_p^w \in \{0, 1\}$	binary variable related to existence of technology w during p
f^w	maximum size of technology w
y^w	overall existence of technology w
$\text{OP}_{1,p}^w$	[€/h] fixed operating cost for using the technology w during period p
$\text{OP}_{2,p}^w$	[€/h] proportional operating cost for using technology w during period p and is scaled with the multiplication factor
IV_1^w	[€/y] annualized, actualized fixed cost related to the investment of technology w
IV_2^w	[€/y] annualized, actualized proportional cost related to the investment of technology w
Δt_p	[h] operating time of period p
occ_p	[1/y] the occurrence of period p

All respective general constraints related to the solar and conventional utilities are derived in Section 2.4.

3.2.4.2 ε -constraint

As mentioned, an ε -constraint was added to the MILP which constrains the CO₂-equivalent emissions of the system. The total CO₂-equivalent emissions depicted in Equation 3.2 are found by taking into account emissions from natural gas consumption and the electricity grid. Life cycle assessment of the associated technologies is not considered. The positive impact on the grid created by selling solar electricity was as well disregarded.

$$\text{CO}_{2,\text{tot}} = \sum_{p \in \mathbf{P}} \left(\text{CO}_{2,\text{el}} \cdot \dot{E}^{\text{GRID}} \cdot f_p^{\text{GRID},\text{in}} + \text{CO}_{2,\text{ng}} \cdot \dot{Q}_{\text{ng}}^{\text{BOI}} \cdot f_p^{\text{BOI}} \right) \cdot \Delta t_p \cdot \text{occ}_p \quad (3.2)$$

Where CO_{2,el} [kgCO₂eq/kWh_{el}] are the life cycle emissions related to buying electricity from the

Swiss grid and $CO_{2,ng}$ [kgCO₂eq/kWh_{ng}] are the life cycle emissions from natural gas burning, \dot{E}^{GRID} [kW] is the reference electricity supply of the grid utility, $f_p^{GRID,in}$ [-] is the multiplication factor of the incoming grid utility in period p , f_p^{BOI} [-] is the multiplication factor of the boiler in period p , and \dot{Q}_{ng}^{BOI} [kW] is the reference natural gas consumption in the boiler.

The ε -constraint ensures that the total emissions do not exceed ε , which is specified as a fraction of the reference emissions and which is incrementally changed in this work (between 95 and 60% of the reference emissions).

$$\frac{CO_{2,tot}}{CO_{2,tot}^{ref}} \leq \varepsilon \quad (3.3)$$

3.2.5 Performance calculation (C)

After the optimization step the non-linear functions, such as the investment cost are recalculated as well as other performance indicators depicted below. The necessary parameters are presented in Table 3.2.

Operating cost During the MILP optimization step, the buying price of electricity is set to the market price displayed in Table 3.2, while the selling price is set to a very small negative number. This serves as a protection against oversizing the photovoltaic systems not to become pure electricity exporters due to potentially high profits from selling electricity. The solar utilities should be sized with the ε -constraint on the emissions.

In the performance calculation step, the operating cost are recalculated with adequate numbers. It is assumed that the solar utilities do not have operating costs. Therefore, the total operating costs are composed of the electricity bought from or sold to the grid and the natural gas consumption in the boiler. The selling price of electricity is set to 80% of the buying price to represent the current market situation more realistically. The yearly operating expenses (opex), C^{opex} [€/y], are a function

Table 3.2 – Data related to emissions, primary energy consumption and operating cost in Switzerland (CH).

Parameter	Symbol	Unit	Value	Source
Ambient temperature	T_a	[K]	298	[-]
Interest rate	i	[-]	0.05	[-]
Equipment lifetime	n	[y]	20	[-]
Maintenance cost fraction of total investment	m	[1/y]	0.05	[-]
Cost of buying electricity	$OP_{2,p}^{el}$	[/€/kWh]	0.142	[168]
Cost of buying natural gas	$OP_{2,p}^{ng}$	[/€/kWh]	0.081	[168]
Emissions electricity	$CO_{2,el}$	[kgCO ₂ eq/kWh]	0.11257	[169]
Emissions natural gas	$CO_{2,ng}$	[kgCO ₂ eq/kWh]	0.20196	[169]

Chapter 3. Comprehensive integration method

of the resource prices and their annual net requirements (natural gas and electricity).

$$C^{opex} = \sum_{p=1}^P \left(OP_{2,p}^{el} \cdot \dot{E}^{GRID} \cdot \left(f_p^{GRID,in} - 0.8 \cdot f_p^{GRID,out} \right) + OP_{2,p}^{ng} \cdot \dot{Q}_{ng}^{BOI} \cdot f_p^{BOI} \right) \cdot \Delta t_p \cdot occ_p \quad (3.4)$$

Where $OP_{2,p}^{el}$ [€/kWh_{el}] is the electricity cost, $OP_{2,p}^{ng}$ [€/kWh_{ng}] is the natural gas price during period p , \dot{E}^{GRID} [kW] is the reference grid electricity inlet/outlet, \dot{Q}_{ng}^{BOI} [kW] is the reference natural gas consumption of the boiler, $f_p^{GRID,in}$ [-] is the multiplication factor of the incoming grid utility in period p , $f_p^{GRID,out}$ [-] is the multiplication factor of the outgoing grid utility in period p , The natural gas and electricity prices are depicted in Table 3.2.

Investment cost The investment cost of the units in-place (the boiler and standard refrigeration cycle) are not considered. Other investment cost functions can be found in B.2.2. All cost data are actualized with the Marshall and Swift index [6]. The total investment cost, C^{INV} [€], is calculated as a function of the maximum sizes of each utility technology w over all periods p .

Total annual cost The total annualized costs (TAC), C^{TAC} [€/y], is derived from yearly operating expenses (opex), C^{opex} [€/y], the annualized capital expenses (capex), where $\tau = \frac{i \cdot (1+i)^n}{(1+i)^n - 1}$ [1/y] is the investment cost annualization factor, and the maintenance cost, which is a fraction m [1/y] of the total investment, see Table 3.2.

$$C^{TAC} = C^{opex} + C^{INV} \cdot (\tau + m) \quad (3.5)$$

Note Calculating the maintenance cost as a fraction of the investment cost constitutes a neglect of the running costs of the utilities in place. Their investment cost and with that their maintenance cost is in this way assumed to be zero. This displays a simplification which, however, generates conservative utility integration results in underestimating the total cost of the current status quo of the plant.

Carnot factor The Carnot factor permits re-scaling the temperature levels on the standard composite curve. This has two advantages: firstly, the representation is more compact since the y-axis will always be between -1 and 1 (equivalent to a temperature range of [-124,∞] °C) which makes visualization of the process easier; and secondly, the factor is proportional to the exergetic potential of a temperature level and therefore exergetic losses between sources and sinks can be visualized.

$$\eta_{Carnot} = 1 - \frac{T_a}{T} \quad (3.6)$$

Where T_a [K] is the ambient temperature and T [K] is the temperature of the stream.

3.3 Results and discussion

3.3.1 Scenario definition

A set of cases is analyzed in order to gain a proper understanding of the different options for energy efficiency improvement and emissions reduction of the studied dairy plant. In Table 3.3, all utility technologies and investigated cases are presented. The Original case refers to the current energy consumption of the plant without process integration (no maximum heat recovery) based on the utilities in place (boiler, one-stage ammonia based refrigeration cycle, and cooling water); the Reference case is based on the Original case, however, considering process integration with maximum heat recuperation. Subsequently, mechanical vapor re-compression around the process pinch (1. MVR) and a heat pump superstructure (2. heat pump superstructure (HPS)) improving the refrigeration cycle are proposed. The MVR was similarly proposed by Becker [140]. The subsequent cases including different solar scenarios and the heat pump superstructure display an extension to the previous analysis.

3.3.2 Daytime operation of the process (Δ)

Throughout this section, daytime only operation is investigated. Due to fewer operating hours and with that lower operating costs less space for investment decisions is left.

3.3.2.1 Reference scenario and heat pump integration

In this Subsection, the Reference case and efficiency improvements related to heat pump integration are investigated. Therefore, a mechanical vapor re-compression (1. MVR), and a multi-stage heat pump superstructure (2. HPS) are subsequently added to the Reference case which consists of the process demands considering heat recovery and the utilities in place (as described in Section 3.3.1). Figure 3.6 depicts the integrated Carnot factor enthalpy profiles of the dairy process and respective

Table 3.3 – Investigated utility integration scenarios, first four cases: non-renewable utilities, next four: solar utilities. The grid (GRID) and cooling water (CW, Appendix B.2.2.1) utility technologies are present in all cases. Detailed models can be found in: App. B.2.2.2 - boiler (BOI), App. B.2.2.3 - heat pumping (REF, MVR& HPS), Section 2.3.1.2 - FP, Section 2.3.1.4 - HCPVT, Section 2.3.1.3 - PV.

Case	Heat recovery (PA)	Boiler (BOI)	Ref-rigeration (REF)	Vapor re-comp. (MVR)	Heat pump superstructure (HPS)	Solar flat plate (FP)	Solar concentrated (HCPVT)	Solar PV (PV)
Original		✓	✓					
Reference	✓	✓	✓					
1. MVR	✓	✓	✓	✓				
2. HPS	✓	✓	✓	✓	✓			
2.1. FP	✓	✓	✓	✓	✓	✓		
2.2. PV	✓	✓	✓	✓	✓			✓
2.3. PV&FP	✓	✓	✓	✓	✓	✓		✓
2.4. HCPVT	✓	✓	✓	✓	✓		✓	

three utility systems. The process curve is a rescaled version of the GCC presented in Figure 3.3 and represents the net heating and cooling demands of the dairy process considering maximum heat recovery. The active utilities for each case, which are responsible for closing the energy balance, were selected and sized during the utility targeting step (in Section 3.2.4.1) by minimizing the total annual costs. The three investigated utility systems are depicted in this *integrated* Carnot factor enthalpy diagram as an envelope to the process GCC (thus ensuring energy conservation). Figure 3.7 and Table 3.4 provide an illustration and the resulting data of the discussed scenarios, respectively.

Reference case The utility envelope (black, Figure 3.6) of the Reference case shows at a high temperature plateau ($T \approx 1000^\circ\text{C}$, $\eta_{\text{Carnot}} = 0.77$) the radiative heat release of the boiler (BOI) and down to 50°C the convective heat release of its combustion gases. At 30°C ($\eta_{\text{Carnot}} = 0.02$) the condensation level of the refrigeration system (REF) in place is visible. Cooling water (CW) is consumed at 15°C ($\eta_{\text{Carnot}} = -0.03$) to remove the waste heat from the condensation of the refrigeration systems as well as part of the medium temperature waste heat from the process. The energy balance is closed with the evaporation level of the refrigeration cycle which provides refrigeration at -2°C ($\eta_{\text{Carnot}} = -0.1$).

The exergy losses between the utility system and the process GCC are represented by the area between the two curves. Especially between the boiler producing heat at very high temperatures, but also in the lower temperature range between the process self-sufficient pocket and the utility system drastic exergy losses are visible. This becomes increasingly clear when looking at the cooling water which is used for final cooling of the evaporation stage of the refrigeration cycle and partial cooling of the steam from the concentrated milk production which summed up to a cooling water consumption of 23.6 kWh/t of raw material (see Table 3.4).

The total annual costs, TAC, between the Original case and the Reference case were reduced from 5.9 to 4.3 €/t of raw material if only the reduction in heating and cooling needs are considered and it reduced to 5.1 €/t of raw material, if the estimated capital investment of the retrofit heat exchanger network (HEN) analysis are considered.

1. MVR Introducing a mechanical vapor re-compression unit (1. MVR) elevates the pressure of the steam exiting the milk evaporation unit to produce useful heat above the process pinch. In Figure 3.6, this can be seen by two horizontal lines surrounding the process pinch ($T = \{56, 76\}^\circ\text{C}$, $\eta_{\text{Carnot}} = \{0.1, 0.15\}$). What has to be noted is that by reusing the steam released in the milk production, the self-sufficient pocket is provided with less heat, meaning that the process can no longer be self-sufficient in the lower temperature range. This is, however, compensated by the evaporation stage of the refrigeration cycle which provides useful heat (at elevated condensation levels of 35°C) to the process in this scenario. Exergetic losses were thus drastically diminished, as well as the cooling water (from 23.6 to 7.8 kWh/t of raw material, Table 3.4) and the natural gas consumption (from 47.9 to 28.1 kWh/t of raw material). The electricity usage was slightly increased (from 2.6 to 4.6 kWh/t of raw material) which permits the calculation of the incremental coefficient of performance

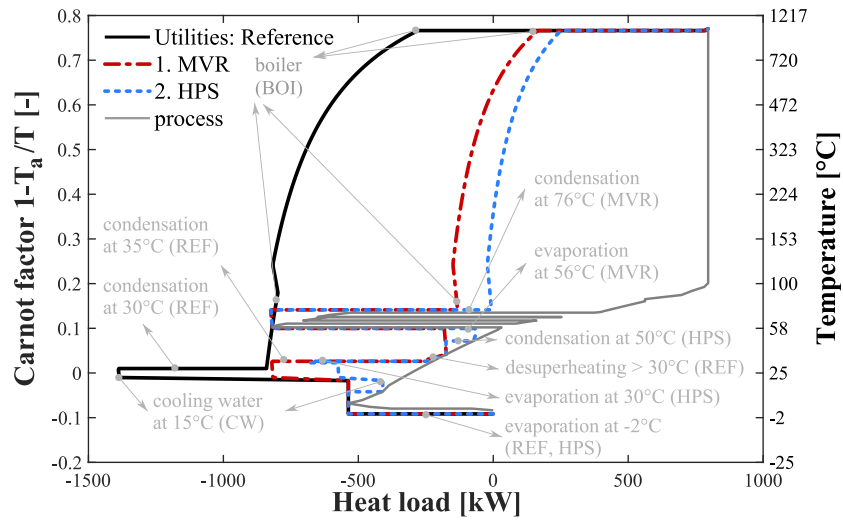


Figure 3.6 – Integrated composite curves (ICCs) of the dairy process and respective utility system. [Reference] case with utilities in place, compared to case [1. MVR] with additional mechanical vapor re-compression around 67°C, and [2. HPS] with additional heat pump superstructure between -2, 15, 30, and 50°C.

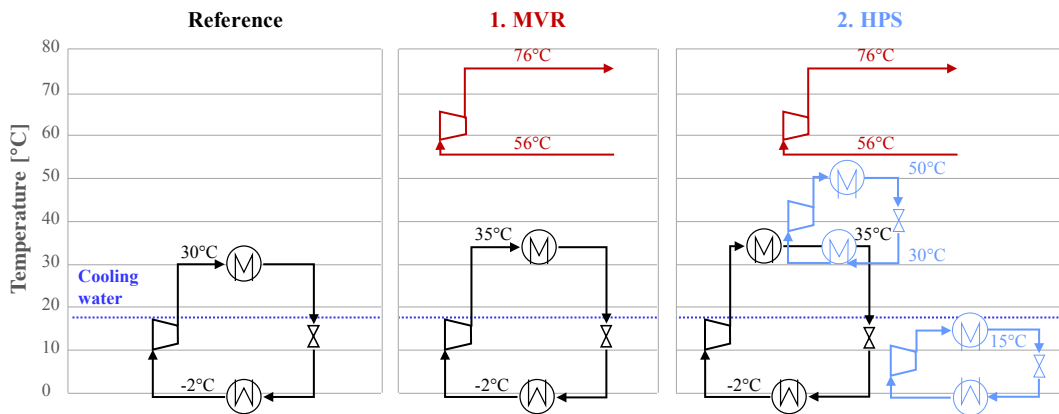


Figure 3.7 – Illustration of the conversion cycles involved in the respective scenarios.

Table 3.4 – Utility integration scenarios as described in Section 3.3.1. Costs and energy specific consumption data (referred to ton of raw material. (*) total annualized costs (TAC) neglecting HEN retrofit cost estimation

			Original	Reference	1. MVR		2. HPS			
Operating costs	C^{opex}	[€/t]	5.9	4.3	2.9		2.6			
Natural gas cons.	\dot{Q}_{ng}	[kWh/t]	64.6	47.9	28.1		24.3			
Electricity cons.	\dot{E}^{GRID}	[kWh/t]	4.6	2.6	4.6		4.8			
Compressor size	\dot{E}^{COMP}	[kW]	167.0	94.7	111.8	55.2	87.5	65.1	10.4	9.7
Cold coeff. of performance	COP_c	[-]		5.7	4.8	11.6	4.8	11.6	11.0	11.0
Cooling water cons.	\dot{Q}^{CW}	[kWh/t]	n.a.	23.6	7.8		4.5			
Compressor cap. exp.	C^{COMP}	[€/t]		0	0	0.190	0	0.221	0.042	0.040
Heat exchang. area	A^{HEN}	[m ²]		826	1032		1161			
Number of HEX	N^{HEN}	[-]		48	64		85			
HEN capital cost est.	C^{HEN}	[€/t]		0.9	1.2		1.5			
TAC w/o HEN	C^{TAC*}	[€/t]	5.9	4.3	3.1		3.0			
Total annual costs	C^{TAC}	[€/t]	5.9	5.1	4.3		4.4			

Chapter 3. Comprehensive integration method

$COP = \Delta \dot{Q}_{ng} / \Delta \dot{E}^{GRID} = 9.9 [-]$. Where \dot{Q}_{ng} and \dot{E}^{GRID} are the natural gas and electricity consumption respectively (as reported in Table 3.4). On top of this improvement in efficiency, the total annual cost dropped from 5.1 in the Reference case to 4.3 €/t of raw material due to drastic reductions in the operating costs.

The elevation of the condensation level (from 30 to 35 °C) is an engineering choice which was motivated by the fact that the size of the mechanical vapor re-compression unit is constrained by how much heat could be delivered to the process from the evaporation stage of the refrigeration cycle. By elevating this temperature and considering de-superheating of the superheated vapor exiting the compressor (at slightly elevated temperature) more use of vapor re-compression could be made and a higher incremental COP was achieved. However, there is a limit to increasing the upper pressure of an existing compressor.

2. HPS Therefore, a heat pump superstructure (2. HPS) is introduced to explore further installation of heat pumps with respect to the total annual costs. Adding the heat pump superstructure provides various options for single- and multi stage cycles between -2 and 50 °C (in 2 °C intervals) to the system resolution. With this, a new utility system configuration was found consisting of the refrigeration cycle in place, the mechanical vapor re-compression unit, and two new heat pump cycles between -2 and 15 °C and between 30 and 50 °C. In Figure 3.6 it can be seen that this led to a higher use of the mechanical vapor re-compression unit, because more heat could be provided to the process by the heat pumps. And this imposed a further decrease in the boiler consumption and, consequentially, a reduction of the exergy losses in the system. The total annual costs not considering the HEN costs (disregarded in the MILP) were reduced as well. However, considering the estimated capital expenses for the HEN, the TAC slightly increased from 4.3 to 4.4 €/t of raw material. The cooling water consumption was further decreased from 7.8 to 4.5 kWh/t of raw material; and the electricity consumption was only slightly increased from 4.6 to 4.8 kWh/t. This originated from the use of a lower temperature refrigeration cycle (-2 to 15 °C) with a higher COP_c of 11, which resulted in a reduction of the consumption of the refrigeration in place (COP_c 4.8). Thereby the incremental COP was further improved to 24.2 [-] with respect to the previous scenario (1. MVR).

Summary What can be concluded from here is that more complex systems (in terms of heat pumping) offer higher potential from the energetic point of view. And more complex systems require more complex tools (as illustrated with integration of the heat pump superstructure). However, there is always a trade-off between efficiency improvements accompanied by potential operating cost reduction and increase of the complexity of the system and therewith the heat exchanger network. The presented results indicate the strong potential of such installations and enunciates the importance of investigating selected case studies in further detail.

In the next section, the relation between efficiency improvements (through heat pumping) on solar sizing is presented and general guidelines are provided.

3.3.2.2 Heat pump & solar integration

Process schedule Figure 3.8 depicts the process operating scheme and solar GHI and DNI radiation during the typical periods. The winter days are marked by DNI levels exceeding the GHI, meaning that the sun elevation is not very high. The starting hours of the process operation was set to 8:00 o'clock in the morning lasting between 7 and 8 hours per day in order to form 2625 operating hours per year. This is a design choice attempting to overlap process operation with the sunshine hours. Observing the overlap between solar radiation and process operation, it becomes clear that there are several instances in which the overlap would be more aligned with the solar insolation if the process starting time was shifted to later in the morning. However, knowing that many manufacturing schedules traditionally start at earlier hours, 8:00 o'clock was the accepted trade-off.

In the daytime operation, the option of storage is not considered. As seen in Figure 3.8, the main lack of solar energy occurs in the early morning hours. It is difficult to store thermal energy over night and thus it was unreasonable to consider storage of solar energy for these periods of low solar productivity.

ϵ -constraint optimization The results from the ϵ -constraint optimization can be seen in Figure 3.9. The two heat pump cases (1. MVR 6.2 & 2. HPS 5.5 kg CO₂-eq/t) were determined without ϵ -constraint as described in Section 3.3.2.1. Among these, the best scenario in terms of emissions was chosen as reference for the solar integration (2. HPS). For integration of the solar components the ϵ -constraint was gradually set to a fraction of these reference emissions (between 95 and 60%) while minimizing the total system cost. In this way a Pareto type curve was produced (Figure 3.9 (a)) between the annualized investment cost and the specific emissions. As expected, with decreasing emissions the annualized investment costs increased. The solar cases are presented with error bars

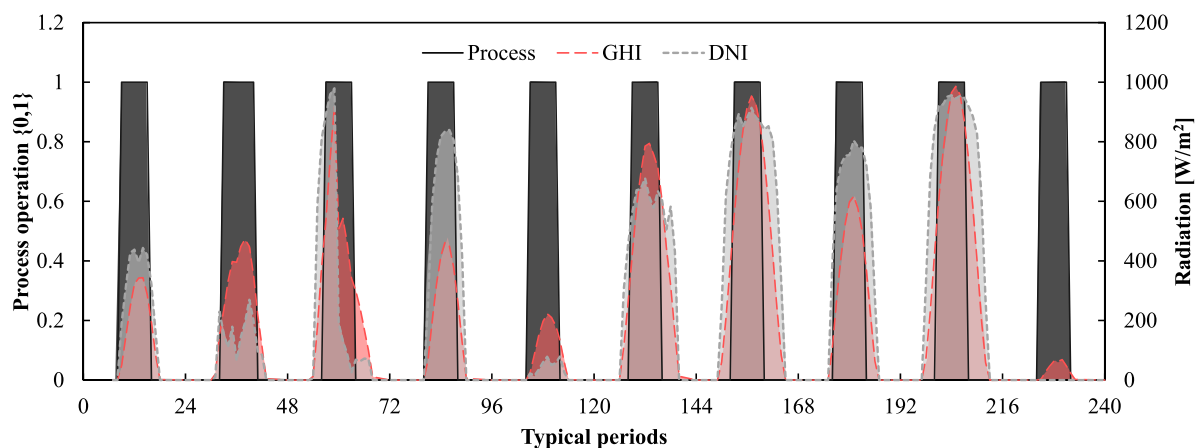


Figure 3.8 – Process operation scheme and solar radiation during typical periods. (GHI: global horizontal irradiation, DNI: direct normal irradiation.)

Chapter 3. Comprehensive integration method

(the data of which can be found in Sections 2.3.1.3, 2.3.1.2, 2.3.1.4). Especially for the HCPVT system which is the most novel technology with the most volatile prices, this is a reasonable assumption. Under the current input data, the solar cases performed very similarly in terms of investment cost. The total annual cost in Figure 3.9 (b) include besides the investment cost also the operating expenses. This leads to a different distribution of the data points. In terms of total annual cost, both heat pumping scenarios and most solar options were profitable with respect to the Reference case (of the utilities in place). The relative emission reductions amounted to 27% (between Original and Reference scenario) due to heat recuperation, 38% due to mechanical vapor re-compression (from Reference to 1. MVR), and 12% due to improved refrigeration (from 1. MVR to 2. HPS). The solar scenarios further decreased the emissions by 5-40% ($\epsilon = 95\text{-}60\%$) with respect to the 2. HPS scenario.

It can be observed that some solar technologies potentially resulted in higher emission reductions than others. With PV modules the least reductions were achieved since they could not replace the boiler natural gas consumption; however, their advantage is the ability to sell overproduction to the grid. Still, up to 20% emission reduction was achieved integrating solar PV. The reduction is achieved by replacing the incoming electricity from the grid with green electricity. The HCPVT

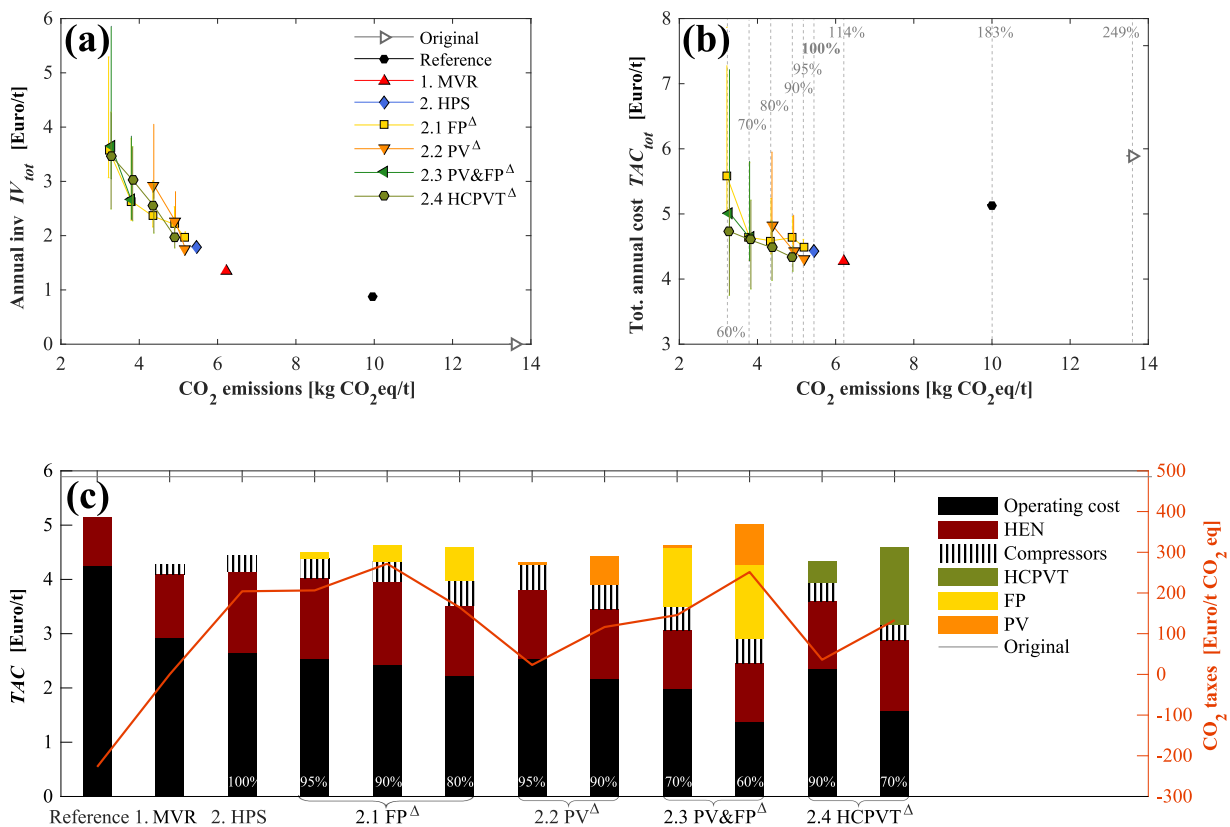


Figure 3.9 – Results from ϵ -constraint optimization of different solar options for daytime only process operation. (a) Annualized capital expenses (capex) versus carbon dioxide (CO₂)-equivalent emissions, (b) TAC versus CO₂ emissions, (c) detailed cost analysis of various cases.

system and combined FP and PV can reach the highest emission reductions at reasonable cost. At specific CO₂ reductions of 3.8 kg CO₂-equivalent/ton of raw material, which is equivalent to 70% of the best heat pump only (reference) case, the TAC of all solar systems overlap, which indicates that this establishes an appropriate balance between operating, investment cost and energy waste.

The uncertainty related to the solar investment cost is indicated on Figure 3.9, but not the uncertainty related to the heat exchanger area cost estimation. This is a rough estimation with errors varying between 20 and 40%; therefore, grand conclusions should not be drawn when considering a difference in TAC between 10 and 20%.

Figure 3.9 (c) illustrates the associated total costs of the different scenarios. The operating cost are predominant in the Reference case, which explains the fact that the total cost of the solar scenarios did not drastically increase. This is attributed to a shift from operating expenses to specific investment cost.

A break even CO₂ tax was calculated with respect to the case with lowest TAC (1. MVR). If the respective tax was applied all cases would exhibit the same costs as scenario 1. MVR. The tax lied between 100 and 300 €/ton CO₂-equivalent which is slightly higher than the current prices, but in the same order of magnitude.

Figure 3.10 (a) depicts the optimal active solar area for different CO₂-equivalent emissions ($\epsilon \in [60\%, 95\%]$) of all studied solar collector types. It can be observed that the required solar area increased with decreasing CO₂-equivalent emissions. The relationship between emission reduction and active solar area does not follow a linear regression, but rather flattens out, especially for HCPVT and PV (and the lowest three FP data points) systems. This is attributed to the interconnectivity of the system, where higher solar thermal production has an influence also the utilization of the heat pumps and mechanical vapor re-compression and therewith on the electricity inflicted CO₂-equivalent emissions. And vice versa, the solar electricity production directly affects the utilization of the heat pumps which influences the boiler consumption.

The HCPVT system required the smallest active area in comparison to the other solar technologies. This stems from the high total conversion efficiency. It has to be noted though that due to two axis tracking and the danger of shading, the actual required land area may be increased by a factor of 2.

Figure 3.10 (b) shows the integrated Carnot factor enthalpy profiles of the dairy process and respective utility systems. Flat plate collectors (scenario 2.1 FP) at 80% emissions with respect to the 2. HPS case (at 4.3 kg CO₂-equivalent/ton of raw material) are shown at solar noon during different typical days. The optimization results show that in comparison to the 2. HPS scenario, a different heat pump configuration was chosen: instead of two heat pumps (30 to 50 °C and -2 to 15 °C) a two stage heat pump between -2, 15, and 50 with flash gas removal and inter-cooling at 30 °C was selected during the MILP. In the curve, this can be traced with help of the missing evaporation plateau at 30°C

Chapter 3. Comprehensive integration method

which is present in case 2 .HPS. The higher operational cost due the higher electricity consumption were compensated by reduced natural gas consumption and apparently higher flexibility towards solar variations. This supports again the advantage of the holistic approach that takes into account the complete system for the complete operating range. It is further visible that the solar thermal production drastically contributed to reducing the exergetic losses between process and utility system, as it produces heat at temperatures much closer to the actual requirements.

Figure 3.11 shows a graphical representation of the multi-period results of case 2.1 FP at 80% emissions with respect to case 2. HPS. In (a) the hot utility streams heat load and meteorological input data are shown, illustrating that the solar flat plate collector output (filled area) reduces the boiler consumption. The solar output follows the available global radiation drawn in gray. In Figure 3.11 (b) the respective ICCs are shown for multiple periods. Close investigation shows the pattern

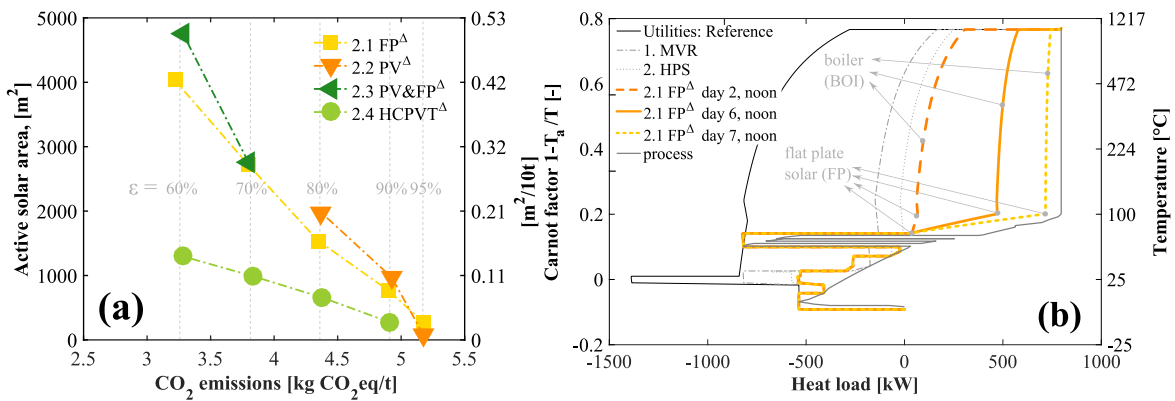


Figure 3.10 – (a) Optimal active solar area, from ϵ -constraint optimization (ϵ between 95 and 60%), (b) ICCs of the dairy process and respective utility system. Conventional utility [reference, 1. MVR, 2. HPS] and solar integration of Case 2.1 FP at 80% emissions with respect to the reference and 4.3 kg CO₂-equivalent/ton of raw material during different typical days.

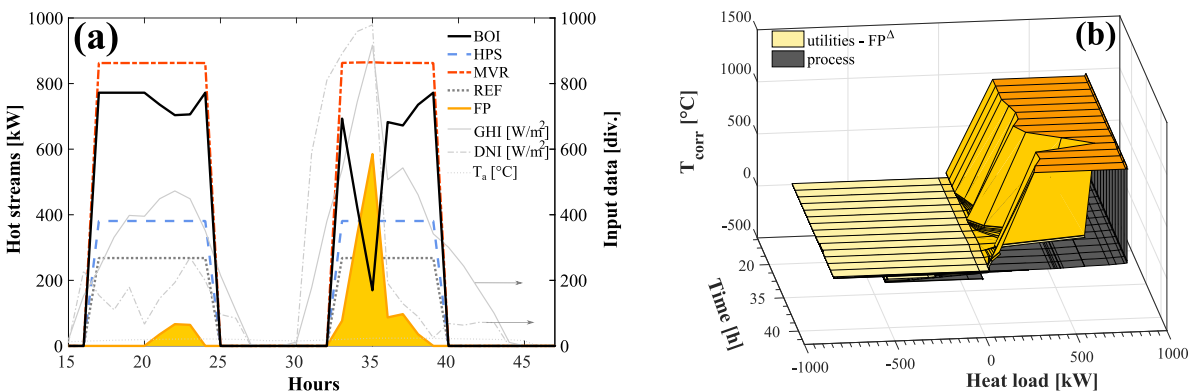


Figure 3.11 – Solar integration, Case 2.1 FP^Δ at 80% emissions with respect to 2. HPS case i.e. 4.3 kg CO₂-equivalent/ton of raw material, multi-period MILP results: (a) hot utility streams heat load vs time, (b) multi-period ICCs of the dairy process and respective utility system.

of the solar output from Figure 3.11 (a) in the high temperature plane of the boiler in the curves in Figure 3.11 (b). This is related to the much lower operating temperatures of the solar system compared to the boiler and the related drop on the temperature axis.

It should be noted that the required boiler output changes drastically over time when solar heat is present. This might have an influence on the overall efficiency of the energy conversion if part load performance of the boiler is modeled in more detail, which was not considered here.

In conclusion, it can be stated that there is high economic and environmental potential for this type of industrial dairy plants for heat pump and solar integration. Results may be extrapolated to other low temperature food processing plants especially when operated in the underlying temperature range. Integration of both types of systems, solar and heat pumping should always be investigated with a holistic approach. For further steps, it is crucial to investigate the heat exchanger network design to explore technical feasibility of integrated systems.

3.3.3 Continuous process operation (O)

Throughout this section, continuous process operation is investigated. Due to a higher number of operating hours (8760 vs 2625h) and with that increased operating costs more space for investment decisions is potentially available.

Figure 3.12 shows the results from the ϵ -constraint optimization. It can be observed that the raw material specific annualized investment cost were lower than the cost for the daytime only operation. This is explained by the higher operating hours and thus increased yearly raw material consumption. This increase had no influence on the specific operating cost which scale linearly with the raw material consumption. But the estimated HEN area and compressor sizes remains unchanged compared to daytime only operation and, therefore, the specific capital cost estimations decrease for a higher yearly raw material consumption. This leads to lower TAC of the 2. HPS scenario in comparison to 1. MVR and daytime operation.

This decrease in relative specific investment costs also showed improvements for the flat plate thermal collectors (FPs) and photovoltaic modules (PVs) at low emission reductions ($\epsilon=95\%$), which in this case are both profitable with respect to the best non-solar case (2. HPS). The PV system could not reach higher emission reductions than 95%, because batteries are not considered and the positive impact from a renewable source to the grid is not counted. With increasing emission reductions the solar size and cost increased and the flat plate scenarios' TAC reached slightly above best non-solar case. The HCPVT exhibited the smallest specific TAC of all solar options as the overproduced electricity could be sold and therefore the operating costs decrease.

The option of storage was only chosen by the optimizer for emission reductions below and including 80% (FP) and 70% (HCPVT), respectively. This is attributed to the additional investment cost imposed

Chapter 3. Comprehensive integration method

by the storage. Therefore, if the emission goals could be achieved without storage, the storage was not selected. The storage volume of the FP cases amounted to 182 m³ (80%) which resulted in an investment cost of about 5% of the investment cost for the solar collectors, and for the HCPVT to 80 m³ (70%) which corresponded to 3% of the solar investment cost.

Figure 3.13 (a) depicts the optimal active solar area for different CO₂-equivalent emissions ($\epsilon \in [70\%, 95\%]$) of all studied solar collector types. Similarly to the daytime only operation, it can be observed that the required solar area increased with decreasing CO₂-equivalent emissions. This was, however, not the case between the FP 80 and 75% emission reductions. Referring to Figure 3.12 (c), it becomes clear that the improvement in emission reductions was achieved by an increase in operating cost and compressor investment cost, rather than an increase in solar collector area. This solution together with the 70% FP&PV case should be excluded from further conclusions as they lead to an extreme oversizing of the heat pump system without thermodynamic needs in order to fulfill the ϵ -constraint. This could be prevented by choosing more carefully the variable bounds for the heat pump cycles. As seen in the case of daytime only operation, it can be seen that the HCPVT system required the smallest active area in comparison to the other solar technologies for strong emission reductions due to high efficiency and high uptime.

Figure 3.13 (b) shows the ICCs of the dairy process and respective utility systems. The HCPVT system (scenario 2.1 HCPVT) at 70% emissions with respect to the 2. HPS case (at 3.8 kg CO₂-equivalent/ton of raw material) are shown at solar noon and evening during two typical days. The same heat pump configuration as for the daytime operation scheme was chosen by the optimizer: instead of two heat pumps (30 to 50 °C and -2 to 15 °C, 2. HPS) a two stage heat pump between -2, 15, and 50 with flash gas removal and inter-cooling at 30°C. During noon at day 1, there was not enough solar heat available to cover the process demand completely which is why the boiler was required to back-up.

On day 7 at solar noon, the HCPVT produced heat which was not required by the process. As a result, the storage system was filled which can be seen by the little nose in the curve. This permits to store the surplus of heat in the thermal storage unit, which can then be released in the evening when solar heat is not available. This can be seen on the third curve, where the storage system provides the low temperature heat for the process and the HCPVT system is not active any more. The behavior of the storage system, boiler, and solar dish is further illustrated in Figure B.5 (in Appendix B.2.3.5) indicating a prolongation of the solar operation between 1-4 hours (at $\epsilon=70\%$).

It has to be noted that with the HCPVT the boiler is always active to provide high temperature heat that cannot be provided by the HCPVT due to a process utility pinch. Limiting the operating range of the boiler between the maximum and a minimum at 80% of the maximum would make a study of the storage system even more interesting and put aside the question of part load performance of the boiler, but this was not considered in the work.

3.3. Results and discussion

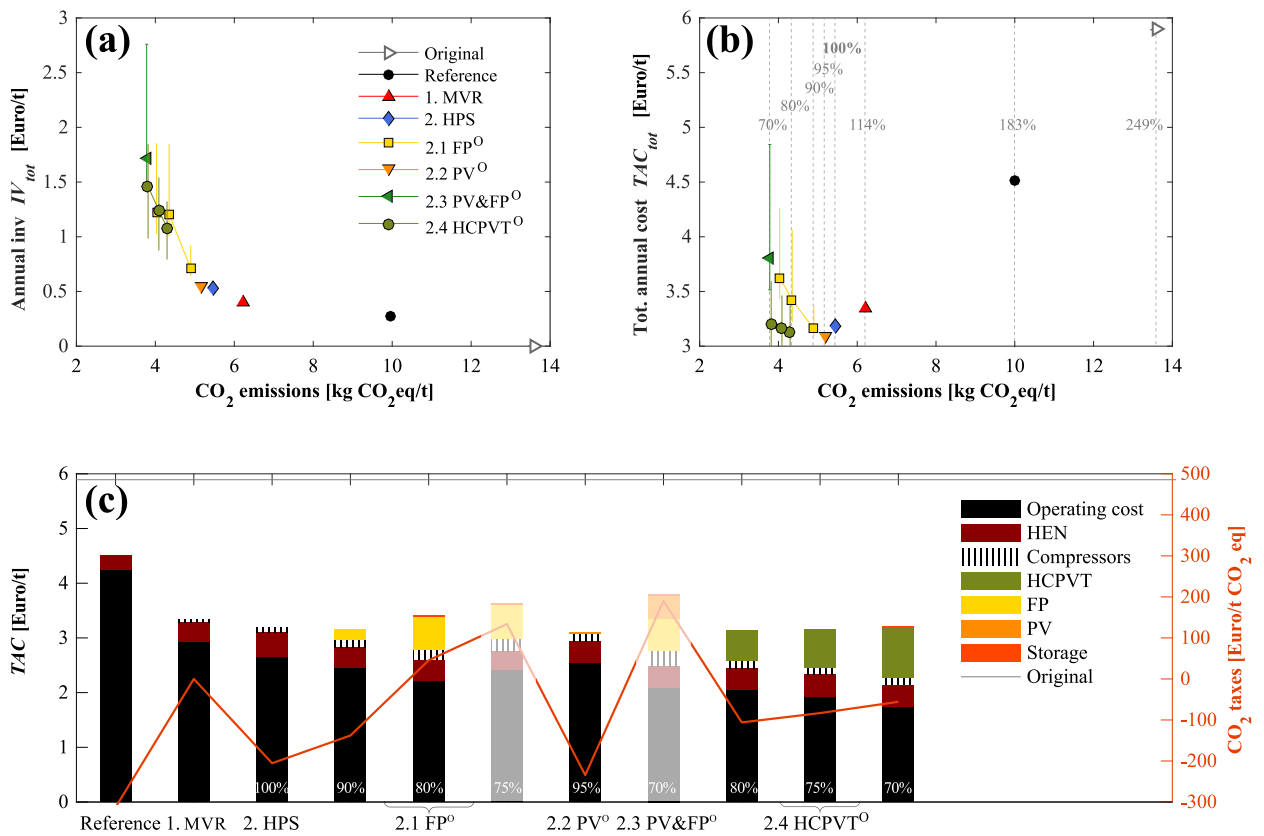


Figure 3.12 – Results of ϵ -constraint optimization of different solar options for continuous process operation. (a) Capex versus CO₂-equivalent emissions, (b) TAC versus CO₂ emissions, (c) detailed cost analysis of various cases. **White-shaded cases:** extreme end of ϵ -constraint with slightly unrealistic results, such as oversizing of refrigeration system.

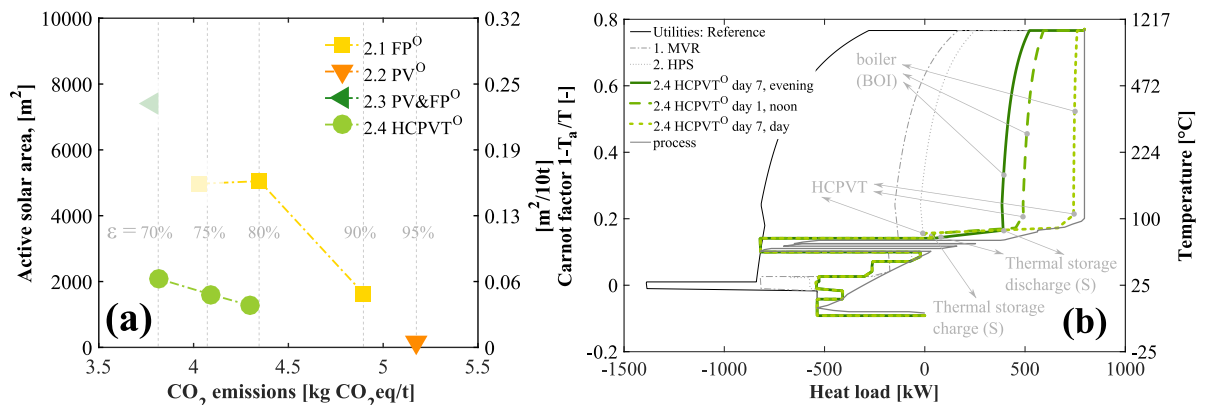


Figure 3.13 – (a) Optimal active solar area, from ϵ -constraint optimization (ϵ between 95 and 70%), (b) ICCs of the dairy process and respective utility system. Conventional utilities [Reference, 1. MVR, 2. HPS] and solar integration of Case 2.4 HCPVT⁰ at 70% emissions with respect to the reference i.e. 3.8 kg CO₂-equivalent/ton of raw material during different typical days.

3.4 Conclusions

What problem formulation is required for a comprehensive design method for solar-assisted low-temperature processes?

A comprehensive method was proposed which addressed simultaneous optimization of the process heat recovery, the conventional utilities, and the renewable utility system (including thermal storage) using ϵ -constrained parametric optimization. The method, tailored for the low-temperature industry, is based on multi-period utility targeting, including process heat recovery through PA and re-use through heat pumping, and identifies the optimal design and operation of the utility and storage system. The proposed methodology was demonstrated on the basis of a Swiss dairy plant where different solar components were compared and evaluated based on economic and environmental criteria. The methodology permitted to derive cost optimal solar field, heat pump, and thermal storage tank sizing as well as optimal operation of the system during all operating periods at selected emission levels.

Optimization of heat recovery, heat pump, and mechanical vapor re-compression placement showed reduced exergy destruction and total costs at increased energy efficiency in the system. Integration of a MVR brought emission reductions of $\approx 38\%$ at 15% reduced TAC, while adding a HPS to study more complex refrigeration systems decreased CO₂ emissions by 12% at comparable TAC. The preliminary version of a heat pump superstructure (HPS), which was used to model the MVR, refrigeration cycle, and the HPS proved to be flexible in handling various heat pump types, and indicates great potential thus motivating more thorough analysis (as conducted in Chapter 4).

Three solar systems were investigated for daytime only and continuous operation of the dairy process: photovoltaic modules (PVs), flat plate thermal collectors (FPs), and a high concentration photovoltaic and thermal system (HCPVT). One major conclusion was that integration of solar energy can contribute to reduce the environmental impact and exergetic losses of the process at beneficial total costs. Solar energy was, however, only selected by the thermo-economic optimization algorithm in combination with an optimized system comprising heat recuperation, mechanical vapor re-compression, and heat pumping. This supports the choice of a comprehensive approach.

For continuous operation of the process, the reduction in specific emissions was not as significant as for daytime only operation. Due to the capital cost of the thermal storage system, it was only chosen by the optimization for high emission reductions requirements. Photovoltaic panel integration offered the least emission reduction potential (up to 20% reduction in daytime only operation with respect to the best non-solar case). However, installation is simple, independent, and if overproduced, can be exported to the grid. In comparison, the HCPVT system, had high potential with very high efficiencies bringing emission reductions easily up to 40% (daytime only) at uncertain cost and shading losses. The low cost, very low efficiency flat plate collectors offered a simple solution providing more reliability of the system performance capital cost expenses with emission reductions of up to 30% (daytime only).

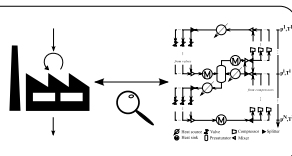
Generic heat pump superstructure

4

Overview

- A comprehensive MINLP superstructure synthesis method for industrial heat pumps
- Optimization of heat pump design, operating conditions, and integration with the process and utility system
- The superstructure includes sub-cooling, multi-stage phase-changes, presaturators, HEN cost estimation and fluid selection
- Multi-objective bi-level solution strategy allowing augmentation by expert judgment
- Benchmarking with three literature case studies shows improvements by 5–30%

Chapter 4: Heat pump superstructure



This chapter is based on Wallerand et al. [170]

Heat pumping has gained increasing attention during the past decades not only for household applications but also for improving energy efficiency of industrial processes through waste heat recovery and valorization at elevated temperatures [89, 90]. As demonstrated in Chapter 1.3 (Figure 1.3), research in the field of industrial *waste heat recovery* is largely dominated by organic rankine cycle (ORC) applications and thermoelectric devices. This may stem from a fully explored state-of-the-art of industrial heat pumps and integration methods; however, the marginal penetration of industrial heat pump systems (apart from basic refrigeration and air-conditioning) [90, 94] contradicts this notion. The main barriers for broad usage in industry were identified as lack of knowledge and of comprehensive heat pump integration methods to provide improvement potentials [90, 94]. This chapter mainly covers single fluid, mechanically driven systems due to their advanced technological development and operative flexibility (as discussed in Sections 1.3 and 1.4.4).

After a state-of-the-art analysis of current synthesis methods, this chapter presents a novel heat pump superstructure with a bi-level solution strategy in the methodology section, followed by application of the method to various literature cases in the results and discussion section.

4.1 State-of-the-art

The focus of this chapter lies on synthesis methods for mechanically driven heat pump integration with industrial processes. Since these techniques rely on modeling state-of-the-art heat pump technologies, a short review of available heat pump features was conducted. Chua et al. [90] and most recently Arpagaus et al. [104] presented comprehensive literature reviews on advances in mechanically driven (multi-temperature) heat pump systems. The most recurring features relevant for large-scale modeling of industrial heat pumps were identified and are presented in Table 4.1. These include multi-stage compression and expansion, ejectors, cascaded cycles, gas-cooling, subcooling, economizers, and presaturators. Other developments, which impose different system architectures (desiccant cooling [90]) or more refined equipment modeling (scroll and oil-free compressors [90, 104, 171, 172]) are not discussed in this chapter.

Table 4.2 provides an overview of the studies introducing synthesis methods discussed in this section. In the presented approaches, it is differentiated between conceptual methods which are based on expert judgment, heuristic rules, or graphical analysis; and mathematical methods, which rely of mathematical programming to perform systematic optimization. This chapter presents a contribution to the latter which is thus discussed at greater length.

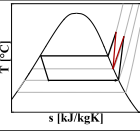
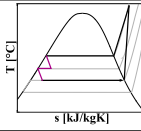
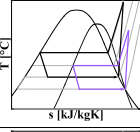
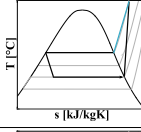
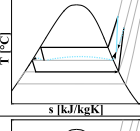
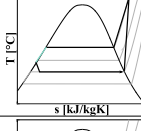
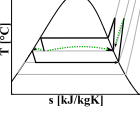
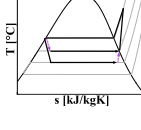
4.1.1 Conceptual methods

Conceptual, or insight-based, methods are not limited by the problem size and therefore always lead to a solution though global optimality will seldom be reached. As early as 1974, Barnés and King [173] and later Cheng and Mah [174] proposed methods based on a set of heuristic rules, dynamic programming, and expert judgment for synthesis of industrial heat pump systems.

In 1978, a milestone was achieved, when Linnhoff and Flower [97] proposed a method now commonly known as pinch analysis (PA) [99] which, for the first time, allowed systematic analysis of a process net thermodynamic requirements and maximum heat recovery potential. This led Townsend and Linnhoff [100] to derive the theoretical foundation for ideal placement of heat engines and heat pumps based on the principles of PA. They concluded that system improvement from a thermodynamic standpoint can only be achieved if heat pumps are placed across the process pinch temperature (1.4.2).

Industrial capital budgeting, however, is seldom based upon thermodynamic objectives. Other drivers play a major role including economic and environmental concerns as well as technical constraints. Therefore, subsequent researchers added thermo-economic principles and technical constraints into their decision process as shown e.g. by Ranade [175] with a trade-off formula between the temperature lift and heat exchanger cost in total site analysis (TSA) (see Table 4.2).

Table 4.1 – Heat pump features considered in this work as identified by Chua et al. [90] and Arpagaus et al. [104].

Feature	Description		Feature	Description	
(A) Multi-stage compression [104, 176–178]	Provide higher coefficient of performance (COP) through intermediate vapor cooling while imposing challenges for direct vapor injection (multi-stage compressor) or lubrication management (multiple single-stage compressors)		(B) Multi-stage expansion (inter-cooling) [179, 180]	Offers lower technical complexity and higher performance through cooling at intermediate pressure level (with aid of several expansion valves for a single-stage compressor)	
(C) Cascaded cycles [181]	Enable coverage of wider temperatures ranges due to the possibility of working fluids switching with applications in natural gas liquefaction or other cryogenic processes, or waste heat recovery with a strong temperature lift		(D) Gas-cooling expansion [182]	Allows to recover heat from the superheated vapor at the compressor outlet (e.g. in a separate heat exchanger), and therefore generates a multi-temperature profile at a single pressure level at higher capital expenses	
(E) Economizer [182]	Permits to preheat the saturated vapor before entering a compressor by mixing with superheated vapor at the same pressure level		(F) Subcooling [178, 180, 181]	Subcooling before expansion improves the performance of heat pumps, however, possibly at the cost of additional heat exchanger installation	
(G) Presaturators (flash-drums) [178, 182, 183]	Enable to saturate superheated vapor and to remove flash gas between expansion stages which improves the coefficient of performance in multiple ways		(H) Ejectors [104, 180, 183–185]	Allow compression of a low pressure fluid through the expansion of a high pressure fluid (principle of suction) at low maintenance and capital expenses. <i>Ejectors were not considered in this work, but are mentioned due to their promising characteristics</i>	

4.1.2 Mathematical methods

Mathematical methods ensure identification of an ideal point with regard the selected objective(s); however, convergence of optimization techniques becomes increasingly difficult with growing problem size. Therefore, many studies considered a reduced solution space, such as discretized temperature levels, simplified heat pump cycles, disregarding PA principles, or preselecting working fluids. The studies presenting mathematical methods are analyzed in the following paragraphs based on selected characteristics.

Temperature level selection In the literature, temperature level (used here interchangeably with pressure level) selection was handled in two ways. The primary approach relies on predefined or discretized temperature levels among which compressor units are activated using integer variables. The first comprehensive methodology for optimal industrial heat pump design based on discrete temperature levels was presented by Shelton and Grossmann [101, 102] in the form of a mixed integer linear programming (MILP) superstructure. Many subsequent authors used discretized temperature levels (as depicted in Table 4.2), resulting in a diminished solution space and therefore increasing the risk of identifying a sub-optimal solution. Fewer authors presented methods with continuous temperature levels as part of the decision variables, which renders the problem structure nonlinear as presented e.g. by Colmenares and Seider [186].

Pinch analysis The principles of PA were considered in most methodologies listed in Table 4.2. Few authors presented algorithms neglecting PA, which reduced the problem size at the cost of disregarding the heat recovery system and its dependencies.

Table 4.2 – State-of-the-art summary of synthesis methods for heat pump design and integration with industrial processes.

Authors	Year	Focus	Method		PA	Property calc.	Temp. discret.	Detail	Objective	Cycle features							Fluid		
			Conc.	Math.						(A)	(B)	(C)	(D)	(E)	(F)	(G)	T	Selection	
<i>Current work</i>		HP	TC	MINLP	✓	CP	0.5 K	3	opex, capex	✓	✓	✓	✓	✓	✓	✓	S	✓	Integers
Yang et al. [187, 188]	2017	HP		MINLP	✓	-	contin.	3	power	✓	✓	✓	✓	✓	✓	✓	S		
Zhang et al. [189]	2016	AHP		MINLP		-	contin.	1	TAC			✓					G		
Oluleye et al. [190]	2016	HP/AHP/HE/AHT	TP		✓	HYSYS	10 K	2	fuel			✓					S	✓	TP
Oluleye et al. [191]	2016	HP/AHP/HE/AHT		MILP	✓	HYSYS	10 K	2	TAC			✓					S	✓	Binary
Dinh et al. [192]	2015	HP		MILP	✓	PR	fixed	3	power	✓		✓			✓	✓	S	(✓)	Flowrates
Kamalinejad et al. [160]	2015	HP		MINLP	✓	RP	contin.	3	TAC	✓		✓	✓	✓	✓	✓	S	(✓)	Flowrates
Liu et al. [193]	2014	HP	TP		✓	-	fixed	3	power	✓	✓	✓					S	✓	TP
Khan and Lee [194]	2013	HP		NLP	✓	PR	contin.	3	power	4 ^(*)							M	(✓)	Composition
Hackl and Harvey [195]	2013	HP	TP		✓	simple	fixed	1	-			✓					G		
Becker [140, 196]	2012	HP		MINLP	✓	Belsim	contin.	2	opex, capex			✓	✓		✓		S	✓	Binary
Zhang and Xu [159]	2011	HP	TC	MINLP	✓	-	fixed	3	exergy	✓		✓	✓	✓	✓	✓	S	(✓)	Flowrates
Hasan et al. [197]	2009	HP		MINLP		simple	contin.	3	power	✓		✓				✓	S/M	(✓)	Flowrates
Nogal et al. [106]	2008	HP		MINLP	✓	HYSYS	contin.	3	capex/power	✓	✓	✓				✓	M	(✓)	Composition
Aspelund et al. [198]	2007	HP	TP			HYSYS, SRK	fixed	3	exergy	✓	✓	✓				✓	S	✓	TP
Bagajewicz and Barbaro [199]	2003	HP		NLP	✓	simple	contin.	1	opex			✓					G		
Holiastos and Manousiouthakis [156]	2002	HE/HP		LP	✓	simple	fixed	1	TAC			✓					G		
Vaidyaraman and Maranas [105]	2002	HP		NLP	✓	SRK	contin.	3	power		✓	✓				✓	M	(✓)	Composition
Maréchal and Kalitventzeff [157]	2001	HP	TC	MILP	✓	Belsim	fixed	3	exergy	✓		✓				✓	S	✓	Binary
Vaidyaraman and Maranas [103]	1999	HP		MILP	✓	[200]	1- 8 K	3	TAC	✓		✓	✓			✓	S	✓	Binary
Kauf [201]	1999	HP	TP			-	contin.	2	COP								S		
Wallin and Berntsson [202]	1993	HP/AHP/AHT	TEP		✓	generic	fixed	1	TAC								G		
Linnhoff and Dhole [203]	1992	HP	TP		✓	simple	fixed	3	power	✓		✓				✓	S		
Swaney [204]	1989	HE/HP		LP	✓	simple	fixed	3	TAC	✓		✓				✓	S		
Colmenares and Seider [186]	1989	HE/HP		NLP	✓	PR	contin.	2	TAC			✓					S	✓	Flowrates
Ranade [175]	1988	HP	EP		✓	simple	contin.	1	TAC								G		
Colmenares and Seider [205]	1987	HE/HP		NLP	✓	PR	fixed	2	TAC			✓					S	✓	Flowrates
Shelton and Grossmann [101]	1986	HP		LP	✓	[206]	1 K	3	TAC	✓		✓				✓	S		
Shelton and Grossmann [102]	1986	HP		MILP	✓	[206]	10 K	3	TAC	✓		✓				✓	S		
Townsend and Linnhoff [100]	1983	HE/HP	TP		✓	Tabl.	fixed	2	exergy								S		
Cheng and Mah [174]	1980	HP	HR			SRK	contin.	3	TAC	✓		✓	✓	✓	✓	✓	S	✓	TP
Barnés and King [173]	1974	HP	HR	MIP		SRK	contin.	3	TAC	✓		✓	✓	✓	✓	✓	S		

(*) Fixed four stages in optimization study

Focus: HP - compression heat pumps, HE - heat engines, AHP - absorption heat pumps, AHT - absorption heat transformers

Conceptual methods: TP - Thermodynamic principles, TC - Technical constraints, EP - Economic principles, HR - Heuristic rules, TEP - Thermo-economic principles;

PA: pinch analysis [99, 207]

Property calculation: CP - CoolProp [208], RP - Refprop [209], SRK - Soave-Redlich-Kwong [210] equation of state, HYSYS - Aspen HYSYS software [211], simple - simplified estimations, PR - Peng-Robinson [212], Belsim - Belsim Vali software [213]

Detail: Level of detail in modeling: 1 - general modeling based on thermodynamic estimations for a generic fluid, 2 - modeling of simplified (single-stage) cycles for specific fluids, 3- full detail modeling of (multi-stage) heat pumps with advanced features for different fluids

Objective: TAC (min), fuel - primary fuel consumption (min), exergy - exergy losses (min), opex (min), capex (min), power - compression power (max)

Cycle features: (A) Multi-stage compression, (B) multi-stage expansion, (C) cascaded cycles, (D) gas cooling, (E) Economizer (preheating before compression), (F) sub-cooling, (G) presaturators

Fluid: T (types): S - single component fluid, M - fluid mixture, G - generic fluid; Selection: TP: thermodynamic principles

Heat pump features In modeling heat pump features, three approaches addressing different levels of detail were observed in the literature. In the first group (1), heat pump performance was modeled based on general thermodynamic principles [107, 156, 175, 189, 195, 199]. It aids in estimating potentials for improvements reachable with heat pump integration but lacks specification of real fluids or system design. Works contained in the second group (2) modeled basic single-stage heat pump cycles based on real fluids assuming that superposition of simple cycles could represent more complex systems [100, 140, 186, 190, 201, 205, 214, 215]. This leads to underestimation of performance and thus sub-optimal solutions could be generated. The third group (3) contains work presenting rigorous heat pump models including technical features from Table 4.1. Most of these included multi-stage compression and pre-saturation [101, 102, 158, 197, 203], while some additionally considered liquid sub-cooling, preheating before compression, or gas-cooling [105, 159, 173, 174], and very few authors examined multi-stage expansion including Vaidyaraman and Maranas [105], Nogal et al. [106], Liu et al. [193], Aspelund et al. [198, 198]. No previous work has comprehensively included all identified heat pump features.

Objective function Apart from the work of Becker et al. [140], the studies discussed here have presented mathematical approaches for single-objective optimization of industrial heat pump systems with objectives such as minimizing exergy losses [159, 195] or total cost [101, 102, 160, 186]. In praxis, decision-making is based on many factors and it is thus difficult to obtain the global solution from single-objective optimization. Therefore, it is advantageous to derive multiple solutions such that the final decision can be based on several criteria including expert judgment, which could be facilitated by multi-objective optimization.

Fluid selection Fluid selection has not been considered extensively in heat pumping literature. Some authors have compared different working fluids based on thermodynamic principles, such as Oluleye et al. [215], while others mainly derive the optimal mass flow rates or composition from preselected fluids, including Kamalinejad et al. [160]. Few researchers have integrated fluid selection into the optimization in the form of integer, binary, or continuous variables such as Vaidyaraman and Maranas [103], Becker [140], or Colmenares and Seider [205]. The candidate fluids were principally selected based on fluid critical properties and triple point.

4.1.3 Discussion and contribution

The discussion of studies presenting conceptual and mathematical methods for optimal heat pump design and integration with industrial processes is summarized as follows.

1. Conceptual methods provide important insight to problems but cannot assess solution optimality. The advantage is, however, that technical infeasibilities and practical constraints can be considered without facing computational problems.
2. Mathematical methods may experience convergence issues for large scale problems due to

increasing complexity. Therefore, many studies considered a reduced solution space.

3. Few studies provide a combination of conceptual and mathematical approaches, which can harvest the advantages of both methods, e.g. through introduction of technical constraints, or multi-solution generation.
4. The potential impact of heat pumping for industrial waste heat recovery is not clearly communicated.

This chapter addresses the gaps denoted (2) and (3) by presenting a novel comprehensive superstructure synthesis method which is solved using mathematical programming for optimal integration of industrial heat pump systems. Preliminary versions of this heat pump superstructure (HPS) as presented in the previous Chapter, and in [111, 167] were generalized and extended to incorporate temperature level and fluid selection, heat exchanger network (HEN) cost estimation, technical constraints and a comprehensive list of heat pump features. A multi-objective decomposition solution strategy allows convergence for large problems and provides multiple solutions for expert judgment adapted to the diverse criteria relevant in industry. This strategy addresses the shortcomings of previous work and provides a clear design method based on a comprehensive superstructure and mathematical programming.

4.2 Methodology

4.2.1 Problem statement

This method aims at providing a utility target and preliminary design of the heat pump system as the basis for detailed design considering dynamic behavior in a subsequent step (not treated here). The problem statement is depicted below.

Problem statement

Given

- industrial process thermal and material demands
- set of candidate utility technologies, including potential heat pumps with operating ranges

Determine

- optimal utility system design
- optimal design of the heat pump system including:
 - specification of technologies
 - features
 - working fluid
 - operating conditions (temperatures, pressures, etc.)

4.2.2 Superstructure synthesis

A flowsheet and a temperature entropy diagram of the novel heat pump superstructure (HPS) are depicted in Figure 4.1. It illustrates the various potential pathways and features considered in the superstructure. Some features are represented in sample cycles.

The superstructure is equipped with a condenser and evaporator at the highest and lowest pressure levels, respectively. The intermediate levels additionally contain a presaturator, a post-compression gas-cooler, a subcooling heat exchanger, and a superheater. Compressors and valves are made available between all pressure levels. Superheated vapor exiting the compressor can be de-superheated in a heat exchanger (gas-cooler) and condensed (represented by one heat exchanger), and/or sent to a presaturator which saturates the fluid and separates it into its phases. Two-phase flow leaving the expansion valves can be evaporated (and potentially superheated by mixing or heat exchange) and then compressed or mixed with condensate with options of inter-cooling and/or subcooling before expansion.

4.2.3 Mathematical formulation

The statement above corresponds to a non-convex Mixed Integer Nonlinear Programming (MINLP) problem. The integer variables relate to activation of different technology options while nonlinearities mainly arise from capital cost correlations and the intrinsic nonlinearity of thermodynamic property correlations. Therefore, a decomposition strategy [125] is applied as presented in Figure 4.2 which incorporates the nonlinearities at the master level solving the linear problem at the slave

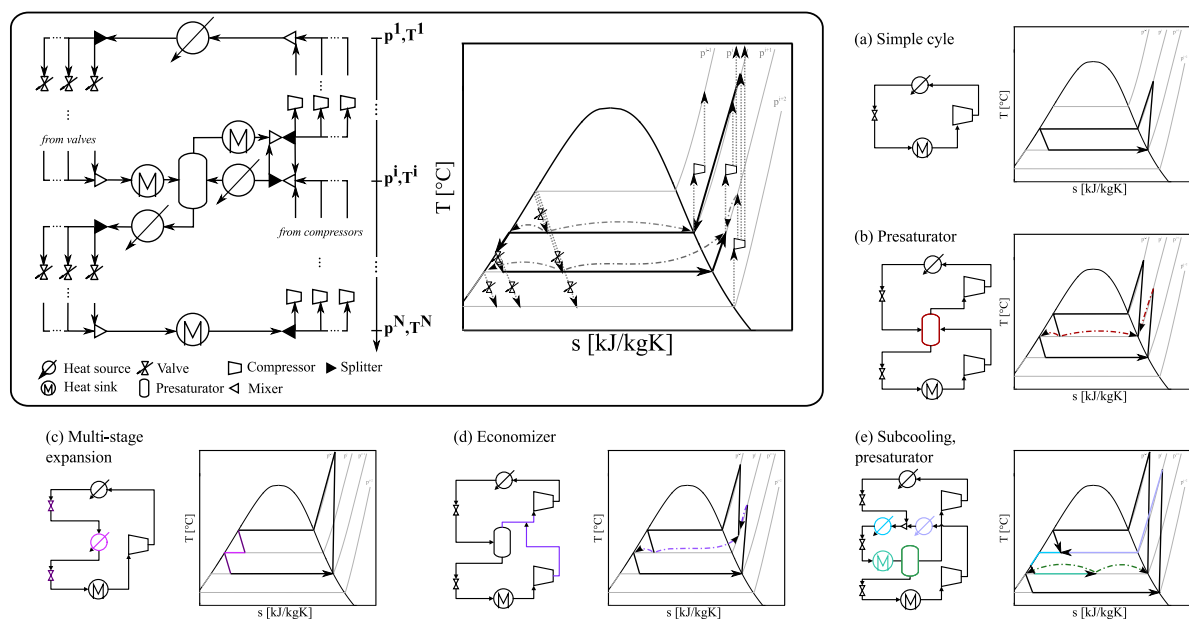


Figure 4.1 – Flowsheet and temperature-entropy diagram of the HPS with sample cycles.

Chapter 4. Generic heat pump superstructure

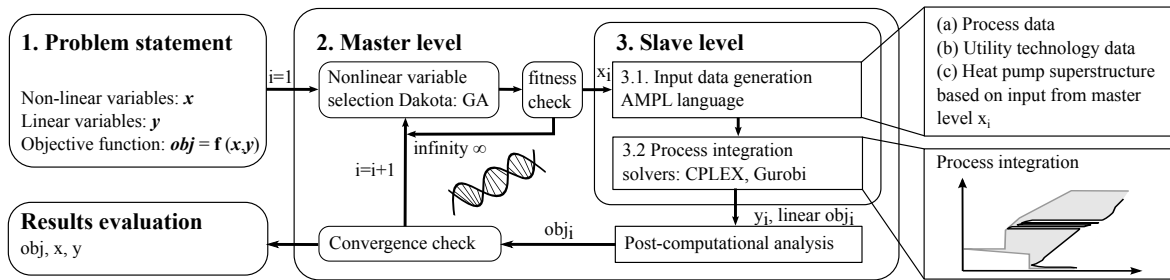


Figure 4.2 – Method proposed in Chapter 4 based on decomposition strategy solving mixed integer nonlinear programming (MINLP) superstructure implemented in Lua OSMOSE platform [125, 143].

level. The variables present in the nonlinear constraints are set at the master level and thus act as parameters for the slave optimization. At the slave level, the linear problem is solved and the decision variables contained in the linear constraints and the linear objective function are transferred to a post-computational analysis where the nonlinear capital cost correlations and objectives are calculated. Based on the objective function values, a convergence check is performed and a new iteration is initiated at the master level.

The main assumptions considered in the heat pump superstructure are:

- the thermodynamic behavior is at steady-state
- heat losses and pressure drops in piping and the components are negligible
- the outlet of a condenser is either saturated or subcooled
- the outlet of an evaporator is either saturated or superheated
- isenthalpic expansion in the valves
- the minimum approach temperature difference is fixed for every stream (and follows the indications from the literature cases)

4.2.3.1 Master level

At the master level, a black box optimization is performed where the variables present in the nonlinear constraints are the decision variables. These are mainly the heat pump saturation temperature levels (T_i), the fluid (d), the subcooling, gas cooling, and compressor preheating temperature differences ($\Delta T_{i,SC}$, $\Delta T_{i,DSH}$, $\Delta T_{i,PRE}$), and all thermodynamic properties derived from these. An additional variable is introduced in order to vary the weight (ξ) of the two components in the objective function at the slave level (see Section 4.2.3.2 - objective function). The properties are retrieved from the open-source database CoolProp [208]. The variables and objective functions at the master level are found in Table 4.3.

Black-box multi-objective nonlinear optimization is performed by Dakota [216] using a multi-objective genetic algorithm (MOGA) [217] which allows analysis of a wide solution space. The specifications used are presented in Appendix C.1.1.

Objective function Different objective functions are of interest when optimizing industrial heat pumps such as the exergy efficiency, coefficient of performance (COP), environmental impact, or cost. Based on the literature cases considered in the results and discussion section, the objectives of the multi-objective optimization were based on economic criteria, i.e. annualized capital expenses (capex) and yearly operating expenses (opex) as shown in Equation 4.1.

$$\min_{T_i, \Delta T_{i,DSH}, \Delta T_{i,SC}, \Delta T_{i,PRE}, d, \xi} \{C^{opex}, C^{capex}\} \quad (4.1)$$

The capex (depicted in Equation 4.4) consists of the investment costs of all technologies w and the HEN cost estimation calculated using Equation 4.3. The HEN area is estimated as suggested by Townsend and Linnhoff [99, 218] based on vertical intervals in the composite curves. HEN design based on mathematical principles, as well as optimization of the minimum approach temperature (ΔT_{min}) was not performed in this work, but could be added to the solution strategy.

Link to slave level The utility and heat pump technology sizing is performed at the slave level. The results from the slave optimization serve as input to calculate the master level objective functions. These are the maximum size (f^w) and existence (y^w) of each technology w influencing the equipment investment and heat exchanger network cost estimation.

4.2.3.2 Slave level

The HPS is embedded in the utility targeting problem of Maréchal and Kalitventzeff [75] where the optimal utility system for an industrial process is found based on the thermal and material needs considering maximum heat recovery. This means that all elements of the heat pump, namely condensers, evaporators, compressors, presaturators (flash-drums) and gas-coolers, are present as utility technologies in the targeting approach. The main variables at the slave level are the size and existence of each utility technology, including all heat pump elements. The size of each technology is decided by optimization based on the objective function while remaining subject to physical and thermodynamic laws.

To ensure mass and energy conservation within the heat pump, additional constraints are added at all saturated liquid, vapor, and superheated vapor points. Since the saturation temperature and respective pressure levels as well as the subcooling and superheated properties are set at the master level, component sizing is linearly dependent on the state properties. Therefore, the problem can be described as a multi-period Mixed Integer Linear Programming (MILP) problem which is solved using commercial software based on AMPL [3] with CPLEX [5]. The specifications are presented in Appendix C.1.2.

Table 4.4 depicts the objective function and variables at the slave level. The utility targeting constraints are described in further detail in Section 2.4. The heat pump parameters for utility targeting

Chapter 4. Generic heat pump superstructure

Table 4.3 – Variables and objective function at master level.

Description	Symbols	Equation
<i>Objectives</i>		
Yearly operating expenses (opex) [\$/y]	C^{opex}	from slave level, see Table 4.4
Total investment cost [\$]	C^{INV}	$\sum_{w \in \mathbf{W}} C^w (f^w, y^w) + C^{HEN} \quad (4.2)$ <p> \mathbf{W} set of utility technologies w f^w maximum size of technology w y^w existence of technology w C^w investment cost function of technology w, see Appendix C.3.1 </p>
Heat exchanger network cost (*) [\$]	C^{HEN}	$\max_p \left\{ \left[c_1 + c_2 \cdot \left(\frac{A_{tot,p}^{HEN}}{N_{min,p}^{HEN}} \right)^{c_3} \right] \cdot N_{min,p}^{HEN} \right\} \quad (4.3)$ $A_{tot,p}^{HEN} = \sum_{k \in \mathbf{K}} \frac{1}{\Delta T_{log,k}} \cdot \left[\sum_{c \in \mathbf{C}} \frac{\dot{Q}_{p,k}^c}{\alpha^c} + \sum_{h \in \mathbf{H}} \frac{\dot{Q}_{p,k}^h}{\alpha^h} \right] (*)$ <p> \mathbf{K} set of temperature intervals {1,2,3, ...,n_d} $\mathbf{H,C}$ set of hot, cold process and utility streams $\Delta T_{log,k}$ [K] logarithmic mean temperature difference $\dot{Q}_{p,k}^{h,c}$ $f_p^{h,c} \cdot Q^{h,c}$ [kW] contribution of hot h, cold stream c to temperature interval k in period p α^h, α^c [kW/m²K] hot, cold stream h, c heat transfer coefficient $A_{tot,p}^{HEN}$ [m²] total heat exchanger network area $N_{min,p}^{HEN}$ [-] minimum number of heat exchanger units c_1 [\$] fixed cost parameter c_2 [\$/m²] scaling cost parameter c_3 [-] non-linear parameter </p>
Annualized capital expenses (capex) [\$/y]	C^{capex}	$C^{INV} \cdot (\tau + m) \quad (4.4)$ <p> τ [1/y] $\frac{i(1+i)^n}{(1+i)^n - 1}$ investment cost annualization factor m [1/y] maintenance cost as fraction of total investment </p>
Total annualized costs (TAC) [\$/y]	C^{TAC}	$C^{capex} + C^{opex} \quad (4.5)$
<i>Variables</i>		
Temperature levels	T_i	$[T_i^{\min}, T_i^{\max}]$, [K] saturation temperature levels
Subcooling	$\Delta T_{i,SC}$	$[0, T_{i,SC}^{\max}]$, [K] temperature difference between condensate and subcooling outlet
De-superheating	$\Delta T_{i,DSH}$	$[0, T_{i,DSH}^{\max}]$, [K] temperature difference in gas-cooling heat exchanger
Pre-heating	$\Delta T_{i,PRE}$	$[0, T_{i,PRE}^{\max}]$, [K] temperature difference for preheating before compression
Fluid index	d	{1, 2, ..., n _d } from set of fluids \mathbf{F}
Weighting factor	ξ	$[0, 1]$, [-] for objective function of slave optimization

(*) Area estimation based on Townsend and Linnhoff [218] and Kemp [99]. The minimum number of heat exchangers (units) N_{min}^{HEN} is estimated following the suggestion of Linnhoff et al. [98] based on graph theory.

as well as mass and energy balances are found in Appendix C.3.1 and C.3.2.

Objective function The MILP problem is solved with commercial solvers [3, 5] based on branch and cut methods for a single objective function. Investigation of a wide solution space regarding both objectives from the master level leaves two options for consideration.

- Constraining one objective with a variable controlled from the master level and minimizing the second objective or
- Defining a weighted sum of the two objectives (wC^{TAC}) where the weighting factor (ξ) is controlled at the master level.

Since alternative (a) generates more infeasible solutions and therefore leads to longer solution times, option (b) was selected and is expressed in Equation 4.6.

$$\min_{f_p^w, f^w, y_p^w, y^w} \{wC^{TAC}\} \quad (4.6)$$

Heat cascade The MILP slave model is subject to heat cascade constraints [75] which ensure heat transfer feasibility for maximum heat recovery. The set of equations are provided in Chapter 2.4 (Equation 2.14 - Equation 2.15).

Mass and energy balances All material and non-thermal energy requirements are described by a set of constraints. These equality constraints ensure that material/energy consumption and conversion are balanced within the system boundaries or compensated with help of the grid (utilities) which factors into the operating cost, as described in more detail in Section 2.4.

Variables The variables present at the slave level are the existence (y_p^w) and sizing (f_p^w) of each of the utility technologies w during each period p and the maximum size considering the entire operating range. Based on the objective function and thermodynamic input parameters selected at the master level, optimal sizes and operating conditions of all utilities including the heat pump technologies are derived within the optimization.

Heat pump specific constraints The general heat pump parameters such as the reference heat load of the evaporator and condenser and the reference electricity consumption of the compressors are presented in Appendix C.3.1. These enter into the targeting constraints and are sized based on the process thermal requirements minimizing the objective function. Enforcing energy and mass conservation within the HPS requires additional constraints to be introduced. These are illustrated in further detail in Appendix C.3.2.

Mass and energy conservation are introduced at three different points on each pressure level, namely: the superheated vapor point after compression, the de-superheated or saturated vapor point before compression or condensation, and the saturated or subcooled liquid point after condensation or before evaporation. Since these points are fixed at the master level, all equations can be formulated with purely linear dependencies. Mass balances at all three points ensure that the working fluid mass flow rate is conserved throughout the heat pump system. Energy balance equations ensure that mixing (e.g. of two compressor outlets at the same pressure level) do not violate the energy conservation law. Superheated vapor mass and energy balances are introduced to study the effect of sensible heat recovery from the vapor (gas-cooling). This can either be achieved by installation of a separate heat exchanger (gas-cooler) or by accounting for sensible heat release in the condenser unit. Both options are separately modeled in this superstructure but does not have a major impact on the heat exchanger network cost estimation (since gas cooling in both cases imposes higher

Chapter 4. Generic heat pump superstructure

investment). The de-superheating temperature difference ($\Delta T_{i,DSH}$) selected at the master level can be understood as the temperature from which sensible heat release is considered. This temperature difference does not influence the energy balance but by manipulating the inlet temperature of the de-superheating, HEN solutions which require stream splitting can be avoided, which has an influence on the heat cascade. If it is set to zero, gas-cooling is neglected and the sensible heat contained in the superheated vapor is considered as if it was available only at saturation temperature levels.

Apart from energy and mass conservation, technical constraints can be considered as introduced below.

Number of heat pump stages The maximum number of stages of a heat pump cycle consisting of one fluid can be restricted as shown in Equation 4.7.

$$\sum_{i=2}^{n_l} \sum_{j=1}^{i-1} y_p^{g,COMP\ i \rightarrow j} \leq n_g^{\max} \quad \forall g \in \mathbf{G} \quad (4.7)$$

Where

\mathbf{G}	set of heat pumps with one working fluid
\mathbf{L}	set of saturation temperature levels $\{1,2,3,..n_l\}$
$y_p^{g,comp\ i \rightarrow j}$	overall existence of compressor between level i and j of heat pump g
n_g^{\max}	maximum number of heat pump stages of heat pump g

Compression ratio and minimum pressure Compressors with compression ratios or with pressure levels outside the bounds cannot be activated. This is depicted in Equation 4.8, which forces the existence of compressor "COMP $i \rightarrow j$ " to zero, if one of the criteria is met.

$$\left\{ y_p^{g,COMP\ i \rightarrow j} = 0 \mid \frac{p^{g,j}}{p^{g,i}} > CR_g^{\max} \vee \frac{p^{g,j}}{p^{g,i}} < CR_g^{\min} \vee p^{g,i} < p^{\min} \right\} \quad \forall i, j \in \mathbf{L} \mid j < i, g \in \mathbf{G} \quad (4.8)$$

Where

$p^{g,k}$	[bar] saturation pressure level of heat pump g at saturation temperature level k
$CR_g^{\min, \max}$	[bar/bar] minimum, maximum accepted compression ratio of heat pump g
p^{\min}	[bar] minimum accepted saturation pressure level

Heat exchanger size A minimum size for heat exchangers is introduced in the form of a soft constraint. Thereby, a fixed penalty cost (IV_1^q) is added to the heat pump units containing thermal

streams as shown in Equation 4.9.

$$C^{\text{fix}} = a \cdot \left(\frac{Q^{\text{min}}}{U \cdot A \cdot \Delta T} \right)^b \quad \forall h \in \mathbf{H}^g, g \in \mathbf{G} \quad (4.9)$$

$$IV_1^g = C^{\text{fix}}$$

Where

\mathbf{H}^g	set of thermal heat pump units {condensers, evaporators, presaturators, gas-coolers} in heat pump g
U	[kW/m ² K] overall heat transfer coefficient
A	[m ²] reference heat exchange area
Q^{min}	[kW] minimum heat exchanger size
ΔT	[K] log mean temperature difference in the heat exchangers
a, b	[\$,-] cost parameters

4.2.4 Fluid selection

Presuming fluid selection from known fluids and sub-critical operation, there are two options for conducting a fluid selection in the presented method.

- (a) the list of candidate fluids is added to the **slave level**, in which every unit (condenser, evaporator, compressors, etc.) is reproduced as many times as there are fluids; the fluids are then activated using binary variables connected to the existence of each unit (y^u), or
- (b) an integer variable referencing the fluid is added to the **master level**

The advantage of selection at the slave level, (a), is that cascaded cycles with different fluids can be designed and convergence of the decomposition strategy is reached after fewer iterations (due to fewer variables at the master level). The disadvantage is that the slave problem size increases proportionally with the number of fluids which impacts the MILP resolution time significantly. Both options were applied in this study depending on the respective problem statement (which will be indicated).

4.3 Results and discussion

This section is divided into three parts. In the benchmarking analysis, three case studies presenting optimal heat pump designs for industrial processes from the literature were selected. The literature results were reproduced with the heat pump superstructure (HPS) to validate its flexibility. During the optimization study, the multi-objective bi-level approach presented in the methodology is applied to the three literature cases, and compared to the previous solutions from the literature. In an extended analysis, one literature case is expanded to consider fluid selection, technical boundary conditions, and HEN cost estimations better representing the reality of industrial problems.

Chapter 4. Generic heat pump superstructure

Table 4.4 – Variables and objective function at slave level.

Description	Symbols	Equation
<i>Objectives</i>		
Weighted total annualized costs (TAC) [\$/y]	wC^{TAC}	$\xi \cdot C^{capex} + (1 - \xi) \cdot C^{opex}$ (4.10)
		ξ weighting parameter controlled from master level
Yearly operating expenses (opex) [\$/y]	C^{opex}	$\sum_{p \in \mathbf{P}} \left(\sum_{w \in \mathbf{W}} OP_{1,p}^w \cdot y_p^w + OP_{2,p}^w \cdot f_p^w \right) \cdot \Delta t_p \cdot occ_p$ (4.11)
Sizing constraint		$f_p^{w,\min} \cdot y_p^w \leq f_p^w \leq f_p^{w,\max} \cdot y_p^w \quad \forall p \in \mathbf{P}, w \in \mathbf{W}$
	\mathbf{P}	set of time periods $p \{1,2,3, \dots, n_p\}$
	\mathbf{W}	set of utility technologies
	f_p^w	continuous variable for sizing technology w during period p
	y_p^w	binary variable related to existence of technology w during p
	$OP_{1,p}^w$	[\$/h] fixed operating cost in period p
	$OP_{2,p}^w$	[\$/h] proportional operating cost in period p
	Δt_p	[h] operating time during period p
	occ_p	[1/y] occurrence of period p
Annualized capital expenses (capex) [\$/y]	C^{capex}	$\sum_{w \in \mathbf{W}} IV_1^w \cdot y^w + IV_2^w \cdot f^w$ (4.12)
	f^w	maximum size of technology w
	y^w	overall existence of technology w
	IV_1^w	[\$/y] fixed cost related to the annualized, linearized investment of technology w
	IV_2^w	[\$/y] proportional cost related to the annualized, linearized investment of technology w
<i>Variables</i>		
Multiplication factor	f_p^w	$[f_p^{w,\min}, f_p^{w,\max}]$, [-] sizing factor of technology w during period p
Use factor	y_p^w	$\{0,1\}$, [-] existence of technology w in period p
Maximum multiplication factor	f^w	$\geq f_p^w \quad \forall p \in \mathbf{P}$ maximum size of technology w
Overall use factor	y^w	$\geq y_p^w \quad \forall p \in \mathbf{P}$ overall existence of technology w

4.3.1 Benchmarking analysis

The selection of the benchmark cases was based on their recurrence in the literature, even though not many cases were treated repeatedly, and the diversity in their characteristics. Suitable cases could not be identified in the most recent literature due to insufficient data provision in terms of process stream data, cost functions, or detailed heat pump configurations. The selected cases were each treated in several publications.

- Case *E2* was selected because it was treated in two consecutive studies by Shelton and Grossmann [101, 102] and due to its heating and cooling requirements which span over a continuous temperature range as shown in Figure 4.3 (a). This case provides exploration potential of a multi-temperature, multi-stage heat pump system which crosses the pinch located at -8°C .
- An *ethylene plant* separation train [219] discussed by Colmenares and Seider [186] was chosen due to the refrigeration needs at extremely low temperatures (-115°C) as shown in Figure 4.3 (b). The pinch point is located at approximately 130°C , which leaves little room for a heat

pump crossing the pinch. Vaidyaraman and Maranas [103] discussed a slightly modified version of the same problem (different ΔT_{\min}) with higher total cost, which is not treated here.

(c) A *Cold Tray* distillation sequence presented by Colmenares and Seider [205] and later studied by Swaney [204] was selected to revisit the original solution which disregarded an obvious improvement of heat pumping across the process pinch (≈ 60 °C). Figure 4.3 (c) shows the process temperature enthalpy profile indicating the process thermal demands and pinch point. Swaney [204] considered a solution with heat pumping across the process pinch for this case study, however with modified input data (isentropic compressor efficiency of 0.8) and is, therefore, not considered here.

The literature optimal cases were reproduced by adding constraints at the slave level of the HPS to force the resulting heat pump layout to contain the same features and operating conditions as those presented in the literature. This was achieved by pre-selecting temperature levels and fixing the active compressor stages and fluids. In this way, the HPS flexibility was tested and reference values for later comparison were calculated, given that most literature studies used different thermodynamic property calculations.

An analysis of the original and the reproduced data (referred to as *Reference* since they serve for later comparison) is presented in Table 4.5. The results are compared based on the total annualized costs (TAC) which was the objective function in the literature. It was observed that the results from literature cases *E2* and *Cold Tray* could be reproduced with a negligible difference (below $\pm 1\%$) in each of the categories including the TAC. The slight difference in results is explained by different property calculation methods. Reproduction of the *Ethylene* case generated around 23% higher electricity consumption which resulted in 22% higher TAC. The thermodynamic conditions are

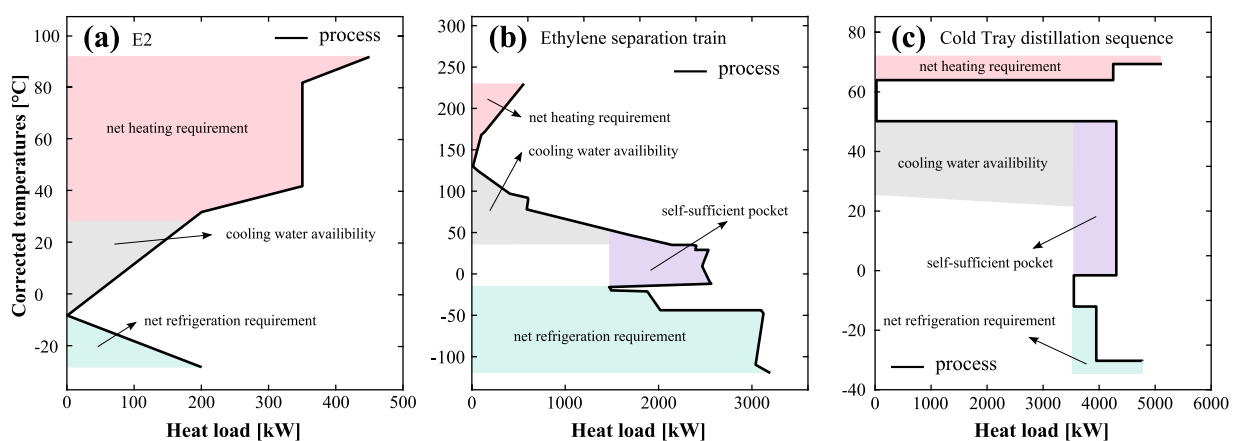


Figure 4.3 – Grand composite curves (GCCs) (temperature enthalpy profiles) from process thermal streams of three benchmark cases, reproduced from (a) Shelton and Grossmann [102], (b) Lincoff et al. [219], (c) Colmenares and Seider [205], respectively.

Chapter 4. Generic heat pump superstructure

Table 4.5 – Comparison of original data and data reproduced (*Reference*) in this work with the HPS. A detailed description of the parameters is presented in Appendix C.2.1.

	<i>E2</i>			<i>Ethylene</i>			<i>Cold Tray</i>			
	Original [101]	<i>Reference</i>	Δ	Original [186]	<i>Reference</i>	Δ	Original [205]	<i>Reference</i>	Δ	
Opex										
Cooling water	\$/y	0	0	-	23'950	25'020	4.5%	29'950	29'930	-0.1%
Steam	\$/y	10'440	10'460	0.2%	-	-	-	287'100	287'090	0.0%
Electricity	\$/y	27'370	27'620	0.9%	266'080	327'580	23.1%	97'260	96'370	-0.9%
Capex										
Compressors	\$/y	54'370	54'710	0.6%	188'990	230'810	22.1%	56'880	56'380	-0.9%
TAC	\$/y	92'180	92'790	0.7%	479'020	583'410	21.8%	471'190	469'770	-0.3%

quite extreme (very low temperature) and thus advanced property estimations are necessary. The literature case consists of five cascaded heat pump cycles over a wide temperature range. Even small underestimation or overestimation of the electricity consumption in the lower cycles is therefore cascaded over the entire range. This, in combination with the property estimation methods, could explain the discrepancy.

4.3.2 Optimization

In this section, the generic HPS and multi-objective solution strategy were applied to the three literature cases. Parameters of the master level optimization are presented in Appendix C.1.1. The MOGA algorithm was terminated after 10^5 function evaluations if the convergence criterion of 0.1 percent change in the non-dominated frontier was not reached. Multi-objective optimization was carried out with regard to the two competing objectives being the opex and capex. The saturation temperature levels and sub-cooling temperature differences (only in case *E2*) were the variables at the master level. Due to the more or less constant temperature requirements in the *Ethylene* and *Cold Tray* case studies, liquid subcooling and gas-cooling were not considered here. However, for these two cases, fluid selection was considered following the data from the literature [186, 205]. To investigate the potential for cascaded cycles, the set of candidate fluids was added at the slave level. Input data and variable boundaries to the different cases are presented in Appendix C.2.1. Figures 4.4 (a), 4.5 (a), 4.6 (a) show the results from the multi-objective optimization. The minimum TAC point of each case was selected and compared to the *Reference* case in an integrated temperature enthalpy diagram in Figures 4.4 (b), 4.5 (b), 4.6 (b) in addition to the flowcharts in Figure 4.7. The three cases are each discussed in the next paragraphs.

Temperature ranges, *E2* The multi-objective results in Figure 4.4 (a) exhibit a pattern of diagonal lines with interstitial gaps. These lines can be explained by the differing numbers of compressors. A trade-off is constituted between a reduction of opex by multi-stage compression, and an increase in capex related to a higher number of compressors with their associated variable and fixed investment costs. The number of compressors for solutions in the non-dominated frontier between opex and capex ranges from three to six. Minimum TAC was achieved with four compressors in contrast to

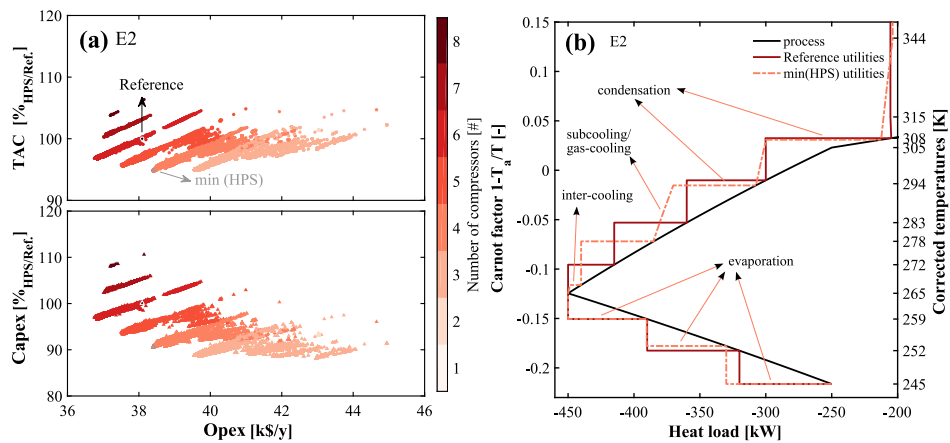


Figure 4.4 – E2. (a) Multi-objective results, (b) utility integrated composite curves (ICCs) (Carnot factor enthalpy profiles) of Reference and min(HPS). Termination: 100k iterations (961 generations); last 50 000 iterations displayed.

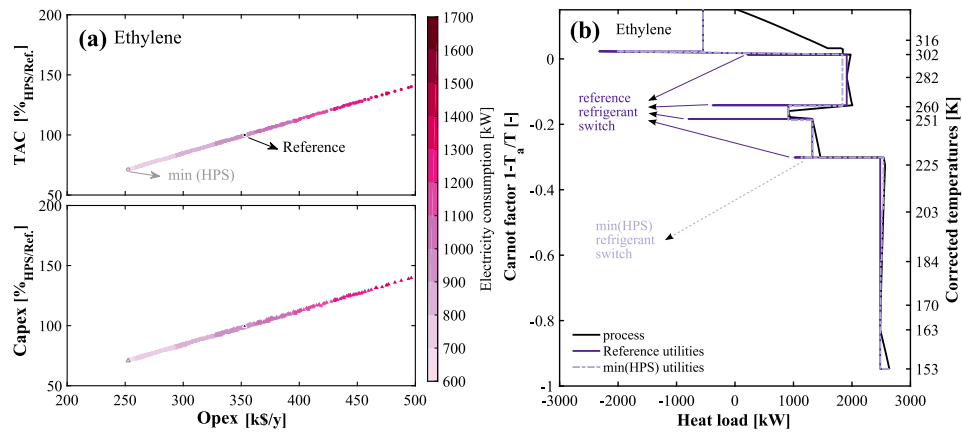


Figure 4.5 – Ethylene. (a) Multi-objective results, (b) utility ICCs. Termination: 118 generations; all 2'852 iterations displayed.

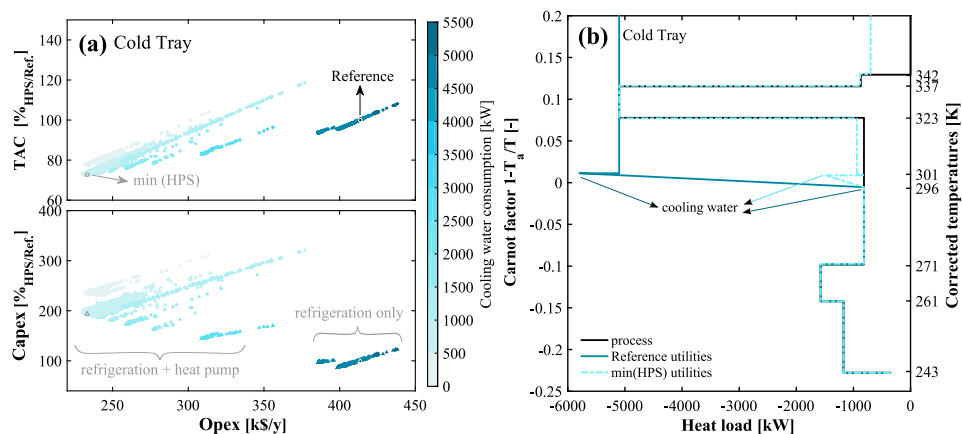


Figure 4.6 – Cold Tray. (a) Multi-objective results, (b) utility ICCs. Termination: 100k iterations (229 generations); last 50'000 iterations displayed.

the six suggested in the Reference. One additional advantage of this multi-objective optimization approach is also that sub-optimal solutions with lower system complexity can be identified. The best solution with three compressors e.g. bears similar TAC ($< +1\%$) as the overall minimum cost solution with four compressors and may therefore be a better solution from the practical perspective. The HPS allows for a comprehensive analysis of heat pump features and operating conditions. The proposed minimum TAC solution consists of a heat pump with inter-cooling, subcooling, and gas-cooling heat exchangers as depicted in Figure 4.4 (b) and Figure 4.7 (a) which contribute to achieving similar performance (in terms of opex) at reduced compressor fixed costs capex compared to the Reference. This leads to a potential overall 5% reduction in TAC as displayed in Table 4.6.

Cascaded cycles, Ethylene separation train Results from the multi-objective optimization in Figure 4.5 (a) show that the two objective functions, opex and capex, are not conflicting. Two main reasons were identified: (1) Due to the elevated process pinch point at 130°C , a pinch-crossing heat pump (as presented in case *E2*) is not feasible, thus there is no trade-off between (higher) compressor investment (capex) and (lower) hot utility requirements (opex); (2) The fixed investment costs of the compressors are distinctly smaller than the proportional costs which translates to the heat pump capex depending primarily on the electricity consumption (opex). Thus all objectives point in the same direction, which would make a Single Objective Genetic Algorithm (SOGA) [217] more appropriate. Running SOGA led to an equivalent result. The minimum point reveals an approximate 30% reduction in the TAC compared to the *Reference* (shown in Table 4.6) driven by the drastically diminished electricity consumption. As illustrated in Figure 4.5 (b) and Figure 4.7 (b), the power consumption was reduced due to a decrease in number of refrigerant switches from four to one, which avoided the minimum temperature difference ($\Delta T_{\min} = 10\text{ K}$) in the switching heat exchangers. Inter-cooling at three levels (174.5 K, 189.5 K, 208.5 K) additionally improved the refrigerator performance leading to an improvement of the COP from 1.8 to 2.6. Due to the constraint on the compression ratio (unlike in the original) to be below 10, which may still be extremely high, the compressor is changed at 180.5 K. This leads to a more complicated, however, beneficial flow management to saturate the superheated compressor outlet.

Process pinch point, Cold Tray distillation Results from the multi-objective optimization in Figure 4.6 (a) indicate a pattern of diagonal lines with gaps in between. Unlike case *E2* this is unrelated to the number of compressors in the system, which are mostly at their maximum (five) due to low compressor fix cost. However, it can be observed that the cooling water consumption correlates with the formation of lines. At highest opex, the largest amount of cooling water is consumed. It is used to cool the process and the refrigeration cycle as reported in the *Reference* displayed in Figure 4.6 (b) and Figure 4.7 (c). By adding a heat pump around the process pinch, the cooling water and hot utility consumptions were drastically reduced. The increase in capex is off-set by a larger decrease in opex leading to a maximum reduction of 27% in TAC in the best point, as depicted in Table 4.6. The HPS minimum TAC solution consists of two separate (ammonia based)

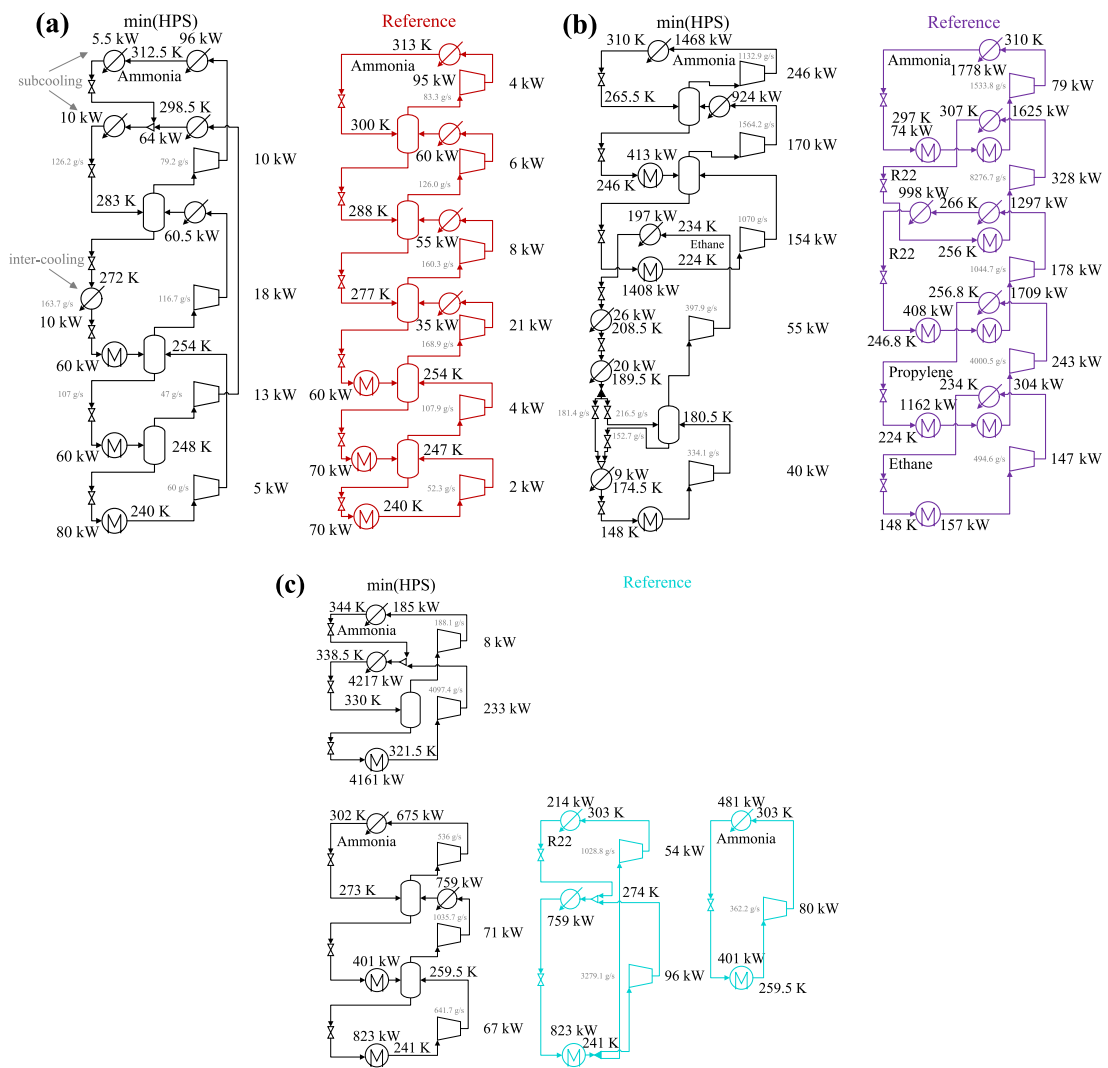


Figure 4.7 – Flowchart of min(HPS) solutions heat pump designs (a) E2, (b) Ethylene, (c) Cold Tray of benchmark analysis.

Table 4.6 – Optimization results. Data shown as Reference was generated with HPS based on the respective literature input data (Section 4.3.1).

	E2		Ethylene		Cold Tray	
	Reference	min(HPS)	Reference	min(HPS)	Reference	min(HPS)
Opex						
Cooling water	\$/y 0	0	25,020	23,150	29,930	4,810
Steam	\$/y 10,460	10,370	0	0	287,090	39,310
Electricity	\$/y 27,620	28,040	327,580	223,340	96,370	189,900
Capex						
No. of compressors	# 6	4	5	5	3	5
Compressors	\$/y 54,710	49,630	230,810	159,140	56,380	109,220
TAC	\$/y 92,790	88,050	583,410	405,630	469,770	343,230
Improvement	% 0	5.1%	0%	30.5%	0%	26.9%
COP _{refrigeration}	- 4.4	4.3	1.8	2.6	5.3	5.8

heat pump systems, one satisfying the refrigeration needs (three compressors), and one across the process pinch (see Figure 4.7 (c) and Figure 4.6 (b), two compressors). With the refrigeration configuration a lower cost, higher COP solution could be derived compared to the reference case which consists of two separate heat pump cycles (R-22 (two compressors) and ammonia). The utility ICCs in Figure 4.6 (b) show that the HPS solution with the pinch heat pump not only reduces cost, but also exergy losses (proportional to the area between the curves) of the system.

Synthesis In conclusion, the HPS can represent a wide range of heat pump features and cycle architectures, while at the same time providing improved solutions to different literature optimal cases. This is attributed to a wider range of heat pump features considered and variable temperature level selection. As demonstrated, the level of complexity, variety of heat pump features considered, and technical constraints added depends on the choice of the user, which makes the superstructure flexible to handle. The solution strategy allows to generate a set of non-dominated solutions which enable the user to perform further analysis, thereby gaining deeper insight to the problem, and to apply other selection criteria. The literature cases discussed in this section serve for benchmarking the underlying approach, however, important criteria are neglected, such as HEN costs, compressor isentropic efficiencies, "real" utilities, and technical constraints thus generating "theoretical" solutions. In the Section 4.3.3, an extended version of the presented case *E2* is, therefore, discussed.

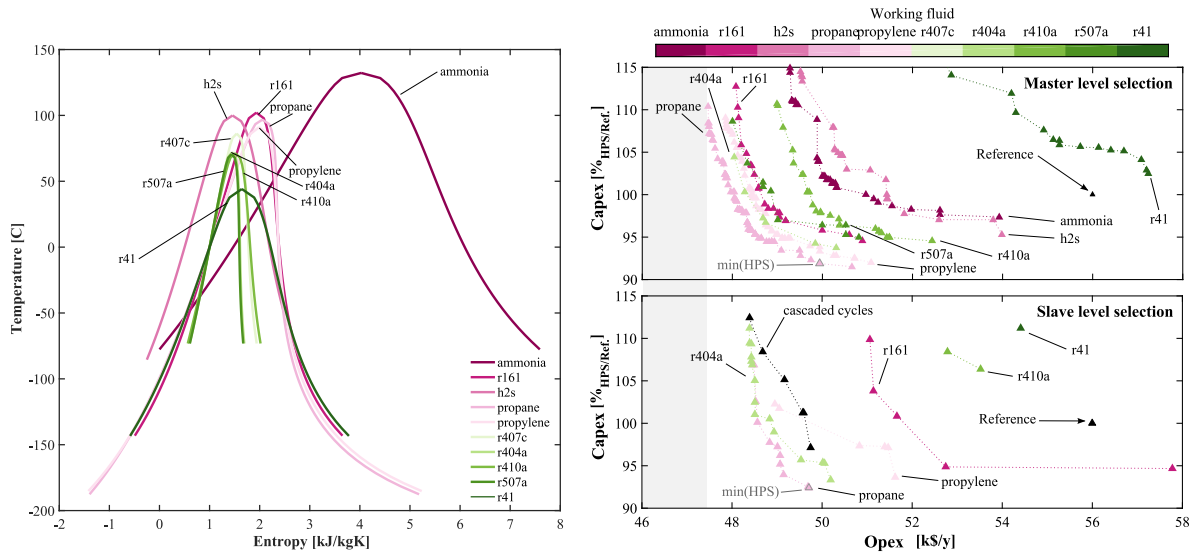
4.3.3 Extended analysis

The heat pump system for the extended case *E2* was optimized with respect to opex and capex assuming an isentropic compressor efficiency of 70%, a maximum compression ratio of 8 [bar/bar] in each compressor, and HEN cost estimation functions from the literature (section 4.2.3.1, Table 4.3). All input data is reported in Appendix C.2.2.

4.3.3.1 Fluid selection

The choice of fluids considered for the extended case *E2* was based on the critical temperature ($T_{crit} \geq 40^\circ\text{C}$), the boiling point ($T_{boil} \leq -33^\circ\text{C}$), and the global warming potential ($\text{GWP} \leq 4 \cdot 10^3$). The fluid investment cost was not considered in this analysis. An interactive parallel coordinate visualization tool developed by Kermani et al. [220] was used to facilitate the fluid screening step which led to ten relevant fluids (see results in Figure 4.8a and Figure C.2). Both fluid selection methods described in Section 4.2.4 were applied and compared during this analysis. To ensure reasonable propagation of the MOGA algorithm during fluid selection at the slave level, a time limit of 600 seconds was imposed for the MILP solver. If the limit is reached, the solver returns the best integer solution at that point even if it is above the specified optimality gap. Nevertheless, a total of 25,000 MOGA iterations required higher computational time than 100,000 iterations with master level fluid selection.

Figure 4.8b shows the non-dominated frontiers of the different fluids generated over all MOGA



(a) Vapor-liquid saturation curves of selected fluids in temperature entropy diagram. (b) Top: Selection at master level; 100k iterations, 211k sec. Bottom: Selection at slave level; 25k iterations, 890k sec.

Figure 4.8 – (a) Fluid set and (b) multi-objective optimization results. In black: multi-fluid solution. R407c is not present, due to a Coolprop [208] problem with this fluid.

iterations by both fluid selection methods. The results from the slave level selection (after intense computational effort) are dominated by the frontier of the master level selection, and it is thus concluded that if not necessary (e.g. for studying cascaded cycles) this method should be avoided.

In the master level selection, propane dominates the other fluids over the entire range of solutions. This outcome was reproduced multiple times by rerunning MOGA with different seeds. Since the MOGA algorithm is aimed at improving the global non-dominated frontier, the frontier of propane yields a good approximation of the global Pareto frontier for this case. The minimum TAC solution generated a total reduction of approximately 9.5%. This solution consists of three compressors between -33 and 41.5°C with propane as working fluid (see Figure C.3).

To study the dominance of propane over the other fluids, the minimum TAC solution was investigated more closely. Therefore, the fraction $\Delta\dot{Q}^{\text{ref}}(T_2)/\Delta\dot{E}^{\text{COMP},2\rightarrow 1}$ between evaporation enthalpy and compressor power amidst the two saturation temperature levels T_1 and T_2 of the first compressor was calculated for all fluids. Figure 4.9 shows the fraction versus the slope of the entropy vapor saturation curve $\Delta s/\Delta T=(s_v(T_1)-s_v(T_2))/(T_1-T_2)$. Figure 4.9a reveals that the compression work correlates with the slope $\Delta s/\Delta T$. Propane is among the fluids which show the most isentropic behavior ($\Delta s/\Delta T \approx 0$) which leads to lower compression work and therefore a higher fraction $\Delta\dot{Q}/\Delta\dot{E}$. When calculating the fraction based on the enthalpy of a complete evaporation (as done in Figure 4.9a), propane is outperformed by r404a and r507a. In a real system, however, irreversibilities related to the expansion work will prevent complete evaporation. Accounting also for those irreversibilities, as shown in

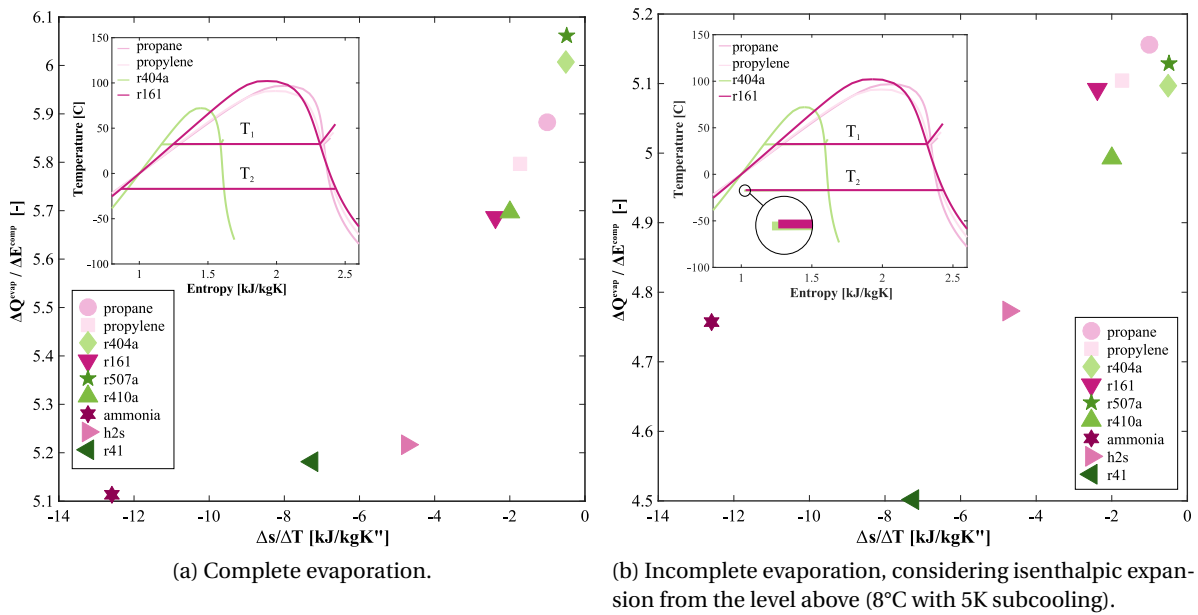


Figure 4.9 – Performance of compressor between saturation levels T_1 (32.5°C) and T_2 (-17°C).

Figure 4.9b, propane yields the highest fraction $\Delta\dot{Q} / \Delta\dot{E}$ hence exhibiting ideal thermodynamic properties in this temperature range.

Comparing the sequence of fluid frontiers (from Figure 4.8b, top) to the thermodynamic performance (Figure 4.9b) indicates a close agreement between thermodynamic and economic performance, which will be further investigated. The closest competitors to propane were: propylene, r161, r404a, r410a, and r507a. Ammonia and hydrogen sulfide generated higher cost solutions, still strongly outperforming r41. All solutions (except r41) outperform the solution presented by the reference case updated with equivalent input data.

The dominance of propane over the entire solution space agrees with other reports indicating superior performance in that temperature range [221]. Further fluid selection criteria could include safety factors (such as flammability or toxicity), fluid cost, ozone layer depletion potential (ODP), global warming potential (GWP) and heat transfer characteristics. Each of these criteria would favor different refrigerants and thus the filtering of potential solutions should be completed carefully to find the best solution for a given case.

4.3.3.2 COP, cycle complexity and HEN costs

Figure 4.10 illustrates the final non-dominated frontier of the results from the master level fluid selection including several properties of these solutions. The (cold) COP increases with decreasing opex, thus, reduced electricity consumption at increased number of compressors; the difference between the lowest (2.9) COP and highest (3.3) is achieved through a higher number of compression stages, increased subcooling and gas-cooling. The highest reduction in TAC (-9.5%) was achieved

with opex of 49.9 k\$ (from Figure 4.8b, top). It can be further noted that the entire frontier spans a relatively small range of operating costs. This is attributed to the simple problem formulation of this benchmark case.

In Figure 4.10, the expected inverse relationship between opex and HEN costs is clearly visible which is impacted by two main factors. The first factor relates to activation of gas-cooling. Since the heat transfer coefficients of gases are distinctly lower than those of condensing fluids, recuperation of sensible heat contained in superheated vapor requires more heat exchange area and therefore increases the HEN costs. The second factor increasing HEN cost is related to a higher number of compression stages, which implies installation of more heat exchangers; thus, influencing both opex and capex. It is also observed that the amount of subcooling increases in tandem with the COP thus providing another option for improving operational efficiency with increased investment. Subcooling was activated in the minimum TAC solution which indicates that its advantageous characteristics should not be overlooked in cycle design. In contrast to non-extended case *E2*, gas-cooling was not activated in the minimum TAC solution, which was attributed to an unfavorable relation between performance benefits and additional HEN cost.

A HEN design of the reference and minimum TAC case was conducted (as shown in Appendix C.2.2, Figure C.4). The optimal solution requires one more heat exchanger than the reference case which is mildly penalized by the HEN cost function thereby being outweighed by the benefits of the reduced opex. The HEN cost estimation from the area targeting compares satisfactorily to the actual design with an overestimation between 8-11% (optimal case design: 53.6, estimation: 57.8 k\$/y; reference case design: 52.8, estimation: 58.8 k\$/y). Likewise compares the total estimated area and the

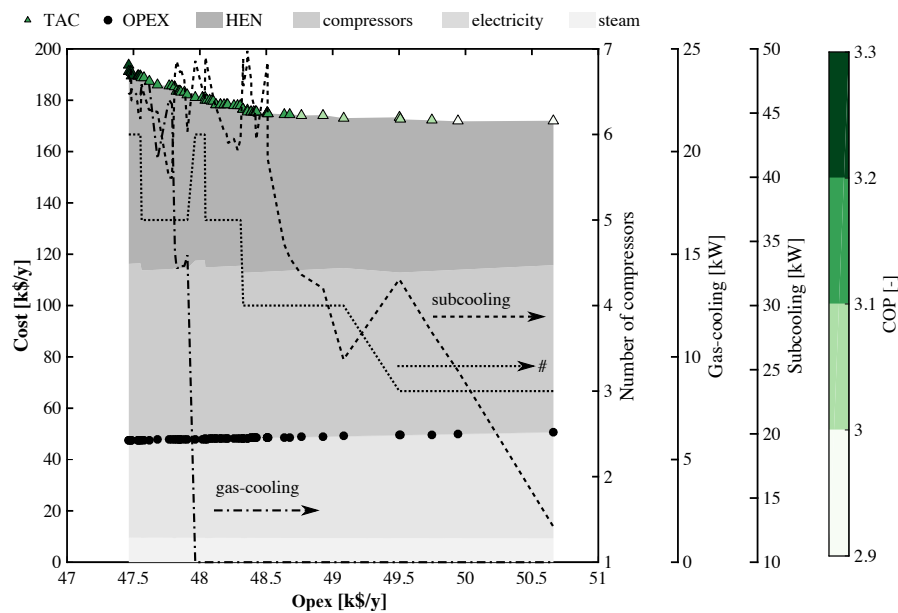


Figure 4.10 – Overall non-dominated frontier of MOGA results from master level fluid selection.

minimum number of heat exchangers.

4.4 Conclusions

How can design of an optimal industrial heat pump system be conducted?

This study has presented a mathematical approach for optimal design of industrial heat pumps spanning a wide variable solution space. The method provides a framework for deriving utility targets, including optimal heat pump component sizes and operating conditions. This provides a basis for detailed system design in a subsequent step to account for dynamics and off-design operation.

The novel superstructure-based synthesis method is embedded in a computational framework and is solved in a decomposition approach. A comprehensive list of heat pump features are taken into account while technical limitations are considered and a set of solutions is provided which allows for expert-based decision making and further in-depth analysis of the solutions.

For benchmarking, the method was compared to a set of literature cases generating between 5 and 30% cost improvements to the optimal solutions reported. An extended version of one case was presented considering fluid selection, HEN cost estimations, and technical constraints within the problem formulation.

The extended case highlighted a trade-off between energy efficiency and system complexity expressed by the increase of heat exchanger network costs with the number of compression stages, level of gas-cooling and subcooling which all improve the COP. This is especially evident when comparing the solutions with 3 and 5 compression stages causing an increase of the COP from 2.9 to 3.1 at 3% increase in TAC. Subcooling was activated in the minimum TAC solution which indicates that its advantageous characteristics should not be overlooked in cycle design. In contrast to non-extended case *E2*, gas-cooling was not activated in the minimum TAC solution, which was attributed to an unfavorable relation between performance benefits and additional HEN cost.

Fluid selection was successfully performed indicating that propane is the most favorable fluid both in economic and thermodynamic terms in this temperature range. The HPS proves to be flexible for different requirements serving in a variety of cases. It has to be noted that a comprehensive analysis of an industrial process should always comprise optimization of the entire utility network, including the hot utilities. This was neglected in this work to be in accordance with the literature input data. In subsequent analysis, the trade-off with other utility technologies should be considered. Future work should also include supercritical cycles, refined fluid and component selection strategies, as well as consideration of off-design performance in multi-time problems.

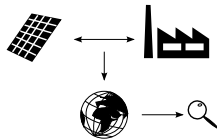
Generalization (A): heat pumping and co-generation

5

Overview

- Derivation of a methodology for environmental and economic (environomic) potential estimation of technologies in industrial sectors, regions, and countries
- Generalization of methodologies derived in previous chapters
- Applied to heat pumping and co-generation in the overall dairy industry
- Presentation of on-line parallel coordinates decision making tool
- Method addresses multiple stake-holders ranging from policy makers to plant operators and technology manufacturers

Chapter 5 & 6:
Generalization



This chapter is based on Wallerand et al. [222]

Having derived methods for optimal solution generation of specific cases, in specific countries, under specific conditions in the previous chapters, this chapter addresses the question of how these methods could be generalized and extended to a wider scope. Therefore, method for estimating the general environmental and economic (environomic) potential of various technologies in industrial processes with application of optimization techniques is derived, generalizing the methodologies derived in the previous chapters. This includes derivation of a publicly available database¹ of solutions based on a wide range of possible economic and environmental conditions.

In agreement with the literature [89, 90], Chapters 3 and 4 demonstrate that heat pumping can be considered as a major contributor for improving energy efficiency and reducing the environmental impact of industrial processes through waste heat recovery and reuse [89, 90] in low temperature

¹ The data can be accessed via an on-line parallel coordinate [76] decision-making platform.

sectors. However, analysis of recent publications in the field of *waste heat recovery* in Section 1.3 reveals that heat pumping is considered far less frequently than other heat recovery technologies such as organic Rankine cycles. A general skepticism towards heat pump technologies among process engineers was reported by several sources [94, 223]. This was assumed to be driven by a lack of knowledge of the heat pump potential and integration methods and a perceived threat of having to compromise the process' operational flexibility [94, 224]. It is further noted that current methods require extensive on-site analysis, which are often unrealized due to economic or time constraints. Proper assessment and clear communication of energetic and economic saving potentials are indispensable for achieving a turning point and, therefore, encouraging more efficient operations through better use of energy resources. Thorough understanding of process operation and optimal heat pump placement is the basis for such analysis.

After a state-of-the-art analysis, a novel methodology for heat pump potential estimation in industrial processes is presented. It considers detailed heat pump modeling and a wide range of input parameters for a generic plant, thus enabling a pre-feasibility assessment. For illustration, the method is applied to the dairy industry in the results and discussion section.

5.1 State-of-the-art

Table 5.1 presents a summary of the relevant literature on synthesis methods and potential studies for heat pump integration in industrial processes. The literature is split between design studies addressing heat pump design for specific processes, and potential studies which estimate the technological potential in specific industries.

5.1.1 Design studies

In the past decades, multiple efforts were made to develop methods addressing optimal design and integration of heat pumps in industrial processes. A general distinction is commonly observed between conceptual and mathematical methods. Conceptual methods rely on heuristics to generate good-practice solutions, while mathematical methods are more likely to generate optimal or near-optimal solutions based on mathematical programming and are hence discussed in more detail. Mathematical methods are often based on linear and nonlinear problem formulations within the domain of optimization. Linear problems can be solved by exact methods, which guarantee optimality in the final result (if terminating in a reasonable time). Nonlinear problems typically consider different aspects of the problem in more detail and allow investigation of an extended solution space; however, solving the problem is a more difficult procedure and optimality is not guaranteed.

In the late 1970s, Linnhoff and Flower [97] developed an important conceptual method aimed at structurally analyzing a process' heat recovery potential nowadays known as pinch analysis (PA) [99, 207].

Table 5.1 – State-of-the-art summary of synthesis methods and potential studies for heat pump integration with industrial processes.

Citation	Year	Topic	Opt.	HR	Market	Model	Integration		Par.	Synthesis
							CU	HU		
<i>Current work</i>		D,Pb	MINLP	✓	X	ME	✓	✓	✓	Bottom-up potential analysis based on optimization of detailed heat pump features for the dairy industry.
Potential studies										
Wilk et al. [225]	2017	D,Pb	X	✓	X	COP	✓	✓	X	Analysis of different industrial processes and the benefits related to installation of heat pumps based on flow sheet software.
Brückner et al. [226]	2015	D,Pt	X	X	X	COP	X	✓	X	Economic potential for compression and absorption heat pumps and heat transformers in different industrial sectors (in Europe) based on estimated heat demands.
Wolf et al. [227]	2014	Pt	X	X	X	COP	X	✓	X	Potential estimation in industrial sectors in the German context by analysis based on the temperature ranges.
Seck et al. [228]	2013	Pb	LP	X	✓	COP	✓	✓	X	"Bottom-up" technical (TIMES) model used to estimate the potential for heat pumping in the French food and beverage sector.
Design studies										
Wallerand et al. [111, 167, 170]	2018	D	MINLP	✓	X	ME	✓	✓	X	Bi-level superstructure including various features which were not considered by other studies such as multi-stage expansion, fluid selection and heat exchanger network (HEN) cost estimation and multi-criteria decision making.
Yang et al. [187, 188]	2017	D	MINLP	✓	X	ME	✓	✓	X	Comprehensive superstructure considering temperature level selection and component sizing.
Oluleye et al. [191, 215]	2016	D,Pb	MILP	✓	X	COP	✓	✓	X	Method for heat engine, mechanical and absorption heat pump and transformer design based on coefficient of performance (COP) fitting functions.
Kamalinejad et al. [160]	2015	D	MINLP	✓	X	ME	✓	✓	X	Two-step approach considering various heat pump features.
Becker [140, 196]	2012	D	MINLP	✓	X	ME	✓	✓	X	Bi-level decomposition strategy [125] with simple heat pump cycles solved for continuous temperature levels.
Zhang and Xu [159]	2011	D	MINLP	✓	X	ME	✓	✓	X	Approach for energy optimal synthesis of cascaded heat pump cycles considering multiple heat pump features in a retrofit problem with fixed temperature levels
Maréchal and Kalitventzeff [157]	2001	D	MILP	✓	X	ME	✓	✓	X	Method based on technology database and expert system
Vaidyaraman and Maranas [103]	1999	D	MILP	✓	X	ME	✓	✓	X	Extended superstructure [101] with economizers and working fluid selection.
Swaney [204]	1989	D	LP	✓	X	COP	✓	✓	X	Heat engine and heat pump integration based on a transportation array.
Colmenares and Seider [205]	1987	D	NLP	✓	X	ME	✓	✓	X	Design of superpositioned simple (one-stage) heat pump cycles (and engines)
Shelton and Grossmann [101, 102]	1986	D	MILP	✓	X	ME	✓	✓	X	Superstructure-based approach, considering multi-stage heat pumping with flash-gas removal.
Townsend and Linnhoff [100]	1983	D	conceptual	✓	X	ME	✓	✓	X	Demonstration that exergetically optimal placed heat pumps need to cross the process pinch temperature.

Topic: D - design methods; P - potential studies (t: top-down, b: bottom-up).

Opt.: - optimization approach: conceptual; mathematical - mixed integer nonlinear programming (MINLP), mixed integer linear programming (MILP), nonlinear programming (NLP), linear programming (LP).

HR: heat recovery in the process is considered, e.g. through PA.

Market: economic model considering market competition between technologies.

Model: - heat pump modeling: ME - based on mass and energy balances; COP: based on Carnot factor efficiencies.

Integration: HU - integration of heat pump as hot utility; CU - integration of heat pump as cold utility

Par.: - parameter variation: variation of input parameters.

Based on these principles, Townsend and Linnhoff [100] demonstrated that optimally-placed heat pumps need to cross the process pinch temperature to improve the overall energy and exergy efficiency. In this way, they highlighted the need to investigate the thermodynamic requirements of the entire system. Most subsequent studies integrated the principles of PA in their methods. Noted contributions to mathematical methods are presented in Table 5.1.

The methods described in the studies presented in this section allow detailed analysis of a process' heat recovery potentials and optimal industrial heat pump and refrigeration placement including the ideal operating conditions. The results are obtained with aid of rigorous mathematical, or conceptual methods based on economic, energetic, and environmental criteria considering detailed technical features of the heat pump cycles. Unfortunately, generalization of the obtained results cannot be conducted due to the dependence on the highly case specific problem input data.

5.1.2 Potential studies

Estimation of the general potential for heat pumping in various industrial sectors was not treated frequently in the literature. Seck et al. [228] and Wilk et al. [225] presented analyses of different industrial processes and the benefits related to installation of heat pumps considering the hot and cold side of the heat pump, modeling them based on the Carnot efficiency. The potential in these bottom-up approaches is extrapolated assuming that the analyzed processes are representative of the respective industry. Other studies [226, 227] addressed the problem from a top-down perspective, estimating the total industrial waste heat potential and the thermal requirements including the temperature levels, which allowed derivation of the total potential heat pump capacity in certain industrial sectors in specific countries or regions.

The presented publications are a foundation for further in-depth analysis highlighting the general potential of heat pumps in certain industrial sectors. Most bottom-up approaches consider the hot and cold side integration of a heat pump into the industrial process; one addresses the heat recovery potential within the process. Heat pumps are typically modeled based on the Carnot efficiency. This circumvents detailed conclusions with recommendations for experimentalists, equipment developers or process operators while only providing policy-makers with coarse estimations of potentials.

5.1.3 Discussion and contribution

The state-of-the-art analysis can be summarized in three main points.

1. Design studies provide complex (multi-stage) heat pump models and results for specific case studies. Generalization of the obtained results has limited impact due to dependence on case-specific input data.
2. Potential studies provide estimations of heat pump potentials in various industrial sectors. The heat pump modeling and industrial process analysis is conducted in a coarse manner

aiming at deriving overall capacities and temperature levels rather than detailed designs.

3. No studies effectively combine potential estimations with detailed modeling and optimization techniques thus offering a comprehensive bottom-up approach for technological potential estimation.

This chapter attempts to close the gaps mentioned in (1-3) by proposing a method for estimating the general environomic potential of heat pumps in industrial processes with improved fidelity and application of optimization techniques. The method includes generation of a publicly available database of optimal solutions (which are based on a reduced input parameter set) via generalized multi-objective optimization. Based on user-selected input criteria, case-specific solutions are drawn from the database and investigated. The data can be accessed via an on-line parallel coordinates decision-making platform. The publicly-available results may be used to conduct a pre-feasibility study in a plant, and in general, to identify potentials from the side of policy-makers or equipment developers. The proposed method may be applied to a variety of technologies and processes and is illustrated in this chapter on potential estimation of heat pumping and co-generation in the general dairy industry based on analysis of various typical plants. Optimal design is achieved with a heat pump superstructure (HPS) including a wide range of technological features [111, 167, 170] and a comprehensive integration method.

5.2 Methodology

5.2.1 Problem statement

The methodology derived and the results obtained may be used to address a variety of research questions, some of which are depicted below.

Problem statement

Given

- (A) certain industry/process, a geographical region
- (B) specific technology (feature)

Determine

- (A)
 - economically viable emission reduction measures
 - key political drivers to enable emission reduction goals
 - favorable technologies and system designs which contribute to emission reduction goals
- (B)
 - target industry/process
 - key geographical region

which provide economically/environmentally viable options for integration of the technology

5.2.2 Overview

A classical deterministic utility design optimization problem, as discussed in Section 5.1.1, is depicted in Figure 5.1. The required input parameters can be grouped into two categories. Imposed parameters (Π) are given by the boundary conditions of the problem, such as the geographical location of the plant which determines energy prices, interest rates, electricity mix emissions, etc., while decision influenced parameters (Π_D) depend on the decisions (D) of the plant manager e.g. (operating time, production volumes). With aid of these input parameters, a (multi-objective) optimization problem can be formulated and solved. The computational burden of this approach is quite high, especially considering that the solution is only valid for the specific case considered.

To overcome this limitation, this work presents a methodology in which the computationally expensive optimization problem is solved once, independent from most input parameters. Thereupon, the solutions are stored in a database from which a quasi-infinite number of scenarios with varying input conditions can be derived.

The method is depicted in Figure 5.2. During the comprehensive solution space generation, the problem scope is defined including the fixed and free parameters, followed by solution generation and pruning to identify the relevant solutions which are added to the database of good solutions. Once this step has been carried out, the database can be accessed on demand to generate the desired output which is referred to as results retrieval.

Parallels may be drawn with classic approaches for dealing with uncertainty of input parameters. Robust optimization addresses uncertainty in mixed integer linear programming (MILP) problems [229]. The most commonly used approach for mixed integer nonlinear programming (MINLP) problems is stochastic programming [230] and accounting for parameter variation in post-computational analysis [231]. The former requires intense computational effort, while the latter approach only allows recalculation of the objective function, not accounting for the fact that different input parameters yield different solutions.

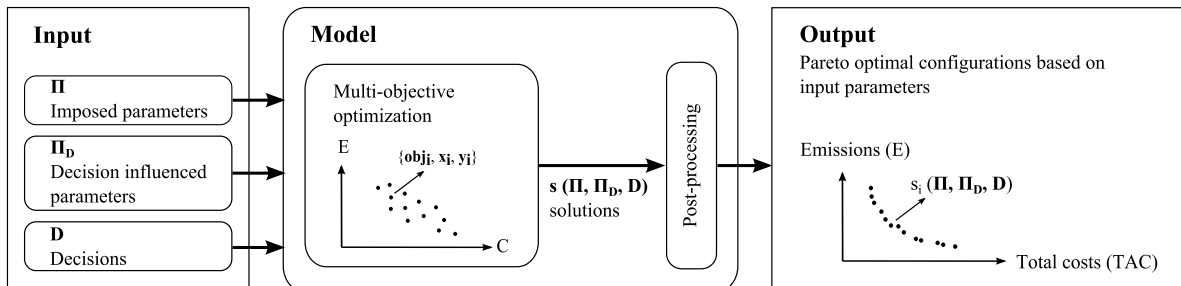


Figure 5.1 – Standard deterministic multi-objective optimization problem statement.

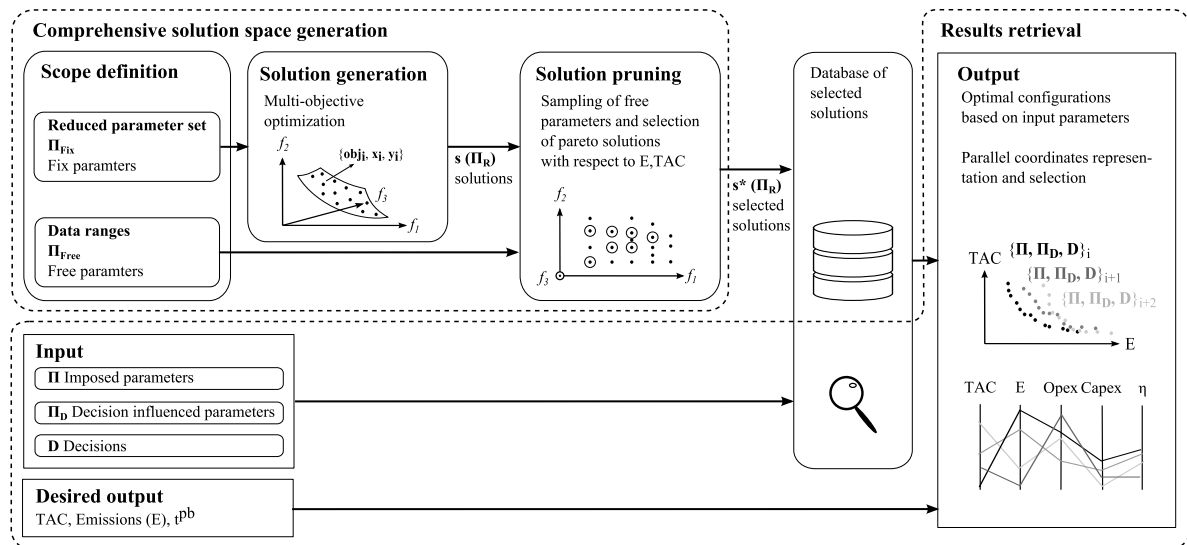


Figure 5.2 – Method proposed in Chapter 5.

5.2.3 Comprehensive solution space generation

5.2.3.1 Scope definition

The goal in most optimization approaches for industrial processes is the derivation of more efficient or less emitting solutions at minimum cost. The scope definition aims at defining the objectives and input parameters required to formulate the optimization problem. The procedure is illustrated for the case of minimizing the total annualized costs (TAC) and emissions, though it can be applied for any problem. Formulating the problem correctly requires understanding of the influence of the different input parameters on the desired output. The input parameters required to model the TAC and emissions of a particular process are classified into four categories:

1. Economic inputs

- Economic parameters influencing the **yearly operating expenses (opex)** are the cost of all incoming material and energy streams, as well as yearly operating time.
- The **annualized capital expenses (capex)** are dependent on the equipment cost functions, the interest rate, and the fraction of maintenance cost (related to the initial investment).

2. **Utility-specific inputs** The performances (efficiency, fuel consumption and technical constraints) of the utility technologies influence the opex and are determined by input parameters.

3. **Process-specific inputs** The process configuration and its heat recovery potential have a major influence on the system cost and emissions, and are therefore treated as an input.

4. **Environmental parameters** of process conversion steps and the impact of the incoming material streams allows for a simplified quantification of the process' environmental impact.

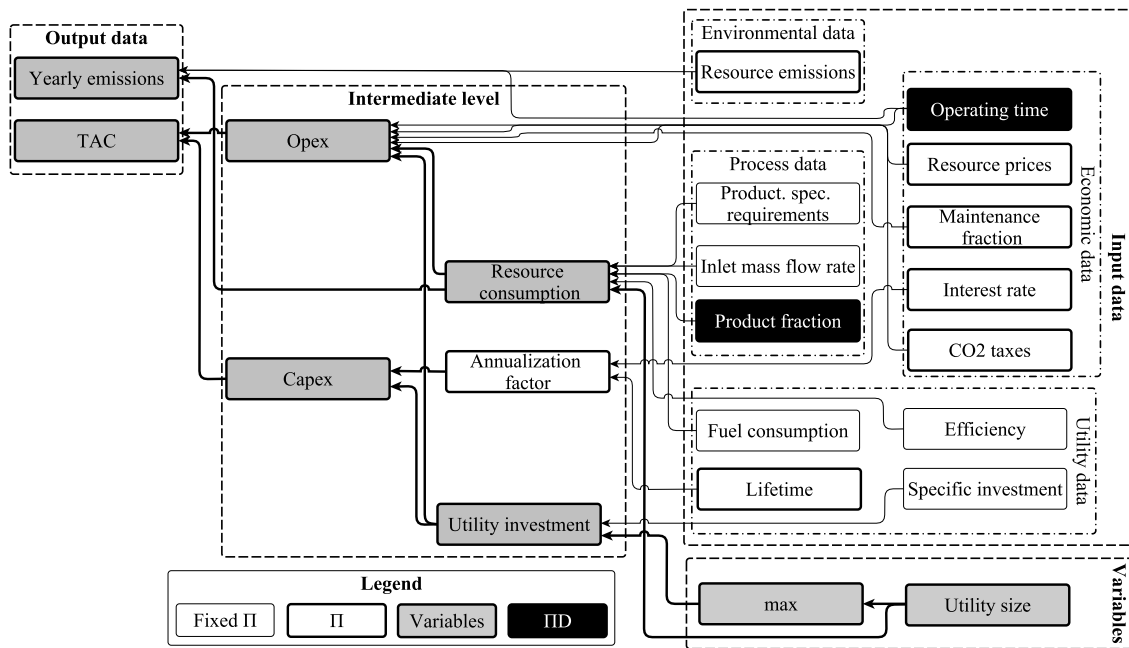


Figure 5.3 – Relations between input data and desired output, imposed parameters (II), decision (D) influenced parameters (IID).

The goal is to identify which input parameters need to be fixed to effectively generate a large solution space; hence, the relations of all influential parameters on the TAC and emissions are shown in Figure 5.3.

The figure highlights that choosing TAC and emissions as objective functions would require fixing the entire input parameter set. The main variables describing the system are the utility sizes which directly influence the resource consumption and utility investment. It follows that selecting the **resource consumption** and **utility investment** as objectives leads to a full description of the system; however, with dependence on less than half the input parameters compared to the TAC and yearly emissions. In this way, the optimization problem can be formulated independently of most location-dependent, volatile, or uncertain input parameters as depicted in Figure 5.3. Of the parameters which require fixing (the product specific requirements, utility specific fuel consumption and efficiency), most are weakly dependent on specific conditions such as the location of the plant and thus can be fixed without the same concerns.

The utility specific investment cost has the least clarity among input parameters to be fixed, since it is subject to a certain level of variation in different countries [232] ($\pm 30\%$ for machinery and equipment in Europe). However, the parameters fixed during the optimization problem can easily be adapted during the results retrieval phase. Additionally, the interest rate and fraction of maintenance cost per year are not fixed, so that the overall investment cost is further re-adjusted during the results retrieval.

5.2.3.2 Solution generation

As derived during the scope definition, a multi-objective optimization is carried out with the objectives being the **resource consumption** and **utility investment cost**. The problem is formulated as an MINLP which is solved by decomposing the problem into an nonlinear programming (NLP) at the master level and MILP at the slave level as shown in Figure 5.4 and discussed by Wallerand et al. [170] and Weber et al. [125], which is described in more detail below.

Master level The master level optimization is conducted with a multi-objective genetic algorithm (MOGA) [217] implemented in Dakota [216]. The objectives at the master level, **total investment cost** and **resource consumption**, are depicted in Equation 5.1.

$$\min_{T_i, \Delta T_{i, DSH}, \Delta T_{i, SC}, \Delta T_{i, PRE}, d_i, \xi, \epsilon^r} \{C^{INV}, \dot{E}_r\} \quad \forall r \in \mathbf{R} \quad (5.1)$$

Where \mathbf{R} is the set of resources {electricity, natural gas}, and \dot{E}_r [kW] is the resource consumption. The total investment costs are derived from the investment cost, C^w , of each utility equipment $w \in \mathbf{W}$, and the HEN cost estimation, C^{HEN} as shown in Equation 5.2.

$$C^{INV} = \sum_{w \in \mathbf{W}} C^w + C^{HEN} \quad (5.2)$$

The decision variables at the master level, including the minimum heat recovery approach temperature difference of the process streams, the HPS features, as well as the equipment cost functions of the specific problem are discussed in the application section.

Slave level At the slave level, the multi-period utility targeting problem from Maréchal and Kalitventzeff [75] is solved for several utility technologies including the heat pump superstructure presented by Wallerand et al. [170]. It should be noted that the underlying problem does not necessarily require a multi-period formulation (and in the applied case study, the number of periods

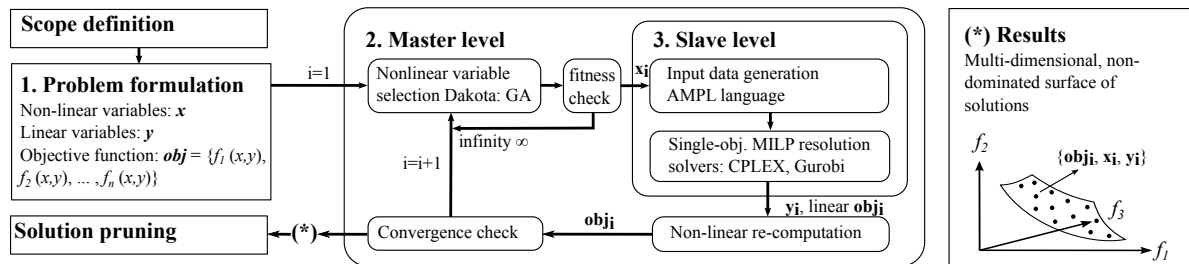


Figure 5.4 – Generalized multi-objective optimization strategy.

Chapter 5. Generalization (A): heat pumping and co-generation

is set to 1); however, the problem framework is presented as such to be generalizable. Commercial software based on AMPL [3] with CPLEX [5] is used to formulate and solve the multi-period MILP problem. The MILP is formulated and solved as a single-objective optimization problem. To span the entire objective solution space given by the master level, two options are considered in this study.

ε -constraint The first option addresses the problem by minimizing one of the objectives while the others are constrained (ε -constraint) with a variable from the master level. As shown in Equation 5.3-5.6, the utility investment cost, C_{slave}^{INV} , is minimized while the consumption of resource r , f_p^r , is restricted.

$$\min_{f_p^w, f^w, y_p^w, y^w} \{C_{\text{slave}}^{INV}\} \quad (5.3)$$

Due to the linearity of the MILP, the utility investment cost at the slave level depicted in Equation 5.4 is derived from linearized cost functions based on the maximum size and existence of each equipment w .

$$C_{\text{slave}}^{INV} = \sum_{w \in \mathbf{W}} (IV_1^w \cdot y^w + IV_2^w \cdot f^w) \quad (5.4)$$

Where IV_1^w [\$] and IV_2^w [\$] are the fixed and proportional cost of equipment w , respectively. The main variables at the slave level are the sizing factor, $f_p^w \in [f^{w,\max}, f^{w,\min}]$, and existence, $y_p^w \in \{0,1\}$, of each technology w during period p as well as their maximum size, f^w , and existence, y^w . In Equation 5.5, the sizing constraints are depicted.

$$f^w - f_p^w \geq 0, y^w - y_p^w \geq 0, f^{w,\min} \cdot y_p^w \leq f_p^w \leq f^{w,\max} \cdot y_p^w \quad \forall p \in \mathbf{P}, w \in \mathbf{W} \quad (5.5)$$

The remaining objectives from the master level are restricted with an ε -constraint depicted in Equation 5.6.

$$f_p^r \leq \varepsilon^r \quad \forall r \in \mathbf{R}, p \in \mathbf{P} \quad (5.6)$$

where f_p^r [-] is the grid sizing factor of resource r during period p and ε^r [-] is the grid unit resource limit fixed at the master level.

Weighted sum of objectives The second option is to define a weighted sum of all objectives, wC^{TAC} , where the weighting factors are controlled from the master level. The objective in this case is shown in Equation 5.7.

$$\min_{f_p^w, f_p^w, y_p^w, y_p^w} \{wC^{TAC}\} \quad (5.7)$$

The weighted total annual cost ($wTAC$) are defined in Equation 5.8 based on the annualized capital expenses (capex), C^{capex} [\$/y]², the yearly operating expenses (opex), C^{opex} [\$/y], the total weighting factor, ξ [-], and the resource prices (weights), $OP_{z,p}^r$ [\$/kWh].

$$\begin{aligned} wC^{TAC} &= \xi \cdot C_{slave}^{capex} + (1 - \xi) \cdot C^{opex} \\ &= \xi \cdot \tau \cdot C_{slave}^{INV} + (1 - \xi) \cdot \sum_{p \in \mathbf{P}} \sum_{r \in \mathbf{R}} \left[OP_{z,p}^r \cdot f_p^r \right] \cdot \Delta t_p \cdot occ_p \end{aligned} \quad (5.8)$$

Where Δt_p [h] is the operating time, and occ_p [1/y] is the occurrence of period p .

The advantage of the ε -constraint method is full control over exploration of the solution space while more infeasible scenarios or unnecessary solutions may be generated. The weighted sum of objectives does not allow direct control over exploration of the solution space; however, it encounters infeasibility less frequently.

5.2.3.3 Solution pruning

Solution pruning is introduced at this stage to reduce the set of solutions so that only the most relevant ones are stored in the database. The first step towards solution space reduction happens during solution generation, where results are slightly rounded so as to reduce the total number of solutions by combining those which are very similar in several objectives and typically exhibit marginal differences in the values of continuous decision variables. During the solution pruning, the relevant solutions are identified by sampling the free input parameters (Π_{Free} within their specified ranges) and storing the minimum TAC solutions as shown in Figure 5.5³. Several sampling algorithms were applied to the generated solutions. Each led to similar results (see Appendix D.2.1) and thus, Matlab [137] intrinsic Latin hypercube sampling [233] was selected as the method for further use in this work.

² The slave capex C_{slave}^{capex} [\$/y] are derived from the slave total total investment C_{slave}^{INV} [\$], and the annualization factor $\tau = \frac{i \cdot (1+i)^n}{(1+i)^n - 1}$ [1/y], with i [1/y] being the interest rate and n [y] the equipment lifetime.

³ The entire set of minimum TAC solutions, instead of only the non-dominated solutions (with respect to TAC and emissions) are stored; As demonstrated in the following sections, lower payback times can be achieved in the dominated region.

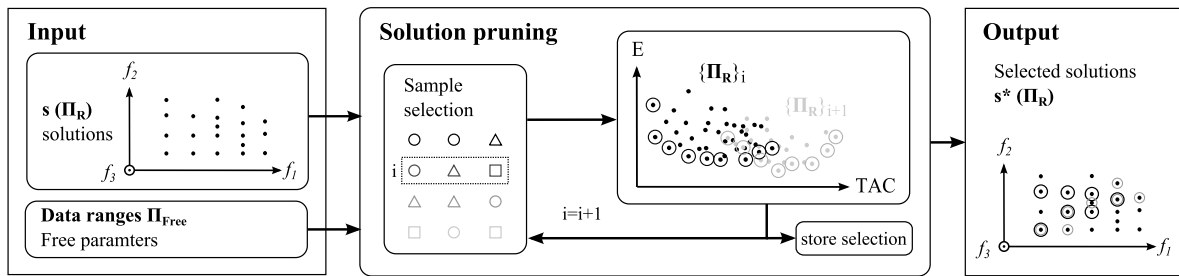


Figure 5.5 – Flowsheet of the pruning step.

If all minimum TAC solutions from each sample are selected, a reduction with respect to the original population of approximately 25% was observed by applying the pruning technique. Accounting for the occurrence of each solution during the sampling, and selecting only the 99% most recurring solutions generates a reduction up to 60% with respect to the original population while keeping the diversity in the solution space, which is the recommended approach for future studies.

5.2.4 Results retrieval

Results retrieval is the subsequent step once the comprehensive solution space generation has been finalized. It contains all activities involving analysis, documentation, and investigation of the solutions stored in the database. Based on selected input parameters and the desired output, solutions are retrieved from the database and investigated by various key performance indicators (KPI), which are elaborated in Table 5.2, including the total system cost and emissions, exergy efficiency, and payback time. As indicated in Figure 5.2, extended analysis of the set of minimum TAC solutions in various forms, including interactive parallel coordinate plots [76], is presented in detail in the results section and demonstrates the gain for multiple stakeholders. This provides an example for assessing and drawing conclusions from the methods to support decisions from various perspectives.

5.3 Application

This section introduces the industrial case study of with all related data. Since the methodology is applied to the dairy industry, a modular dairy plant is presented, followed by the scope definition of the underlying problem. The detailed problem statement of the solution generation is further elaborated.

5.3.1 Modular dairy plant

The modular dairy plant presented here is based on industrial data from Becker[140, 161, 196], which was already presented in Chapter 3, and data from the reference document for best available techniques in the food, drink and milk industry [81]. Figure 5.6 depicts the pathways for conversion of raw milk into milk-based products as derived by Kantor et al. [234]. Based on European production

Table 5.2 – Key performance indicators (KPI) calculated during post-computational analysis.

Description	Symbols	Equation
Total annualized costs (TAC) [\$ / y]	C^{TAC}	$C^{capex} + C^{opex} = C^{INV} \cdot \tau + C^{opex} \quad (5.9)$
		τ [1/y] $\frac{i(1+i)^n}{(1+i)^n - 1}$ investment cost annualization factor, i [-/y] interest rate, n lifetime [y] C^{INV} [\$] total investment cost, see Equation 5.2
Total emissions [t CO ₂ eq / y]	\dot{E}_{CO_2}	$\sum_{r \in \mathbf{R}} \sum_{p \in \mathbf{P}} \text{CO}_2^r \cdot \dot{E}_r \cdot f_p^r \cdot \Delta t_p \cdot \text{occ}_p \quad (5.10)$
		\mathbf{P} set of time periods {1,2,3, ..., n _p } f_p^r [-] grid sizing factor of resource r during period p \dot{E}^r [kW] reference (thermal, electrical) power of grid resource unit r CO_2^r [kgCO ₂ eq/kWh] specific emissions of resource r Δt_p [h] operating time of period p occ_p [1/y] occurrence of period p
System exergy efficiency [%]	η_{exergy}	<p>The exergy efficiency of the system is derived by the process exergy requirements and production, respectively, as well as the resource exergy import and export.</p> $\frac{\sum_{p \in \mathbf{P}} \left(\sum_{s \in \mathbf{S}_{\text{required}}} \dot{E}_{\text{ex}}^s + \sum_{r \in \mathbf{R}_{\text{export}}} \dot{E}_{\text{ex},r,p} \right) \cdot \Delta t_p \cdot \text{occ}_p}{\sum_{p \in \mathbf{P}} \left(\sum_{s \in \mathbf{S}_{\text{produced}}} \dot{E}_{\text{ex}}^s + \sum_{r \in \mathbf{R}_{\text{import}}} \dot{E}_{\text{ex},r,p} \right) \cdot \Delta t_p \cdot \text{occ}_p} \quad (5.11)$ <p>The exergy production within the process stems from the hot streams above and the cold streams below the ambient temperature ($T_a = 15^\circ\text{C}$), respectively.</p> $\sum_{s \in \mathbf{S}_{\text{produced}}} \dot{E}_{\text{ex}}^s = \sum_{c \in \mathbf{C} T_{\log,c} \leq T_a} \dot{Q}_p^c \cdot \left(1 - \frac{T_a}{T_{\log,c}} \right) + \sum_{h \in \mathbf{H} T_{\log,h} \geq T_a} \dot{Q}_p^h \cdot \left(1 - \frac{T_a}{T_{\log,h}} \right)$ <p>The exergy requirement within the process stems from the cold streams above and the hot streams below the ambient temperature (T_a), respectively.</p> $\sum_{s \in \mathbf{S}_{\text{required}}} \dot{E}_{\text{ex}}^s = \sum_{c \in \mathbf{C} T_{\log,c} \geq T_a} \dot{Q}_p^c \cdot \left(1 - \frac{T_a}{T_{\log,c}} \right) + \sum_{h \in \mathbf{H} T_{\log,h} \leq T_a} \dot{Q}_p^h \cdot \left(1 - \frac{T_a}{T_{\log,h}} \right)$
		\mathbf{S} set of process streams $\mathbf{H}, \mathbf{C} \subset \mathbf{S}$ set of hot, cold process streams $\mathbf{R} \subset \mathbf{W}$ set of imported/exported resources including [electricity, natural gas, etc.] $\Delta T_{\log,s}$ [K] logarithmic mean temperature difference of stream s \dot{Q}_p^s [kW] process stream s heat consumption/release $\dot{E}_{\text{ex},r,p}$ $f_p^r \cdot \dot{E}_{\text{ex},r}$ [kW] exergy of each resource r during period p
Payback time [y]	t^{pb}	$\frac{C^{INV}}{C^{opex,ref} - C^{opex}} \quad (5.12)$
		C^{INV} [\$] total investment cost, as shown in Equation 5.1
Yearly operating expenses (opex) [\$ / y]	C^{opex}	$\sum_{p \in \mathbf{P}} \left(\sum_{w \in \mathbf{W}} \text{OP}_{1,p}^w \cdot y_p^w + \text{OP}_{2,p}^w \cdot f_p^w \right) \cdot \Delta t_p \cdot \text{occ}_p + m \cdot C^{INV} + \dot{E}_{CO_2} \cdot c_{CO_2} \quad (5.13)$
		\mathbf{W} set of utility technologies f_p^w [-] continuous variable for sizing technology w during period p y_p^w [-] binary variable related to existence of technology w during p $\text{OP}_{1,p}^w$ [\$/h] fixed operating cost in period p $\text{OP}_{2,p}^w$ [\$/h] proportional operating cost in period p c_{CO_2} [\$/t CO ₂ eq] CO ₂ taxes m [1/y] maintenance cost as fraction of total investment
Investment discount [%]	b^{INV}	<p>Percentage of investment reduction (by subsidies or lower utility investment costs) required to achieve the desired payback time.</p> $1 - \frac{C^{INV, \text{desired}}}{C^{INV}} = 1 - \frac{t^{pb, \text{desired}} \cdot (C^{opex,ref} - [C^{opex} - m \cdot C^{INV}])}{1 + t^{pb, \text{desired}} \cdot m} \cdot \frac{1}{C^{INV}} \quad (5.14)$
		$t^{pb, \text{desired}}$ [y] desired payback time, set here to 2 years
Exergy discount [\$/Δ%]	b^{exergy}	<p>Investment discount per exergy reduction (by subsidies) required to achieve the desired payback time.</p> $\frac{C^{INV} - C^{INV, \text{desired}}}{\eta_{\text{exergy}} - \eta_{\text{exergy}}^{\text{ref}}} \quad (5.15)$
COP of heat pumps [-]	COP	$\frac{\sum_{e \in \text{EVAP} T_{in} \leq 0V \geq 40^\circ\text{C}} \dot{Q}^e + \sum_{c \in \text{COND} T_{in} \geq 40^\circ\text{C}} \dot{Q}^c}{\sum_{q \in \text{COMP}} \dot{E}^q} \quad (5.16)$
		EVAP set of all evaporator units in heat pump COND set of all condensation units in heat pump COMP set of all compressor units in heat pump \dot{Q}^e heat consumption by evaporator e \dot{Q}^c heat release by condenser c \dot{E}^{co} electricity consumption by compressor co

volumes [235], the fabrication of fresh dairy products (such as butter, desserts and concentrated milk) and the production of cheese were identified as the two main routes. The specific energy requirement of cheese-making is considerably higher than that of fresh dairy products due to the drying and exporting of whey as a co-product. A combination of cheese-making and fresh products would, by inspection, lead to a design mainly dominated by the cheese making requirements and is, hence, not considered. As shown by Kantor et al. [234], the dairy pathways can be decomposed into functional subprocesses, so-called modules, and their specific thermal requirements (per unit of product) can be extracted. Scaling these requirements with specified product mass flowrates or ratios permits generation of a profile for any dairy plant.

In this manner, three different fresh dairy production plants were generated to study the heat pump potential in this industry. Table 5.3 presents the respective data, which stem (1) from the actual plant studied by Becker [140], (2) from the average production volumes of dairy goods in the European Union [235], and (3) a combination of (1) and (2) without the concentrated milk production to investigate plants with a lower pinch point temperature. Figure 5.7 displays the utility integrated composite curves (ICCs) of the three plants, revealing the different net thermal requirements and temperature ranges considering maximum heat recovery. As indicated in Figure 5.6, the process and utility system are separately modeled so that heat exchange between the utilities and the process is only allowed through energy carriers such as steam, water, or refrigerant. Figure 5.7 (d) shows the utility heat cascade of the reference boiler at high temperature heating with high and medium pressure steam. The curves of the utilities in place and the available energy carriers are shaped by steam (medium pressure at $\approx 200^\circ\text{C}$, low pressure at $\approx 100^\circ\text{C}$) generated by a natural gas boiler, cooling water ($15\text{--}17^\circ\text{C}$), and a two-stage refrigeration cycle ($30, -3, -33^\circ\text{C}$, R161). The reference resource (natural gas and electricity) consumption of these configurations is shown in Table 5.3.

Having assumed a minimum approach temperature, $\Delta T_{\min}/2$, of 5 K for all process streams (except the milk evaporation/condensation streams), the energetic requirements of the modelled plant are in good accordance with the actual plant from Becker [140]. Hence, it is assumed that this approach temperature represents the actual level of heat recovery in the considered plants, and the derived resource consumption of each case is treated as its reference.

5.3.2 Scope definition

The scope definition aims at formulating the problem and deriving the data for the solution generation. Table 5.4 shows the identified free and fixed parameters for the underlying problem. As shown in Section 5.2.3.1, the fixed parameters are the utility- and HEN-specific (installed) investment cost, fuel consumption, utility efficiencies, and process data. Data ranges are provided for the free input parameters. It was assumed that the specific investment of the components already installed in the plant (boiler and refrigeration cycle) were negligible. The potential utilities to be considered were selected as a natural gas co-generation engine (COGEN), a mechanical vapor re-compression (MVR),

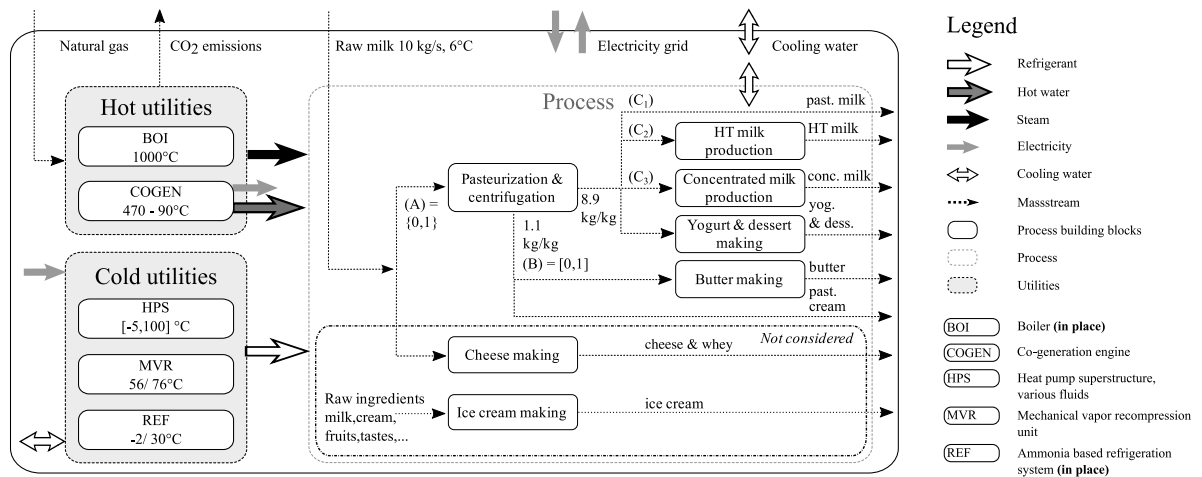


Figure 5.6 – Flowsheet of the modular dairy plant. Utility and process data depicted in Appendix D.3.

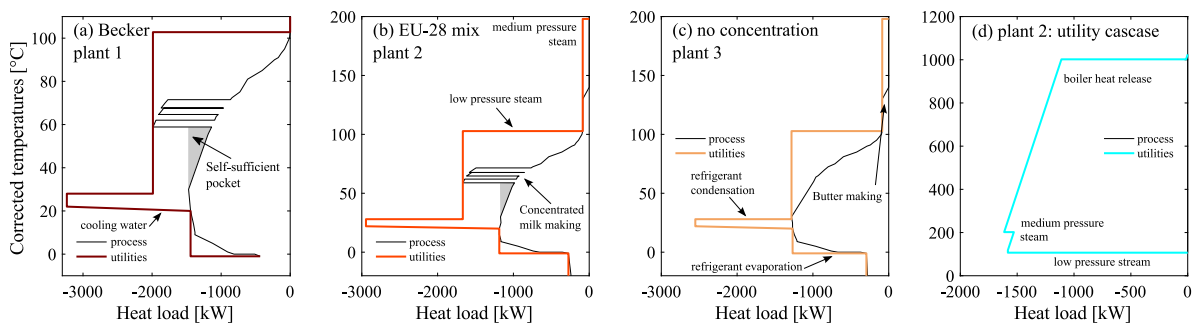


Figure 5.7 – Dairy plants’ utility integrated composite curves (ICCs).

Table 5.3 – Product mass flow rates and reference resource consumption of examined dairy plants.

Name	Plant	(A)	(B)	(C1)	(C2)	(C3)	(C4)	Flow rate kg/s	Flow name	Mass fraction processing step outlet/inlet	Electricity kW	Natural gas kW
Becker [140]	1	1	0	0.157	-	0.225	0.618	10	raw milk		238.8	2208.6
								1.1	past. cream			
								1.40	past. milk			
								0.86	concentrated milk	1 [conc. milk]/2.33 [past. milk]		
EU-28 mix	2	1	0.69	0.25	0.25	0.18	0.32	5.50	yogurt & dessert (*)	1 [yog. & dess.]/1 [past. milk]	266.4	1852.6
								10.00	raw milk			
								0.341	past. cream	1/1		
								0.759	butter	1 [butter]/1 [past. cream]		
								2.23	past. milk	1/1		
								2.23	HT milk	1/1		
No concentration	3	1	0.3	0.2	0.25	0	0.55	10.00	raw milk		252.5	1424.8
								0.77	past. cream	1/1		
								0.33	butter	1/1		
								1.78	past. milk	1/1		
								2.23	HT milk	1/1		
								4.90	yogurt& dessert (*)	1/1		

(*) Assumption: 50/50 dessert / yogurt production

Original plant [140]: cheese 0%, butter 0%, cream 11 %, drinking milk 14%, milk powder 20%, fresh products 55%

European milk consumption [235], 2015: [cheese 36 % *not considered*], butter 29 %, cream 13 %, drinking milk 11%, milk powder 4%, fresh products 7%; Assumption: 50% of drinking milk is UHT

No concentration: removal of the milk concentration unit

Chapter 5. Generalization (A): heat pumping and co-generation

and a heat pump superstructure (HPS). The HEN cost is estimated based on a retrofit assumption. Correspondingly, the minimum number of connections, the minimum heat exchange area, and the HEN cost were derived for the reference plant and for each new design. The investment cost difference generates the estimate for the retrofit heat exchanger network (HEN). Thereby, it must also be noted that if a new solution generates fewer connections (N), or a smaller area (A), they are set to the reference values. Applying this concept enforces that the HEN cost is always positive or zero (and is with respect to the reference plant). Designs with higher ΔT_{\min} , meaning less heat recovery and higher resource consumption will always be inferior to the reference case and, hence, will be discarded.

Figure 5.8 shows available electricity and natural gas prices in OECD countries, commercial bank lending rates, and emissions associated with grid electricity, which serve as indications for the free parameter data ranges, and provide the basis for later analysis.

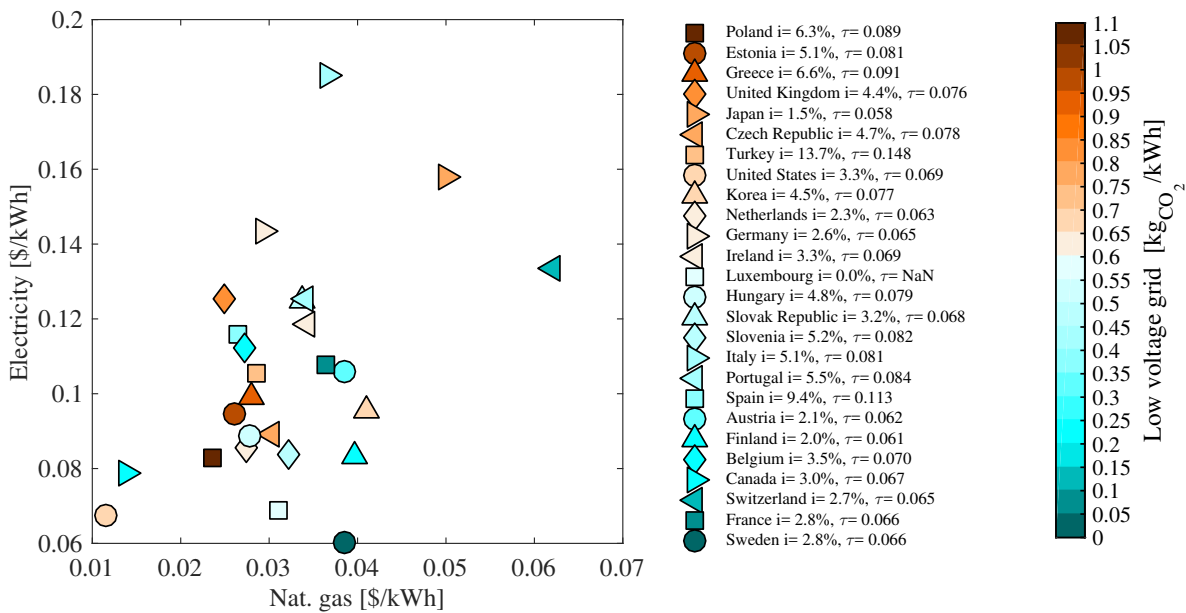


Figure 5.8 – Resource prices (2017) [238][*], commercial bank lending rates (i) [239] (mostly 2015), annualization factor (τ) based on Equation 5.9 (20 y. lifetime), low voltage electricity grid emissions [240] (Reference year 2014, allocation, cut-off by classification, ICC 2013, GWP 100a). [*] Gas price Japan [241] (2015).

5.3.3 Solution generation

All variables and objectives at both levels of the multi-objective optimization approach described in Section 5.2.3.2 are depicted in Table 5.5. The general variables at the master level include the minimum approach temperature difference of the process streams, and the variables controlling the slave objective function as described by Equation 5.5-5.8. The heat pump superstructure (HPS) specific variables at the master level are the saturation temperature levels, subcooling tempera-

Table 5.4 – Free and fixed input parameter set to optimization problem.

	Symbol	Units	Fix	Free	Sub-category	Data values / data ranges
Economic data						
Operating time	Δt_p	h		✓		[2000, 8000]
Resource prices	c_r	\$/kWh		✓	Electricity	[0.04, 0.30]
					Natural gas	[0.01, 0.10]
Interest rate	i	-		✓		[0.03, 0.15]
CO ₂ taxes	c_{CO_2}	\$/tCO ₂		✓		[0, 100]
Maintenance frac.	m	%INV		✓		[0.03, 0.1]
Utility data						
Spec. installed investment	C^w	\$ ₂₀₁₆	✓		Compressors	Installed cost function from industrial data [140], updated with CEPCI [4], converted to \$ (1.33 \$ ₂₀₁₀ /€ ₂₀₁₀), installation factor (1.5), and $\dot{E}_{el}^{COMP} = f^{COMP} \cdot \dot{E}_{el}^{COMP} \in [20, 500]$ kW _{el} . $C^{COMP} = \frac{541.7}{550.8} \cdot 1.33 \cdot 1.5 \cdot 1500 \cdot 160^{0.1} \cdot (\dot{E}_{el}^{COMP})^{0.9} \quad (5.17)$
					Co-generation engine	Installed cost function [140], updated with CEPCI [4], converted to \$ (1.07 \$ ₁₉₉₉ /€ ₁₉₉₉), and $\dot{E}_{el}^{COGEN} = f^{COGEN} \cdot \dot{E}_{el}^{COGEN} \in [100, 600]$ kW _{el} . $C^{COGEN} = \frac{541.7}{390.6} \cdot 1.07 \cdot \left(\begin{array}{l} -0.0391 \cdot (\dot{E}_{el}^{COGEN})^2 \\ +850.89 \cdot \dot{E}_{el}^{COGEN} \\ +306016 \\ +125 \cdot (\dot{E}_{el}^{COGEN})^{0.8} \end{array} \right) \quad (5.18)$
					Boiler in place	$C^{BOI} = 0$
					Refrigeration in place	$C^{REF} = 0$
HEN cost estimation	C^{HEN}	\$ ₂₀₁₆	✓		General function	Installed cost function [236, 237] (CS-SS), updated with CEPCI [4], total HEN area estimation A [m ²] based on vertical intervals [99, 218], minimum number of heat exchangers N [-] is estimated based on graph theory [98]. $C(A, N) = \frac{541.7}{402} \cdot \left(8500 + 409 \cdot \left(\frac{A}{N} \right)^{0.85} \right) \cdot N \quad (5.19)$
					Investment of specific design	Installed cost of HEN area is estimated as difference from the reference plant theoretical investment cost, to approximate a retrofit design. $N^* = \max(N^{ref}, N)$ $A^* = \max(A^{ref}, A)$ $C^{HEN} = C(A^*, N^*) - C(A^{ref}, N^{ref}) \quad (5.20)$
Efficiency	η_r^w	%	✓		Compressors	$\eta_{el}^{COMP} = 60\%_{el}$ (min. [140], Table 4.1)
					Co-generation engine [140]	$\eta_{el}^{COGEN} = 37.5\%_{el}$ $\eta_{th}^{COGEN} = 49.5\%_{th}$
					Boiler [140]	$\eta_{th}^{BOI} = 90\%_{th}$
Lifetime	n	y		✓	Equipment	[10, 30]
Fuel consumption	\dot{E}_r	kW	✓		General	$\dot{E}_r = \dot{E}_r^w / \eta_r$ (5.21)
Exergy consumption	$\dot{E}_{ex,r}$	kW	✓		Electricity	$\dot{E}_{ex,el} = 1.0 \cdot \dot{E}_{el}$ (5.22)
					Nat. gas	$\dot{E}_{ex,ng} = 1.04 \cdot \dot{E}_{ng}$ (5.23)
Process data						
Product fraction	A,B,C1-4	-	(✓)			three cases depicted in Table 5.3
Product spec. requ.	\dot{Q}^{PROC}	kJ/kg	✓			Table D.7
Inlet mass flow rate	m_{raw}	kg/s	✓		raw milk inlet	10 kg/s
Environmental data						
Resource emissions	CO ₂	kgCO ₂ /kWh		✓	Electricity	[0.1, 1.1]
					Natural gas	[0.15, 0.25], general assumption if not otherwise stated 0.24 kgCO ₂ /kWh [169], 0.15 kgCO ₂ /kWh assuming partially biogas

Set of periods is $p \in \mathbf{P} = \{1\}$

Chapter 5. Generalization (A): heat pumping and co-generation

ture difference, temperature difference below which gas-cooling can be considered, preheating temperature difference (for dry fluids, which were not considered in this work), and three fluid indices (to consider cascaded cycles). The slave variables and objective function were introduced (in Section 5.2.3.2). A set of heat pump specific parameters were also introduced to constrain the compression ratio, number of compressors per fluid cycle, and compressor size.

Table 5.5 – Variables and objective function of the problem.

Description	Symbols	Range	Unit	ε -constraint	weighted sum of objectives
<i>Master level</i>					
Objective function	$f_{\text{master}}^{\text{obj}}$	$\{C^{\text{INV}}, \dot{E}_r\}, r \in \mathbf{R}$	div.	✓	✓
<i>General variables</i>					
Min. approach temp. diff.	$\Delta T_{\text{min}}/2$	{2,3,5}	K	✓	✓
Max. consumption of resource r (Eq. 5.6)	$c^{r,\text{max}}$	{0,1}	-	✓	X
TAC weighting fraction (Eq. 5.8)	ξ	{0.05,0.1,0.2,0.5,0.6,0.7,0.8,0.95,1}	-	X	✓
Electricity price (Eq. 5.8)	c_{el}	{0.01,0.1,0.2,0.5,0.8,1,2,5}· c_{ng}	\$/kWh	X	✓
Nat. gas price (Eq. 5.8)	c_{ng}	{0.06}	\$/kWh	X	✓
Plant index	x	{1,2,3}	-	✓	✓
<i>Heat pump superstructure (HPS) specific variables</i>					
Saturation temperature	$T_i = T_{i+1} + \Delta T_i$				
	ΔT_1	{5,5.5,...,50}	K	✓	✓
	ΔT_2	{5,5.5,...,50}	K	✓	✓
	ΔT_3	{5,5.5,...,50}	K	✓	✓
	ΔT_4	{5,5.5,...,50}	K	✓	✓
	T_5	{-35,-34.5,...,50}	°C	✓	✓
Subcooling temperature difference	$\Delta T_{1,SC}$	{0,1,...,30}	K	✓	✓
	$\Delta T_{2,SC}$	{0,1,...,30}	K	✓	✓
	$\Delta T_{3,SC}$	{0,1,...,30}	K	✓	✓
	$\Delta T_{4,SC}$	{0,1,...,30}	K	✓	✓
Gas-cooling temperature difference	$\Delta T_{i,DSH}$	$\begin{cases} T_{i-1} - T_i, & DSH == 1 \\ 0, & \text{else} \end{cases}$	K	✓	✓
De-superheating condition	DSH	{0,1}	-	✓	✓
Preheating temperature difference	$\Delta T_{i,PRE}$	0	K	✓	✓
Fluid index	d_1	{1,...,9}	-	✓	✓
	d_2	{1,...,9}	-	✓	✓
	d_3	{1,...,9}	-	✓	✓
Fluid set	\mathbf{F}	{NH3,H2S,PROPANE, PROPYLENE,R161 R404A,R410A,R507A,R41}		✓	✓
<i>Slave level</i>					
Objective function	$f_{\text{slave}}^{\text{obj}}$		div.	$C_{\text{slave}}^{\text{INV}}$	wC^{TAC}
Constraints (additional)	Resource constraint	$f_p^r \leq f^{r,\text{max}} \forall r \in \mathbf{R}$		✓	X
<i>Variables</i>					
Multiplication factor of techn. w during p	f_p^w	{ $f^{w,\text{max}}, f^{w,\text{min}}$ }	-	✓	✓
Use factor of techn. w, p	y_p^w	{0,1}	-	✓	✓
Maximum multiplication factor	f_p^w	$\geq f_p^w \forall p \in \mathbf{P}$	-	✓	✓
Overall use factor	y_p^w	$\geq y_p^w \forall p \in \mathbf{P}$	-	✓	✓
<i>HPS parameters</i>					
Compressor isentropic efficiency	$\eta_{\text{isentropic}}$	0.6	-	✓	✓
Minimum temperature difference	$\Delta T_{\text{min}}/2$	2	K	✓	✓
Min/max compression ratio	$CP^{\text{min,max}}$	{1,2,7}	bar/bar	✓	✓
Min/max valve differential pressure		{0.5,18}	bard	✓	✓
Min/max compressor power		{10,500}	kW	✓	✓
Maximum number of compressors per fluid d		2	-	✓	✓
Maximum number of compressors per HPS		4	-	✓	✓

5.4 Results and discussion

5.4.1 Comprehensive solution space generation

5.4.1.1 Solution generation

The results from the multi-objective optimization problem introduced in Section 5.3.2 and 5.3.3, are depicted as surfaces of non-dominated solutions in Figure 5.9 and Figure 5.10. The discontinuities in the surface are created by the binary variables related to activation and deactivation of units. It can be observed that the ϵ -constraint method shows a more uniform distribution of solutions compared to the weighted sum of objectives method. This was attributed to the brute-force nature of the constrained optimization. The weighted sum objective function method generated more feasible points, though the position cannot be controlled to explore specific regions of the solution space.

The resource plane⁴ reveals a non-dominated frontier between the natural gas and electricity consumption. It marks the limit of the feasible solution space. Considering conventional technologies, this line cannot be breached. Several solutions using the weighted objectives method are closer to the infeasibility frontier, though at higher capital expenses. The original plant with its reference consumption is marked at highest total resource consumption with zero capital cost. Every other solution improves either the electricity or natural gas consumption. Determining the preferential optimization approach requires a more detailed analysis to evaluate the homogeneity and frequency of solution occurrence in the distribution of solutions as discussed in Section 5.2.3.3. Solution pruning was thus applied on the solutions generated here.

⁴ The resource plane refers to the plane formed with the two types of resource consumption as axes, and hence spans the natural gas and electricity consumption.

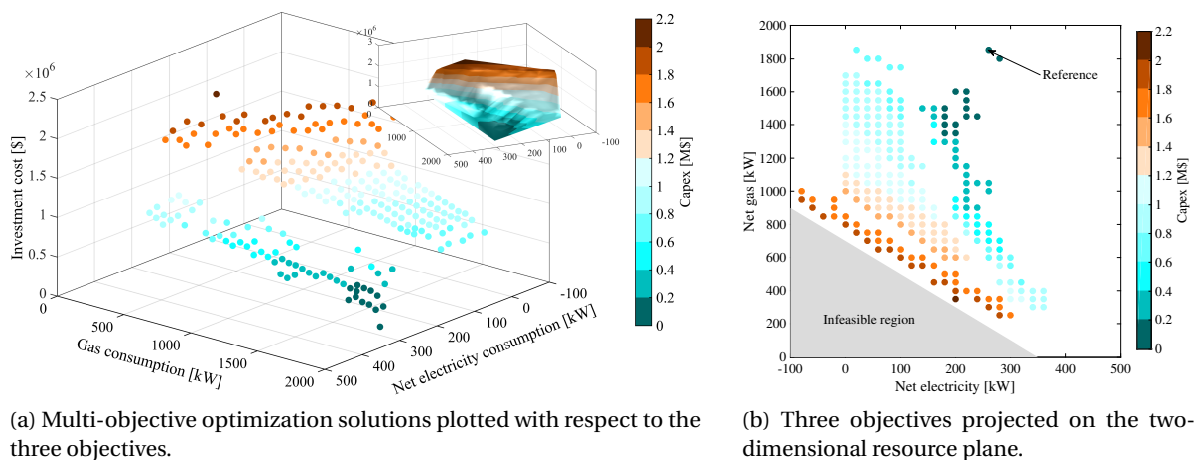


Figure 5.9 – ϵ -constraint case: results from multi-objective optimization of plant 2.

Chapter 5. Generalization (A): heat pumping and co-generation

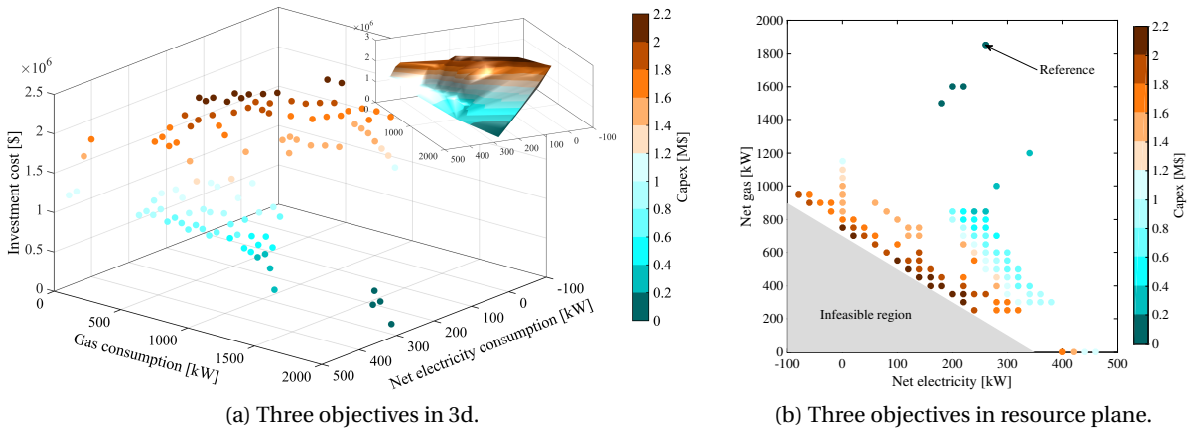


Figure 5.10 – Weighted sum of objectives: results from multi-objective optimization of plant 2.

5.4.1.2 Solution pruning

For each sample of free input parameters, a different set of minimum TAC solutions with respect to their emissions was found. To identify the most recurring solutions, the free parameters indicated in Table 5.4 were sampled based on the proposed ranges and the minimum TAC indexes were stored. Figure 5.11 shows the occurrence of all minimum TAC solutions selected during the sampling step. Relatively few solutions are never selected and therefore discarded. The encircled points mark the 99% most recurrent solutions. On closer investigation of the sampling results, it can be observed that a great number of solutions selected as minimum TAC points (even in the 99% most recurrent) during the sampling of the constrained optimization are not present in the weighted results. The solutions which are common to both approaches exhibited lower investment cost for the constrained optimization. Hence, the ϵ -constraint optimization approach was selected for future applications.

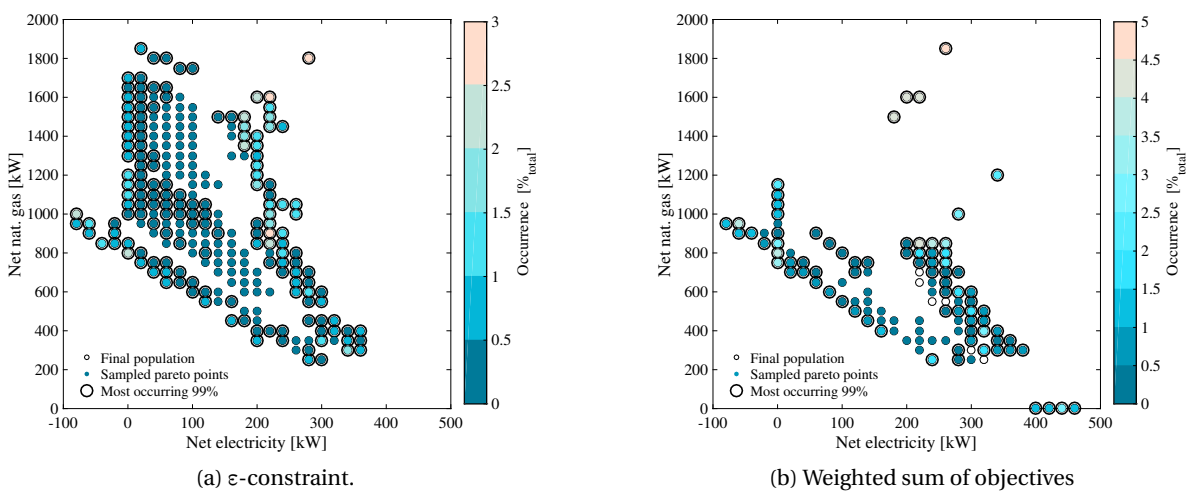


Figure 5.11 – Occurrence of minimum TAC solutions during the sampling of plant 2.

The selected solutions are depicted in Figure 5.12 and Figure 5.13. Figure 5.12a displays the exergy efficiency of the selected solutions (of plant 2) in the resource plane, highlighting that the exergy efficiency of the solutions is strongly linked to the net electricity import. This was explained by the high exergy value attributed to electricity, which neglects the generation process and hence creating a small bias. This bias could be avoided by considering the electricity generation, though this is highly dependent on the location of the plant and hence cannot be treated in the generalized solutions generated in this work.

The utility selection of plants 2 and 3 are shown in Figures 5.12b and 5.12c, respectively. The solutions without additional utility integration (apart from the utilities in place) are found at the upper right of the cloud of solutions, at highest resource consumption. From there, heat pump (hp) integration stretches toward higher net electricity consumption, while co-generation (cogen) towards lower electricity consumption. It has to be noted that the heat pump designs which are derived from the HPS, could be integrated at any temperature level (Table 5.5) by the optimizer. However, it can be observed that for lower capex solutions, the heat pump was placed across the process pinch, interacting with the milk concentration streams. The mechanical vapor re-compression (MVR) was never observed in low capex (high resource consumption) solutions due to imposed sizing limits which are related to the limited availability of process steam for MVR. In the case of plant 2, the MVR was activated with higher electricity consumption. Since plant 3 does not have a concentrated milk production unit, MVR was not activated. The lowest combined resource consumption was achieved with co-generation, mechanical vapor re-compression, and heat pumping.

The characteristics of these selected solutions of plant 2 were further analyzed in Figure 5.13 with respect to the exergy efficiency. Various trends can be observed. As expected the cooling water, natural gas, and boiler consumption decreased, while the electricity consumption increased with increasing exergy efficiency (dropping with the availability of co-generation, since co-generation generates electricity). The co-generation engine, as stated before, increased initially and then decreased with increasing exergy efficiency. Heat pumping was utilized with increasing exergy

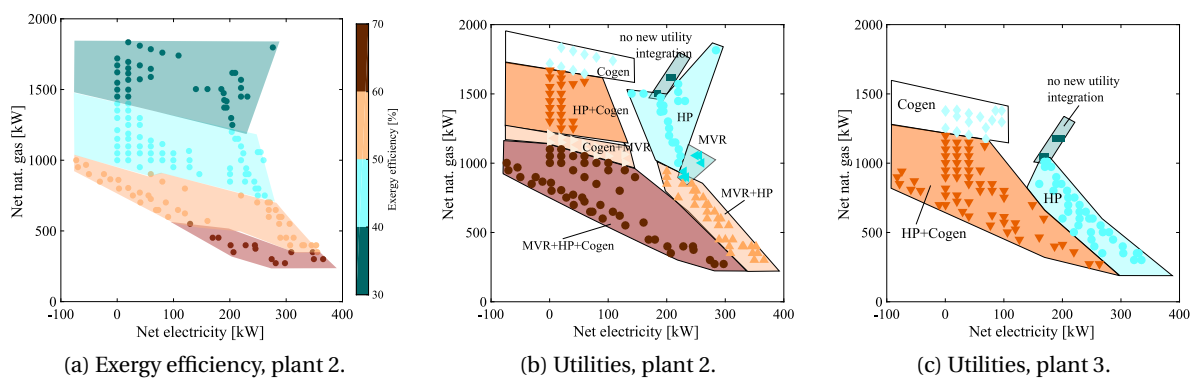


Figure 5.12 – Exergy efficiency and utility selection of selected plants.

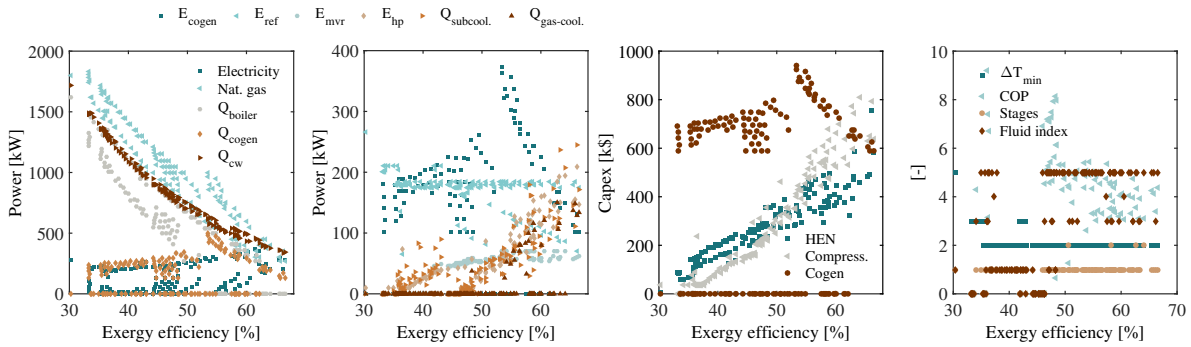


Figure 5.13 – Pruned solution characteristics, plant 2.

efficiency, until MVR was activated, at which point it restarted from zero. It is interesting to note that subcooling was always present when heat pumping was active. This indicates that sub-cooling is a favorable feature considering the balance between cost and performance. Gas-cooling, in contrast, was activated mainly in the high efficiency region which indicates that specific technologies need to be considered for reaching especially efficient operation.

The fluid indexes which were mainly used in the heat pump were 1, 3 and 5, corresponding to ammonia, propane and R161, respectively. Slight tendency toward higher indexes is observed with increasing exergy efficiency, which appears to be related to the temperatures and performance of the heat pumps.

Further, it can be observed that almost all solutions had a $\Delta T_{\min}/2=2\text{K}$ in the process heat exchangers, meaning that the first step in terms of cost and energy efficiency was to increase heat recovery in the process. These results are consistent with process integration principles. Assessing the economic feasibility may not support the same solutions, as the cost estimation functions applied may underestimate the real cost of a retrofit HEN, or that compressor costs may be overestimated⁵. Independent from uncertainty related to the capex, a general discomfort of modifying the HEN was observed across the industry. Therefore, plant 2 was re-assessed with fixed $\Delta T_{\min}/2=5\text{K}$, in order to compare the results. The data of all plants can be found in Appendix D.2.2.

5.4.2 Results retrieval

Once the database of solutions was created, various investigations could be conducted. Additional interest in this approach stems from the fact that this analysis can be carried out from different stakeholder perspectives.

⁵Feedback from the industry suggests that the compressor cost function overestimates especially large heat pumps, due to the high exponential.

5.4.2.1 Country analysis

As indicated in Figure 5.8, different countries are subject to a large range of resource prices, emissions associated with grid electricity, and bank lending rates. The goal in this section was to identify which political and operational boundary conditions were required to generate economically viable emission reduction measures in the dairy industry in different countries. So-called *utility maps* were created, which capture the best *economically viable* emission reduction measures based on different boundary conditions (operating time, CO₂ tax, electricity generation emissions). *Economically viable* was defined here as a payback time below three years. The least emitting solution below this payback time was selected. If no solution below three years payback time could be identified, the reference (marked as 0) was assumed.

Heat recovery improvement Figure 5.14 depicts the solutions and respective cost distribution and emissions of selected OECD countries of plant 2. The number indexes the solution id which can be found in Table D.3, Figure D.7a, and Figure D.9. One immediate result was that countries with the lowest resource prices (United States of America (US) and Canada (CA)) exhibited no economically viable solution for operating times of 2500 hours per year. When adding a CO₂ tax, it became profitable in CA to invest in the first emission reduction measures.

Solution 2 and 142 (143) were similar to the reference utility configurations with different a minimum approach temperature, $\Delta T_{\min}/2$, of 2K and 3K, respectively (143 - small difference in refrigeration cycle). Solution 1 represented a single-stage MVR added across the process pinch point to recover steam from the concentrated milk production (see Figure D.9). This can also be visualized in the resource price plane in Figure 5.15. The utility map reveals that with introduction of the CO₂ tax (20 \$/tCO₂), the line between reference and measures with no additional installed equipment moves toward lower resource prices. For the context of dairy plants operating in the US, this indicated that the CO₂ tax considered here was insufficient to incentivize owners to invest in reducing emissions given the imposed economic conditions. Increasing the operating time to 8000h led to a drastic increase in economically viable measures in all countries. Higher yearly operating expenses (opex) logically yielded decreased payback times (considering the same investment cost).

Overall, assuming 2500 operating hours, an average viable CO₂ emission reduction of 21% across the considered OECD countries could be achieved, which increased to 25% by adding a CO₂ tax. Higher operating hours logically incentivized investment in emission reductions; this is supported by looking at the case with 8000 h/y of operation where 55% and 58% emission reductions could be achieved in an economically viable manner without and with CO₂ taxes, respectively. A further improvement to 65% reduction was observed when assuming a CO₂ tax and tax incentives for the investor which amounted to 20% of the total investment. Co-generation became viable for countries with high resource prices and high electricity grid emissions, due to its high efficiency and comparatively low emissions. The background was plotted with an average grid emission

Chapter 5. Generalization (A): heat pumping and co-generation

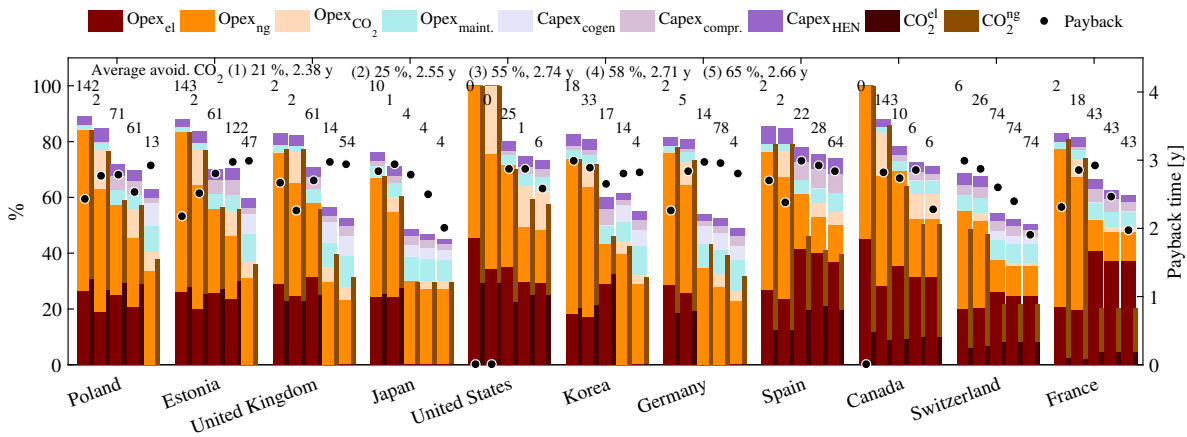


Figure 5.14 – Cost data, CO₂ equivalent emissions, plant 2. Five bars per country: (1) operating time 2500 h, tax 0 \$/tCO₂, (2) 2500 h, 20 \$/tCO₂, (3) 8000 h, 0 \$/tCO₂, (4) 8000 h, 20 \$/tCO₂, (5) 8000 h, 20 \$/tCO₂, 20% investment reduction through tax incentives.

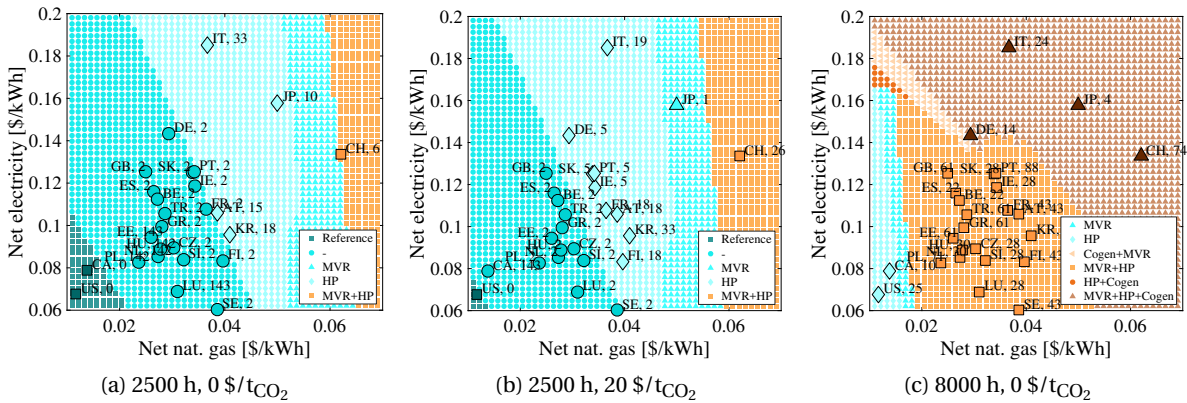


Figure 5.15 – Plant 2, utility maps with maintenance fraction 0.05, background: $\tau=0.08$, 0.5 kgCO₂/kWh_{el}.

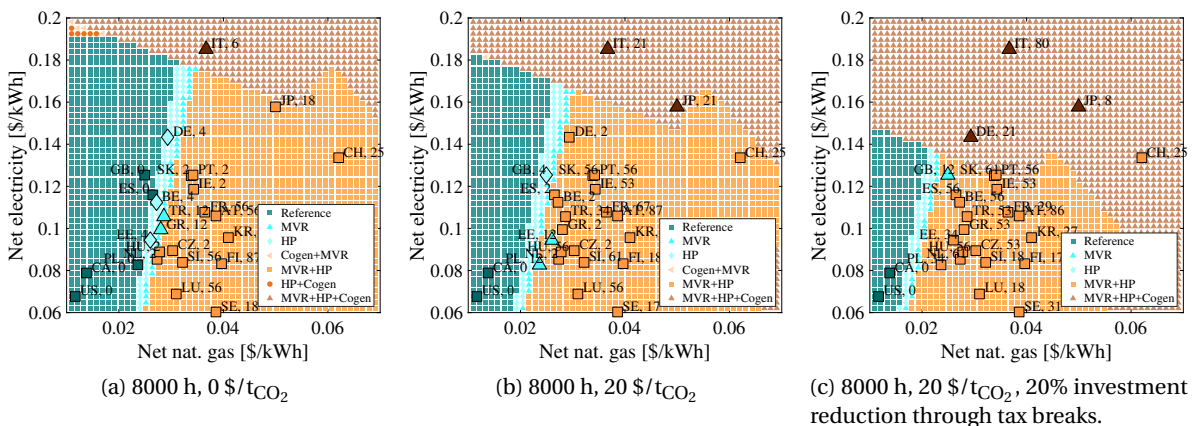


Figure 5.16 – Plant 2, $\Delta T_{\min}/2=5K$ fixed HEN, utility maps with maintenance fraction 0.05, background: $\tau=0.08$, 0.5 kgCO₂/kWh_{el}.

assumption of $0.5 \text{ kgCO}_2/\text{kWh}_{\text{el}}$, which explains the difference for several countries.

Fixed heat exchanger network (HEN) These promising results were all achieved by increasing the heat recovery in the process. Fixing the $\Delta T_{\text{min}}/2$ to 5K and thereby assuming that the process heat recovery system cannot be altered (even though it might be economically feasible), and thereby bounding the upper level of the exergy efficiency, leads to different results. Figure 5.16 depicts the results for 8000 operating hours, since the lower operating times do not generate economically feasible solutions (i.e. payback times are above three years). This is linked to the fact that a reduction in operating expenses cannot be achieved as "easily" (from an economical point of view) as by decreasing the ΔT_{min} . With 8000 operating hours (Figure 5.16a), the first economically feasible solutions were observed for natural gas prices above 0.025 \$/kWh. By adding a CO₂ tax, and investment cost reduction, the economically viable utility lines were pushed toward low resource prices. The ICCs of the economically viable solutions are shown in Figure D.10.

As mentioned before, plants with 2500 operating hours per year could not economically reduce CO₂ emissions given the technologies available. Operation for 8000 h/y could economically reduce 20% and 26% of the CO₂ emissions without and with CO₂ taxes, respectively, indicating that the CO₂ taxes have higher impact on less efficient systems with high opex. A further decrease to 31% was achieved by assuming a CO₂ tax and incentives for the producer which amounted to 20% of the total investment.

Synthesis Figure 5.17 depicts two solutions selected frequently during the countries' analysis with a fixed heat recovery network. Solution 21 consists of a MVR system and small heat pump which provides heat to the self-sufficient pocket, so that the MVR can be used at higher capacity. A co-generation system provided electricity, so that the net electricity requirement amounted to zero. The utility ICC of this solution may be misleading since the engine heat release through cooling water which accounts for more than half of the heat released by the engine is not visible since it was directly transferred to the process. Table D.5 depicts the detailed data of that solution.

The heat pump did not create a utility pinch with the process grand composite curve (GCC) which reduced the HEN cost. The COP of the MVR system added up to 11.2, which corresponded to a second law efficiency of 58.2% due to the low temperature increment. The COP of the heat pump (HP) according to Equation 5.16 was calculated to be 7.8, corresponding to a second law efficiency of 57.2%. The overall exergy efficiency of the system was 36.9%.

Solution 27 comprises a MVR and a HP, which was operated from sub-ambient (replacing part of the refrigeration cycle) to above the process pinch point. Subcooling at two points increases the COP reaching 3.0 (which is equivalent to a high second law efficiency of 63.8% achieved through extensive sub-cooling). The system overall exergy efficiency was 45.0%, due to a strongly reduced natural gas consumption compared to solution 21 (see Table D.5).

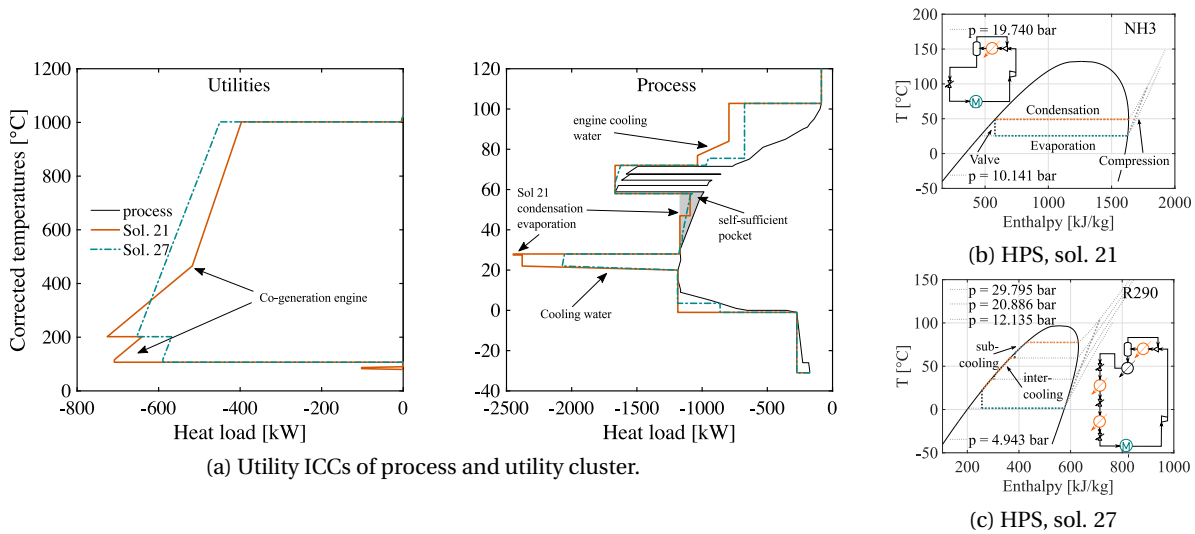


Figure 5.17 – Most occurring solution of ε -constrained objective of plant 2, $\Delta T_{\min}/2=5\text{K}$ fixed HEN; (b,c) T-h diagrams of HPS.

Several intermediate conclusions may be drawn from this analysis. Firstly, it was shown that the selected solutions provided a wide range of system complexity, from improvement of the heat recovery system, to single-stage MVR systems (with and without sub-cooling) and multi-stage HPS systems (illustrated in Table D.5). A decision-making process was suggested which was based on commonly accepted KPIs such as payback time and emissions.

Political incentives, such as CO₂ taxes and tax breaks for investment in emission reduction measures could increase the economically viable emission reductions from an average of 56% to 67% for an average plant (including concentrated milk production Figure 5.14, Figure D.8a) in the investigated OECD countries (assuming 8000 operating hours). In plants, which do not contain a concentrated milk production unit the numbers were slightly lower (46% to 54%, Figure D.8c). If a fixed process heat recovery network was considered, these numbers were distinctly lower (20% to 31%, Figure D.8b) for the analyzed plant (with milk concentration unit), though the relative effect of political incentives was drastically increased.

The analysis could be used by policy-makers aiming at understanding market drivers which lead to less-emitting industry, or by equipment manufacturers aiming to identify their potential markets. The following section addresses both these issues at more depth.

5.4.2.2 Decision-making platform

This section presents the decision-making platform and providing exemplary analysis from different stakeholder perspectives. The platform is available on-line and contains the solutions of all plants presented in the previous sections. It can be found in [242] and provides the minimum TAC points for each range of emissions of each input parameter sample (depicted in the first seven bars) consisting

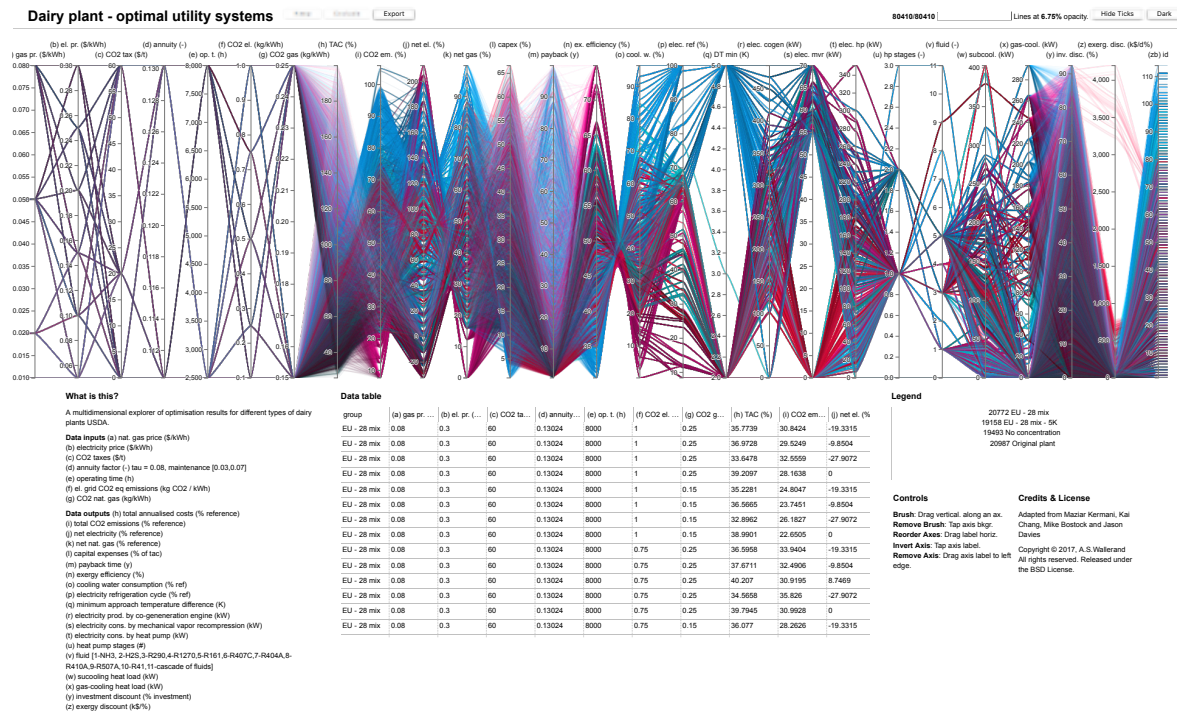


Figure 5.18 – On-line decision making platform [242].

of resource prices, CO₂ taxes, annuity⁶, operating time, resource emissions (electricity, natural gas⁷). The different plants are marked in different colors and can be (de-)activated in the legend. Different parameter samples can be selected with help of the sliders and the resulting data can be exported.

The next paragraph provides the motivation for selecting the minimum TAC points for their emissions, and discusses the influence of political actions on the economic viability of the solutions. The data shown in each of following paragraphs can be found in the decision making platform.

Political actions Figure 5.19 shows the influence of different political actions on the viability of emission reduction measures. The minimum TAC solution for each emission reduction and the respective payback time is depicted for plant 2 in three different countries with fixed $\Delta T_{min}/2$ of 5 K. The lowest payback time was achieved in many cases at higher emissions than the lowest TAC. This justifies why the entire range of minimum TAC solutions were taken into account, and not only the non-dominated Pareto frontier between TAC and emissions. It could be observed that the payback time for solutions close to the reference was quite low (due to low investment costs) and then increased (with another potential decrease). Five different cases in three different countries were investigated ranging from 2500 operating hours to 8000 h with CO₂ taxes of 0, 20 (with and without investment cost reduction of 20% through tax incentives), and 60 \$/tCO₂. It could be observed that political measures had less influence in Switzerland, which had the highest resource prices, than in

⁶The annuity [1/y] is defined as the sum of the annualization factor, τ , and the maintenance fraction, m.

⁷Two options were provided for natural gas: 100%_{mol} fossil gas: 0.25 kgCO₂/kWh [169]; 40%_{mol} biogas: 0.15 kgCO₂/kWh.

Chapter 5. Generalization (A): heat pumping and co-generation

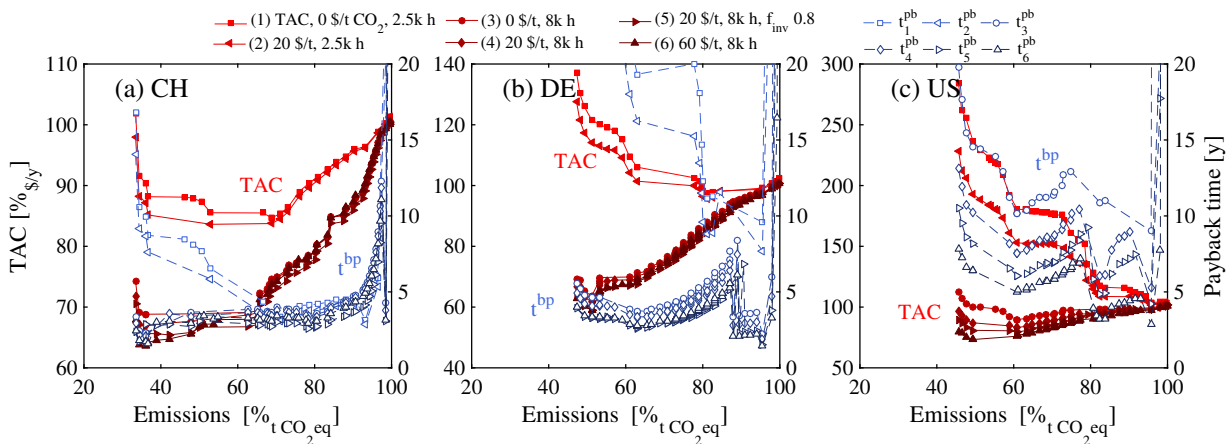


Figure 5.19 – Minimum TAC solutions and respective payback time. Influence of political actions on economically viable solutions, plant 2, $\Delta T_{\min}/2=5\text{K}$, 8000h.

the other countries. Political measures in Switzerland (CH) reduced the payback time by a maximum of 1.5 years. This impact, however, may influence the success or failure of a project. For 8000 h, the tax incentive of 20% of the total investment generated in general the lowest payback times followed by 60 \$/tCO₂ especially for high emission reductions.

In the United States of America, where the resource prices are extremely low, the CO₂ taxes (especially 60 \$/tCO₂) had a strong impact, meaning that the payback time was reduced by 5 to 10 years. This could be easily explained by the fact that the CO₂ tax can be understood as an absolute increase of the resource prices⁸, and hence is equivalent to increasing the natural gas price in the US by 100%, whereas in CH, the relative increase is only 20%.

In conclusion, CO₂ taxes have distinctly higher impact in countries with low resource prices, while to achieve a change in countries with high resource prices, tax breaks may be a good incentive.

Plant operators and heat pump manufacturers One goal of this work was to allow pre-feasibility assessment based on the generated results, which is illustrated in this section. The solutions discussed during the political actions, are further depicted in Figure 5.20 (without incentives for 8000 h). Negative values in the opex arise from the export of electricity. It can be seen that in CH, for example, in a plant of type 2 one of the first emission and cost reduction measures is installation of a co-generation engine, since the electricity prices were relatively high. For high emission reductions in CH, the co-generation engine should be phased out in favor of investing in a more complex heat pump system and, hence, in compressors due to the fact that the electricity grid emissions were very low. These solutions also generated the lowest payback times which coincided with the minimum TAC points. Therefore, from the perspective of plant operators and heat pump manufacturers, heat pumps are worth considering for dairy plants (of type 2) in Switzerland, should be one conclusion

⁸For natural gas (0.24 kgCO₂/kWh): 20, 60 \$/tCO₂ leads to 0.005, 0.014 \$/kWh; for electricity (assuming 0.5 kgCO₂/kWh): 0.01, 0.03 \$/kWh

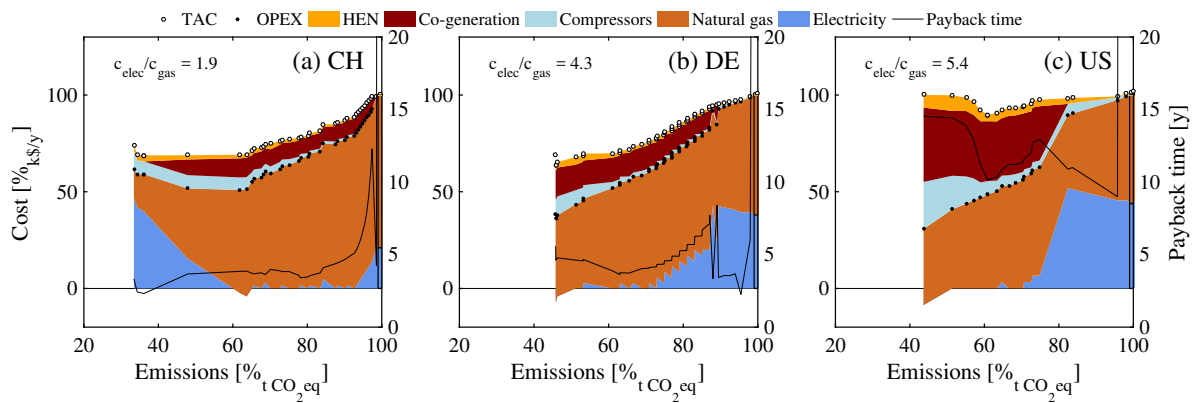


Figure 5.20 – Detailed cost data versus CO₂ equivalent emissions for min(TAC) points, plant 2, 0 \$/tCO₂, ΔT_{min}/2=5K, 8000h.

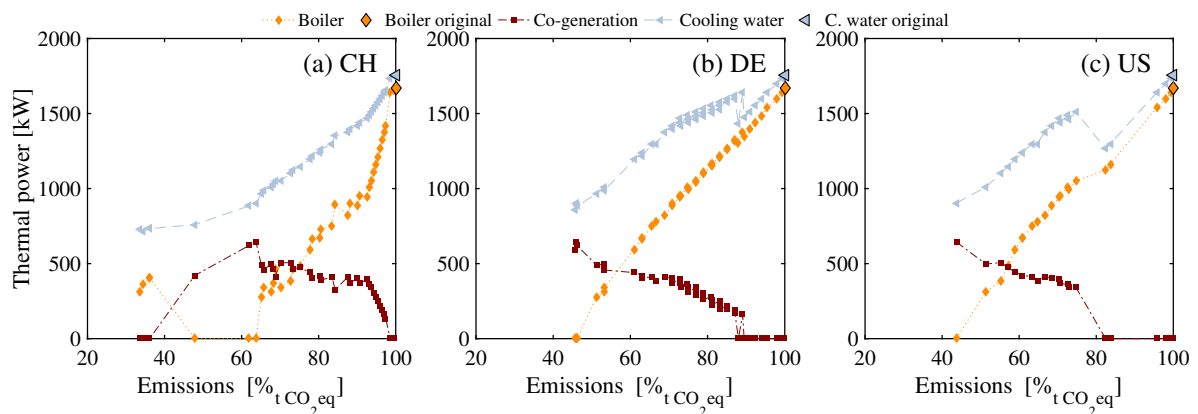


Figure 5.21 – Boiler, co-generation engine and cooling water loads versus CO₂ equivalent emissions for min(TAC) points, plant 2, 0 \$/tCO₂, ΔT_{min}/2=5K, 8000h, solution id in black.

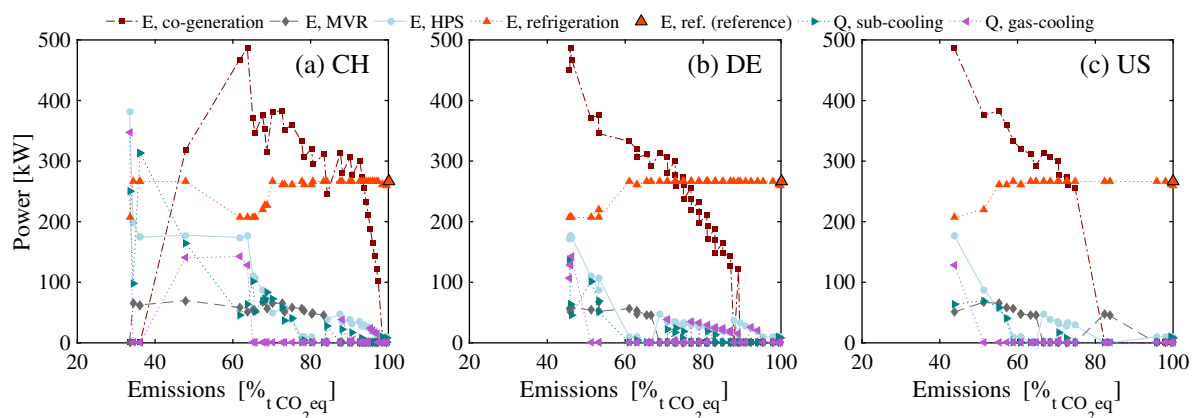


Figure 5.22 – Electrical power loads (and heat pump data) versus CO₂ equivalent emissions for min(TAC) points, plant 2, 0 \$/tCO₂, ΔT_{min}/2=5K, 8000h.

drawn from this pre-feasibility assessment.

In Germany (DE) and the US, the highest emission reductions were actually achieved with co-generation and heat pumping, due to the high electricity grid emissions. Interestingly, in both DE and US, the minimum payback time did not coincide with the minimum TAC cost. The minimum payback time was found close to the reference consumption suggesting a small heat pump (10 kW_{el}) installation across the pinch point. It is arguable as to whether such a small installation is worthwhile achieving a mere emission reduction of less than 5%. At lower emissions (60% compared to reference) another low payback time can be observed (in both countries). As shown in Figure 5.22, these solutions required installation of a MVR across the process pinch and of a co-generation engine. Applying CO₂ taxation at the level of 20 \$/tCO₂ would make these solutions more attractive (payback time of 4 years in DE and 8 years in the US). The HEN cost of all solutions was comparatively small, since the process $\Delta T_{\min}/2$ was fixed to 5K, and only the utility integration needed to be accounted for.

Figure 5.21 and Figure 5.22 illustrate the thermal, electrical power and exergy efficiency of various equipment in these solutions. As noted previously, the exergy efficiency shows an inversely proportional relationship with the cooling water consumption. Figure 5.22 reveals that gas-cooling was present in various minimum-cost solutions and subcooling even more so. Due to the size limitation of the MVR unit, heat pumping was the first unit to be activated together with the co-generation unit (in CH). The refrigeration cycle (in place) was typically operated at its reference size, only high emission reduction solutions showed heat pumping interfering with the operation of the refrigeration cycle to create better system efficiencies.

5.5 Conclusions

How can the results be extrapolated to a wider scope?

This chapter presented a methodology for the generation of a database of optimal utility solutions for industrial processes, independent from the most volatile (cost related) input data. The method was applied to heat pumping and co-generation in the dairy industry. A modular dairy plant was presented and three dairy plant types were analyzed with environomic boundary conditions of various OECD countries. The generated data was discussed at great length from the perspective of multiple stakeholders. A parallel coordinate on-line decision-making platform was introduced which grants access to the publicly-available database encompassing a detailed utility design of each solution and performance data for various contextual parameters, which enabled a cost-free pre-feasibility assessment of emission reduction measures.

The results indicated that heat pumping contributes to emission reductions and increases exergy efficiency in the dairy industry, independent from location until a certain threshold. If emissions

must be reduced beyond that point, the CO₂ equivalent emissions of the grid electricity in the specified location have a great influence. The outcome of the optimization further indicated that internal heat recovery should be the first step for efficiency and emissions reduction at lowest capex. Restructuring the HEN of a plant may not be a practicable solution and thus plants with fixed HEN were also investigated. It could be demonstrated that the operating time and energy resource prices drastically influenced the economic viability of emission reduction measures. Political incentives, such as CO₂ taxes and tax breaks for investment in emission reduction measures could increase the economically viable emission reductions from an OECD average of 20% to 26% and 31%, in the least favorable case of a fixed process heat recovery network. These are equivalent to 30% and 55% increase in viable emission reduction measures achieved through a CO₂ tax of 20 \$/tCO₂ without and with 20% tax breaks on the investment, respectively. It was found that CO₂ taxes had distinctly higher impact in countries with low resource prices, while to achieve a change in countries with high resource prices, tax breaks might be a better incentive.

The methodology provides a wide range of applications and valuable insights for multiple stakeholders. The main limitation of the presented approach is identified as the fixing of the equipment investment cost, which are uncertain values and may have an influence on the utility selection. In future work this may be addressed by re-calculating the investment cost with varying cost functions, or using stochastic programming.

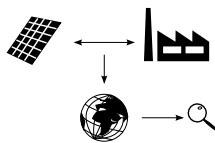
Generalization (B): addition of solar utilities

6

Overview

- Extension of the methodology developed in Chapter 5 to include solar utilities
- Potential analysis of solar utilities, heat pumping, and co-generation in the overall dairy industry
- Results allow determination of solar break-even costs

Chapter 5 & 6:
Generalization



This chapter is based on Wallerand et al. [243]

Potential studies aim at identification of the total energetic, economic, and/or environmental potential of certain technologies in specific sectors or industries, at a regional, national, or global level. The derived results may be used by multiple stakeholders to generate policy strategies [72], or to identify sectors and regions most viable for installation of certain technologies [67]. The methodology derived in the previous chapter adds a further dimension to the available literature: Through generation of a publicly available database of detailed solutions plant-operators are enabled to conduct cost-free pre-feasibility assessment, while equipment manufacturers gain insights of the potential of specific technological features in certain industries and under different environmental and economic (environomic) conditions.

This chapter presents an extension to the methodology presented in Chapter 5 taking into account solar utilities. The methodology presented in Chapter 5 is based on generalized multi-objective optimization stripped of all location-dependent input parameters. Therefore, it is assumed that the specific investment cost of conventional utilities does not depend on the location. This assumption cannot be applied to solar utilities, since the required installed capacity needed to satisfy a fixed constant load depends strongly on the location and its available yearly irradiation.

After a state-of-the-art analysis of current potential analysis methods for solar energy for industrial processes (SEIP) applications, this chapter presents an extension to the potential analysis presented in Chapter 5, in the methodology section. For illustration, the method is applied to the dairy industry in the results and discussion section.

6.1 State-of-the-art

The studies discussed in this section are compared in various points in Table 6.1. The potential studies are distinguished between bottom-up and top-down approaches.

6.1.1 Top-down

Classical top-down approaches are presented by Brown et al. [66], Beath [67], and Lauterbach et al. [68], in which the total energy demands of different industrial sectors at the national level were estimated, categorized by temperature levels, and matched with solar technologies. Some went as far as identifying industrial clusters in specific regions and matching those with the annual irradiation [66, 67]. Sharma et al. [69, 70, 71] presented a more detailed methodology in which the plants associated with certain sectors were individually identified, classified by their hot utility type (boiler or co-generation). The solar systems were then sized by plant capacity and the annual CO₂ emission mitigation potentials were derived.

6.1.2 Bottom-up

A bottom-up approach was published by Murray [244] who discussed the theoretical potential and conceptual integration for highly concentrated solar thermal systems in the primary aluminum industry concluding that integration would be difficult. A more applied study was introduced by Schweiger et al. [56] who presented a potential analysis and design of solar heat for industrial processes (SHIP) applications in Spain (ES) and Portugal (PT) through steam production and integration with conventional utility systems based on selected examples. Calderoni et al. [72] considered three textile plants and estimated the economic feasibility of solar integration and the key drivers enabling economic viability. The solar modeling approach was unfortunately not specified.

Müller et al. [148] derived a methodology to estimate the potential for solar heat integration in the liq. food industry in general and in specific plants based on the available land area, the process temperature levels, and an annual average of the specific solar production. Meyers et al. [73] compared solar (non-concentrating) thermal system (ST) with photovoltaic module (PV) systems combined with resistance heating for a fixed process load, which is an exergetically inefficient way to provide heating. Based on a regression model, the results were extrapolated to various meteorological conditions to derive the break-even cost based on current and future specific project investment costs.

Table 6.1 – State-of-the-art summary of potential estimation studies for SEIP applications.

Author	Year	Foc	Appr	Obj	Vars	Siz.	Econ.	Solar modeling				Proc. m.		SC	Process	Uti.	Description.
								M	dT	Tool	Stor.	PA	HEN				
<i>Current work</i>	2018	SP-I	D,Pb	E	C	M - GA	✓	S	year	MEB	(✓)	✓	X	various	dairy	Co-gen., HP	Bottom-up optimization-based potential analysis for estimation of solar, co-generation and HP in low-temp. industries.
Meyers et al. [73]	2018	SP	M,Pb	E	C	B	✓	D,S	year,	R,	✓	X	X	various	-	-	Method for cost comparison between solar thermal and photovoltaics via resistance heating based on regression model for (kWp/m ²).
Brown et al. [66]	1980	SP-A	Pt	TP	LOC,L	C	✓	S	year	MEB	X	X	X	PT	various	-	End-use matching analysis of parabolic trough collectors with industrial process heat.
Murray [244]	1999	SP-A	Pb	TP	energy	C	X	-	-	MEB	-	X	X	CSE)	aluminum	-	Conceptual analysis of potentials for highly concentrating solar heat in the primary aluminum industry.
Schweiger et al. [56]	2000	SP-A	Pb,D	TP	C, T	B	✓	S	year	MEB	X	X	X	various	various	-	Potential analysis and design of SHIP in ES and PT through steam production and integration with conventional utility system.
Beath [67]	2012	SP-A	Pt	TP	location, load	C	X	S	year	MEB	X	X	X	various	various	-	Top-down analysis of industrial heat demand, temperature ranges, and location, matched with solar availability in Australia.
Calderoni et al. [72]	2012	SP-A	A,Pb	E	-	F	✓	S	-	-	✓	X	✓	PT	textile	-	Economic feasibility study of solar-assisted process plants in Tunisia.
Lauterbach et al. [68]	2012	SP-A	Pt	TP	load	C	X	S	-	-	X	X	X	various	various	-	Top-down analysis of industrial heat demand, temperature ranges in DE.
Müller et al. [148]	2014	SP-A	Pb	TP	FD,L	C	X	S	year	MEB	✓	X	X	various	food (liq.)	-	Methodology: how to estimate the potential for solar heat in the liq. food industry, based on available area, and temperature levels.
Sharma et al. [69, 70]	2016	SP-A	Pt,D	TP	SF	C	X	S	year	MEB	X	X	X	PT	paper	Co-gen.	Potential analysis of solar heat for paper industry in India, considering solar sizing (by capacity), location, and co-generation.
Sharma et al. [71]	2017	SP-A	Pt,D	TP	SF	C	X	S	year	MEB	X	X	X	PT	dairy	-	Potential analysis of solar heat for dairy industry in India, considering solar sizing (by capacity) and locations of plants.

Focus: Solar (S), Solar integration to urban system (SU), *SP, SP-A, SP-I* based on notation presented in the introduction Section, Figure 2

Approach: Design (D), modeling (M), analysis (A), potential (P), review (R), empirical (E)

Objective: Thermodynamic principles (TP), economic (E), thermoeconomic (TEP), technical (T)

Variables: temperature (T), collector area (C), storage size (S), load (L), irradiation (IRR), field design (FD), solar fraction (SF), location (LOC)

Sizing: Fixed (F), brute forcing (variation of parameters, identification of maxima) (B), mathematical programming (M - genetic algorithm (GA) - sequential quadratic programming (SQP)), conceptual methods (C), R-curve analysis (R), analytical (A), polynomial regression (PR)

Economic (Econ.): economics considered in study (✓/X)

Modeling (M): (Quasi-) static (S), dynamic (D)

Time discretization (dT): instantaneous (ins.), variable time step (VST); horizon: unless stated differently: yearly analysis

Tool: Mass and energy balances (MEB), design space method (DSM), regression (R), measurements (MEA)

heat exchanger network (HEN): ✓ - full HEN design (analysis), (✓) - focus on identification of relevant HEX for solar integration, X - no specific HEN design

Solar collector types (SC): Evacuated tube collectors (ETC), flat plate (FP), power tower heliostat field (HPF), parabolic trough (PTC), flat plate photovoltaic and thermal systems (PVT), compound parabolic concentrator (CPC)

6.1.3 Discussion and contribution

The state-of-the-art analysis can be summarized in four main points.

1. Top-down approaches provide estimations of the general potential for solar energy in certain industrial sectors and geographical regions. However, the results are coarse and some options may be overlooked.
2. Bottom-up approaches aim at derivation of profitability of solar integration measures in specific sectors. The studies presented in the literature either focus on the solar system or on the industrial process, but do not consider them in a combined framework.
3. Current literature focuses on conceptual approaches. A lack of systematic potential studies applying rigorous methods (such as mathematical programming) is found.
4. A gap is identified for a bottom-up approach which considers both the process and solar system, as well as a wider set of utilities and integration options, to identify relationships between energy prices and utility selection at a national or international level.

This work attempts to close the gaps mentioned in (3-4) by expanding a bottom-up method for estimating the general environomic potential of conventional technologies (heat pumps and co-generation) in industrial processes to consider solar technologies. This requires a complex post-computational framework including parameter sampling.

The method includes enhancing the databased of solutions generated in Chapter 5 with various solar technologies, identification of solar system break-even cost, and specific potential estimation. Based on user-selected input criteria, case-specific solutions are drawn from the database and investigated. The data would be accessible via an on-line parallel coordinates decision-making platform (which is in planning). The presented method illustrates, how specific solar performance models can be generalized to provide indication for industries in various countries.

6.2 Methodology

6.2.1 Problem statement

Since the method presented here is an extension to the method introduced in Chapter 5, the same research questions can be formulated as depicted in Section 5.2.1. Additionally, the following questions are derived.

Problem statement*Given*

- (A) certain industry/process, a geographical region
- (B) set of solar technologies

Determine

- (A) technologies and costs
 - solar technologies, which bring the highest emission reductions
 - break-even cost of each solar technology
- (B) economically viable emission reduction potential and measures

6.2.2 Derivation

As mentioned before, the methodology presented in Chapter 5 is based on generalized multi-objective optimization stripped of all location-dependent input parameters. Therefore, it was assumed that the specific investment cost of conventional utilities do not depend on the location. This assumption cannot be applied to solar utilities for obvious reasons.

Therefore, another approach is suggested to account for solar utility contribution. If a correlation between collector area and the solar fraction can be identified, multi-objective, multi-period specific optimization can be avoided and the solar utilities contribution could solely be accounted for in a post-computational step based on the desired solar fraction and performance solar parameters. The solar fraction, f^{ws} [-], is defined as the fraction of energy that the solar utilities provide to the process compared to what the is the actual process (thermal or electrical) requirement, as shown in Equation 6.1.

$$f^{ws} = \frac{\dot{E}^{ws}}{\dot{E}^{\text{PROC}}} \quad (6.1)$$

The solar fraction can be defined instantaneously, or based on a maximum day. In this work, it refers to the average solar contribution over the whole year, \dot{E}^{ws} [kW], with respect to the average process requirement, \dot{E}^{PROC} [kW].

In order to study the optimal solar collector area for different solar fractions, the ϵ -constrained mixed integer linear programming (MILP) model for flat plate collectors with thermal storage, presented in Chapter 3, was run for various process operating hours and with different solar fractions. The results are presented in Figure 6.1a. As expected, it can be observed that with increasing process operating times, more solar collector area is required to satisfy the same fixed average contribution. And it can further be observed that the required solar area seems to follow a linear relation with the process operating time.

From this observation, an *intuitive correlation* presented in Equation 6.2 was derived and compared to the results. The correlation links the required solar utility collector area, A^{ws} [m²], yearly efficiency, η^{ws} [-], the yearly available solar radiation (GHI), \mathbf{g}_h [kWh/m²y], the constant process (thermal or electrical) requirement, \dot{E}^{PROC} [kW], and the process operating time, Δt^{PROC} [h/y], with the solar fraction, f^{ws} [-].

$$f^{ws} = \frac{\sum_{p \in \mathbf{P}} \mathbf{g}_{h,p} \cdot \eta^{ws} \cdot A^{ws}}{\dot{E}^{\text{PROC}} \cdot \Delta t^{\text{PROC}}} \quad (6.2)$$

The approximation of the collector area based on this correlation are shown in Figure 6.1a. A good agreement between the approximated collector area and the results from the detailed parametric optimization from Chapter 3 can be observed for solar fractions ranging from 0.1 to 0.3. The storage cost of the individual solutions (for solar fraction of 0.3) remains below 10% of the collector costs.

When increasing the solar fraction to 0.4 and 0.5 as shown in Figure 6.1b, the approximation given by Equation 6.2 drastically underestimates the solar collector area requirement derived by the MILP model. The discrepancy is linked to the fact that the *intuitive correlation* relies on a yearly average, therewith assuming a seasonal storage option. The MILP model, which relies on typical days, considers only daily storage. This is further illustrated in Figure 6.2 and Figure 6.3. For a solar fraction of 0.3, the storage in Figure 6.2 is mainly operated on days with high solar radiation, and the cooling water consumption is only increased on two typical days (one being the extreme day with occurrence 1). A forced solar fraction of 0.5 (Figure 6.3) results in a drastic increase of cooling water consumption due to the cyclic constraint of the storage unit (chapter 2.4.2) and the accompanying overproduction of the solar system.

Since a detailed model of seasonal storage is not available and the cost functions cannot be anticipated, it is recommended to use solar fractions below 0.4 for this type of problem.

The agreement between the *intuitive correlation* and the results from the multi-period MILP is promising, especially since the correlation does not rely on fitted data. For wider application, a cross-verification may be recommended, though. In this study, the results from the flat plate thermal collectors (FPs) are assumed to be applicable also to the high concentration photovoltaic and thermal system (HCPVT). Since, the photovoltaic modules (PVs) are operated without storage, the *intuitive correlation* for PV is assumed without limits on the solar fraction.

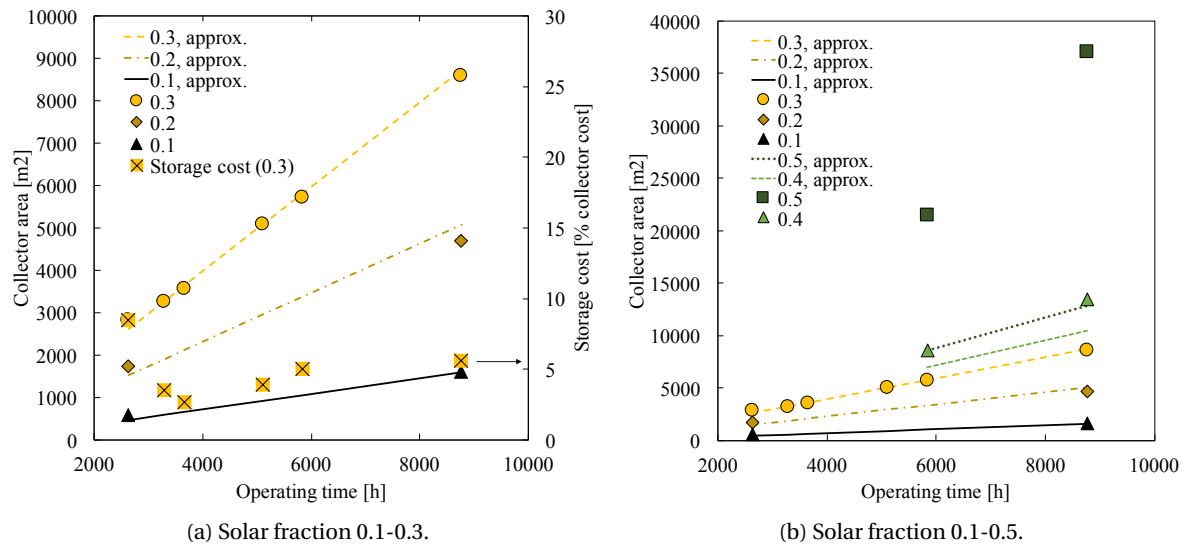


Figure 6.1 – Results from MILP in Chapter 3, flat plate collector area for different process operating times.

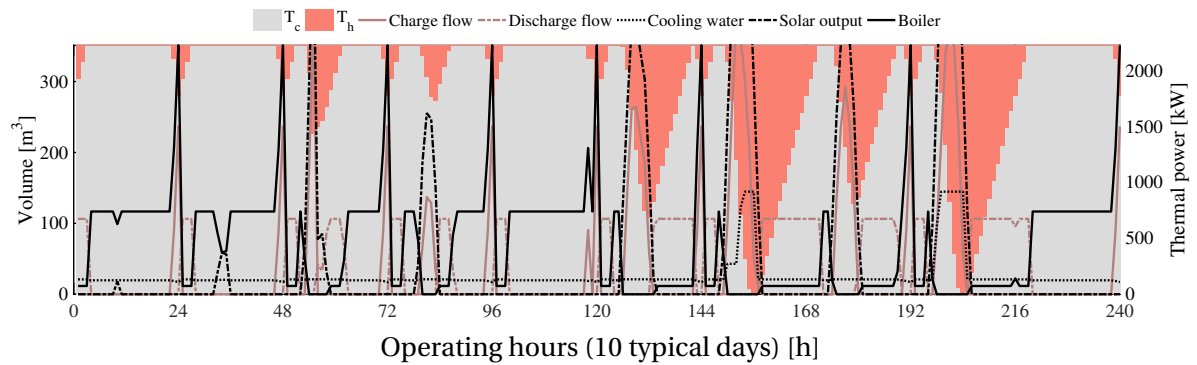


Figure 6.2 – Thermal utility operation for flat plate collector integration, from Chapter 3, non-stop operation, solar fraction of 0.3.

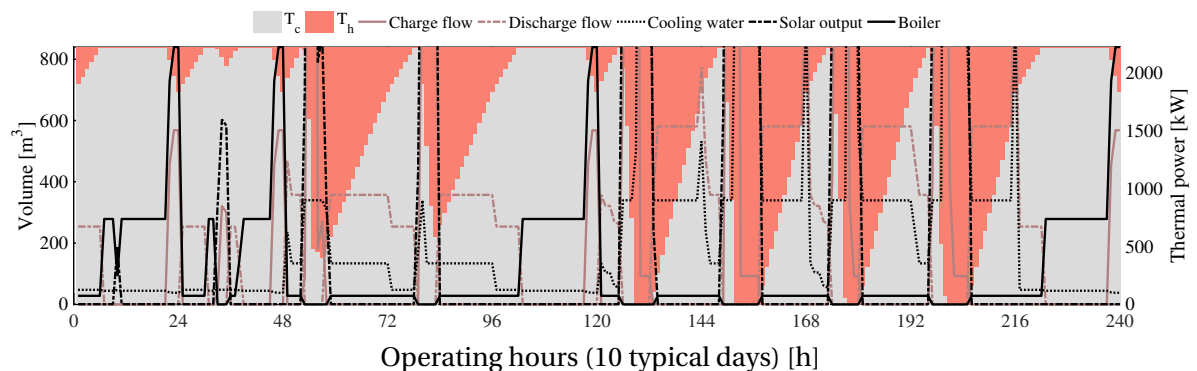


Figure 6.3 – Thermal utility operation for flat plate collector integration, from Chapter 3, non-stop operation, solar fraction of 0.5.

6.2.3 Approach

The analysis conducted in Section 6.2.2, forms the basis for the suggested approach. Figure 6.4 illustrates the method which aims at incorporating solar utilities into the database of solutions presented in Chapter 5. Therefore, the solar fraction and utilities under scrutiny need to be selected. With the selected solar fraction and utilities, the original database created in Chapter 5, is expanded. Each point in the database is thereby replicated for each solar technology considered and its data is re-calculated based on the selected solar fraction.

Photovoltaic module (PV) For installation of photovoltaic modules (PVs), the new net electricity consumption from the grid, \dot{E}_{el}^{GRID*} [kW_{el}], is derived by the old consumption and the solar fraction, as depicted in Equation 6.3.

$$\dot{E}_{el}^{GRID*} = (1 - f^{ws}) \cdot \dot{E}_{el}^{GRID} \quad (6.3)$$

The constant solar contribution is given by $\dot{E}_{el}^{ws} = f^{ws} \cdot \dot{E}_{el}^{GRID}$ [kW_{el}].

Flat plate thermal collector (FP) Likewise, the installation of flat plate thermal collectors (FPs) is treated, though the new natural gas consumption depends on hot utility w of the solution. Therefore, the new natural gas consumption, \dot{E}_{ng}^{GRID} , is derived by the old consumption, the solar fraction and the hot utility thermal efficiency, as depicted in Equation 6.4.

$$\dot{E}_{ng}^{GRID*} = (1 - f^{ws}) \cdot \frac{\dot{Q}_{th}^w}{\eta_{th}^w} \quad (6.4)$$

The constant solar contribution is given by $\dot{Q}_{th}^{ws} = f^{ws} \cdot \dot{Q}_{th}^w$ [kW_{th}].

High concentration photovoltaic and thermal system (HCPVT) The HCPVT co-generates thermal and electrical power. Since the thermal storage imposes the highest constraints, the sizing is conducted based on the thermal power, $\dot{Q}_{th}^{ws} = f^{ws} \cdot \dot{Q}_{th}^w$ [kW_{th}]. The new natural gas consumption, \dot{E}_{ng}^* , is derived by the old consumption, the solar fraction and the hot utility thermal efficiency, as depicted in Equation 6.5 and Equation 6.6.

$$\dot{E}_{ng}^{GRID*} = (1 - f^{ws}) \cdot \frac{\dot{Q}_{th}^w}{\eta_{th}^w} \quad (6.5)$$

$$\dot{E}_{el}^{GRID*} = \dot{E}_{el}^{GRID} + \frac{\dot{Q}_{th}^{ws} \cdot \eta_{el}^{ws}}{\eta_{th}^{ws}} \quad (6.6)$$

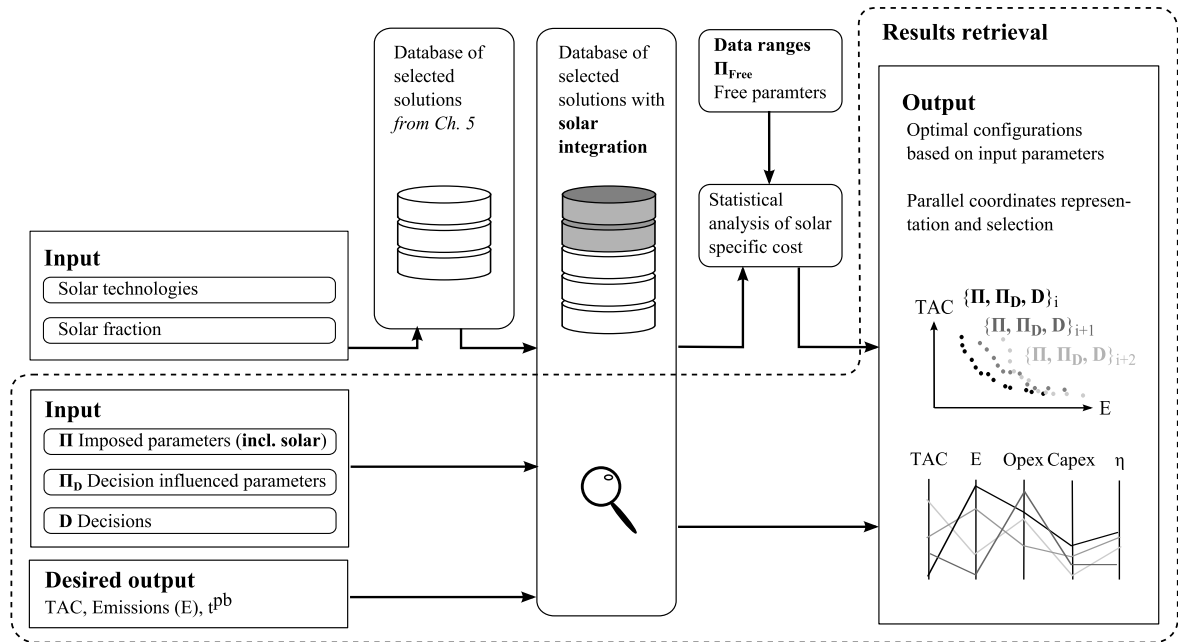


Figure 6.4 – Methodology proposed in Chapter 6: Combined potential estimation method for solar and conventional utilities.

The constant solar contribution is given by $\dot{Q}_{th}^{ws} = f^{ws} \cdot \dot{Q}_{th}^w$ [kW_{th}].

Co-generation If the thermal utilities replace part of the co-generation unit, the solution's net electricity demand needs to be adapted, as illustrated in Equation 6.7.

$$\dot{E}_{el}^{GRID**} = \dot{E}_{el}^{GRID*} - f^{ws} \cdot \frac{\dot{Q}_{th}^{COGEN} \cdot \eta_{el}^{ws}}{\eta_{th}^{ws}} \quad (6.7)$$

In this way the database of solutions is enlarged considering integration of solar energy by a fixed solar fraction in each of the additional solutions. When results are retrieved from the database, the specific solar collector cost [\$/m²], the efficiency [-], and the irradiance of the location need to be submitted, so that the location-dependent solar cost can be accurately estimated.

Break-even cost A second approach is applied, in which the break-even solar cost is determined based on statistical analysis. Therefore, the data ranges of the free parameters presented in Chapter 5 are sampled (Latin hypercube [233]), and in each run the maximum feasible specific solar energy cost [\$/kWh] of each technology is determined, under the condition that 10% of the best total annualized costs (TAC) solutions must incorporate the specified solar technology. The details are presented in the results and discussion section.

6.3 Results and discussion

The solutions of plant plant 2, $\Delta T_{\min}/2=5K$, were enhanced with solar utilities to study integration of further emission reductions. The imposed solar fraction of the different technologies under scrutiny is depicted in Table 6.2.

The enlarged set of solutions is depicted in Figure 6.5a in the resource plane¹. The effect of the respective technology on the set of solutions can be clearly identified. The integration of PV effectuated a fractional reduction of net electricity consumption, therefore, distorting the points towards the left. Integration of FP resulted in a distortion to the bottom, induced by reduced natural gas consumption.

Figure 6.6 shows the total annualized costs (TAC) and total emissions of all solutions in the three different countries, assuming the solar cost and efficiency values depicted in Table 6.2, the radiation data of the individual countries as written in the caption of Figure 6.6, and electricity and natural gas prices as depicted in Figure 5.8. As extensively discussed in Chapter 5, the respective minimum TAC solutions were selected and are depicted in Figure 6.7. Negative values in the yearly operating expenses (opex) arise from the export of electricity. The conclusions drawn from this analysis confirm the conclusions derived in Chapter 3, indicating that under current solar system cost metrics, solar systems should be installed as the last of multiple emission reduction measures. The first option is heat recovery (not depicted here), followed by mechanical vapor re-compression (MVR), and heat pump (HP) integration. Solar integration was only selected as additional measure for emission reduction, after other options had been employed. With solar integration though additional emission reductions by up to 20% could be achieved, reaching a total reduction of up to 80% compared to the reference in Switzerland (CH). It has to be noted, that integration of HCPVT in Switzerland (CH), together with mechanical vapor re-compression (MVR) showed reduced TAC, compared to the reference TAC -10%, which confirms the solutions presented in Chapter 3.

Table 6.3 provides the ranges of free parameters which were sampled. The statistical analysis was conducted in order to derive the maximum viable solar cost, assuming uniformly distributed parameters. Of course, this assumption is more than simplified, but there was not sufficient data available to derive more precise correlations. Figure 6.5b depicts the results of this analysis, indicating that the maximum feasible cost ranges from 0.29 to 0.001 $\$/kWh_{\text{lifetime prod.}}$ ². The 90th percentile was used to identify the maximum viable cost for each of the technologies, leading to 0.0098 $\$/kWh_{\text{th, lifetime}}$ for FP, 0.0392 $\$/kWh_{\text{el}}$ for PV, 0.0098 $\$/kWh_{\text{el+th}}$ for HCPVT, and 0.0294 $\$/kWh_{\text{el+th}}$ for the combined version of FP and PV. A difference was observed between the two co-generation cases (HCPVT and FP+PV) due to different imposed solar fractions.

¹ The resource plane refers to the plane formed with the two types of resource consumption as axes, and hence spans the natural gas and electricity consumption.

² The solar investment costs are derived in dollars per kWh of lifetime energy production, and the lifetime is assumed to be 20y.

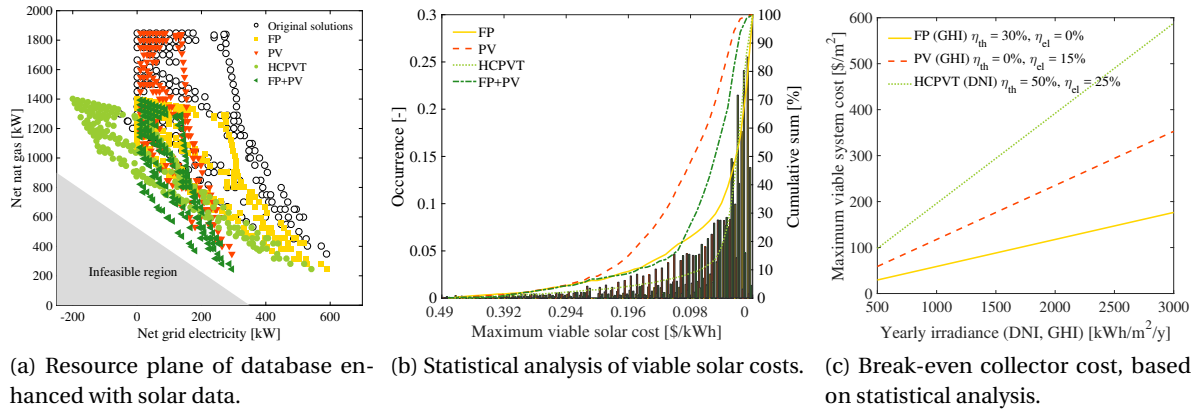


Figure 6.5 – Database enhanced with solar data, results of statistical analysis, and break-even collector cost.

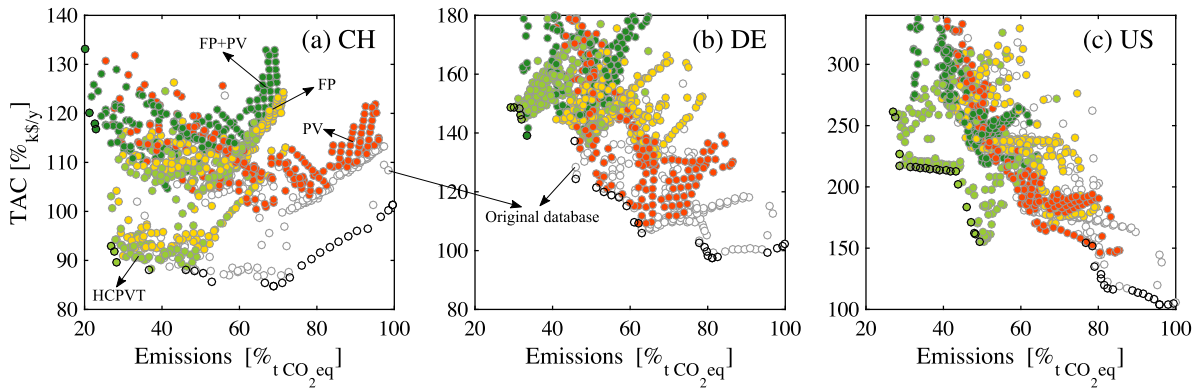


Figure 6.6 – TAC versus emissions of solar enhanced database of plant 2, $\Delta T_{\min}/2=5K$, 2500 h, 0 $\$/t_{CO_2}$, solar performance data Table 6.2, global horizontal irradiation (GHI) of three locations 1400,1100,2000 kWh/m²/y (a,b,c) DNI 1500,1000,2500 (a,b,c).

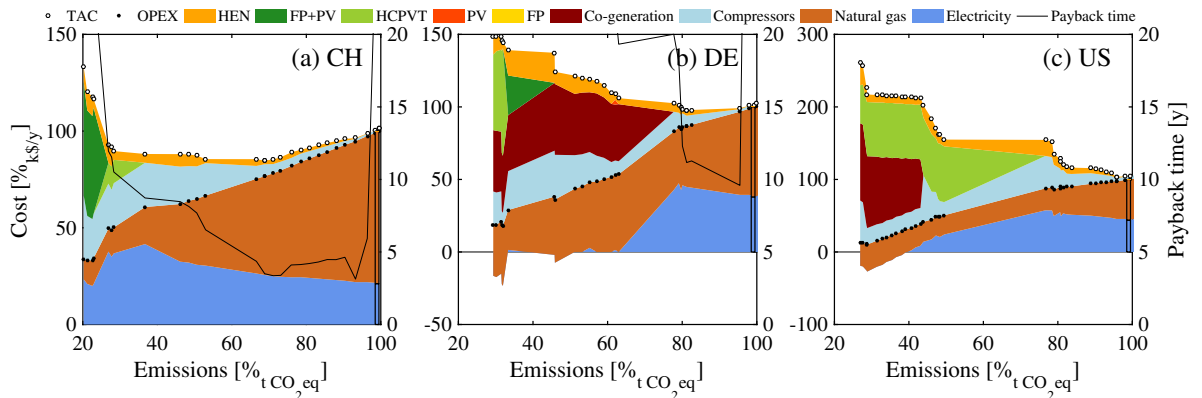


Figure 6.7 – Cost analysis of min(TAC) points of solar enhanced database of plant 2, $\Delta T_{\min}/2=5K$, 2500 h, 0 $\$/t_{CO_2}$.

Chapter 6. Generalization (B): addition of solar utilities

Table 6.2 – General solar data assumed, based on Philibert [1], Kalogirou [18], and Kalogirou and Tripanagnostopoulos [121].

Solar system	η_{th} [-]	η_{el} [-]	Cost [\$/m ²]	f^s [-]
Flat plate thermal collector (FP)	0.3	-	400	0.3
Photovoltaic module (PV)	-	0.15	500	0.5
High concentration photovoltaic and thermal system (HCPVT)	0.5 (DNI)	0.25 (DNI)	400	0.3 (thermal)
FP + PV	0.3	0.15	400, 500	0.3, 0.5

Table 6.3 – Data ranges of free parameters as derived in Chapter 5.

Parameter	Range	Unit
Natural gas price	[0.01, 0.1]	\$/kWh
Electricity price	[0.04, 0.18]	\$/kWh
CO ₂ tax	[0, 60]	\$/t CO ₂ eq.
Annuity factor ($\tau + m$)	[0.08, 0.25]	1/y
Operating time	[2000, 8000]	h
El. grid CO ₂ eq. emissions	[0.1, 1]	t CO ₂ /kWh
Nat. gas CO ₂ eq. emissions	[0.15, 0.25]	t CO ₂ /kWh

Assuming these numbers as break-even costs, the area specific collector costs, could be derived based on a chosen efficiency and a given annual irradiance, as shown in Figure 6.5c. It can be observed that FP costs should in many cases not exceed 150 \$/m² (which is quite below current market prices), while viable PV systems are be in the range of 100 to 300 \$/m² (closer to current market prices), and cost of the HCPVT system should be between 200 and 500 \$/m² (below current prices). These number will change, if different efficiencies are assumed.

When applying the break-even cost on the enhanced database of solutions, a change in results was observed. Figure 6.8 and Figure 6.9 show the minimum TAC points for 2500 and 8000 operating hours of plant 2, $\Delta T_{min}/2=5K$, respectively. The results from with 2500h show installation of PV in Switzerland (CH) and Germany (DE), which was replaced by FP, HCPVT and combined FP and PV with increasing emission reductions. Interestingly, at 8000h operating hours, PV (in CH and Germany (DE)) and HCPVT (in United States of America (US)) is replaced by a co-generation unit, bringing the advantage of co-producing thermal and electrical power, constantly. Due to the high investment cost of the co-generation unit, this option is only selected for operating hours.

Figure 6.10 depicts the thermal production of the units present in the minimum TAC solutions (excluding the heat pump units). It can be shown that some of the solar installations generate increased cooling water consumption, thereby suggesting lower exergy efficiencies, as seen for United States of America (US) and Germany (DE) at around 50% emission reductions. This confirms that economic, and even environmental objectives, cannot verify that solar energy is used in the exergetically optimal way. This could be avoided by choosing different objectives. However, considering economic criteria at a certain point cannot be avoided.

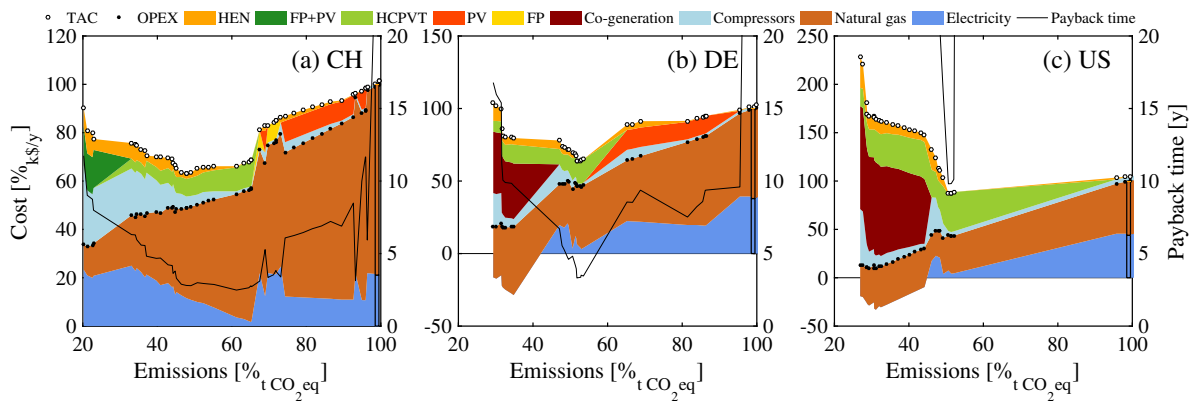


Figure 6.8 – Cost analysis of min(TAC) points of solar enhanced database of plant 2, $\Delta T_{\min}/2=5K$, 2500 h, 0 $\$/t_{CO_2}$, with break-even costs: FP: 0.0098 $\$/kWh_{th, lifetime}$, PV: 0.0392 $\$/kWh_{el}$, HCPVT 0.0098 $\$/kWh_{el+th}$, FP+PV 0.0294 $\$/kWh_{el+th}$.

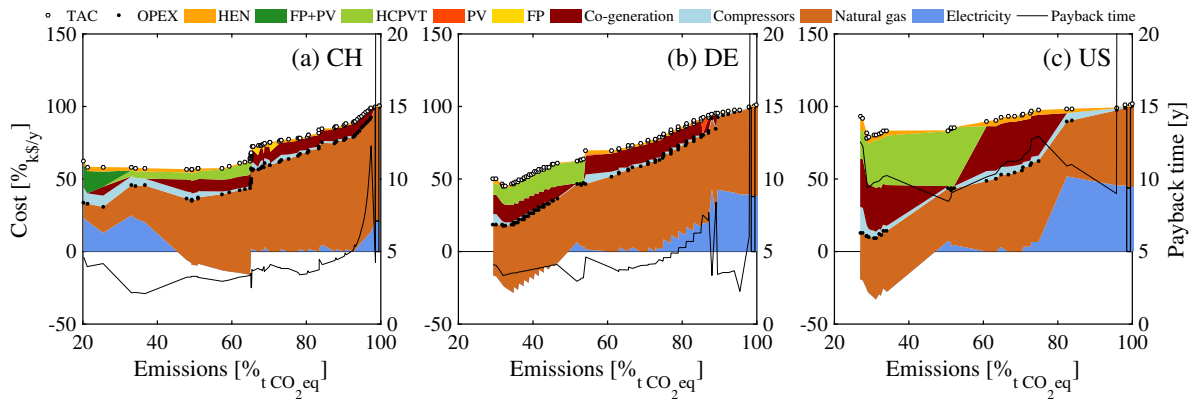


Figure 6.9 – Cost analysis of min(TAC) points of solar enhanced database of plant 2, $\Delta T_{\min}/2=5K$, 8000 h, 0 $\$/t_{CO_2}$, with break-even costs.

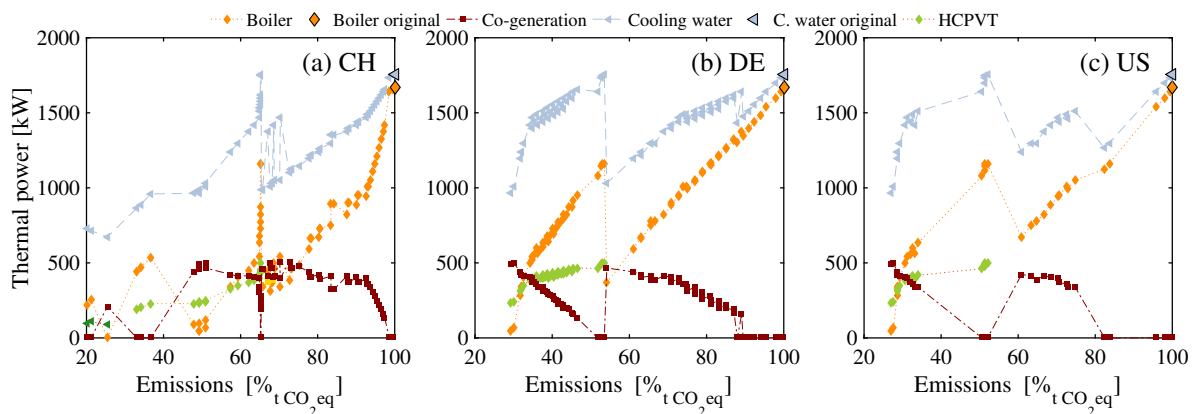


Figure 6.10 – Thermal units of min(TAC) points of solar enhanced database of plant 2, $\Delta T_{\min}/2=5K$, 8000 h, 0 $\$/t_{CO_2}$, with break-even costs.

6.4 Conclusions

How can the results be extrapolated to a wider scope?

This chapter presents an extension to the methodology presented in Chapter 5 taking into account solar utilities. The presented method illustrates, how specific solar performance models can be generalized to provide indication for industries in various countries.

The method includes enhancing the databased of solutions generated in Chapter 5 with various solar technologies, identification of solar system break-even cost, and specific potential estimation. Based on user-selected input criteria, case-specific solutions were drawn from the database and investigated. The data could be accessed via an on-line parallel coordinates decision-making platform (which is in planning).

The method is based on an *intuitive correlation* derived from the model presented in Chapter 3, which is employed to assess the annual solar collector and storage performance under optimal control. Results indicated that ST only achieved economic viability for collector costs ranging from below 100 \$/m² in areas of low solar radiation to 200 \$/m² in areas with higher incident insolation. Similarly the cost for PV and HCPVT were derived. Results confirmed the conclusions derived in Chapter 3 indicating that under current solar system cost metrics, solar systems would be installed as the last of multiple emission reduction options, favoring heat recovery improvements, mechanical vapor re-compression, and heat pumping in the first place. When analyzing the results assuming break-even solar costs, solar systems became more profitable, however, this also promoted solutions in which the solar energy was used inefficiently, which was manifested in a high cooling water consumption. This could be avoided using different objectives such as the exergy efficiency.

Conclusions

Overview

- Summary of the main results
- Significance of the work
- Recommendations and guidance
- Future perspectives

This thesis explored the multi-dimensional problem formulation of optimal solar integration in industrial processes through elaboration of methodologies tailored to low-temperature processing industries. The intricacies behind this goal were addressed in five main chapters. The main findings and contributions are presented below, followed by recommendations and future perspectives.

Main results summary

Chapter 1 Chapter 1 provides the wider context of the topics discussed in this thesis. It motivates the case study selection and technologies studied, and introduces concepts and nomenclature used throughout the work.

Chapter 2 *How can solar system design be accurately and rigorously addressed?*

The second chapter presented a **rigorous solar system modeling and design approach** which allows estimation of collector and storage performance at sufficient precision and limited computational effort. This development addressed shortcomings identified in the literature related to a lack of rigorous solar design methods at sufficient precision. Comparison of the static collector model with transient results yielded sufficient precision (<5 % deviation). Application of a clustering approach reduced the resolution time successfully while guarding the accuracy for sufficient numbers of clusters. For low cluster numbers a deviation of the results was revealed, highlighting a need to proper investigation of the clustering results.

Chapter 3 *What problem formulation is required for a comprehensive design method for solar-assisted low-temperature processes?*

Conclusions

In Chapter 3, a **comprehensive method** was proposed which addressed simultaneous optimization of the process heat recovery, the conventional utilities, and the renewable utility system (including thermal storage) using ϵ -constrained parametric optimization. The method, tailored for the low-temperature industry, is based on multi-period utility targeting, including process heat recovery through pinch analysis (PA) and re-use through heat pumping, and identifies the optimal design and operation of the utility and storage systems. In the literature, utility integration and solar system design has not been treated in a comprehensive manner for the low-temperature industries. The proposed method was demonstrated on the basis of a dairy plant located in Switzerland (CH) where different solar components were compared and evaluated based on economic and environmental objectives.

The results demonstrated that the use of a comprehensive method is unavoidable, since the sizing of all components was shown to be interrelated. Of particular interest was the fact that solar utility integration was only economically viable in combination with integration of a mechanical vapor re-compression system, which reduced the hot utility requirements. It could be shown that from an economic, environmental, and exergetic point of view internal heat recovery was the most effective measure, followed by mechanical vapor re-compression and improvements in the refrigeration system. After these measures were in place, solar energy integration yielded economically feasible solutions (15% reduction in total annualized costs (TAC)) reducing the overall emissions by up to 70%.

For continuous operation of the process, the reduction in specific emissions was not as significant as for daytime only operation. Due to the capital cost of the thermal storage system, it was only chosen by the optimization for high emission reductions requirements. Photovoltaic module (PV) integration offered the least emission reduction potential (up to 20% reduction in daytime only operation with respect to the best non-solar case). However, installation is simple, independent, and if overproduced, could be exported to the electricity grid. In comparison, the high concentration photovoltaic and thermal system (HCPVT) system, had high potential with very high efficiencies bringing emission reductions easily up to 40% (daytime only) at uncertain cost and shading losses. The low cost, very low efficiency flat plate thermal collector (FP) collectors offered a simple solution providing more reliability of the system performance capital cost expenses with emission reductions of up to 30% (daytime only).

Chapter 4 *How can design of an optimal industrial heat pump system be conducted?*

Results from Chapter 3 revealed that mechanical vapor re-compression, heat pumping and advanced refrigeration cycles are key measures for process emission reductions and efficiency improvements in low-temperature industries, which outperformed solar systems in terms of cost-effectiveness in emission reductions. Therefore, Chapter 4 focused on the development of a comprehensive and novel **generic heat pump synthesis method for industrial applications**.

The superstructure-based approach was solved with mathematical programming, and addressed a comprehensive list of heat pump features, while technical limitations were considered and a set of solutions was generated which allowed for expert-based decision-making and further deep solution analysis.

For benchmarking, the method was compared to a set of literature cases, generating between 5% and 30% cost improvements compared to the optimal solutions reported. An extended version of one case was presented considering fluid selection, heat exchanger network (HEN) cost estimations, and technical constraints within the problem formulation. The extended case highlighted a trade-off between energy efficiency and system complexity expressed by the increase of heat exchanger network costs with the number of compression stages, level of gas-cooling and subcooling which all improve the coefficient of performance (COP). This was especially evident when comparing the solutions with 3 and 5 compression stages causing an increase of the COP from 2.9 to 3.1 at 3% increase in TAC. Subcooling was activated in the minimum TAC solution which indicated that its advantageous characteristics should not be overlooked in cycle design. In contrast to the non-extended case, gas-cooling was not activated in the minimum TAC solution, which was attributed to an unfavorable relation between performance benefits and additional HEN cost. Fluid selection was successfully performed indicating that propane is the most favorable fluid both in economic and thermodynamic terms in this temperature range. The heat pump superstructure (HPS) proved to be flexible for different requirements serving in a variety of cases.

Chapters 5 and 6 *How can the results be extrapolated to a wider scope?*

Having derived methods for optimal solution generation of specific cases, in specific countries, under specific conditions in the previous chapters, Chapter 5 and Chapter 6 addressed the question of how these methods could be generalized and results could be extended to a wider scope. Therefore, a **method for estimating the environomic potential of technologies in industrial process applications** was derived, which was based on generalized optimization techniques. This method contributes to the state-of-the-art by offering a detailed bottom-up optimization-based approach based on mathematical programming. Current bottom-up approaches lack rigorous methods, and often rely on qualitative and (seldom) simple quantitative assessment.

The method was first derived for heat pump and co-generation equipment only, and later extended to include solar utilities. Applied to the dairy industry, the method revealed a wide applicability from evaluation of policy measures (CO₂ taxes and tax incentives), to pre-feasibility assessment for project planners. The on-line decision-support tool developed in the context of this work yielded additional, realistic solutions to guide various stakeholders toward efficient solutions.

It could be demonstrated that the operating time and energy resource prices drastically influenced the economic viability of emission reduction measures. Political incentives, such as CO₂ taxes and tax breaks for investment in emission reduction measures were found to increase the economically

Conclusions

viable emission reductions from an OECD average of 20% to 26% and 31%, in the least favorable case of a fixed process heat recovery network. These are equivalent to 30% and 55% increase in viable emission reduction measures achieved through a CO₂ tax of 20\$/t_{CO₂} without and with 20% tax breaks on the investment, respectively. It was shown that CO₂ taxes had distinctly higher impact in countries with low resource prices, while to achieve a change in countries with high resource prices, tax breaks might be a better incentive.

Integration of the solar utilities in Chapter 6 allowed derivation of break-even solar system costs, which were found to range from below 200 \$/m² for FP, to 250 \$/m² and 450 \$/m² for PV and HCPVT, respectively.

Results confirmed the conclusions derived in Chapter 3 indicating that under current solar system and heat pump cost metrics, solar systems would be installed as the last of multiple emission reduction options, favoring heat recovery improvements, mechanical vapor re-compression, and heat pumping in the first place. When analyzing the results assuming break-even solar costs, solar systems became more profitable, however, this also promoted solutions in which the solar energy was used inefficiently, which was manifested in a high cooling water consumption. This could be avoided using different objectives such as the exergy efficiency.

In summary Integration of solar energy in industrial processes is a wide field of research with various applications, foci, and objectives. Dependent on the particular subject of study, different tools should be applied, as demonstrated within this work. One main conclusion persists throughout the course of this thesis: In order to quantify the added value of solar integration to industrial processes, analysis of the entire utility network and process improvement measures (heat recovery) need to be completed. The developed methods aim at providing guidance to reach optimal solutions backed by metrics to justify their feasibility to decision makers.

Significance of the work

The benefit of models and explicitly optimization models can be argued. A true representation of reality by a model is impossible to achieve, and optimization models, in particular, require additional simplification due to computational limitations. This marks a trade-off between the accuracy of the model and the computational effort. If the optimization model is drastically simplified, the computational effort is low but the results may not be meaningful, since the model may not have captured the actual system behavior and the main bottlenecks. If the model is too complex, the computational effort can be so high that it does not allow to study a wide solution space and it is, therefore, unlikely to find optimal points.

Chapter 2 addresses this issue briefly by comparing the modeled performance of solar technologies with static hourly equations and with transient models, and in a further step the influence of clustering on the precision. However, this trade-off is not the main focus of this thesis.

Despite these shortcomings, (optimization) models are usually the only mean to derive quantitative results, if there is a lack of measured data that could otherwise be used for statistical or artificially-driven analysis. And if this notion is agreed upon, then the role of models is to provide quantitative results backed up with metrics to aid decision makers. This is (best) achieved in several phases. General, broader models can identify potentials in a first phase and more detailed, specific models can aid in planning and execution during the next phases. This thesis has contributed to the first phase by developing generic synthesis models that support pre-feasibility assessment, pre-design, and potential estimation of solar energy involving efficiency improvement measures for the low-temperature industry.

In the first three chapters (2, 3 and 4) this was achieved by the development of easy-to-use generic methods and models that may be applied by other researchers. These methods aim at enabling pre-feasibility assessment and pre-design of solar-assisted industry.

The second part of the thesis (Chapters 5 and 6) presented a general method for potential estimation based on the models developed in the previous chapters. The method itself is a contribution which can be generally applied, while also the results themselves may be used by process engineers or decision makers to estimate and weigh up the potential of technologies and efficiency measures in different global settings.

Recommendations and guidance

- **Adapt level of detail to needs.** Depending on what goal is pursued, adaption of discretization and level of detail of the models is imperative. This was illustrated for the generalization of the solar potential in Chapter 6. If detailed analysis of the optimal control strategy and sizing is required, it is recommended to use detailed models as presented in Chapters 2 and 3. However, if general cost estimation is required, a model of reduced complexity as presented in Chapter 6 is sufficient.
- **Comprehensiveness.** Instead of focusing on modeling one single technology at high detail, it is strongly advised to focus on a comprehensive consideration of technologies, which aids in providing directions on follow-up detailed analysis. It was observed multiple times in literature [59–61, 151], that the process cold/sub-ambient side together with the refrigeration system or mechanical vapor re-compression (MVR) was disregarded. This leads to sub-optimal solar integration and wasted energy.
- **Choice of objective function.** The choice of the objective function is crucial to the outcome of the optimization. Economic objectives are uncertain and may not favor renewable resources. Constraining the objective as performed in Chapter 3, or addressing thermodynamic and environmental criteria permit assessment from a broader perspective.

Future perspectives

The **solar modeling and design strategy** proposed in this work focused on the collector performance. Several aspects were simplified which could be addressed in future work.

- Solar collector field losses were simplified with a constant loss factor. More refined models should include:
 - Pressure drop and pumping power
 - Shading
 - Thermal losses
- The cost and availability of land were not considered. They would increase the economic model accuracy if data are known.

The **Comprehensive integration method** was tailored to the low-temperature processing industries, adaptation and extension could include:

- Multi-objective, non-linear optimization which would aid in identifying optimal utility temperature levels, though the problem size might drastically increase.
- Identification of additional utility technologies such as: steam network, high temperature/absorption heat pumps.
- A major issue is unwillingness of operators to change process heat recovery networks. The method could, therefore, be adapted for total site analysis (TSA), or include fixed HENs in a different way.

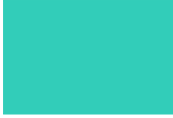
The **heat pump superstructure** addresses multiple feature, but could be extended to consider

- Equipment selection
- Super-critical fluids
- Mixed refrigerants
- Absorption systems

As mentioned previously, the **generalization methodology** provides numerous advantages, though the main limitation of the presented approach is identified as:

- Currently, the equipment investment cost is fixed, which is an uncertain value and may have an influence on the utility selection. In future work this may be addressed by re-calculating the investment cost with varying cost functions, or using stochastic programming.

Appendix



A.1 Introduction

The global availability of the direct normal irradiation (DNI) and global horizontal irradiation (GHI) are depicted in Figure A.1.

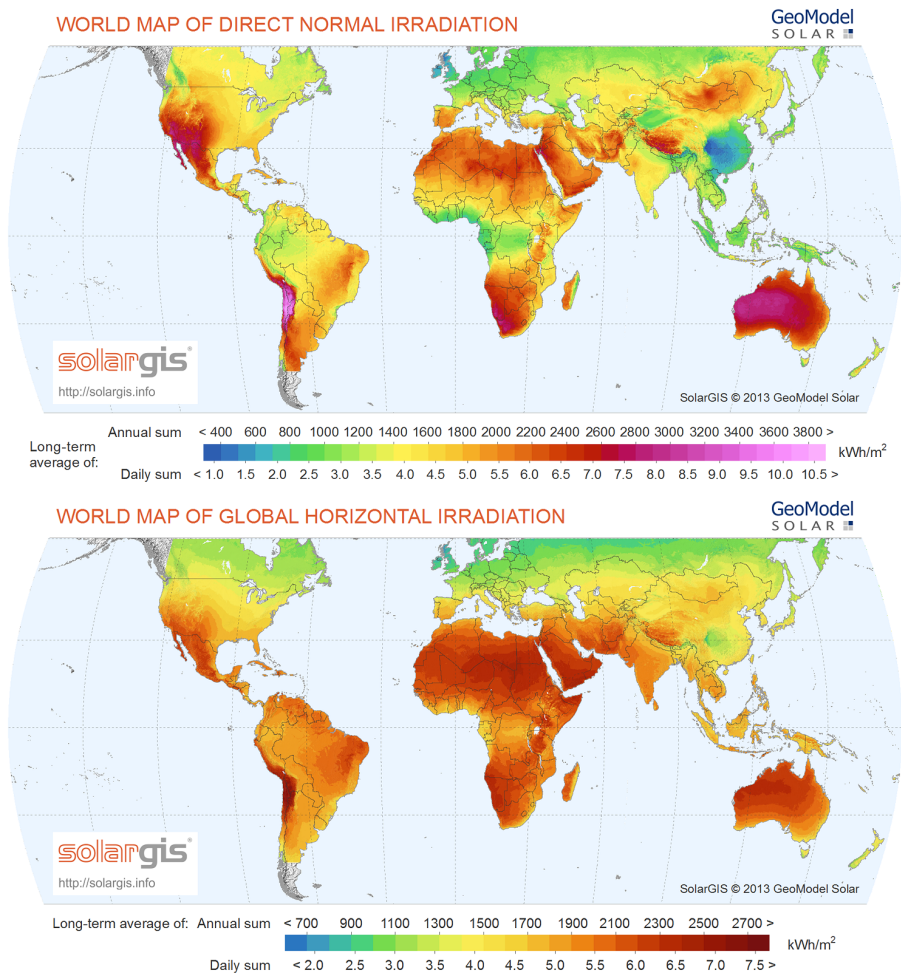


Figure A.1 – Global availability of DNI and GHI [kWh/m²y] [135].

Comprehensive integration method B

(Chapter 3)

B.1 Additional results

Figure B.1 shows the primary energy, fuel, electricity, and CO₂ emission savings of the non-stop operation solutions. It can be seen that for all solutions the electricity savings are "negative", meaning that more electricity is required due to the additional heat pump and MVR units. With increasing solar installations, the emissions and natural gas consumption are continuously reduced. The total annual cost and the primary energy savings are decreased with increasing solar system sizes.

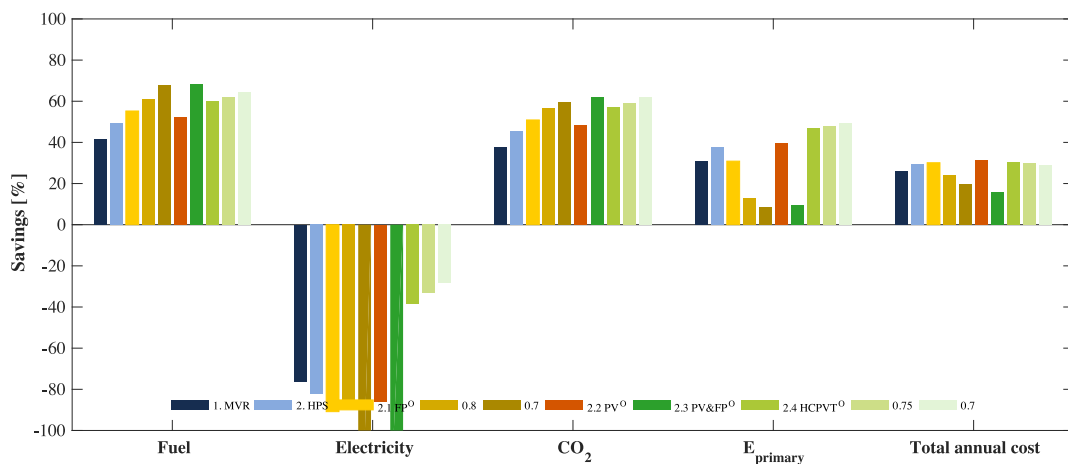


Figure B.1 – Primary energy, fuel, electricity, and CO₂ emission savings of non-stop operation solutions.

B.2 Performance parameters and cost functions

B.2.1 Heat exchanger network (HEN) cost estimation

The heat exchanger area is estimated as presented by Kemp [99, 218, 245] (area targeting) based on vertical intervals placed between the hot and cold composite curves. In each interval the approximate heat exchanger area is estimated based on the logarithmic mean temperature difference, the hot and cold average heat transfer coefficients, and the heat transferred within the interval. The total area A_{tot}^{HEN} [m²] is found by the summing over all intervals. Estimation of the installed heat exchanger capital expenses springs from the assumption that all heat exchangers are equal.

$$C_p^{HEN} = \left[a + b \cdot \left(\frac{A_{tot,p}^{HEN}}{N_{min,p}^{HEN}} \right)^c \right] \cdot N_{min,p}^{HEN} \quad (B.1)$$

The minimum number of heat exchangers (units) N_{min}^{HEN} to be placed in each zone (between pinches) is estimated following the suggestion of Linnhoff et al. [98] based on graph theory. The cost correlations are taken from Taal et al. [236] reprinted from Hall et al. [237] and can be found in Table B.1 for retrofit heat exchanger costs. The total cost is calculated for each period $p \in \mathbf{P}$ and the final installed cost is then found as the maximum of all periods.

$$C^{HEN} = \max_p \left(C_p^{HEN} \right) \quad (B.2)$$

Table B.1 – Heat exchanger network (HEN) cost estimation parameters Hall et al. [237] reprinted by Taal et al. [236] (2.33) updated to 2015 €, Carbon steel (CS)-CS heat exchangers.

Parameter	Symbol	Value	Unit
Heat exchanger cost estimations	HEN		
Fixed parameter	a	9'500	€
Scaling parameter	b	460	€/m ²
Non-linear parameter	c	0.8	-

B.2.2 Non-renewable technologies

B.2.2.1 Cooling water (CW)

The cooling water is modeled by one cold stream between 15 (T_{in}^{CW}) and 17 °C (T_{out}^{CW}). The operating cost are negligible as the cooling water is assumed to origin from a river close by the plant. The cooling thermal stream is formulated by the following relation, where c_p^{CW} [kJ/kgK] is the specific

heat capacity, and \dot{m}^{CW} , 1 kg/s, is the reference mass flow rate.

$$\dot{Q}^{CW} = \dot{m}^{ref,CW} \cdot c_p^{CW} \cdot (T_{out}^{CW} - T_{in}^{CW}) \quad (B.3)$$

B.2.2.2 Boiler (BOI)

The boiler heat release is modeled by three streams: air preheating, radiative and convective thermal power from natural gas combustion. The total heat release is derived by a multiplication of the lower heating value (LHV) with the reference fuel flow rate including the efficiency. Cooling down the combustion gases from the adiabatic flame temperature to a pre-defined radiation temperature defines the radiative component and is displayed as a hot stream at constant temperature (radiation temperature). The convective component is defined as a hot stream between the radiation temperature and the exhaust gases outlet temperature. The air preheating is written as a cold stream from ambient to preheating temperature. This practice has been published by Maréchal and Kalitventzeff [246] and is applied in the same manner by Becker [140]. The heat release is illustrated below in Equation B.4.

$$\dot{Q}^{BOI} = -\dot{Q}_{pre}|_{T_a}^{T_{preh}} + \dot{Q}_{rad}|_{T_{rad}} + \dot{Q}_{conv}|_{T_{out}}^{T_{rad}} \quad (B.4)$$

The parameters are described in Table B.2. The boiler investment cost is set to zero, since it is already in-place. The natural gas consumption (Equation B.5) is derived from the boiler useful heat release based on a conversion fraction. The conversion fraction includes the thermal losses as well as the part of the heat released in the combustion that is dispensed in the exhaust gases and therefore not delivered to the process as useful heat.

$$\dot{Q}_{ng}^{BOI} = \dot{Q}^{BOI} / f^{BOI} \quad (B.5)$$

Table B.2 – Boiler (BOI) parameters, adapted from Becker [140].

Parameter	Symbol	Value	Unit
Investment (in-place)	IV_2^{BOI}	0	€/kW
Adiabatic flame temperature	T_{ad}^f	2768	°C
Radiation temperature	T_{rad}	1027	°C
Exhaust gases temperature	T_{out}	120	°C
Air preheating temperature	T_{preh}	120	°C
Radiative heat load	\dot{Q}_{rad}	28842	kW
Convective heat load	\dot{Q}_{conv}	15031	kW
Air preheating load	\dot{Q}_{preh}	1740	kW
Boiler conversion fraction	f^{BOI}	90	%

B.2.2.3 Heat pump superstructure (HPS)

To ensure mass and energy conservation within the heat pump, linear constraints are defined at all liquid, vapor and superheated vapor points. These constraint are added to the utility targeting constraints. These equations are further documented in [167]. The constraints and parameters entering the mixed integer linear programming (MILP) are derived and depicted in Appendix C.3.1. The non-linear bare module cost function for compressors COMP [in €, 2010, is not further actualized] of each heat pump g is formulated after reference [247] reprinted by [140] where the installation factor was assumed to be 1.5.

$$C^{\text{COMP}} = 1.5 \cdot 1500 \cdot 160^{0.1} \cdot (\dot{E}^{g,\text{COMP } i \rightarrow j})^{0.9} \text{ [€ 2010]} \tag{B.6}$$

Where the maximum electricity consumption of compressor from level $i \rightarrow j$ of heat pump g , $\dot{E}^{g,\text{COMP } i \rightarrow j}$ [kW], is provided in Equation B.7 shown for any utility technology w .

$$\dot{E}^w = \dot{E}^w \cdot f^w \tag{B.7}$$

Where \dot{E}^w [kW] is the maximum (electrical) power consumption of utility technology w , \dot{E}^w [kW] is the (electrical) power reference consumption of utility technology w , and f^w [-] is the maximum size of technology w . During the MILP problem resolution, the annualized compressor capital costs as a function of the compressor power rating including the maintenance cost, $IV_2^{g,\text{COMP}}$, was based on a linear fitting function of Equation B.6.

Table B.3 – Heat pump parameters.

Parameter	Symbol	Value	Unit
Heat pump superstructure (HPS)			
Investment	IV_2^{HPS}	Eq. B.6	
Temperatures	$T^{\text{HPS, COND } i}$	-2,10,15,20,25,30,35,40,45,50	°C
Isentropic compressor efficiency	$\eta_{\text{isentropic}}$	0.76	-
Fluid	Ammonia		
Refrigeration in-place (REF)			
Investment	IV_2^{REF}	0	€/kW
Condenser temperature	$T^{\text{REF, COND } i}$	30 & 35	°C
Evaporator temperature	$T^{\text{REF, EVAP } i}$	-2	°C
Isentropic compressor efficiency	$\eta_{\text{isentropic}}$	0.76	-
Fluid	Ammonia		
Vapor recompression as proposed by [140] (MVR)			
Investment	IV_2^{HP}	Eq. B.6	
Condenser temperature	$T^{\text{REF, COND } i}$	76	°C
Evaporator temperature	$T^{\text{REF, EVAP } i}$	56	°C
Isentropic compressor efficiency	$\eta_{\text{isentropic}}$	0.76	-
Fluid	Water		

B.2.3 Solar technologies

The solar technologies and typical periods clustering are comprehensively discussed in Chapter 2.

B.2.3.1 Solar cost function

The proportional (installed) cost coefficient of a solar technology s is calculated as depicted in Equation B.8.

$$IV_2^s = f_{\text{inst}} \cdot IV_A^w \cdot A^s \quad (\text{B.8})$$

B.2.3.2 Flat plate thermal collector (FP)

All parameters of the considered flat plate collectors can be found in Table B.4. Figure B.2 shows the thermal conversion efficiency $\eta_{p,\text{tot}}^{\text{FP}} = \dot{Q}_p^{\text{FP}} / (g_{h,p} \cdot A^{\text{FP}})$ of the thermal energy production of a flat plate collector \dot{Q}_p^{FP} in period p with respect to the global horizontal radiation $g_{h,p}$ in each period p . This efficiency is comprised of not only the conductive and radiative thermal losses, but also the losses caused by the non-perpendicular angle of incidence of the sun. Since the collectors are installed in a fixed position, different angles of inclination need to be tested. The graph indicates clearly that in some days (e.g. day number four and eight) collectors with 55° inclination outperform the collectors with smaller inclination angles. This stems from the fact that on these (winter) days the solar elevation angle is not very high (see Figure 3.5) and collectors installed at higher inclination can capture more of the incoming radiation. On days in the middle of the summer (e.g. day number seven and nine), the solar elevation angle is very high and therefore the collectors with the smallest inclination angles exhibit the best performance. In the end, the total yearly performance is the most

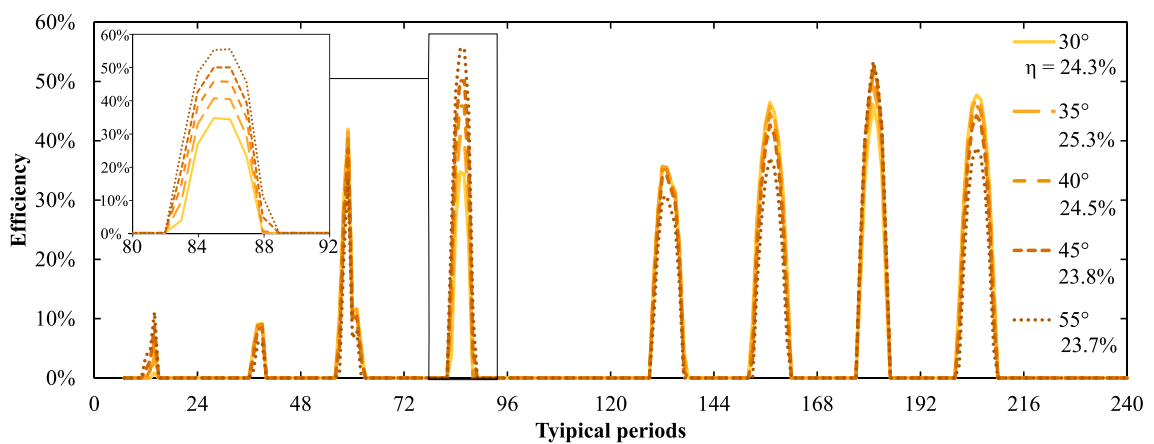


Figure B.2 – Thermal conversion efficiency of flat plate (FP) solar thermal collectors as a function of time for different inclination angles, input data presented in Table B.4, performance equations shown in Section 2.3.1.2.

Appendix B. Comprehensive integration method (Chapter 3)

important indicator which is displayed in Figure B.2 for all the inclination angles. It is weighted by the relative occurrence of each typical period in the year. An inclination angle of 35° with an average efficiency of about 25.3% exhibits the best performance and was therefore chosen for further analysis. This efficiency is however biased, since it is calculated only when the collector produces thermal energy. The overall production versus GHI efficiency yields 17.1%.

This average efficiency of the considered flat plate collectors is far below the theoretical maximum of up to 60%. In this study a balance is struck between performance and capital investment. The efficiency of single glazed flat plate thermal collectors drops with higher operating temperatures, lower ambient temperatures, and the inclination of the sun. These insufficiencies are partly overcome by better insulation or by changing the collector model (e.g. evacuated tube collectors). Both of these options come at distinctly higher costs (factor 2 and higher [164]) and were, therefore, not considered.

Table B.4 – Flat plate solar collector (FP) parameters, if no other indication, data taken for single glazing flat plate collectors from Tehnomont [108] data tested by SPF [164] presented in Table B.4, performance equations presented in Section 2.3.1.2.

Parameter	Symbol	Value	Unit
Ground reflectivity	ρ_g	0.154	-
Heat transfer fluid		water glycol mix	
Investment cost ([164],2012)	IV_A^{FP}	196	€/m ²
Installation cost factor	f_{inst}^{FP}	1.5	-
Total investment {min,max}		{200,600}	€/m ²
Collector area	A^{FP}	2.059	m ²
Standard efficiency/ conversion factor	η_0^{FP}	0.74	-
Efficiency coefficient 1	a_1^{FP}	3.5940	W/m ² K
Efficiency coefficient 2	a_2^{FP}	0.00864	W/m ² K ²
Incidence angle modifier coefficient	a	2.40	-
Fluid inlet temperature	T_{in}^{FP}	80	°C
Fluid outlet temperature	T_{out}^{FP}	105	°C
Slope Inclination (recommended: similar to latitude)	θ_i^{FP}	35	°
Azimuth, shift towards south	γ_i^{FP}	0	°
Thermal field loss factor	f_{field}^{FP}	0.97	-

B.2.3.3 Photovoltaic module (PV)

The photovoltaic modules (PVs) were modeled based on hourly static equations with the assumption that the transient behavior is negligible. All parameters of the considered for the photovoltaic modules can be found in Table B.5.

Figure B.3 shows the conversion efficiency from the global horizontal irradiance (GHI) $g_{p,i}$ in each period p to the electricity produced in the photovoltaic modules $\eta_{p,tot}^{PV} = E_p^{PV} / (g_{i,p} \cdot A^{PV})$, where E_p^{PV} is the electrical production of a PV module in period p . As discussed previously, the GHI only covers the fraction of the solar radiation that hits the earth at a perpendicular angle. This allows the conversion efficiency (if it is described in this manner) to exceed the rated efficiency of the PV

B.2. Performance parameters and cost functions

modules (e.g. on day 1), since the inclined modules may capture more of the inclined sun rays than the GHI takes into account. The assessment also changes if shadowing is taken into account, though this was not considered as a factor in this study. The winter days (1, 4, and 9) show due to this peculiarity and due to lower ambient temperatures the highest efficiencies. In agreement with the observation from the plate collectors, it can be seen that higher inclinations are favored in winter days while lower inclination angles perform better during summer days. The highest overall efficiency is found for the lowest inclination angle of 30° with an average of 18.5%. Such efficiencies may only be reached for high performance PV modules such as the ones assumed. More detailed modeling, considering shading and conversion losses, will most likely show lower performance values.

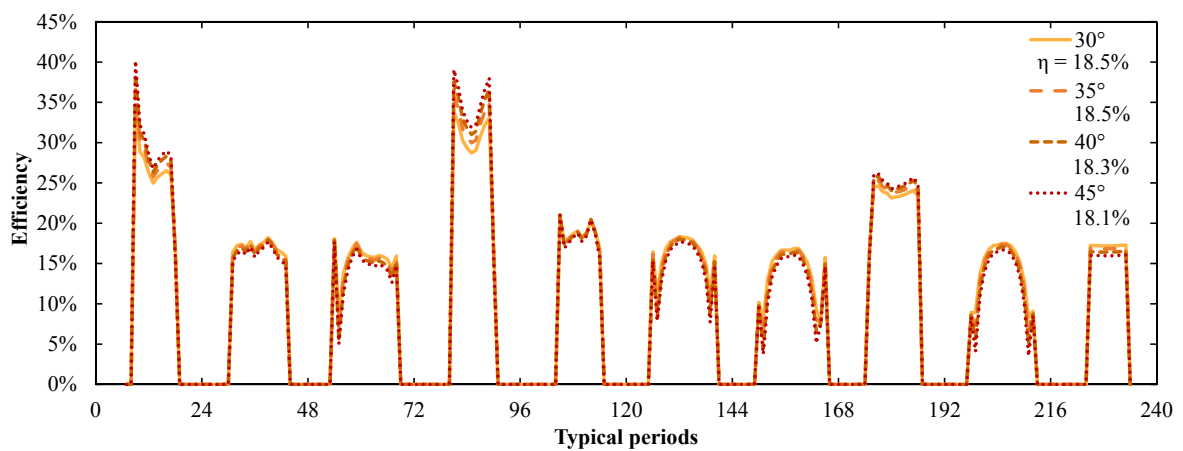


Figure B.3 – Electrical conversion efficiency of photovoltaic modules (PVs) as a function of time for different inclination angles, input data presented in Table B.5, performance equations presented in Section 2.3.1.3.

B.2.3.4 High concentration photovoltaic and thermal system (HCPVT)

The high concentration photovoltaic and thermal system (HCPVT) were modeled based on hourly static equations with the assumption that the transient behavior is negligible. All parameters of the considered for the HCPVT can be found in Table B.6.

The HCPVT conversion efficiencies are not depicted here as they are assumed to be constant over time independent from the irradiance and other potentially influencing factors such as the ambient temperature (active cooling). A comparison between transient and static model was conducted and the results are depicted in Figure B.4 [110]. The dish thermal efficiency is assumed to approximate 55%, and the electrical efficiency 25%. Constant electrical conversion losses and solar thermal losses in the field were considered in this study. The average yearly overall efficiency of the HCPVT system with respect to the DNI was found based on detailed dynamic models, averaging 25%_{el} and 55%_{th} (total), respectively, which is extremely high and may be overestimated.

Appendix B. Comprehensive integration method (Chapter 3)

Table B.5 – Photovoltaic module (PV) parameters, if no other indication, data taken from SunTech [166]. nominal cell operating temperature (NOCT) are a set of conditions which are defined in order to find the nominal cell operating temperature. Standard testing conditions (STC) are at $1000\text{W}/\text{m}^2$, 25°C cell temperature and air mass 1.5.

Parameter	Symbol	Value	Unit
Investment cost [248]	IV^{PV}	260	$\text{€}/\text{m}^2$
Installation cost factor	f^{PV}	1.5	-
Total investment {min,max}		{300,800}	$\text{€}/\text{m}^2$
Maximum power	$\dot{E}_{\text{max}}^{\text{PV}}$	290	W
Module area	A^{PV}	1.63	m^2
Module electrical efficiency	$\eta_{\text{el}}^{\text{PV}}$	0.178	-
Temperature reduction factor	f_T^{PV}	0.004	$-/\text{K}$
Efficiency reduction at $g_{200} = 200\text{W}/\text{m}^2$	f_{200}	0.98	-
standard testing conditions (STC) temperature	T_{STC}	25	$^\circ\text{C}$
STC radiation	g_{STC}	1000	W/m^2
Nominal Operating Cell Temperature	$T_{\text{NOCT}}^{\text{PV}}$	45	$^\circ\text{C}$
NOCT radiation	g_{NOCT}	800	W/m^2
NOCT ambient temperature	$T_{\text{a,NOCT}}$	20	$^\circ\text{C}$
NOCT wind speed	$v_{\text{a,NOCT}}$	1	m/s
Inclination (around latitude)	θ^{PV}	30	$^\circ$
Azimuth, shift towards south	γ_i^{PV}	0	$^\circ$
Effective transmittance-absorptance product	$\tau\alpha$	0.9	-
Electrical conversion factor	$f_{\text{gen}}^{\text{PV}}$	0.95	-

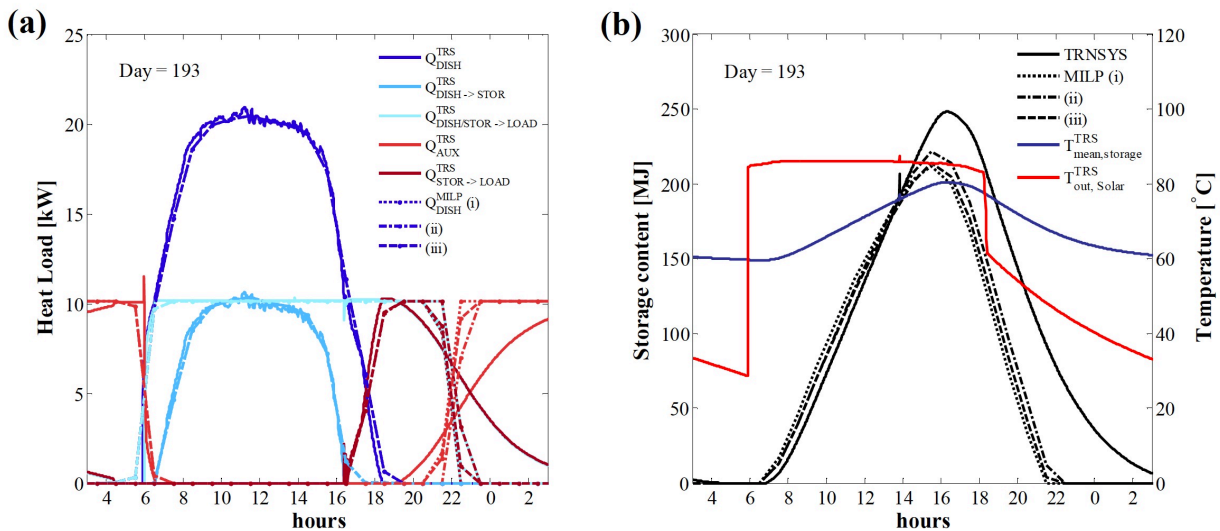


Figure B.4 – Comparison of Transient System Simulation Tool [2] (TRNSYS) results and static model for HCPVT [110], data shown in Table B.6, static performance equations presented in Section 2.3.1.4.

B.2.3.5 Storage

The storage is detailed in Section 2.4.2, where the thermal storage mass and energy balances are formulated based on different temperature levels modeled as different interconnected tanks. The

B.2. Performance parameters and cost functions

Table B.6 – High concentration photovoltaic and thermal system (HCPVT) parameters, data taken from Airlight Energy Holding SA [132].

Parameter	Symbol	Value	Unit
Heat transfer fluid		water glycol mix	
Investment cost	IV^{HCPVT}	700	€/m ²
Dish area	A^{HCPVT}	40.05	m ²
Installation cost factor	f_{FP}	1.5	-
Total investment {min,max}		{500,1500}	€/m ²
Primary efficiency	$\eta_{\text{th,prim}}^{\text{HCPVT}}$	0.5	-
Secondary efficiency	$\eta_{\text{th,sec}}^{\text{HCPVT}}$	0.05	-
Electrical efficiency	$\eta_{\text{el}}^{\text{HCPVT}}$	0.25	-
Fluid temperature primary in	$T_{\text{in,prim}}^{\text{HCPVT}}$	85	°C
Fluid temperature primary out	$T_{\text{out,prim}}^{\text{HCPVT}}$	92	°C
Fluid temperature secondary out	$T_{\text{out,sec}}^{\text{HCPVT}}$	110	°C
Thermal field loss factor	$f_{\text{field}}^{\text{HCPVT}}$	0.9	-
Electrical conversion factor	$f_{\text{gen}}^{\text{HCPVT}}$	0.9	-

implementation relies on the mass storage presented by Moret et al. [141] which is expanded to represent the thermal behavior.

Performance Figure B.5 illustrates the thermal storage filling in addition to the boiler and solar dish behavior over a selected range of operating periods. The storage is charged when the availability of the sun exceeds the process requirements (at around 80% of its total potential) and is consumed with decreasing solar availability. It can be seen that the solar availability is increased by the storage or in other words that the boiler utilization is reduced due to the emptying of the tank, which indicates the advantage of the storage. For higher utilization of the storage, the ϵ -constraint would have to be decreased.

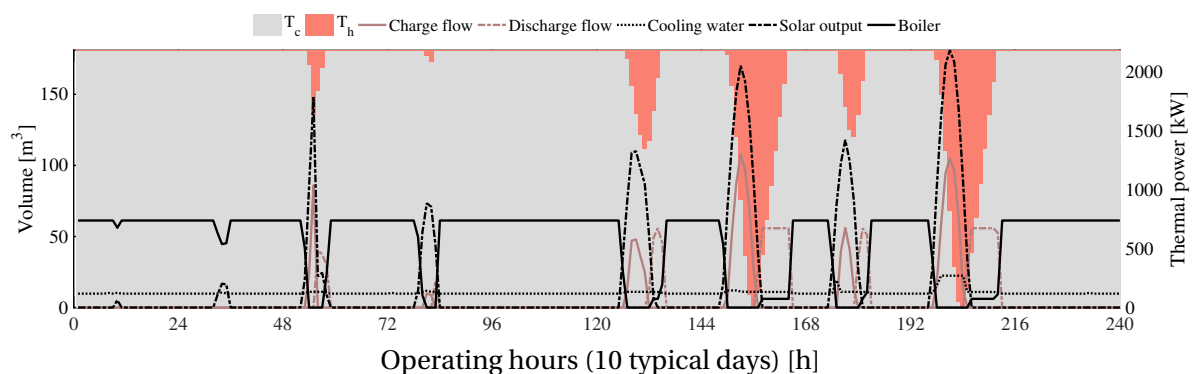


Figure B.5 – Thermal storage volume and temperature distribution for the FP collectors non-stop operation of the industrial process, case 2.1. FP^0 at $\epsilon = 80\%$ of the 2. HPS case.

B.3 Weather data & clustering

Following the indications of Domínguez-Muñoz et al. [126] the typical days are built from n clusters with 2 extreme days. For clustering, 3 indicators are chosen which influence the solar performance the most: DNI, GHI, and the ambient temperature. Since the DNI fluctuates the most on an hourly, daily, and monthly basis with a high influence on the solar output, it is chosen as the main reference for determination of the performance indicator. Also the extreme days are determined based on the DNI, which means that one extreme day is found for the highest daily radiation and lowest solar radiation. In Figure 3.5 in the upper corner the typical days and their occurrence are illustrated. The two last days are extreme days which are represented only once. The operating time of one period is one hour which leads to 240 operating periods.

Table B.7 displays the yearly average values and mean squared error of the six weather data attributes of which only three are subject to the clustering. The yearly means of the three attributes that are used for clustering are very close to the original data and thus the error of the first three indicators is comparably small. Errors for the outside temperature and the wind speed, however, are distinctly higher. This may be explained by stronger fluctuations throughout the year even though the ambient temperature is used as input to the k-medoids clustering.

Table B.7 – Mean data and performance indicators of typical days compared to original.

Attribute	Unit	Mean _{original}	Mean _{typical}	mELDC ² 10 ⁻⁴
GHI	[W/m ²]	163.2	163.3	1.685
DNI	[W/m ²]	192.8	190.1	3.242
Elevation α_s	[°]	14.1	13.4	2.603
Azimuth γ_s	[°]	44.4	45.2	5.592
T _a	[°C]	10.7	10.5	51.321
v _a	[m/s]	2.1	3.1	100.837

B.4 Dairy process

The process streams as presented by Becker [140] are depicted in Table B.8. A detailed description of the process model is provided in Appendix D.3.

Table B.8 – Hot and cold streams of the dairy process, reproduced from Becker [140].

Unit	Name	T _{in} [°C]	T _{out} [°C]	Q̇ [kW]	ΔT _{min} /2 [°C]	Remarks
Regrigeration	ref	6.0	4.0	76.0	2.0	refrigeration inlet milk
Pasteurization	pasto1a	4.0	66.0	2356.0	2.0	preheating
	pasto2a	66.0	86.0	676.4	2.0	pasteurization milk
	pasto3a	86.0	4.0	2773.2	2.0	refrigeration milk
	pasto4a	66.0	98.0	119.7	2.0	pasteurization cream
	pasto5a	98.0	4.0	351.6	2.0	refrigeration cream
Concentration	eva1	4.0	70.3	504.0	2.0	preheating
	eva2	70.3	70.3	904.2	1.2	evaporation 1.effect
	eva3	66.4	66.4	864.1	1.2	evaporation 2.effect
	eva4	60.8	60.8	849.8	1.2	evaporation 3.effect
	eva5	60.8	4.0	151.5	2.0	refrigeration concentrated milk
	eva6	68.9	68.9	904.2	1.2	condensation 1.effect
	eva7	65.9	65.9	864.1	1.2	condensation 2.effect
	eva9	68.9	15.0	87.8	2.0	condensation 3.effect
	eva10	65.9	15.0	80.8	2.0	cooling condensates 1.effect
	Condensates cooling	eva8	60.1	60.1	849.8	1.2
eva11		60.1	15.0	69.7	2.0	cooling condensates 3.effect
Yoghurt production	yog1	4.0	94.0	1026.0	2.0	heating
	yog2	94.0	10.0	957.6	2.0	cooling
Desert production	des1	4.0	90.0	817.0	2.0	heating
	des2	90.0	70.0	190.0	2.0	cooling
Hot water	hw	15.0	55.0	167.2	2.0	hot water prodcutio
Cleaning in place	CIP1a	58.7	70.0	188.6	2.0	maintain temperature CIP1
	CIP1b	65.0	15.0	104.5	2.0	recuperation waste heat CIP1
	CIP2a	67.5	80.0	209.5	2.0	maintain temperature CIP2
	CIP2b	75.0	15.0	125.4	2.0	recuperation waste heat CIP2
Fridge	frig	5.0	5.0	300.0	2.0	maintain storage temperature

Generic heat pump superstructure

(Chapter 4)

C.1 General

C.1.1 MOGA input parameters

All computations were conducted on a machine with 8-Core Xeon 2.4 GHz processor with 16.0 GB of RAM. Table C.1 depicts the data used in the multi-objective genetic algorithm (MOGA [217]) from the Dakota package [216]. Different parameters were used during different runs. Due to danger of getting trapped in local minima, especially during the extended analysis (in Section 4.3.3) with fluid selection at the master level, the mutation and crossover parameters were set more aggressively. These parameters were selected based on a heuristic analysis tracking the propagation of the non-dominated frontier. Figure C.1 shows the propagation of multi-objective genetic algorithm (MOGA) and the dominance of each population over the previous indicating that a total of 10^5 evaluations achieve satisfying convergence for the master level fluid selection, as shown in Figure C.1a. The dominance change of the slave level fluid selection displayed in Figure C.1b, however, indicates that after 25,000 iterations, and significant computation time the MOGA has not reached convergence. These results further support the conclusions derived in Section 4.3.3.1, that the master level selection is more efficient.

Table C.1 – Input parameters for MOGA method [217].

Parameter	Expression	Value	Comment
Initial population	population_size	300, 500	initial set of individuals (section 4.3.2, 4.3.3)
Crossover type	crossover_type	'shuffle_random' 'multi_point_binary 2'	(section 4.3.2) select one of each design var. of the parents for child (section 4.3.3) bit switching at 2 pnts. in the binary encoded genome of two parents
Crossover rate	crossover_rate	0.9	crossover rate of new generation
Mutation type	mutation_type	'replace_uniform', 'bit_random'	(section 4.3.2) randomly choosing variable and reassigning it to a random valid value (section 4.3.3) flips a randomly chosen bit in the string of randomly chosen variable
Mutation rate	mutation_rate	0.1, 0.2	(section 4.3.2, 4.3.3)
Maximum iteration	max_iterations	100, 200×10^3	maximum number of iteration unless convergence is reached (section 4.3.2, 4.3.3)
Convergence type	convergence_type	'average_fitness_tracker'	
Percent change	percent_change	0.1	(default) percent change in non-dominated frontier

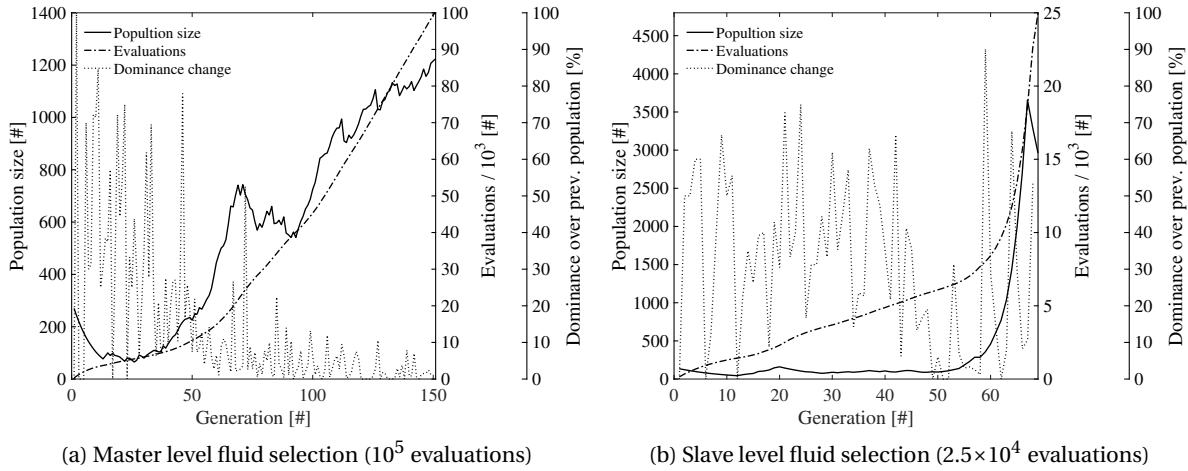


Figure C.1 – Analysis of MOGA propagation of extended case *E2*.

C.1.2 MILP input parameters

The input parameters used for CPLEX [5] are displayed in Table C.2. The last three entries were found based on the parameter tuning performed by CPLEX.

Table C.2 – Input parameters for CPLEX [5], AMPL [3].

Parameter	Expression	Value	Comment
mipgap	'mipgap'	0.001	relative difference between best integer and best bound
time	'time'	300, 600	cpu time limit in seconds (all, selection at slave level)
flow cuts	'flowcuts'	1	(agressive) use of flow cuts in solving MIPs
mir cuts	'mircuts'	1	(moderate) generation of MIP rounding cuts
branch	'branch'	1	branching direction for integer variables

C.2 Benchmark analysis

C.2.1 Benchmark cases

The thermal streams considered in the different benchmark cases are depicted in the original source and were reproduced in Table C.3. The objective functions, variables, boundary conditions, and input data to the respective optimization problems are displayed in Table C.4. The HEN costs were disregarded during this optimization following the literature input data.

In case *E2*, gas-cooling was considered. It has to be noted that the temperature difference below which gas-cooling was realized was not selected as a variable. It was set to the difference between the temperature level i and the one above ($i - 1$), yielding $\Delta T_{i,DSH} = T_{i-1} - T_i$. The main effect of this choice is ensuring that the generated solutions do not require splitting of the gas-cooling thermal streams, in other words, they do not require several heat exchangers cooling gas at one compressor outlet.

Table C.3 – Streams data of the three benchmark cases.

(a) <i>E2</i> [101]					(b) <i>Ethylene</i> [186]					(c) <i>Cold Tray</i> [205]				
Stream name	T _{in}	T _{out}	Q̇	α	Stream name	T _{in}	T _{out}	Q̇	α	Stream name	T _{in}	T _{out}	Q̇	α
	K	K	kW/K	kW/m ² K		K	K	kW	kW/m ² K		K	K	kW	kW/m ² K
Process					Process					Process				
H1	360	320	10	1	H1	408	312	-1186	1	H1	-10.7	-10.7	-400.70	1
H2	320	250	10	1	H2	375	312	-466	1	H2	-28.9	-28.9	-823.38	1
C1	260	310	15	1	H3	375	312	-387	1	H3	51.5	51.5	-4285.30	1
C2	300	360	10	1	H4	375	312	-380	1	C1	67.9	67.9	870.83	1
					H5	375	290	-572	1	C2	-3	-3	758.94	1
					H6	269	260	-20	1	C3	62.5	62.5	4229.65	1
					H7	168	158	-157	1					
					H8	258	256.8	-381	1					
					H9	313	313	-224	1					
					H10	307	307	-141	1					
					H11	234	234	-1081	1					
					H12	290	230	-451	1					
					C1	393	440	111	1					
					C2	277	302	174	1					
					C3	158	311	208	1					
					C4	346	360	516	1					
					C5	436	498	448	1					
					C6	315	358	133	1					
					C7	252	256	1120	1					
					C8	247	298	96	1					
Utilities					Utilities					Utilities				
	K	K				K	K				K	K		
Water for cooling	300	310		0.56	Cooling water for cooling	297.1	300		0.56	Cooling water for cooling	295	300		0.56
Water for heating*	300	290		0.56	Cooling water for heating*	297.1	294.2		0.56	Cooling water for heating*	295	290		0.56
Steam	440	440		0.56	Steam LP	411	411		1	Steam	138	13882		1

Table C.4 – Benchmark case data.

Description	Symbols	E2				Ethylene				Cold Tray			
		Data	Unit	Reference	min(HPS)	Data	Unit	Reference	min(HPS)	Data	Unit	Reference	min(HPS)
<i>Master level</i>													
Objective function	J_{master}^{obj}	{ C^{opex}, C^{capex} }	\$/y	Table 4.6	{ C^{opex}, C^{capex} }	\$/y	Table 4.6	{ C^{opex}, C^{capex} }	\$/y	Table 4.6	{ C^{opex}, C^{capex} }	\$/y	Table 4.6
HEN cost function	C^{HEN}	0	\$/y		0	\$/y		0	\$/y		0	\$/y	
Compressor cost function	C^{COMP}	as slave	\$/y	Table 4.6	$0.15 \cdot 1,925 \cdot (E^{COMP} [kW_{el}])^{0.963}$ [186]	\$/y	Table 4.6	$0.15 \cdot 1,925 \cdot (E^{COMP})^{0.963}$	\$/y	Table 4.6	$0.15 \cdot 1,925 \cdot (E^{COMP})^{0.963}$	\$/y	Table 4.6
<i>Variables</i>													
Saturation temperature	T_1	{300, 300.5, ..., 313}	K	313	312.5	{310, 310.5, ..., 310}	K	310, ammonia	310, ammonia	{333, 333.5, ..., 353}	K	-	344
	T_2	{290, 290.5, ..., 310}	K	300	298.5	{250, 250.5, ..., 290}	K	307, r22	265.5, ammonia	{323, 323.5, ..., 353}	K	-	338.5
	T_3	{280, 280.5, ..., 300}	K	288	283	{230, 230.5, ..., 280}	K	297, ammonia	246, ammonia	{313, 313.5, ..., 343}	K	-	331
	T_4	{265, 265.5, ..., 285}	K	277	272	{220, 220.5, ..., 260}	K	266, r22	234, ethane	{303, 303.5, ..., 333}	K	-	321.5
	T_5	{250, 250.5, ..., 270}	K	254	254	{200, 200.5, ..., 240}	K	256, r22	224, ammonia	{293, 293.5, ..., 323}	K	303, r22, ammonia	302
	T_6	{245, 245.5, ..., 265}	K	247	248	{190, 190.5, ..., 230}	K	256.8, propylene	205, ethane	{283, 283.5, ..., 313}	K	274, r22	298
	T_7	240	K	240	240	{170, 170.5, ..., 210}	K	246.8, r22	189, ethane	{273, 273.5, ..., 303}	K	-	273
	T_8					{160, 160.5, ..., 200}	K	234, ethane	180.5, ethane	{253, 253.5, ..., 283}	K	259.5, ammonia	259.5
	T_9					{150, 150.5, ..., 190}	K	224, propylene	172, ethane	{243, 243.5, ..., 273}	K		257
	T_{10}					148	K	ethane	ethane	241.3	K	r22	
Subcooling temperature difference	$\Delta T_{i,SC}$					0	K			0	K		
	$\Delta T_{1,SC}$	{0, 1, ..., 20}	K	0	14								
	$\Delta T_{2,SC}$	{0, 1, ..., 20}	K	0	15								
	$\Delta T_{3,SC}$	{0, 1, ..., 15}	K	0	0								
	$\Delta T_{4,SC}$	{0, 1, ..., 15}	K	0	2								
	$\Delta T_{5,SC}$	{0, 1, ..., 5}	K	0	0								
	$\Delta T_{6,SC}$	{0, 1, ..., 5}	K	0	0								
Gas-cooling temperature difference	$\Delta T_{i,DSH}$	$T_{i-1} - T_i$	K	0	as shown	0	K			0	K		
Preheating temperature difference	$\Delta T_{i,PRE}$	0	K	0	0	0	K			0	K		
Fluid set	F	{ammonia}		ammonia	ammonia	{ammonia, propylene, r22, r13, ethane, ethylene}				{ammonia, r12, r22}			ammonia
Weighting factor	ξ	{0, 1}	-	0.5	0.47	{0, 1}	-	0.5	0.87	{0, 1}	-	0.5	0.74
<i>Slave level</i>													
Objective function	J_{slave}^{obj}	$wTAC$	\$/y			$wTAC$	\$/y			$wTAC$	\$/y		
<i>Parameters [101]</i>						<i>Parameters [186]</i>						<i>Parameters [205]</i>	
Compressor isentropic efficiency	$\eta_{isentropic}$	1	-			1	-			1	-		
Minimum temperature difference	ΔT_{min}	10	K			10	K			2.78	K		
Set of periods	P	{1}	-			{1}	-			{1}	-		
Operating time of period	Δt_1	1	y			1	y			1	y		
Occurrence of period	occ_1	1	1/y			1	1/y			1	1/y		
Maximum compression ratio	CP^{max}	10				10	bar/bar						
Maximum number of compressors	n^{max}	5				5	-			5	-		
<i>Yearly operating expenses (opex)</i>													
Steam production	$OP_{2,STEAM}$	50.91	\$/kW/y			0	\$/kW/y			56.2866	\$/kW/y		
Electricity grid	$OP_{2,GRID}$	608.33	\$/kW/y			336	\$/kW/y			420	\$/kW/y		
Cooling water	$OP_{2,CW}$	15.97	\$/kW/y			6.011	\$/kW/y			6.011	\$/kW/y		
<i>Annualized capital expenses (capex)</i>													
Compressor cost	$IV_{2,COMP}^{COMP}$	2824.8	\$/y			$0.15 \cdot 3,787.4$	\$/y			$0.15 \cdot 3,787.4$	\$/y		
	$IV_{2,COMP}^{COMP}$	831.67	\$/kW/y			$0.15 \cdot 1,573$	\$/kW/y			$0.15 \cdot 1,573$	\$/kW/y		
Heat exchanger cost parameters	a,b	500, 0.8	\$/-			500, 0.8	\$/-			500, 0.8	\$/-		
	U	1	kW/m ² K			1	kW/m ² K			1	kW/m ² K		
	A	1	m ²			1	m ²			1	m ²		
	Q^{min}	7	kW			100	kW			7	kW		

C.2.2 Extended case E2

The thermal streams considered in this case are depicted in Table C.3(a). Figure C.2a shows the parallel coordinates information generated with the tool from Kermani et al. [220]. The global warming potential (GWP) of most selected Hydrofluorocarbons (HFCs) (r407c, r404a, r410a, r507a) is above 1500 [249] compared to hydrogen sulfide and natural refrigerants (ammonia (r717), propane (r290), propylene (r1270)) with GWP of below 10 [249, 250] and lower-impact HFCs such as r161 (12 [251]) and r41 (97 [252]). The objective functions, variables, boundary conditions, and input data to the extended case E2 are displayed in Table C.5. Figure C.2b depicts the temperature entropy diagram of the optimized HPS solution. Figure C.3a displays the integrated composite curves of the extended case. In the reference case, cooling water is required to cool the highest condenser level which is increased compared to the benchmark case due to the lower compressor isentropic efficiency. Since the cooling water outlet temperature is above the condenser temperature, part of it needs to be heated by the hot utility. Figure C.3b presents a flowsheet of the minimum TAC case. The two HEN design of the reference and optimized case is shown in Figure C.4. It has to be noted that the HPS solution requires one more heat exchangers which is mildly penalized by the HEN cost function thereby being outweighed by the benefits of the reduced opex.

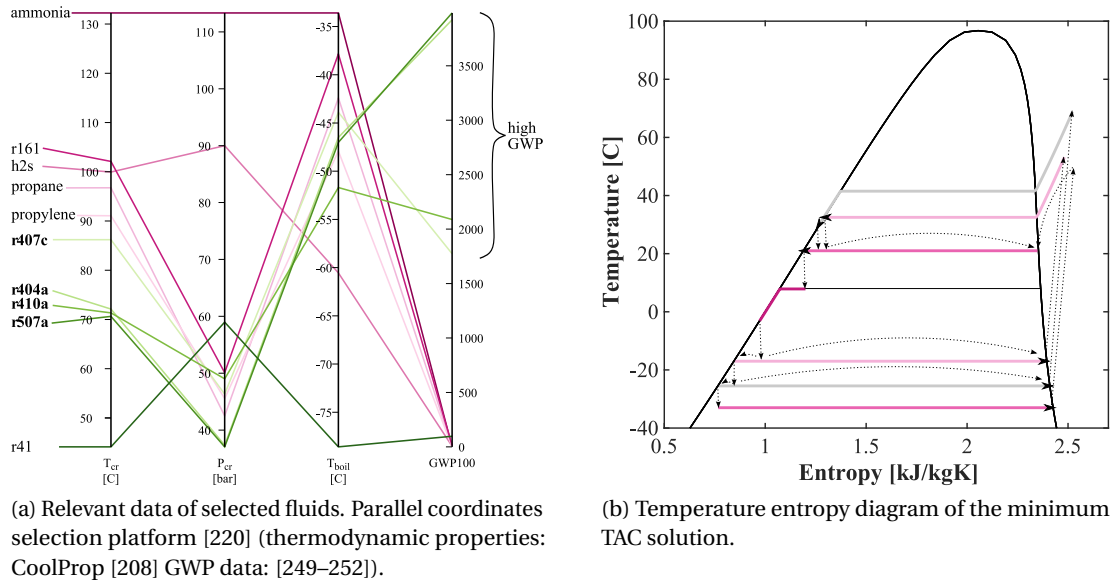
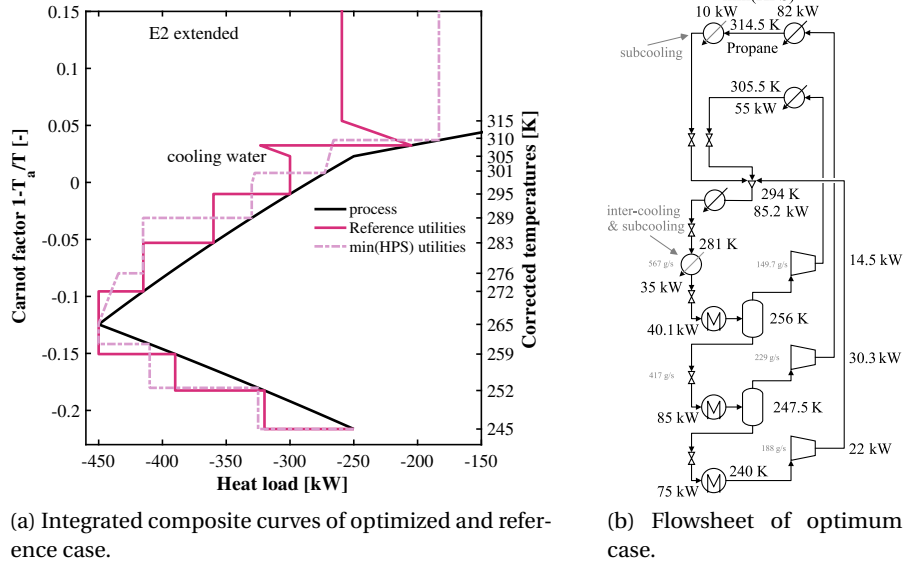


Figure C.2 – Set of selected fluids considered during multi-objective optimization.

Appendix C. Generic heat pump superstructure (Chapter 4)



(a) Integrated composite curves of optimized and reference case.

(b) Flowsheet of optimum case.

Figure C.3 – Extended case E2 minimum TAC solution.

Table C.5 – Optimization problem description: extended case E2.

Description	Symbols	Data	Unit	Reference	min(HPS)
<i>Master level</i>					
Objective function	f_{master}^{obj}	$\{C^{OPEX}, C^{CAPEX}\}$	\$/y	56 005	49 944
Heat exchanger cost function (estimation)	C^{HEN}	C^{HEN} Table 4.3	\$/y	132 608	121 840
HEN design			\$/y	58 800	57 800
	c_1 fitted [101]	0	\$	52 800	53 600
	c_2 fitted [101]	500	\$/y		
	c_3 fitted [101]	0.8	-		
<i>Variables</i>					
Saturation temperature	$T_i = T_{i+1} + \Delta T_i$				
	ΔT_1	{5, 5.5, ..., 40}	K	13	9
	ΔT_2	{5, 5.5, ..., 40}	K	12	11.5
	ΔT_3	{5, 5.5, ..., 40}	K	11	13
	ΔT_4	{5, 5.5, ..., 40}	K	23	25
	ΔT_5	{5, 5.5, ..., 40}	K	7	8.5
	ΔT_6	{5, 5.5, ..., 40}	K	7	7.5
	T_7	240	K	240	240
Subcooling temperature difference					
	$\Delta T_{1,SC}$	{0, 1, ..., 20}	K	0	12
	$\Delta T_{2,SC}$	{0, 1, ..., 20}	K	0	0
	$\Delta T_{3,SC}$	{0, 1, ..., 15}	K	0	0
	$\Delta T_{4,SC}$	{0, 1, ..., 15}	K	0	11
	$\Delta T_{5,SC}$	{0, 1, ..., 10}	K	0	0
	$\Delta T_{6,SC}$	{0, 1, ..., 10}	K	0	0
De-superheating temperature difference	$\Delta T_{i,DSH}$	$T_{i-1} - T_i$	K	0	as indicated
Preheating temperature difference	$\Delta T_{i,PRE}$	0	K	0	0
Fluid set	F	{ammonia, r161, h2s, propane, propylene, r407c, r404a, r410a, r507a, r41}		ammonia	propane
Weighting factor	ξ	{0, 1}	-	0.5	0.58
<i>Slave level</i>					
Objective function	f_{slave}^{obj}	$wTAC$	\$/y		
<i>Parameters</i>					
Compressor isentropic efficiency	$\eta_{isentropic}$	0.7	-		
Minimum temperature difference	ΔT_{min}	10	K		
Set of periods	P	{1}	-		
Operating time of period	Δt_1	1	y		
Occurrence of period	occ_1	1	1/y		
Maximum compression ratio	CP^{max}	8	bar/bar		
<i>Opex</i>					
Steam production	OP^{STEAM}	50.91	\$/kW/y		
Electricity grid	OP_2^{GRID}	608.33	\$/kW/y		
Cooling water	OP_2^{CW}	15.97	\$/kW/y		
<i>Capex</i>					
Compressor cost	IV_1^{COMP}	2824.8	\$/y		
	IV_2^{COMP}	831.67	\$/kW/y		

Appendix C. Generic heat pump superstructure (Chapter 4)

temperature $T_{i,SC}$ [K]. As such, the heat release in a condenser is defined by Equation C.1.

$$\begin{aligned}\dot{Q}^{g,COND\ i} &= -\dot{m}^{ref} \cdot \left([h_{PRE}(T_i) - h_V(T_i)]_{T_i}^{T_{i,PRE}} + [h_V(T_i) - h_L(T_i)]_{T_i} + [h_L(T_i) - h_{SC}(T_i)]_{T_i}^{T_{i,SC}} \right) \\ &= -\dot{m}^{ref} \cdot (\Delta h_{COND}(T_i) + \Delta h_{SC}(T_i) + \Delta h_{PRE}(T_i))\end{aligned}\quad (C.1)$$

Where $T_{i,PRE}$ is the preheating temperature before compression [K], h_{PRE} is the enthalpy before compression [kJ/kg], h_V [kJ/kg] is the vapor and h_L [kJ/kg] is the liquid saturation enthalpy.

The heat consumption of an evaporator (EVAP) at saturation temperature T_i of heat pump g is composed of two parts: evaporation at the saturation temperature and superheating between saturation and preheating temperature. As such, the heat consumption in an evaporator is defined by Equation C.2.

$$\begin{aligned}\dot{Q}^{g,EVAP\ i} &= \dot{m}^{ref} \cdot \left([h_V(T_i) - h_L(T_i)]_{T_i} + [h_{PRE}(T_i) - h_V(T_i)]_{T_i}^{T_{i,PRE}} \right) \\ &= \dot{m}^{ref} \cdot (\Delta h_{EVAP}(T_i) + \Delta h_{PRE}(T_i))\end{aligned}\quad (C.2)$$

The liquid side of the presaturator (PRESAT) also needs to be cooled down to the subcooling temperature which is formulated similarly and shown by Equation C.3.

$$\dot{Q}^{g,PRESAT\ i} = \dot{m}^{ref} \cdot [h_L(T_i) - h_{SC}(T_i)]_{T_i}^{T_{i,SC}} \quad (C.3)$$

Gas-cooling (GAS-COOL) to the compressor inlet temperature from the superheated vapor at the compressor outlet can be achieved by mixing in the presaturator or in a heat exchanger as described in Equation C.4.

$$\dot{Q}^{g,GAS-COOL\ i} = \dot{m}^{ref} \cdot [h_{DSH}(T_i) - h_{PRE}(T_i)]_{T_i,PRE}^{T_{i,DSH}} \quad (C.4)$$

Where h_{DSH} is the enthalpy to which the superheated compressor outlets are mixed [kJ/kg], and $T_{i,DSH}$ is the respective temperature [K].

The electricity consumption of a compressor depends on the isentropic efficiency and the enthalpies of both pressure levels, formulated as Equation C.5.

$$\dot{E}^{g,COMP\ i \rightarrow j} = \dot{m}^{ref} \cdot \left[\frac{h_{isentropic,i}(T_j) - h_V(T_i)}{\eta_{isentropic}} \right] \quad (C.5)$$

Where $h_{\text{isentropic},i}(T_j)$ [kJ/kg] is the isentropic enthalpy after compression from saturated vapor at temperature level T_i to (saturation) temperature level T_j , and $\eta_{\text{isentropic}}$ is the isentropic compressor efficiency [-]. The HPS stream properties are depicted in Table C.6.

Table C.6 – Data of streams of the heat pump superstructure (HPS).

Unit	Name	T_{in} K	T_{out} K	$ \Delta Q $ kJ/kg	α kW/m ² K
Condenser	condensation	T_i	T_i	$h_V(T_i) - h_L(T_i)$	1.6
	sub-cooling	T_i	$T_{i,SC}$	$h_L(T_i) - h_{SC}(T_i)$	0.56
	de-superheating	$T_{i,PRE}$	T_i	$h_{PRE}(T_i) - h_V(T_i)$	0.06
Evaporator	evaporation	T_i	T_i	$h_V(T_i) - h_L(T_i)$	3.6
	preheating	T_i	$T_{i,PRE}$	$\Delta h_{PRE}(T_i)$	0.06
Gas-cooler	gas-cooling	$T_{i,DSH}$	$T_{i,PRE}$	$h_{DSH}(T_i) - h_{PRE}(T_i)$	0.06
Presaturator	sub-cooling	T_i	$T_{i,SC}$	$h_L(T_i) - h_{SC}(T_i)$	0.56

C.3.2 Heat pump specific constraints

In the following the heat pump specific linear equations at the slave level are introduced. The respective units, streams and relations are depicted in Figure C.5.

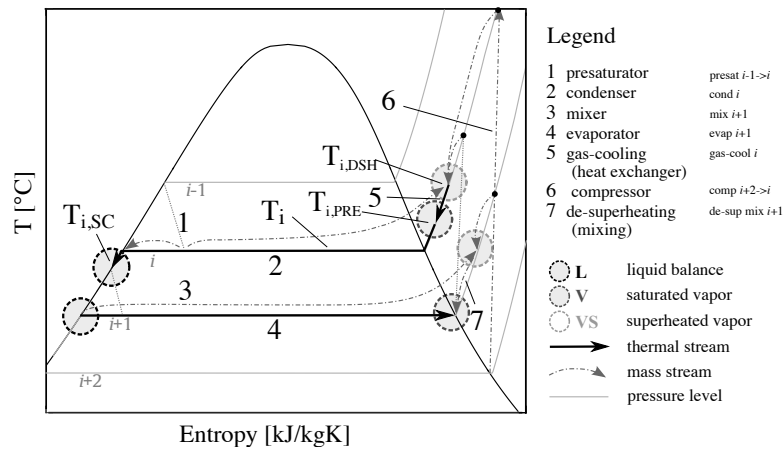


Figure C.5 – Temperature-entropy diagram with mass and energy balances of the HPS.

Liquid mass balance The liquid mass balance at temperature level i can be at saturated or sub-cooled conditions depending whether $\Delta T_{i,SC} > 0$ (sub-cooled) or $\Delta T_{i,SC} = 0$ (saturated). It is shown in Equation C.6 of heat pump g and is composed of:

- the positive contribution from the potential condenser (COND) at level i
- the negative contribution from the potential evaporator (EVAP) at level i
- the positive contribution of the liquid fraction of all valves in combination with presaturators (PRESAT) that end at level i
- the negative contribution from all valves that exit from level i

Appendix C. Generic heat pump superstructure (Chapter 4)

- the negative contribution of the fraction of liquid that may be used to de-superheat the compressor outlets (mix) at level i (MIX)

$$f_p^{g,COND\ i} - f_p^{g,EVAP\ i} + \sum_{j=1}^{i-1} (1 - x_V^{g,j \rightarrow i}) \cdot f_p^{g,PRESAT\ j \rightarrow i} - \sum_{k=i+1}^{n_l} f_p^{g,PRESAT\ i \rightarrow k} - f_p^{g,MIX\ i} = 0 \quad (C.6)$$

$$\forall i \in \mathbf{L}, g \in \mathbf{G}, p \in \mathbf{P}$$

Where

\mathbf{G}	set of heat pumps g consisting of one fluid d
\mathbf{L}	set of heat pump saturation temperature levels $\{1,2,3, \dots, n_l\}$
$f_p^{g,COND\ i}$	condenser (COND) sizing factor of heat pump g (containing fluid f) during period p
$f_p^{g,EVAP\ i}$	evaporator (EVAP) sizing factor of heat pump g during period p
$f_p^{g,MIX\ i}$	mixer (MIX) sizing factor of heat pump g during period p
$f_p^{g,PRESAT\ j \rightarrow i}$	presaturator (PRESAT) after expansion from temperature level $j \rightarrow i$ sizing factor of heat pump g during period p
$x_V^{g,j \rightarrow i}$	vapor fraction after expansion from temperature level $j \rightarrow i$ of heat pump g
$h_{SC}^{g,i}$	[kJ/kg] enthalpy at subcooled or saturated temperature level $T_{i, SC} = T_i - \Delta T_{i, SC}$ of heat pump g

Liquid energy balance The liquid energy balance in Equation C.7 is trivial because all streams enter and exit at the same state of matter and temperature.

$$\left(f_p^{g,COND\ i} - f_p^{g,EVAP\ i} + \sum_{j=1}^{i-1} (1 - x_V^{g,j \rightarrow i}) \cdot f_p^{g,PRESAT\ j \rightarrow i} - \sum_{k=i+1}^{n_l} f_p^{g,PRESAT\ i \rightarrow k} - f_p^{g,MIX\ i} \right) \cdot h_{SC}^{g,i} = 0$$

$$\forall i \in \mathbf{L}, g \in \mathbf{G}, p \in \mathbf{P} \quad (C.7)$$

Vapor mass balance The vapor mass balance at temperature level i can be at saturated or superheated conditions depending whether $\Delta T_{i, PRE} > 0$ (superheated) or $\Delta T_{i, PRE} = 0$ (saturated). It is shown in Equation C.8 of heat pump g and is composed of:

- the positive contribution from the potential evaporator at level i
- the negative contribution from the potential condenser at level i
- the negative contribution from all compressors that exit from level i
- the potential incoming mass flow related to the potential gas-cooling (GAS-COOL) heat exchanger unit from the superheated mass balance at level i
- the potential positive contribution from a de-superheating (DE-SUP) through mixing unit at level i

$$f_p^{g,EVAP\ i} - f_p^{g,COND\ i} - \sum_{j=1}^{i-1} f_p^{g,COMP\ i \rightarrow j} + f_p^{g,DE-SUP\ i} + f_p^{g,GAS-COOL\ i} = 0 \quad (C.8)$$

$$\forall i \in \mathbf{L}, g \in \mathbf{G}, p \in \mathbf{P}$$

Where

The energy balance in this case is trivial, since all streams enter and exist at $h_{PRE}^{g,i}$ [kJ/kg], the enthalpy

$f_p^{g,COMP\ i \rightarrow j}$	sizing factor of compressor from level $i \rightarrow j$	sizing factor of heat pump g during period p
$f_p^{g,DE-SUP\ i}$	sizing factor of the de-superheating (DE-SUP) through mixing unit of heat pump g during period p	
$f_p^{g,GAS-COOL\ i}$	sizing factor of the gas-cooling (GAS-COOL) heat exchanger of heat pump g during period p	

at preheated or saturated temperature level $T_{i,PRE} = T_i + \Delta T_{i,PRE}$ of heat pump g . This balance is not displayed here.

Superheated vapor mass balance The superheated vapor mass balance at temperature level i is conducted at superheated conditions $T_{i,DSH} = T_i + \Delta T_{i,DSH}$. It is shown in Equation C.9 of heat pump g and is composed of:

- the positive contributions of each compressor entering level i
- the positive contribution of the vapor fraction of all valves in combination with presaturators that end at level i
- the negative contribution from the gas-cooling and de-superheating through mixing units at level i
- and the positive contribution from the liquid mixing unit at level i

$$\sum_{k=i+1}^{n_l} f_p^{g,COMP\ k \rightarrow i} + \sum_{j=1}^{i-1} x_V^{g,j \rightarrow i} \cdot f_p^{g,PRESAT\ j \rightarrow i} - f_p^{g,GAS-COOL\ i} - f_p^{g,DE-SUP\ i} + f_p^{g,MIX\ i} = 0 \quad (C.9)$$

$\forall i \in \mathbf{L}, g \in \mathbf{G}, p \in \mathbf{P}$

Superheated vapor energy balance The energy balance given in Equation C.10 ensures that regardless of which compressor is active, the starting point for de-superheating is always fixed. This constraint ensures energy conservation and linearity in the problem formulation.

$$\sum_{k=i+1}^{n_l} f_p^{g,COMP\ k \rightarrow i} \cdot h_{out}^{g,COMP\ k \rightarrow i} - f_p^{g,GAS-COOL\ i} \cdot h_{DSH}^{g,i} - f_p^{g,DE-SUP\ i} \cdot h_{PRE}^{g,i} + f_p^{g,MIX\ i} \cdot h_{SC}^{g,i} = 0 \quad (C.10)$$

$\forall i \in \mathbf{L}, g \in \mathbf{G}, p \in \mathbf{P}$

Where

$h_{PRE}^{g,i}$	[kJ/kg] enthalpy at preheated or saturated temperature level $T_{i,PRE} = T_i + \Delta T_{i,PRE}$ of heat pump g
$h_{DSH}^{g,i}$	[kJ/kg] superheated vapor enthalpy at point $T_{i,DSH} = T_i + \Delta T_{i,DSH}$
$h_{out}^{g,COMP\ k \rightarrow i}$	[kJ/kg] outlet enthalpy of compressor from level k to i

Generalization (A) - heat pumping and co-generation (Chapter 5)

D.1 General

D.1.1 MOGA input parameters

All computations were conducted on a machine with 8-Core Xeon 2.4 GHz processor with 16.0 GB of RAM. Table D.1 depicts the data used in the multi-objective genetic algorithm (MOGA [217]) from the Dakota package [216]. Different parameters were used during different runs. Due to danger of getting trapped in local minima, especially during the extended analysis (in Section 4.3.3) with fluid selection at the master level, the mutation and crossover parameters were set more aggressively. These parameters were selected based on a heuristic analysis tracking the propagation of the non-dominated surface. Figure D.1 shows the propagation of MOGA and the dominance of each population over the previous indicating that after generation 40 the weighted sum of objectives does not propagate very much any more which could explain the dominance of ϵ -constraint. ϵ -constraint propagates continuously until the stopping criterion (at 1.5×10^5 evaluations) is reached. This might indicate that longer runtimes could generate improved solutions, however, reaching already 40 hours of runtime, this option is currently neglected.

Table D.1 – Input parameters for MOGA method [217].

Parameter	Expression	Value	Comment
Initial population	population_size	500	initial set of individuals
Crossover type	crossover_type	'shuffle_random'	select one of each design var of the parents for child (*)
Crossover rate	crossover_rate	0.9	crossover rate of new generation
Mutation type	mutation_type	'replace_uniform'	randomly choosing variable and reassigning it to a random valid value (*)
Mutation rate	mutation_rate	0.1	
Maximum iteration	max_iterations	150e ³	maximum number of iteration unless convergence is reached
Convergence type	convergence_type	'average_fitness_tracker'	
Percent change	percent_change	0.1	(default) percent change in non-dominated frontier

(*) recommended for MOGA in the reference manual

Appendix D. Generalization (A) - heat pumping and co-generation (Chapter 5)

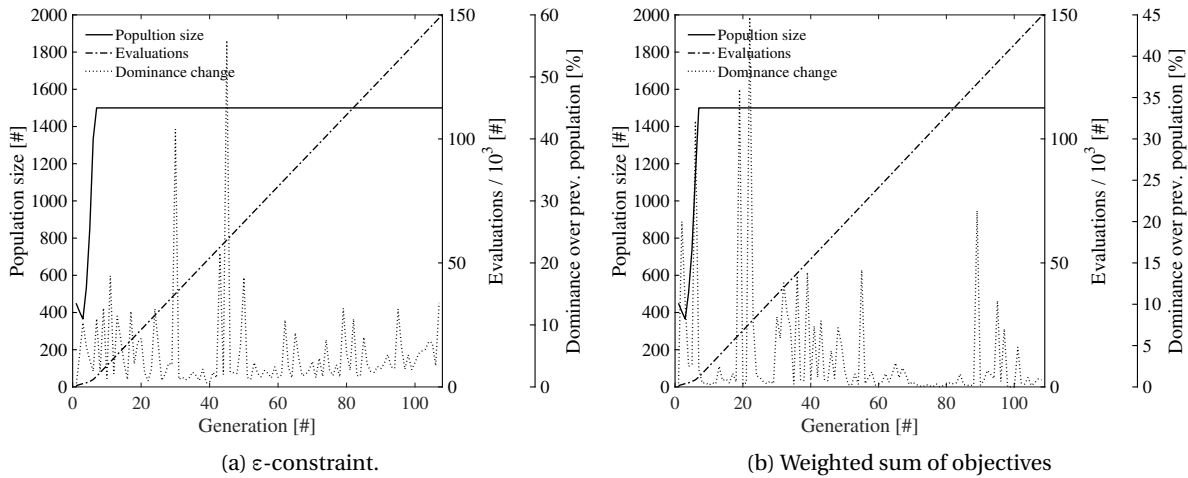


Figure D.1 – Analysis of MOGA propagation of plant $x = 2$.

D.1.2 MILP input parameters

The input parameters used for CPLEX [5] are displayed in Table D.2. The last three entries were found based on the parameter tuning performed by CPLEX.

Table D.2 – Input parameters for CPLEX [5], AMPL [3].

Parameter	Expression	Value	Comment
mipgap	'mipgap'	0.005	relative difference between best integer and best bound
time	'time'	300	cpu time limit in seconds
flow cuts	'flowcuts'	1	(agressive) use of flow cuts in solving MIPs
mir cuts	'mircuts'	1	(moderate) generation of MIP rounding cuts
branch	'branch'	1	branching direction for integer variables

D.2 Additional results

D.2.1 Sampling in detail

The results from the sampling are depicted in Figure D.2 and Figure D.3. Figure D.2a compares the number of evaluations and number of identified solutions (by deriving the non-dominated frontiers) found with the different sampling algorithms. The sample size is set to 80,000 from which samples with an electricity to natural gas price ratio of above 8 and below 1 are removed. The factorial combination of the bounds (of the parameter ranges) is added to the sample size. Brute forcing indicates manually selected parameter spacing (with different degree fineness) and evaluating every combination of these. Naturally, the (finest grid) brute forcing requires the largest number of evaluations as indicated in Figure D.2a. However, investigating the intersection of the Pareto points identified by the different algorithms yields almost 100% overlap as shown in Figure D.2. Hence,

the Matlab [137] intrinsic latin hypercube sampling [233] is suggested and applied within the study. Figure D.3 shows the histogram and cumulative sum of the occurrences of the different solutions during the sampling process. If all Pareto solutions are selected, a reduction with respect to the original of $1-239/239 = 0\%$ is achieved. If further reduction of the selected solutions is desired, the histogram can be used as an indicator. It shows that 170, 121, and 95 solutions represent 99%, 95%, and 90% of the occurrences of the Pareto points thereby achieving a reduction of 29%, 49%, and 60%.

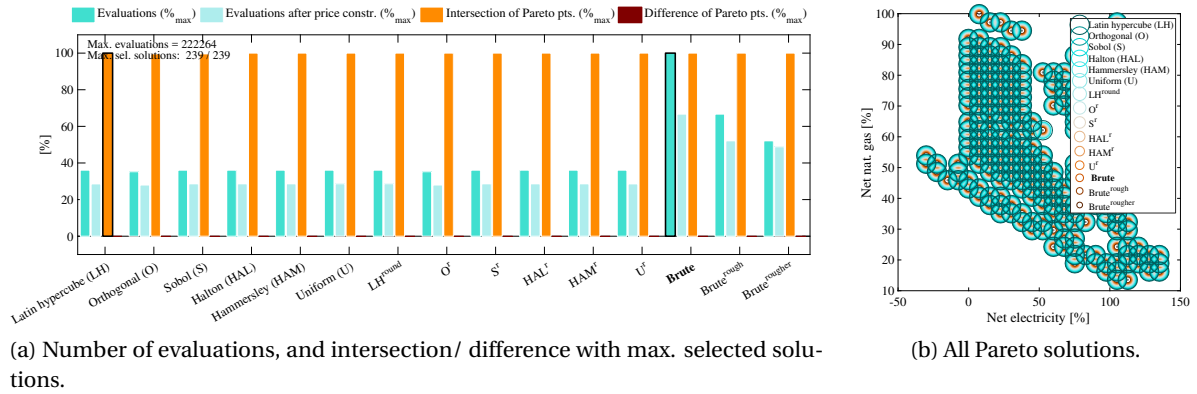
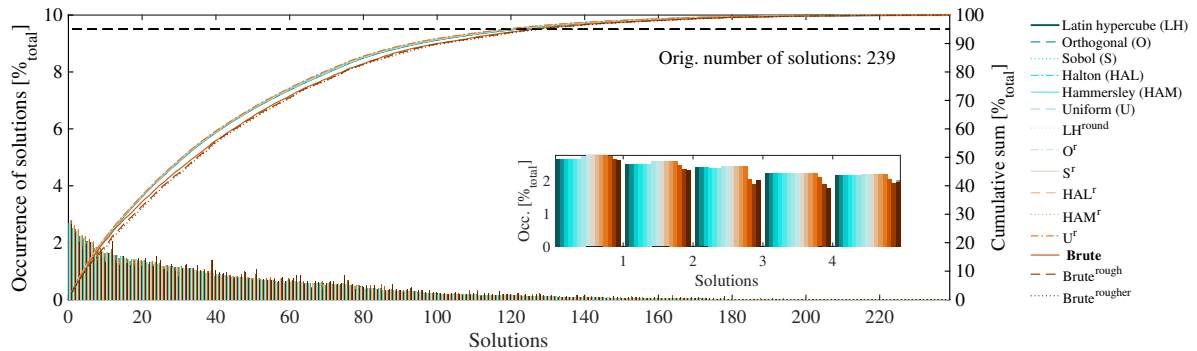


Figure D.2 – Selection of solutions with different sampling algorithms.



D.2.2 Solution generation & pruning: remaining plants

The results from the multi-objective optimization problem with ϵ -constraint introduced in Section 5.3.2 and 5.3.3, are depicted as surfaces of non-dominated solutions in Figure D.4 for the remaining plants (plant 1, Figure D.4a; plant 2 with fixed HEN, Figure D.4b; plant 3, Figure D.4c).

The resource plane¹ reveals a non-dominated frontier between the natural gas and electricity consumption. The original plant with its reference consumption is marked at highest total resource consumption with zero capital cost. Every other solution improves either the electricity or natural

¹ The resource plane refers to the plane formed with the two types of resource consumption as axes, and hence spans the natural gas and electricity consumption.

Appendix D. Generalization (A) - heat pumping and co-generation (Chapter 5)

gas consumption. As expected, it can be observed that the solutions of plant 2 with a fixed HEN, $\Delta T_{\min}/2=5K$, in Figure D.4b are further away from the infeasible region as compared to Figure 5.9b. Due to the fixed HEN and therewith no further possibility for process heat recovery, the resource consumption cannot be as strongly reduced as for the case of process heat recovery.

The plants have different resource consumption ranges. While plant 1 in Figure D.4a shows the highest natural gas consumption, the highest electricity consumption is shown in Figure D.4b. The lowest resource consumption is displayed by plant 3 in Figure D.4c. These values are linked to the plant requirements shown in Figure 5.7 and Table 5.3. Plant 1 has the highest hot minimum energy requirement (MER), while plant 3 does not contain a concentrated milk production unit and has, therefore, the lowest MER and resource consumption.

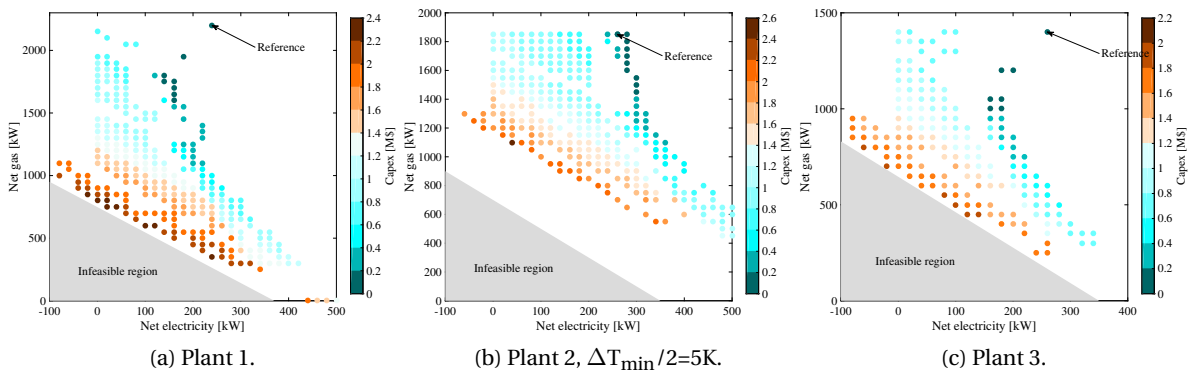


Figure D.4 – Solution generation.

Figure D.5 shows the occurrence of all minimum TAC solutions selected during the sampling step of the different plants: plant 1 (Figure D.5a), plant 2 with fixed HEN (Figure D.5b), plant 3 (Figure D.5c). Relatively few solutions are never selected and therefore discarded. The encircled points mark the 99 percentile of the most recurrent solutions. A similarity between the patterns of selected solutions is observed, indicating, that the solutions at the edges of the surface are the most promising ones.

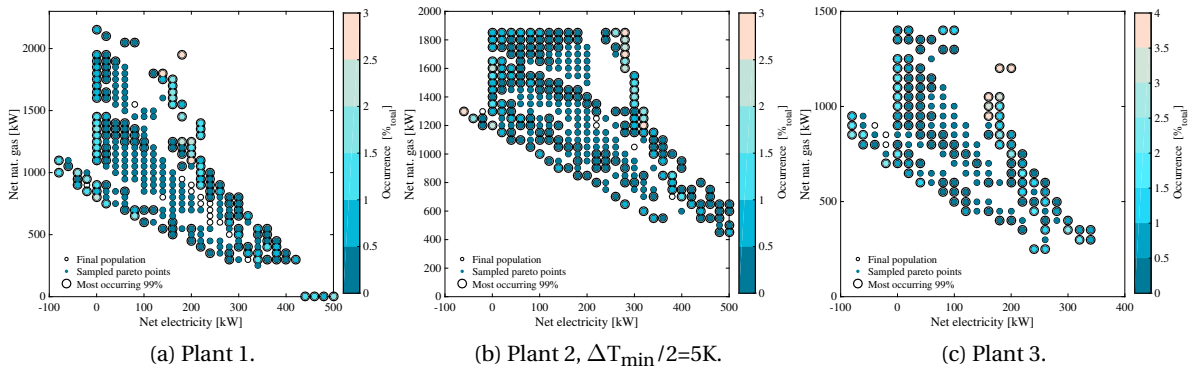


Figure D.5 – Solution pruning.

The characteristics of the selected solutions of the three plants were analyzed in Figure D.6 with respect to the exergy efficiency. Similar trends can be observed for the three plants, as for the results presented in Section 5.4.1.2. The cooling water, natural gas, and boiler consumption decreased, while the electricity grid consumption increased with increasing exergy efficiency. The co-generation engine increased initially and then decreased with increasing exergy efficiency. Heat pumping was utilized with increasing exergy efficiency, until MVR was activated (for all except plant 3), at which point it restarted from zero. The same observations as stated in Section 5.4.1.2 can be drawn regarding subcooling, gas-cooling, and the fluid indexes.

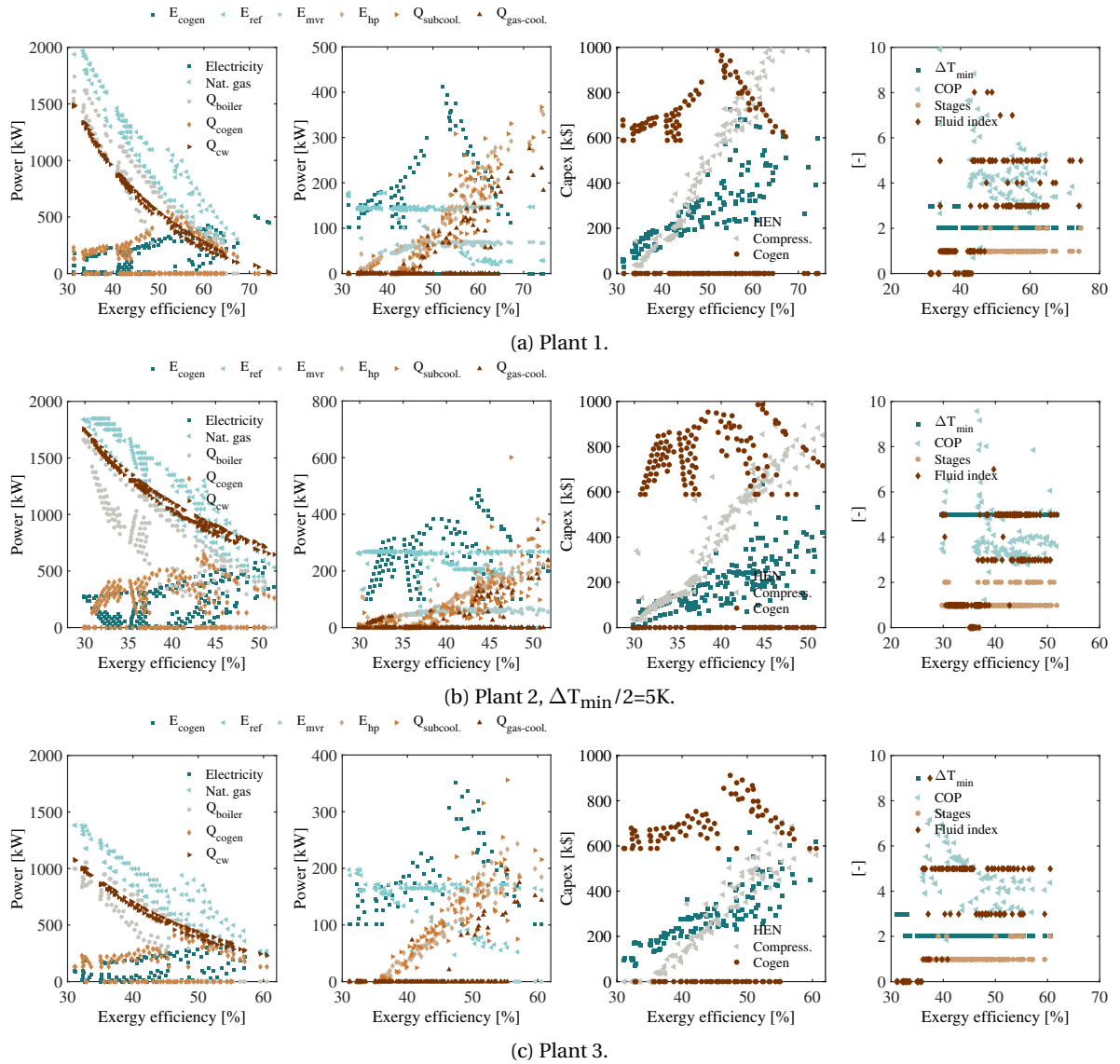


Figure D.6 – Pruned solution characteristics.

D.2.3 Results retrieval: remaining plants

Figure D.8 depicts the solutions and respective cost distribution and emissions of selected OECD countries of the three plants (plant 1, Figure D.8a; plant 2 with fixed HEN, Figure D.8b; plant 3, Figure D.8c).

The number indexes the solution id which can be found in Table D.5, Table D.6, Figure D.7b, and Figure D.10 for plant 2 with fixed HEN. As found in Section 5.4.2.1, it is visible that countries with low resource prices (United States of America (US), Canada (CA), and Poland (PL)) exhibited more seldom economically viable emission reductions measures for operating times of 2500 hours per year. When adding a CO₂ tax and increasing the operating hours, certain measures became more often profitable.

It has to be noted that especially plant 2 with fixed HEN (Figure D.8b) generated fewer cost-viable emission reduction solutions, due to the higher constraints on the heat and resource requirements. And especially plant 1 produced almost exclusively cost-viable emission reduction measures. This was attributed to the smaller range temperature thermal requirements of the plant, and with that more options for heat recovery, heat pumping, and co-generation.

D.2.4 Database of solutions

Figure D.7 shows the indexes of the selected solutions of plant 2 (without and with fixed HEN) on the resource plane. The solutions are represented in more detail in Appendix D.2.4.1 and Appendix D.2.4.2. The number indexes the solution id which can be found in Tables D.3-D.6.

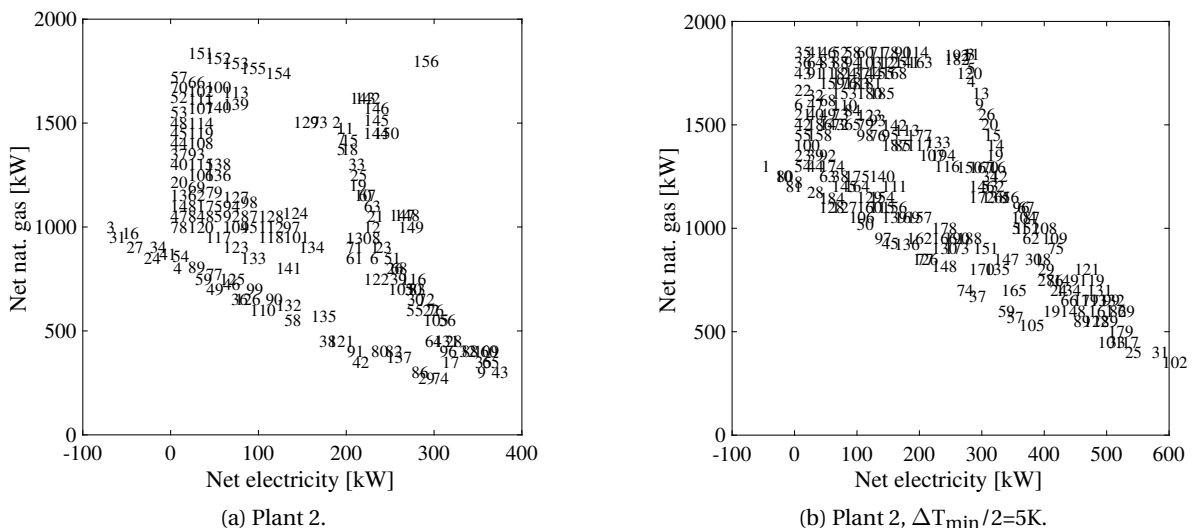
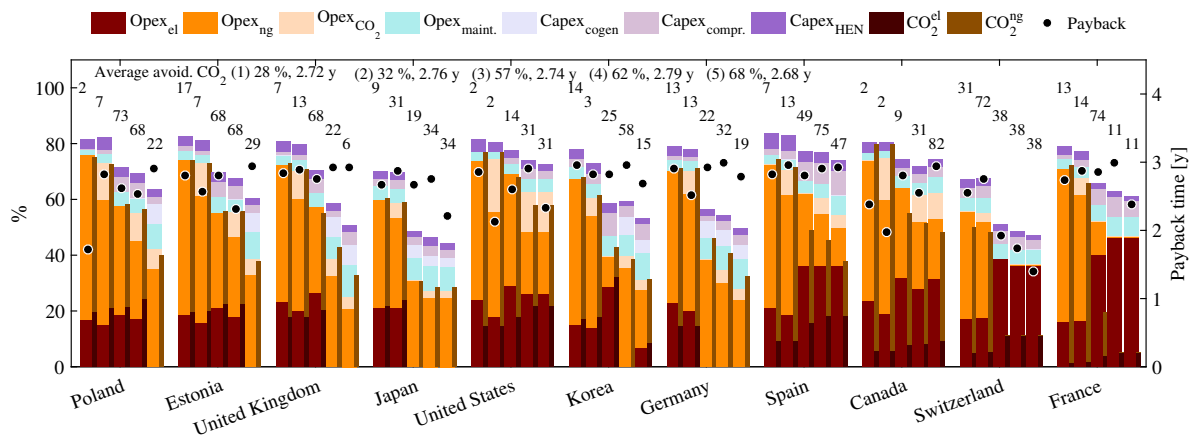
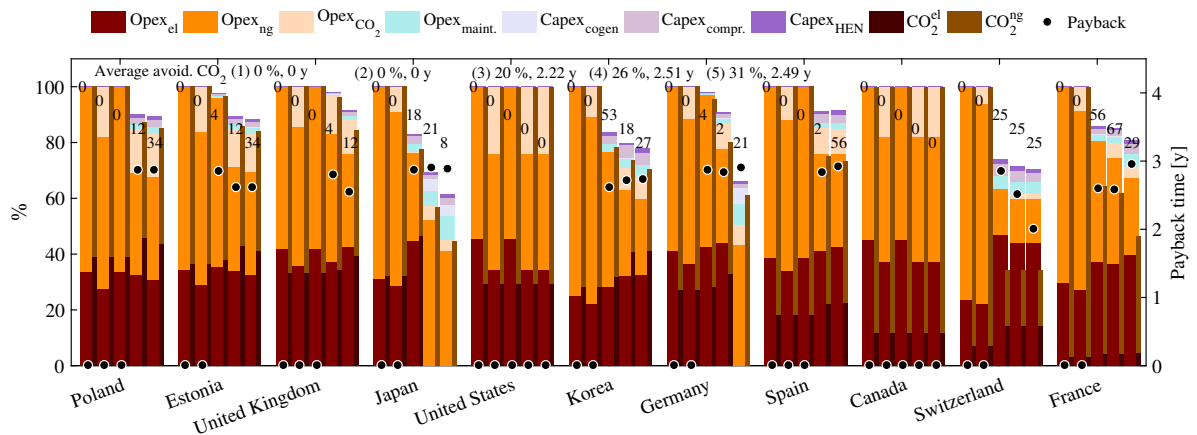


Figure D.7 – Solution indexes.

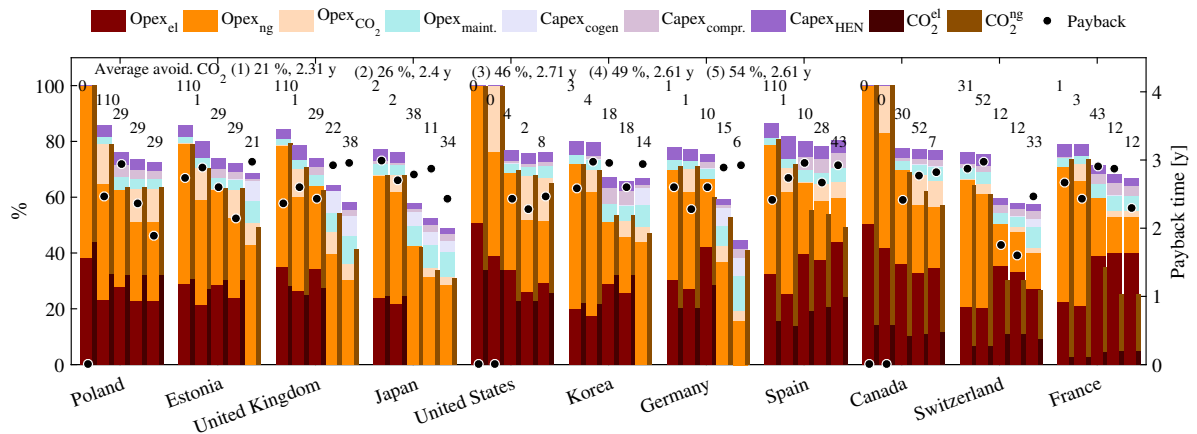
D.2. Additional results



(a) Plant 1.



(b) Plant 2, $\Delta T_{\min}/2=5K$.



D.2.4.1 Plant 2

This section contains a more detailed analysis of the database of solutions generated for plant 2. The integrated composite curves (ICCs) of selected solutions from the country analysis are displayed in Figure D.9. In Tables D.3-D.4, economical, energetic, and technical metrics of the solutions are displayed.

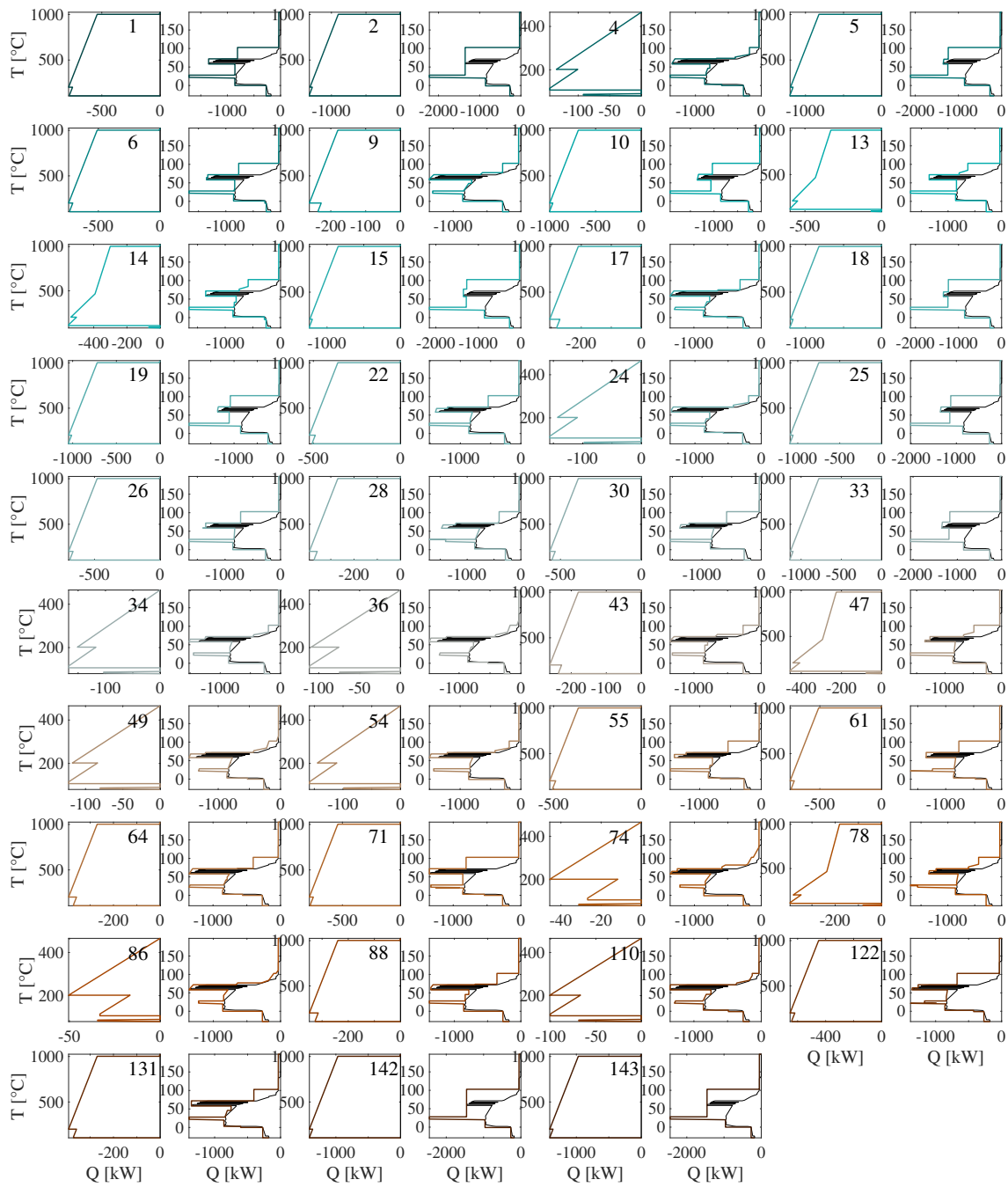


Figure D.9 – ICCs selected during data retrieval of plant 2.

D.2. Additional results

Table D.3 – Database of solutions for plant 2 (I).

Id	Cap.HEN k\$	Cap.Comp k\$	Cap.Cogen k\$	Nat. gas kW	Net. elec. kW	ΔT_{min} K	Q _{boi} kW	Q _{cogen} kW	E _{cogen} kW	E _{ref} kW	E _{mvr} kW	E _{hp} kW	stag.	fluid	subcool. kW	gas-cool. kW	Temp. levels °C	COP	Exerg. eff. %
1	217	161	0.0	900	228	2	810	0	0	180	48	0	0	-	0	0	-	0.0	46.4
2	112	0	0.0	1503	184	2	1353	0	0	184	0	0	0	-	0	0	-	0.0	35.8
3	345	411	940.1	1000	-73	2	0	495	375	174	64	64	1	R161	33	0	25.5,70,Δ12	4.4	53.4
4	430	564	845.0	800	3	2	0	396	300	121	56	127	1	R161	72	0	75.5,Δ13,1,48.5,Δ12	3.0	55.6
5	137	39	0.0	1373	190	2	1236	0	0	180	0	10	1	R161	24	0	Δ16,73,56,Δ2	23.4	37.7
6	233	205	0.0	850	227	2	765	0	0	167	50	10	1	R290	5	0	66.5,Δ1,Δ27,34.5,-7	4.7	47.7
7	122	39	0.0	1424	190	2	1282	0	0	180	0	10	1	R161	14	0	53.5,82.5,Δ17	13.2	36.9
8	199	150	0.0	943	229	2	848	0	0	184	45	0	0	-	0	0	-	0.0	45.3
9	444	531	0.0	300	350	2	270	0	0	180	61	109	1	R290	173	0	50.5,Δ21,26,79.5,Δ17	4.8	62.2
10	169	104	0.0	1150	210	2	1035	0	0	180	0	30	1	NH3	32	0	75,Δ17,55.5,Δ1	20.6	41.3
11	113	39	0.0	1474	189	2	1327	0	0	179	0	10	1	R161	10	0	77,Δ20,2	3.2	36.2
12	208	136	0.0	1000	220	2	900	0	0	180	0	40	1	NH3	31	0	Δ2,56.5,74.5,Δ9	21.5	44.2
13	266	165	748.0	1150	0	2	497	296	224	174	50	0	0	-	0	0	-	0.0	45.6
14	282	216	748.6	1100	0	2	451	297	224	160	54	10	1	R161	8	0	-7,Δ30,43.5	7.2	46.9
15	119	39	0.0	1416	194	2	1274	0	0	184	0	10	1	NH3	1	0	Δ2,54.5,79	14.8	37.0
16	362	399	925.5	969	-55	2	0	480	363	184	70	53	1	R161	65	0	Δ29,66,25.5	5.4	53.4
17	440	638	0.0	350	309	2	315	0	0	100	57	152	1	R161	137	0	77,Δ16,Δ29,45,0.5	3.3	61.7
18	134	39	0.0	1374	194	2	1237	0	0	184	0	10	1	NH3	24	0	Δ5,71.5,54.5,Δ20	22.3	37.7
19	162	86	0.0	1200	204	2	1080	0	0	180	0	24	1	NH3	14	0	56.5,74.5,Δ9	21.5	40.5
20	235	150	748.8	1212	0	2	551	297	225	180	45	0	0	-	0	0	-	0.0	44.2
21	187	133	0.0	1050	224	2	945	0	0	184	0	39	1	NH3	61	0	75,Δ9,55.5,Δ11	19.7	43.1
22	286	353	0.0	600	287	2	540	0	0	180	60	48	1	R161	57	0	26,Δ29,70	5.0	53.2
23	214	161	0.0	900	233	2	810	0	0	184	48	0	0	-	0	0	-	0.0	46.3
24	450	542	868.9	850	-30	2	0	421	318	114	56	118	1	R161	78	0	74,Δ7,Δ28,42,1	3.4	59.8
25	152	73	0.0	1250	204	2	1125	0	0	184	0	20	1	NH3	22	0	Δ4,56,74,Δ11	21.7	39.6
26	236	222	0.0	800	246	2	720	0	0	180	56	10	1	R161	13	0	Δ29,61.5,26	6.1	48.5
27	461	516	892.7	900	-50	2	0	446	337	122	56	109	1	R161	112	0	75.5,Δ22,Δ28,45,0.5	3.3	55.3
28	333	444	0.0	450	313	2	405	0	0	174	70	69	1	R290	110	32	25.5,Δ15,69,53,Δ22	5.4	57.5
29	582	638	589.1	271	282	2	0	134	102	174	62	147	1	R161	172	135	61.5,Δ26,26,82,Δ15	4.4	66.6
30	322	316	0.0	650	269	2	585	0	0	174	57	39	1	R290	57	0	26,69.5,Δ30	5.1	52.1
31	445	491	916.4	950	-70	2	0	471	356	130	57	98	1	R161	50	0	74,Δ2,Δ27,48,1	3.3	54.8
32	401	473	0.0	400	329	2	360	0	0	180	57	92	1	R161	83	0	26,75.5,Δ9,Δ17,58.5	4.6	58.8
33	138	66	0.0	1300	202	2	1170	0	0	184	0	18	1	NH3	26	0	Δ4,56,76.5,Δ19	19.7	38.7
34	324	429	892.7	900	-24	2	0	446	337	180	70	64	1	R161	53	26	Δ21,67,26	5.1	53.8
35	376	523	0.0	350	347	2	315	0	0	180	54	114	1	R161	81	0	26,51,Δ17,78.5	4.1	60.1
36	495	633	773.1	650	69	2	0	322	243	105	70	137	1	R161	75	105	1,70,Δ9,Δ21,46	3.4	58.8
37	223	110	724.6	1350	0	2	721	272	206	174	0	32	1	NH3	35	0	Δ4,56.5,74.5,Δ11	21.7	41.4
38	468	746	676.5	450	169	2	0	223	169	87	58	193	1	R290	124	116	75,Δ13,Δ14,48,1	3.1	63.2
39	318	248	0.0	750	250	2	675	0	0	177	53	21	1	R161	25	0	Δ29,65,24	5.3	49.8
40	234	128	732.3	1300	0	2	661	280	212	174	0	38	1	NH3	47	0	Δ4,56,75,Δ14	20.8	42.4
41	432	425	876.7	866	-13	2	0	429	325	180	70	62	1	R161	63	52	Δ28,66,26	5.4	54.2
42	757	792	627.8	350	207	2	0	173	131	70	60	209	1	R290	244	129	78.5,Δ26,Δ28,41,0.5	3.4	66.2
43	377	560	0.0	300	366	2	270	0	0	184	54	127	1	R161	91	0	80,Δ17,51,26	4.0	61.5
44	206	105	722.6	1400	0	2	769	270	204	174	0	30	1	NH3	47	0	75.5,Δ9,56,Δ11	19.8	40.4
45	204	82	713.3	1450	0	2	832	261	197	174	0	23	1	NH3	76	0	56,Δ26,Δ11,74	21.7	39.5
46	411	482	809.0	725	60	2	0	359	271	180	70	82	1	R161	81	70	Δ29,70,26	5.0	56.3
47	354	246	784.5	1050	0	2	339	334	252	180	53	20	1	R161	24	0	64.5,Δ28,26	5.6	48.1
48	194	64	706.0	1500	0	2	890	253	191	174	0	17	1	NH3	37	0	73.5,Δ12,56.5,Δ12	23.2	38.7
49	485	609	797.1	700	41	2	0	347	262	105	68	130	1	R161	120	100	Δ21,70,1,46,Δ30	3.5	57.9
50	277	293	0.0	700	267	2	630	0	0	180	52	36	1	R290	27	0	70,Δ14,26	4.4	50.7
51	218	200	0.0	850	243	2	765	0	0	184	49	10	1	NH3	4	0	24,45,Δ15,71	4.6	47.3
52	156	39	703.7	1622	0	2	1005	251	190	180	0	10	1	NH3	10	0	Δ4,56,77,Δ11	18.5	36.7
53	177	49	707.5	1550	0	2	932	255	193	180	0	13	1	NH3	18	0	72,Δ5,56.5,Δ9	24.6	37.8
54	341	447	873.9	861	2	2	0	426	322	184	70	70	1	R161	75	0	70,Δ26,26	4.9	53.6
55	340	430	0.0	600	269	2	540	0	0	135	61	73	1	R161	33	0	1,39.5,Δ26,68.5	2.6	53.7
56	295	393	0.0	550	306	2	495	0	0	184	65	57	1	R161	65	0	68.5,Δ29,24	4.9	54.2
57	144	0	690.8	1719	0	2	1115	238	180	180	0	0	0	-	0	0	-	0.0	35.3
58	398	701	724.9	550	129	2	0	272	206	103	70	162	1	R1270	125	121	47.5,Δ11,0.5,71.5,Δ22	3.1	60.5
59	472	591	821.1	750	28	2	0	372	281	118	69	123	1	R161	48	80	68.5,Δ9,Δ11,41.5,0.5	3.3	56.5
60	295	541	0.0	400	353	2	360	0	0	180	70	103	1	R161	60	86	Δ17,68,24	4.6	57.9
61	278	358	0.0	850	200	2	765	0	0	91	52	57	1	NH3	19	37	24,Δ12,1	0.7	48.3
62	255	159	719.5	1150	20	2	550	267	202	174	48	0	0	-	0	0	-	0.0	45.2
63	171	122	0.0	1100	220	2	990	0	0	184	0	36	1	NH3	42	0	Δ4,56.5,77,Δ14	19.3	42.1
64	438	552	0.0	450	290	2	405	0	0	112	59	119	1	R290	161	0	Δ24,75,Δ29,43.5,1	3.5	58.4
65	365	532	0.0	350	355	2	315	0	0	184	55	115	1	R161	65	0	80,Δ13,51,26	4.0	59.8
66	143	0	664.8	1695	20	2	1142	211	160	180	0	0	0	-	0	0	-	0.0	35.3
67	165	105	0.0	1150	214	2	1035	0	0	184	0	30	1	NH3	26	0	75,Δ13,55.5,Δ1	20.2	41.3
68	233	222	0.0	800	251	2	720	0	0	184	56	10	1	R161	13	0	Δ29,61.5,26	6.1	48.4
69	234	150	723.1	1188	20	2	578	271	205	180	45	0	0	-	0	0	-	0.0	44.3
70	149	39	703.7	1669	0	2	1047	251	190	180	0	10	1	R290	36	0	Δ29,52,84,Δ8	10.1	36.0

Appendix D. Generalization (A) - heat pumping and co-generation (Chapter 5)

Table D.4 – Database of solutions for plant 2 (II).

Id	Cap _{HEN} k\$	Cap _{Comp} k\$	Cap _{Cogen} k\$	Nat. gas kW	Net. elec. kW	ΔT_{min} K	Q _{boi} kW	Q _{cogen} kW	E _{cogen} kW	E _{ref} kW	E _{envr} kW	E _{bp} kW	stag.	fluid	subcool. kW	gas-cool. kW	Temp. levels °C	COP	Exerg. eff. %
71	236	310	0.0	900	200	2	810	0	0	107	48	45	1	NH3	15	0	$\Delta 11,23,1$	7.1	47.0
72	276	322	0.0	650	282	2	585	0	0	184	56	41	1	R161	47	0	$\Delta 29,70,24$	4.7	51.8
73	134	88	0.0	1503	160	2	1353	0	0	135	0	25	1	R290	16	0	$\Delta 11,22,5,1$	7.4	36.2
74	491	652	589.1	271	298	2	0	134	102	184	60	155	1	R161	110	149	$67,\Delta 27,84,26$	4.1	65.8
75	265	166	696.7	1100	40	2	548	244	184	174	50	0	0	-	0	0	-	0.0	45.9
76	283	353	0.0	600	292	2	540	0	0	184	60	48	1	R161	57	0	$26,\Delta 29,70$	5.0	53.0
77	396	475	831.8	772	40	2	0	383	289	180	68	82	1	R161	74	69	$\Delta 28,70,24$	4.7	55.3
78	366	292	796.1	1000	0	2	272	346	261	174	54	34	1	R161	40	0	$24,68,5,\Delta 30$	4.9	49.5
79	234	150	697.2	1164	40	2	604	244	185	180	45	0	0	-	0	0	-	0.0	44.4
80	484	595	652.2	400	228	2	0	198	150	184	58	135	1	R161	117	106	$67,\Delta 29,26,81,5,\Delta 2$	4.3	62.9
81	268	204	721.8	1100	20	2	501	269	204	164	50	10	1	R290	6	0	$\Delta 11,71,27,\Delta 13,-7$	4.5	46.4
82	321	655	652.2	400	245	2	0	198	150	180	70	145	1	R290	124	0	$64,5,\Delta 29,26,93,5$	4.0	62.2
83	272	290	0.0	700	271	2	630	0	0	184	52	35	1	R161	20	0	$26,\Delta 13,70$	4.5	50.6
84	288	227	745.2	1050	20	2	412	293	222	174	58	10	1	R161	11	0	$\Delta 21,53,5,26$	7.5	47.6
85	282	216	697.3	1050	40	2	501	244	185	160	54	10	1	R161	5	0	$\Delta 19,41,-7$	7.1	47.1
86	484	631	603.4	300	274	2	0	149	112	180	57	150	1	R161	146	137	$26,79,\Delta 15,\Delta 17,62$	4.3	65.5
87	265	166	645.0	1050	80	2	598	191	144	174	50	0	0	-	0	0	-	0.0	46.2
88	376	480	0.0	400	331	2	360	0	0	180	56	96	1	R161	38	0	$75,5,\Delta 9,47,5,26$	4.4	58.7
89	409	453	847.7	806	20	2	0	399	302	180	54	89	1	R161	53	0	$26,49,\Delta 14,75,5$	4.3	54.9
90	355	538	773.1	650	108	2	0	322	243	180	70	102	1	R1270	100	83	$24,71,\Delta 5,\Delta 20,57$	4.7	57.4
91	457	810	652.2	400	201	2	0	198	150	86	70	195	2	R161	207	0	$49,\Delta 29,\Delta 17,95,1,70,\Delta 11$	3.1	64.1
92	266	204	669.6	1050	60	2	553	216	163	163	50	10	1	R161	10	0	$\Delta 17,-4,5,\Delta 23,68,18,5$	5.1	46.7
93	217	102	695.5	1350	20	2	775	242	183	174	0	29	1	NH3	38	0	$56,5,\Delta 4,\Delta 14,74,5$	22.0	41.0
94	254	159	668.0	1100	60	2	601	214	162	174	48	0	0	-	0	0	-	0.0	45.5
95	277	208	659.5	1000	80	2	527	206	155	174	51	10	1	R161	12	0	$26,66,\Delta 28$	5.4	47.4
96	409	600	0.0	400	307	2	360	0	0	111	58	138	1	R290	94	0	$74,\Delta 11,\Delta 14,45,1$	3.2	59.7
97	253	166	589.1	1000	128	2	656	134	102	180	50	0	0	-	0	0	-	0.0	46.3
98	232	150	645.3	1116	80	2	657	191	145	180	45	0	0	-	0	0	-	0.0	44.7
99	341	516	797.1	700	86	2	0	347	262	184	70	94	1	R161	68	80	$70,\Delta 22,24$	4.5	56.3
100	143	0	638.8	1671	40	2	1168	185	140	180	0	0	0	-	0	0	-	0.0	35.4
101	273	217	589.1	950	129	2	611	134	102	166	54	10	1	R290	9	0	$\Delta 27,49,5,-0,5$	7.3	47.5
102	148	39	677.8	1650	20	2	1078	224	170	180	0	10	1	R290	20	0	$87,5,\Delta 6,54,5,\Delta 13$	9.2	36.0
103	389	333	0.0	700	248	2	630	0	0	147	55	46	1	R290	56	0	$67,5,\Delta 18,\Delta 29,41,5,1$	3.7	51.2
104	290	228	693.8	1000	60	2	463	241	182	174	58	10	1	R161	8	0	$50,\Delta 13,25,5$	8.0	47.9
105	435	372	0.0	550	288	2	495	0	0	174	58	56	1	R161	62	48	$47,\Delta 11,26,71,\Delta 22$	5.0	54.8
106	244	131	714.7	1250	20	2	649	262	198	180	0	39	1	NH3	90	0	$56,\Delta 14,\Delta 14,74$	22.0	43.0
107	170	39	677.8	1569	20	2	1005	224	170	180	0	10	1	R1270	46	0	$70,5,\Delta 6,56,\Delta 13$	23.7	37.2
108	202	93	691.7	1400	20	2	827	238	180	174	0	26	1	NH3	33	0	$75,\Delta 9,56,5,\Delta 7$	20.9	40.1
109	355	524	0.0	400	345	2	360	0	0	184	70	91	2	R290	161	0	$96,5,\Delta 23,\Delta 28,68,5,24$	4.5	58.2
110	444	663	749.0	600	91	2	0	297	225	96	59	160	1	R161	79	80	$48,\Delta 27,1,74,\Delta 2$	3.3	60.0
111	152	39	677.8	1612	20	2	1044	224	170	180	0	10	1	NH3	7	0	$\Delta 5,56,\Delta 6,79,5$	16.0	36.6
112	267	204	616.6	1000	100	2	606	162	123	163	50	10	1	R161	7	0	$-7,\Delta 18,63,5,24,5,\Delta 20$	5.3	47.0
113	142	0	612.8	1647	60	2	1195	158	120	180	0	0	0	-	0	0	-	0.0	35.5
114	192	53	675.8	1500	20	2	946	222	168	174	0	14	1	NH3	30	0	$\Delta 11,56,5,72,\Delta 11$	25.3	38.3
115	228	127	709.3	1300	20	2	704	256	194	177	0	37	1	NH3	75	0	$54,5,\Delta 11,\Delta 17,74$	20.5	42.0
116	277	262	0.0	750	262	2	675	0	0	184	52	26	1	R161	0	0	$67,26$	4.3	49.4
117	329	305	757.2	950	40	2	300	306	231	180	54	38	1	R161	42	0	$24,70,\Delta 29$	4.7	49.8
118	291	228	642.2	950	100	2	514	188	142	174	58	10	1	NH3	2	0	$24,47,\Delta 5$	8.1	48.5
119	193	75	688.2	1450	20	2	878	235	178	177	0	21	1	NH3	83	0	$56,5,\Delta 28,\Delta 17,74,5$	22.4	39.2
120	355	272	769.2	1000	20	2	322	318	240	180	54	27	1	R161	34	0	$\Delta 30,67,5,26$	5.3	49.0
121	394	773	676.5	450	180	2	0	223	169	94	70	185	2	R161	109	151	$\Delta 14,48,72,\Delta 13,1$	3.6	62.7
122	352	462	0.0	750	220	2	675	0	0	81	53	86	2	R161	40	0	$23,5,\Delta 6,\Delta 24,65,5,0,5$	1.3	50.6
123	334	324	739.5	900	60	2	288	287	217	180	57	41	1	R161	50	0	$\Delta 30,70,26$	5.0	50.7
124	227	150	589.1	1064	128	2	714	134	102	184	45	0	0	-	0	0	-	0.0	44.8
125	352	483	821.1	750	56	2	0	372	281	184	70	82	1	R161	78	55	$70,\Delta 27,25,5$	4.9	55.6
126	361	677	773.1	650	73	2	0	322	243	93	70	153	1	R161	134	116	$42,5,\Delta 22,68,5,\Delta 25,1$	3.5	58.7
127	233	150	671.3	1140	60	2	631	218	165	180	45	0	0	-	0	0	-	0.0	44.5
128	254	160	616.2	1050	100	2	651	162	122	174	48	0	0	-	0	0	-	0.0	45.7
129	141	236	0.0	1503	140	2	1353	0	0	66	0	74	1	R161	25	0	$23,5,\Delta 7,0,5$	6.7	36.5
130	219	294	0.0	943	200	2	848	0	0	112	45	43	1	R161	23	0	$24,\Delta 11,1$	6.9	46.0
131	380	553	0.0	450	300	2	405	0	0	122	59	119	1	R161	30	0	$48,\Delta 15,1,74$	3.1	58.0
132	452	541	760.0	623	120	2	0	309	233	180	57	116	1	R161	179	0	$26,64,5,\Delta 29,\Delta 19,88,5$	4.1	58.0
133	334	354	727.0	850	80	2	266	275	208	180	60	48	1	R161	54	0	$26,\Delta 27,70$	4.9	51.6
134	279	228	589.1	900	146	2	566	134	102	180	58	10	1	R161	4	0	$49,5,\Delta 7,26$	8.0	48.4
135	383	584	735.2	571	160	2	0	283	214	184	59	131	1	R161	83	0	$65,\Delta 28,24,91$	3.8	58.5
136	229	128	687.8	1250	40	2	699	234	177	180	0	38	1	NH3	32	0	$56,\Delta 4,\Delta 7,74$	21.2	42.6
137	583	644	639.1	373	246	2	0	185	140	174	61	151	1	R290	237	0	$24,65,\Delta 28,\Delta 11,89,5$	3.9	63.3
138	219	115	674.9	1300	40	2	768	221	167	174	0	33	1	NH3	41	0	$\Delta 4,56,5,75,5,\Delta 14$	20.8	41.6
139	151	39	622.0	1588	60	2	1125	168	127	177	0	10	1	R161	9	0	$52,\Delta 11,84$	11.1	36.3
140	155	39	651.8	1573	40	2	1056	198	150	180	0	10	1	NH3	6	0	$76,5,\Delta 9,56,\Delta 1$	18.8	36.9
141	333	354	675.0	800	120	2	318	221	167	180	60	48	1	R161	57	0			

D.2.4.2 Plant 2, $\Delta T_{\min}/2=5K$

This section contains a more detailed analysis of the database of solutions generated for plant 2 with fixed HEN. The ICCs of selected solutions from the country analysis are displayed in Figure D.10. In Tables D.5-D.6, economical, energetic, and technical metrics of the solutions are displayed.

Analysis of the ICCs in Figure D.10 reveals that most selected economically viable solutions exhibit a heat pump or mechanical vapor re-compression system across the process pinch.

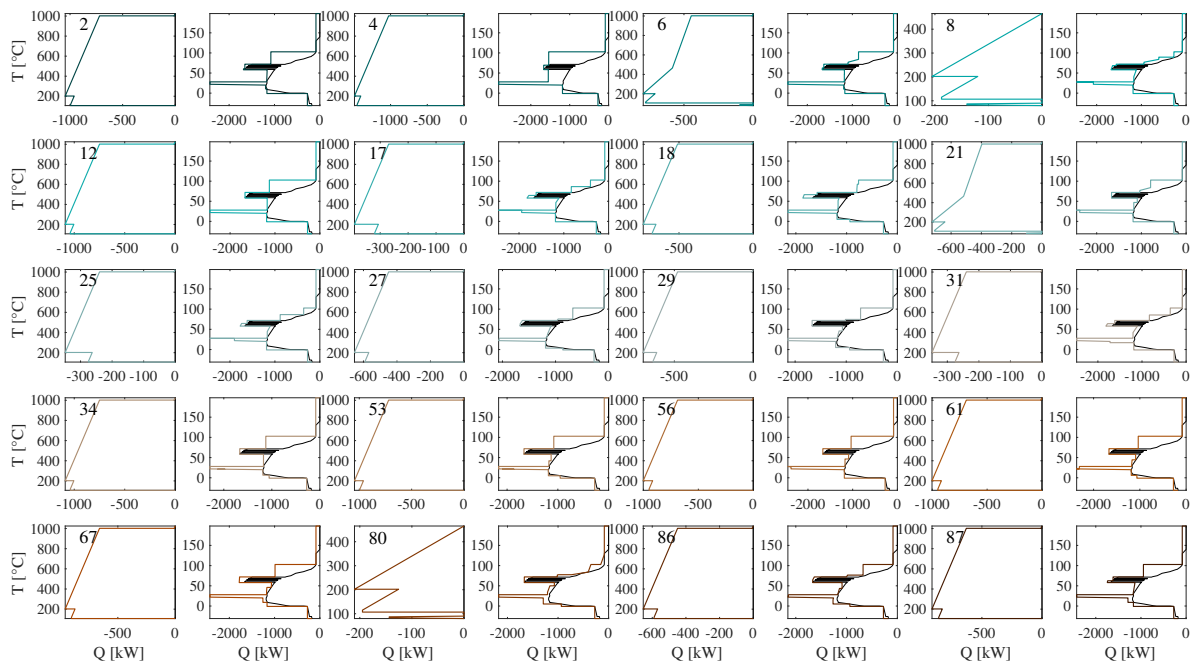


Figure D.10 – ICCs selected during data retrieval of plant 2, $\Delta T_{\min}/2=5K$.

Appendix D. Generalization (A) - heat pumping and co-generation (Chapter 5)

Table D.5 – Database of solutions for plant 2, $\Delta T_{\min}/2=5K$ (I).

Id	Cap _{HEN} kS	Cap _{Comp} kS	Cap _{Cogen} kS	Nat. gas kW	Net. elec. kW	ΔT_{\min} K	Q _{boi} kW	Q _{cogen} kW	E _{cogen} kW	E _{ref} kW	E _{mvr} kW	E _{hp} kW	stag.	fluid	subcool. kW	gas-cool. kW	Temp. levels °C	COP	Exerg. eff. %
1	186	684	1081.4	1300	-52	5	0	644	487	207	51	177	1	R161	63	128	81,Δ17,47,3	2.8	43.7
2	61	207	0.0	1200	323	5	1080	0	0	262	51	10	1	R290	11	0	62.5,Δ30,8.5	4.0	37.5
3	0	39	0.0	1841	276	5	1657	0	0	266	0	10	1	R161	0	0	62,11	3.5	29.8
4	16	39	0.0	1712	276	5	1541	0	0	266	0	10	1	NH3	0	0	71.5,56.5	24.7	31.2
5	6	39	0.0	1775	276	5	1597	0	0	266	0	10	1	NH3	0	0	45.5,67.5	16.4	30.5
6	92	199	870.7	1600	0	5	671	423	320	262	48	10	1	NH3	0	0	49.8,64.5	3.5	36.1
7	1	39	0.0	1821	272	5	1639	0	0	262	0	10	1	R161	10	0	Δ16,77.7	3.4	30.1
8	347	587	1044.5	1221	0	5	0	605	457	266	55	136	1	R161	91	0	91.5,Δ28,70.5,25.5	3.8	42.9
9	41	84	0.0	1600	290	5	1440	0	0	266	0	24	1	NH3	0	26	54,74	18.3	32.4
10	236	719	1057.9	1250	-31	5	0	619	468	207	70	161	2	R161	152	0	3,Δ18,90.5,36.5,Δ15,Δ15,64.5	2.8	43.7
11	12	39	0.0	1841	270	5	1657	0	0	260	0	10	1	R161	8	0	62,Δ30,4.5	3.7	29.9
12	82	160	0.0	1250	315	5	1125	0	0	266	48	0	0	-	0	0	-	0.0	36.8
13	35	69	0.0	1650	285	5	1485	0	0	266	0	19	1	NH3	0	21	53.5,73.5	18.3	31.8
14	68	142	0.0	1400	309	5	1260	0	0	266	0	42	1	NH3	0	0	54,74	18.3	34.7
15	62	128	0.0	1450	304	5	1305	0	0	266	0	38	1	NH3	0	0	54,74	18.3	34.1
16	77	150	0.0	1292	311	5	1163	0	0	266	45	0	0	-	0	0	-	0.0	36.2
17	152	769	0.0	450	525	5	405	0	0	266	70	188	1	R290	111	0	88.5,Δ18,66.5,25.5	3.7	49.4
18	70	564	0.0	850	384	5	765	0	0	207	70	107	2	R161	82	0	68.5,Δ15,94.5,Δ12,3	3.1	42.9
19	97	140	0.0	1350	308	5	1215	0	0	266	0	42	1	NH3	5	0	Δ2,74.5,56.5	20.7	35.4
20	56	114	0.0	1500	299	5	1350	0	0	266	0	33	1	NH3	0	0	54,74	18.3	33.5
21	164	223	887.1	1550	0	5	596	440	333	266	56	10	1	NH3	0	0	49,25.5	7.8	36.9
22	122	150	859.9	1666	0	5	751	412	311	266	45	0	0	-	0	0	-	0.0	35.2
23	227	490	941.4	1350	0	5	313	497	376	221	67	88	1	R161	70	0	4,Δ30,70.5,35	3.2	40.3
24	217	650	0.0	700	410	5	630	0	0	195	56	158	1	R161	97	0	78,Δ15,Δ11,46.2	3.1	45.8
25	316	780	0.0	400	529	5	360	0	0	266	66	198	1	R161	98	0	88.5,Δ20,66.5,25.5	3.8	50.7
26	52	99	0.0	1550	295	5	1395	0	0	266	0	28	1	NH3	0	0	54.5,74.5	18.3	32.9
27	255	611	0.0	750	389	5	675	0	0	190	58	141	1	R290	160	0	1.5,35,Δ13,77.5,Δ12,Δ20,59.5	3.0	45.0
28	387	593	1022.1	1174	20	5	0	582	440	266	56	137	1	R161	126	112	25.5,68,Δ30,Δ5,90.5	3.9	43.5
29	187	565	0.0	800	389	5	720	0	0	207	58	124	1	R161	34	0	76.5,Δ16,48.3	3.2	43.9
30	240	509	0.0	850	369	5	765	0	0	207	54	108	1	R161	98	0	74,Δ15,Δ28,45.5,3	3.5	43.2
31	132	892	0.0	400	572	5	360	0	0	266	70	236	1	R290	137	0	66,Δ22,87.5,15	3.3	49.5
32	121	150	834.4	1642	20	5	777	385	291	266	45	0	0	-	0	0	-	0.0	35.2
33	340	711	0.0	450	503	5	405	0	0	266	62	174	1	R290	314	0	88.5,Δ15,Δ28,66.5,25.5	4.0	50.0
34	112	220	0.0	1250	300	5	1125	0	0	236	48	16	1	NH3	0	0	23.5,4.5	8.1	37.1
35	100	120	847.0	1850	0	5	941	398	301	266	0	35	1	NH3	0	0	53.5,74	17.8	32.7
36	108	133	852.5	1800	0	5	886	404	305	266	0	39	1	NH3	0	0	54.5,74.5	18.3	33.3
37	413	786	783.5	672	280	5	0	333	252	266	68	198	1	R290	315	173	25.5,65,Δ28,Δ15,93.5	3.9	49.8
38	108	537	883.0	1250	60	5	333	436	329	221	51	118	2	R161	115	0	4,Δ22,79.5,3	3.0	41.1
39	198	462	912.0	1350	20	5	368	466	352	227	70	75	1	R290	72	0	65,Δ30,4.5	3.5	40.0
40	96	215	852.4	1550	20	5	661	404	305	262	54	10	1	NH3	5	0	8.5,45.5,Δ22	5.3	36.6
41	116	95	811.5	1850	20	5	1008	362	273	266	0	27	1	NH3	9	0	Δ5,74,56	21.0	32.5
42	188	325	921.7	1500	0	5	485	476	360	262	59	40	1	R290	40	0	8,Δ29,64.5	3.8	37.7
43	114	156	862.3	1750	0	5	822	414	313	266	0	47	1	NH3	0	0	55,76	17.4	34.0
44	250	498	903.5	1300	20	5	339	457	346	207	52	107	1	R161	51	0	3,Δ17,75.5,23,43.5	3.0	40.9
45	486	698	904.4	925	140	5	0	458	346	266	59	161	2	R161	118	0	25.5,65.5,Δ28,95,Δ1,77	4.1	46.6
46	95	101	788.2	1850	40	5	1052	338	255	266	0	29	1	NH3	0	0	54.5,74.5	18.3	32.2
47	128	161	839.2	1600	20	5	731	390	295	266	49	0	0	-	0	0	-	0.0	35.8
48	185	762	0.0	600	440	5	540	0	0	190	54	196	2	R290	108	122	Δ8,76.5,1.5	3.0	47.5
49	91	199	820.0	1550	40	5	722	370	280	262	48	10	1	NH3	0	0	65,40.5,7.5	3.6	36.3
50	364	655	949.9	1021	100	5	0	506	382	266	59	156	1	R290	356	0	25.5,Δ21,94,65.5,Δ28	3.9	45.2
51	195	393	0.0	1000	349	5	900	0	0	227	57	64	1	R161	63	0	71.5,Δ28,Δ13,33.5,4.5	3.2	40.6
52	91	93	759.2	1850	60	5	1106	308	233	266	0	26	1	NH3	0	0	54.5,74.5	18.3	32.0
53	131	304	0.0	1200	300	5	1080	0	0	211	52	36	2	NH3	0	0	23.5,3.44	1.2	37.9
54	278	514	935.6	1300	0	5	279	491	371	207	54	110	1	R161	102	0	3,45.5,Δ30,Δ15,77.5	3.4	41.3
55	193	394	951.1	1450	0	5	384	507	383	262	65	57	1	R290	58	0	65,Δ30,8	3.8	38.5
56	117	223	0.0	1150	333	5	1035	0	0	266	56	10	1	NH3	0	0	25.5,48.5	8.0	38.2
57	533	884	733.1	567	340	5	0	281	212	266	63	223	2	R161	371	0	86,Δ18,101.5,Δ11,Δ20,57.5,24	3.7	51.1
58	86	89	732.0	1850	80	5	1157	280	212	266	0	25	1	NH3	0	0	74.5,53.5	17.4	31.8
59	343	833	749.0	600	326	5	0	297	225	266	59	226	1	R290	287	173	64.5,Δ16,24,89,Δ18	3.6	50.6
60	79	79	702.0	1850	100	5	1213	249	188	266	0	22	1	NH3	0	24	53.5,74	17.8	31.6
61	142	283	0.0	1150	320	5	1035	0	0	237	56	26	2	R161	14	0	46.5,Δ23,24.4	3.5	38.4
62	145	443	0.0	950	366	5	855	0	0	227	68	70	1	R290	66	0	65,Δ29,4.5	3.5	41.2
63	240	525	890.2	1250	40	5	320	443	335	207	57	112	1	R161	52	0	3,45.5,Δ28,75.5	3.4	41.5
64	114	107	816.4	1800	20	5	954	367	277	266	0	31	1	NH3	17	5	Δ9,74,56	21.5	33.1
65	90	199	768.9	1500	80	5	773	318	240	262	48	10	1	NH3	1	0	64.5,Δ4,39.8	3.4	36.5
66	217	711	0.0	650	427	5	585	0	0	190	60	178	1	R290	174	35	1.5,82.5,Δ17,Δ20,55	3.0	46.6
67	73	315	0.0	1100	357	5	990	0	0	262	70	26	1	R161	7	14	48,Δ9,7	4.6	38.6
68	120	150	808.9	1618	40	5	804	359	271	266	45	0	0	-	0	0	-	0.0	35.3
69	120	752	0.0	600	518	5	540	0	0	266	70	182	1	R290	103	0	95.5,18.5,65.5,Δ22	3.3	45.7
70	106	193	0.0	1292	300	5	1163	0	0	244	45	11	1	NH3	0	0	4.5,22.5	9.6	36.4
71	76	68	672.0	1850	120	5	1268	218	165	266	0	19	1	NH3	0	20	53.5,73.5	18.3	31.4
72	96	216	801.5	1500	60	5	712	351	266	262	54	10	1	NH3	0	0	Δ1,42,8.5	5.4	36.8
73	87	193	791.7	1550	60	5	775	341	258	262	46	10	1	NH3	0	0	40.5,7.5,65,Δ2	3.6	36.0
74	423	763	797.9	702	2														

D.2. Additional results

Table D.6 – Database of solutions for plant 2, $\Delta T_{\min}/2=5K$ (II).

Id	Cap-HEN			Nat. gas	Net. elec.	ΔT_{\min}	Q _{oil}	Q _{ocean}	Q _{oxygen}	E _{ref}	E _{min}	E _{ig}	stag.	fluid	subcool.	gas-cool.	Temp. levels	COP	Exerg. eff.
	Cap _{Comp}	Cap _{O₂}	Cap _{CO₂}																
91	131	120	821.5	1750	20	5	899	372	281	266	0	35	1	NH3	22	38	74,Δ11,56	21.7	33.7
92	220	409	863.7	1350	40	5	460	416	314	227	56	71	1	R290	83	0	47,Δ15,Δ25,73,4.5	3.4	39.6
93	118	150	706.0	1522	120	5	910	253	191	266	45	0	0	-	0	0	-	0.0	35.6
94	90	104	738.1	1800	80	5	1100	286	216	266	0	30	1	NH3	0	33	53.5,74	17.8	32.4
95	85	194	689.1	1450	140	5	877	236	178	262	47	10	1	NH3	0	0	7,27,64.5,Δ2,59	3.3	36.4
96	177	293	0.0	1100	350	5	990	0	0	262	60	28	1	NH3	9	0	53,Δ16,8	4.3	38.8
97	294	890	916.4	950	128	5	0	471	356	190	70	225	2	R161	87	75	1.5,Δ23,93,46,5,68	2.8	46.3
98	108	216	750.4	1450	100	5	762	299	226	262	54	10	1	R161	19	0	8.5,Δ20,42,Δ19	5.9	36.9
99	182	700	0.0	650	494	5	585	0	0	262	63	169	1	R290	143	0	Δ3,88,5,65,Δ29,7.5	3.1	45.0
100	333	375	948.9	1400	0	5	343	505	382	266	66	49	1	R290	73	0	68,Δ30,25.5	5.2	39.4
101	399	992	0.0	450	486	5	405	0	0	154	45	287	2	R290	205	190	Δ28,48,79.5,Δ2,-2	5.2	50.5
102	251	1104	0.0	350	589	5	315	0	0	207	0	382	2	R161	251	347	Δ16,48,3,76.5	6.1	50.5
103	85	96	709.0	1800	100	5	1155	256	194	266	0	27	1	NH3	0	30	53.5,74	17.8	32.2
104	187	366	0.0	1050	347	5	945	0	0	235	70	42	1	R404A	46	29	Δ27,53,3	4.1	39.7
105	423	851	714.8	529	360	5	0	262	198	266	56	236	1	R161	215	238	89,Δ18,Δ16,64,5,24	3.6	51.7
106	395	652	963.8	1050	87	5	0	520	393	266	65	149	1	R290	203	113	25.5,59,Δ21,Δ15,91	4.0	44.8
107	87	201	614.4	1350	200	5	925	160	121	262	49	10	1	NH3	3	0	47.5,Δ22,65.5,7.5	3.7	37.0
108	127	385	0.0	1000	380	5	900	0	0	262	54	65	1	R161	0	0	7.5,41,73	3.3	40.0
109	128	432	0.0	950	397	5	855	0	0	262	58	77	1	R161	0	0	7.5,41,73	3.3	40.7
110	120	150	783.2	1594	60	5	830	332	251	266	45	0	0	-	0	0	-	0.0	35.4
111	104	473	760.2	1200	140	5	519	309	233	227	49	97	2	R161	48	0	74.5,Δ16,4.5	3.0	40.6
112	83	85	678.8	1800	120	5	1211	225	170	266	0	24	1	NH3	0	26	54.5,74.5	18.3	31.9
113	117	150	654.2	1474	160	5	963	200	151	266	45	0	0	-	0	0	-	0.0	35.7
114	65	39	589.1	1850	175	5	1421	134	102	266	0	10	1	NH3	0	0	54.5,71	22.3	30.8
115	194	611	827.5	1100	120	5	303	378	286	207	66	133	1	R290	97	78	3,35,5,73,Δ29	3.0	43.0
116	92	217	589.1	1300	224	5	926	134	102	262	54	10	1	NH3	2	1	7.5,41,Δ9	5.5	37.4
117	84	194	637.3	1400	180	5	927	183	138	262	47	10	1	NH3	3	0	49,Δ23,8,64.5	3.8	36.5
118	128	113	793.0	1750	40	5	953	343	259	266	0	33	1	NH3	25	0	Δ12,74,56	21.8	33.5
119	168	597	0.0	750	456	5	675	0	0	262	57	138	1	R161	0	0	8.5,41,5,80,63.5	3.2	43.6
120	79	131	0.0	1749	260	5	1574	0	0	224	0	36	2	NH3	12	0	70,Δ3,3,25,54,Δ9	6.5	31.0
121	132	577	0.0	800	448	5	720	0	0	262	66	121	1	NH3	0	45	7.5,48,5,73	3.2	42.7
122	248	802	0.0	550	463	5	495	0	0	195	55	212	2	R290	286	0	83,Δ22,88.5,Δ2,2	3.1	48.3
123	119	150	731.8	1546	100	5	883	280	211	266	45	0	0	-	0	0	-	0.0	35.5
124	124	107	765.1	1750	60	5	1005	314	237	266	0	31	1	NH3	19	0	Δ10,74,56	21.6	33.2
125	78	79	650.4	1800	140	5	1263	196	148	266	0	22	1	NH3	0	24	53.5,74	17.8	31.7
126	481	760	868.9	850	189	5	0	421	318	266	65	176	2	R161	154	0	25.5,59,Δ20,97.5,Δ10,79.5	4.0	47.3
127	396	627	987.4	1100	60	5	0	545	412	266	60	146	1	R161	51	126	25.5,44,5,87,Δ1,Δ12,65.5	3.9	44.3
128	634	855	987.4	1100	39	5	0	545	412	176	58	218	2	R290	281	55	-2,Δ14,93.5,39,Δ22,70,Δ10	4.2	44.7
129	239	554	827.0	1150	100	5	349	378	286	207	58	121	1	R161	33	0	49,Δ16,3,75.5	3.2	42.4
130	266	681	711.1	900	220	5	341	258	195	190	59	167	1	R290	179	27	54,Δ22,80,Δ19,1.5	3.1	45.3
131	183	631	0.0	700	469	5	630	0	0	262	60	147	1	R161	80	0	81,7,5,63,Δ30	3.3	44.4
132	200	684	0.0	650	488	5	585	0	0	262	62	164	1	R290	195	0	Δ12,85,5,62,Δ29,7	3.2	45.1
133	116	150	589.1	1414	210	5	1029	134	101	266	45	0	0	-	0	0	-	0.0	35.9
134	207	644	0.0	700	419	5	630	0	0	207	58	154	1	R290	155	0	3,48,Δ16,Δ19,80	3.1	45.5
135	316	656	589.1	800	305	5	476	134	102	190	57	160	1	R161	92	125	75,Δ12,Δ20,46,5,1.5	3.2	45.8
136	389	716	902.2	920	160	5	0	456	345	266	66	172	1	R290	142	150	25.5,70,5,Δ26,91	3.8	46.2
137	100	118	743.8	1750	80	5	1045	292	221	266	0	34	1	NH3	0	0	54.5,74.5	18.3	33.0
138	241	442	0.0	1150	300	5	1035	0	0	170	57	73	3	various	0	0	2,-6,23,5,45,23.5	2.5	38.7
139	253	619	806.8	1050	140	5	297	357	270	207	58	145	1	R161	84	0	3,50,Δ18,77.5,Δ9	3.2	43.7
140	98	465	782.0	1250	120	5	523	331	250	227	56	86	2	R161	22	0	4,5,79,61	3.0	40.0
141	74	71	621.0	1800	160	5	1318	166	126	266	0	20	1	NH3	0	21	53.5,74	17.8	31.5
142	118	150	680.1	1498	140	5	936	227	171	266	45	0	0	-	0	0	-	0.0	35.6
143	164	223	836.4	1500	40	5	646	387	293	266	57	10	1	NH3	0	0	45.5,25.5	9.2	37.1
144	97	110	714.8	1750	100	5	1099	262	198	266	0	32	1	NH3	0	0	54.5,74.5	18.3	32.8
145	240	573	886.1	1200	60	5	282	439	332	207	66	119	1	R161	59	43	3,46,5,Δ11,Δ12,73	3.2	42.1
146	261	486	0.0	1200	280	5	1080	0	0	132	52	95	2	R161	47	57	4.5,-2,Δ12,25.5	4.8	38.2
147	100	660	589.1	850	319	5	521	134	102	207	53	161	2	R290	161	0	3,85,Δ14,Δ15,68.5	2.8	44.3
148	423	772	852.8	816	220	5	0	404	306	266	0	259	2	R161	600	0	54.5,Δ20,25.5,Δ4,99,Δ18,75	7.9	47.4
149	185	597	0.0	750	415	5	675	0	0	221	59	136	1	R161	72	0	4,77,Δ30,62	3.2	44.5
150	149	565	0.0	1292	260	5	1163	0	0	76	45	139	1	NH3	11	0	Δ3,23,5,-2	5.8	37.0
151	242	592	589.1	900	286	5	566	134	102	195	58	134	1	R161	61	0	76.5,Δ28,48.2	3.3	43.9
152	179	405	0.0	1000	353	5	900	0	0	227	64	61	1	R161	45	0	65.5,Δ15,Δ16,33,5,4.5	3.2	40.5
153	140	134	776.2	1650	60	5	894	325	246	266	0	39	1	NH3	27	0	Δ11,74,56	21.7	34.6
154	249	516	783.5	1150	120	5	431	333	252	207	57	108	1	R161	41	0	74,Δ1,Δ20,45,5.3	3.4	42.0
155	112	86	679.2	1750	120	5	1165	226	171	266	0	24	1	NH3	18	0	74,Δ12,56	21.8	32.5
156	235	561	779.2	1100	140	5	394	328	248	207	58	123	1	R161	34	0	3,76,5,Δ16,49	3.2	42.6
157	245	553	724.0	1050	180	5	452	272	205	207	56	122	1	R161	38	0	3,48,Δ18,76,63.5	3.2	42.8
158	188	358	910.2	1450	20	5	462	464	351	262	52	58	1	R161	37	0	41,Δ22,73,7.5	3.3	38.2
159	137	130	800.4	1700	40	5	894	350	265	266	0	38	1	NH3	12	0	Δ5,74,5,56.5	21.0	34.2
160	307	623	837.3	1100	100	5	285	388	294	190	57	147	1	R290	197	0	1.5,Δ18,81,5,52,Δ14,Δ22,34	2.9	43.4
161	306	625	0.0	600	471	5	540	0	0	266	62	143	1	R161	92	0	87.5,Δ26,65,5,25.5	4	

D.3 Industrial case study

D.3.1 Dairy process

The process streams as discussed in [140] are depicted in Table D.7. The process was modeled assuming constant, simultaneous operation of all units with a time average approach. As illustrated in Figure 5.6, multiple products are (potentially) created from conversion of raw milk, namely yogurt and dessert, pasteurized milk and cream, high temperature (long lasting) milk, and butter. Upon arrival in the factory, the raw milk is cooled down to an operating temperature of 4 °C.

The first process step is **pasteurization and centrifugation** of the raw milk. This requires heating to 60 °C, centrifugation (consuming electricity), which results in a separation of milk and cream. The milk is then further heated to 86 °C, while the cream is heated to 98 °C, resulting in pasteurized milk and cream which are cooled again to 4 °C. The heating and cooling requirements of the individual process steps (referred to as process streams) are estimated based on the specific heat capacity and temperature levels. The specific heat capacity of (raw) milk was approximated to be 3.8 kJ/kgK, and that of cream to be 3.4 kJ/kgK.

The pasteurized cream can be further converted to **butter**, which requires consecutive refrigeration steps down to -25 °C. The specific heat capacity of butter is assumed to be 2.4 kJ/kgK.

The products are always modeled to reach operating conditions (4 °C) after the conversion steps before being placed in the **storage unit**. The storage unit cooling requirements were modeled at constant temperature and based on data provided by the process operators.

Pasteurized milk can be further converted to various products. Production of **high temperature (HT) milk** requires heating to 135 °C and rapid cooling to ambient conditions. Fabrication of **yogurt and dessert** requires addition of further ingredients and various heating, storing and cooling steps. In agreement with process operators, both were modeled by assuming heating and cooling requirements between 4 and 90 °C. The dessert is packaged at 70 °C, during which the temperature is assumed to drop to 50 °C. For all conversion processes mentioned above, milk properties are assumed with a specific heat capacity of 3.8 kJ/kgK.

Concentrated milk is produced in a three stage evaporation process, at sub-atmospheric pressures between 0.7 and 0.25 bar. Water thermodynamic properties were assumed for partial evaporation. The vapor is assumed to be captured and subsequently condensed and cooled to ambient conditions to harvest the latent and sensible heat.

The **cleaning in place** system requires make-up water at 80 °C.

D.3. Industrial case study

Table D.7 – Hot and cold streams of the generalized dairy process, reproduced from Becker [140], Stadler [254], and the EUROPEAN COMMISSION [81].

Unit	Operation	Stream	T _{in} [°C]	T _{out} [°C]	Q̇ [kJ/kg]	ΔT _{min} /2 [°C]	α [kW/K m ²]	Remarks
Centrifugation & pasteurization Reference: [kg _{raw milk}]	Inlet cooling	ref	6.0	4.0	-7.60	ΔT _{min}	1.0	refrigeration inlet milk
	Pasteurization	pasto1a	4.0	66.0	235.6	ΔT _{min}	1.0	preheating
		pasto2a	66.0	86.0	67.64	ΔT _{min}	1.0	pasteurization milk
		pasto3a	86.0	4.0	-277.32	ΔT _{min}	1.0	refrigeration milk
		pasto4a	66.0	98.0	11.97	ΔT _{min}	1.0	pasteurization cream
		pasto5a	98.0	4.0	-35.16	ΔT _{min}	1.0	refrigeration cream
HT milk Ref: [kg _{HT}]	high temperature milk	uht1	86.0	135.0	186.2	ΔT _{min}	1.0	ultra high temperature heating
		uht2	135.0	86.0	-186.2	ΔT _{min}	1.0	rapid cooling
Concentration Ref: [kg _{concentrated milk}]	Concentration	eva1	4.0	70.3	586.1	ΔT _{min}	1.0	preheating
		eva2	70.3	70.3	1051.4	1.2	10.0	evaporation 1.effect
		eva3	66.4	66.4	1004.77	1.2	10.0	evaporation 2.effect
		eva4	60.8	60.8	988.14	1.2	10.0	evaporation 3.effect
		eva5	60.8	4.0	-176.2	ΔT _{min}	1.00	refrigeration concentrated milk
	Water residuals	eva6	68.9	68.9	-1051.4	1.2	10.0	condensation 1.effect
		eva7	65.9	65.9	-1004.8	1.2	10.0	condensation 2.effect
		eva8	60.1	60.1	-988.1	1.2	10.0	condensation 3.effect
	Condensates cooling	eva9	68.9	15.0	-102.1	ΔT _{min}	1.0	cooling condensates 1.effect
		eva10	65.9	15.0	-94.0	ΔT _{min}	1.0	cooling condensates 2.effect
		eva11	60.1	15.0	-81.0	ΔT _{min}	1.0	cooling condensates 3.effect
Yogurt Ref: [kg _{yogurt}]	Yogurt production	yog1	4.0	94.0	342	ΔT _{min}	1.0	heating
		yog2	94.0	10.0	-319.2	ΔT _{min}	1.0	cooling
Dessert Ref: [kg _{yogurt}]	Dessert production	des1	4.0	90.0	326.8	ΔT _{min}	1.0	heating
		des2	90.0	70.0	-76.0	ΔT _{min}	1.0	cooling to filling temperature
		des3	50	20	-152.0	20.0	1.0	cooling of filled cups
Cleaning in place Ref: [kg _{raw milk}]	Cleaning units	CIP1a	58.7	70.0	18.86	ΔT _{min}	1.0	maintain temperature CIP1
		CIP1b	65.0	15.0	-10.45	ΔT _{min}	1.0	recuperation waste heat CIP1
		CIP2a	67.5	80.0	20.95	ΔT _{min}	1.0	maintain temperature CIP2
		CIP2b	75.0	15.0	-12.54	ΔT _{min}	1.0	recuperation waste heat CIP2
	Hot water Fridge	hw	15.0	55.0	16.72	ΔT _{min}	1.0	hot water production
		frig	5.0	5.0	-30.0	ΔT _{min}	1.0	maintain storage temperature
Butter Ref: [kg _{butter}]	Butter production	but1	4.0	20.0	117.50	ΔT _{min}	1.0	heating
		but2	20.0	10.0	-73.4	ΔT _{min}	1.0	cooling
		but3	10.0	7.0	-7.20	ΔT _{min}	1.0	refrigeration
		but4	7.0	-21.0	-67.2	ΔT _{min}	1.0	refrigeration
		but5	-21.0	-21.0	-60.0	ΔT _{min}	1.0	refrigeration
		but6	-21.0	-25.0	-10.6	ΔT _{min}	1.0	refrigeration

Table D.8 – Utility thermal and resource stream data.

Unit	T _{in} [°C]	T _{out} [°C]	Q̇ [kW]	Ė _r [kW]	r	ΔT _{min} /2 [K]	α [kW/K m ²]	f ^{w,min} [-]	f ^{w,max} [-]	OP _{1,p} ^w [\$/h]	OP _{2,p} ^w [\$/h]	Remarks
Boiler (BOI)	1027	1027	-288.418			25	0.06	0.6	1000	0	0	Radiative heat release
	1027	120	-150.305	487.47	ng	2	0.06					Convective heat release Natural gas consumption
Co-generation engine (COGEN)	470.5	120	-86.6			5	0.06	0.7	1000	0	0	Exhaust gases
	87	79.9	-105.2	387.13	ng	3	2					Engine cool. water Natural gas consumption
Cooling water (CW)	15	17	1000			5	2.0	0	1000	0	0	Cooling water
Electricity (GRID,el in)				-1000	el			0	1000	0	c _{el} ·1000	Electricity grid buy
Electricity (GRID,el out)				1000	el			0	1000	0	0	Electricity grid sell
Nat. gas (GRID,el)				-1000	ng			0	1000	0	c _{ng} ·1000	Nat. gas grid
Refrig., COND 1	30	30	-331.3			2.0	1.6	0	1000	0	0	Refrigeration condenser 1
Refrig., EVAP 2	-3	-3	383.358			2.0	1.6	0	1000	0	0	Refrigeration evaporator 2
Refrig., EVAP 3	-33	-33	420.076			2.0	3.6	0	1000	0	0	Refrigeration evaporator 3
Refrig., COMP 12				73.498	el			0.13606	13.606	0	0	Ref. compressor 2 → 1
Refrig., COMP 13				164.1928	el			0.0609	6.0904	0	0	Ref. compressor 3 → 1
Mechanical vapor re-compression (MVR)	74	74	-2516.97805			2	1.6	0	1000	0	0	Condensation MVR
	56	56	2292.47685			2	3.6	0	1000	0	0	Evaporation MVR
				224.5012	el			0.1822	0.31180	0	0	Compressor MVR

D.3.2 Utilities

Some of the utilities are discussed in Becker [140]. All utility data is depicted in Table D.8. Each utility has at least one thermal and/or resource stream. Negative signs represent energy release, while positive signs represent energy consumption. The utility parameters indicated in the table can be found in the MILP parameters in the list of symbols.

Several compressor cost functions were compared and the one by Becker [140], which was based on industrial projects from France, was found to be well aligned with other functions as depicted in Figure D.11. For this, a bare module factor, F_{BM} , of 2 was assumed based on experience from Becker [140].

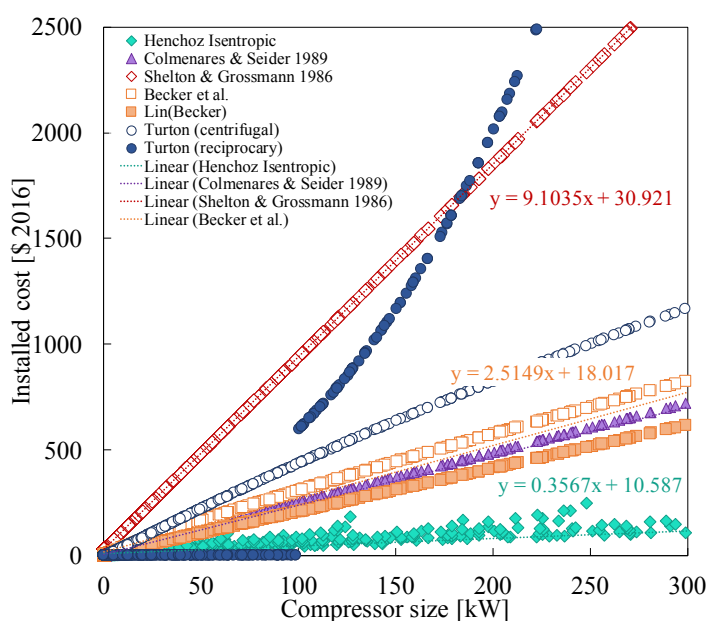


Figure D.11 – Compressor cost functions, installed cost in \$ [2016], updated with Chemical Engineering Plant Cost Index [4] (CEPCI); Turton et al. [79] (Bare module factor, F_{BM} , of 2), Henchoz [255] (F_{BM}), Colmenares and Seider [205], Shelton and Grossmann [102] (annuity estimated to be 0.15 1/y), Becker [140] (Lin(Becker) refers to the linearization applied in Chapter 3), Turton et al. [79] ($F_{BM}=2$).

Bibliography

- [1] Cedric Philibert. Solar Energy Perspectives. Technical report, International Energy Agency (IEA), 2011. URL https://www.iea.org/publications/freepublications/publication/Solar_Energy_Perspectives2011.pdf.
- [2] S.A. Klein, W.A. Beckman, J.W. Mitchell, J.A. Duffie, N.A. Duffie, and T.L. Freeman. TRNSYS 16. 2006.
- [3] Robert Fourer, David M. Gay, and Brian W. Kernighan. *AMPL: A Modeling Language for Mathematical Programming*. Duxbury Press / Brooks/Cole Publishing Company, 2003. ISBN ISBN 0-534-38809-4.
- [4] CEPCI. The Chemical Engineering Plant Cost Index - Chemical Engineering. URL <http://www.chemengonline.com/pci-home>.
- [5] IBM ILOG CPLEX Optimization Studio V12.7.0 documentation, February 2015. URL http://www.ibm.com/support/knowledgecenter/SSSA5P_12.7.0/ilog.odms.studio.help/Optimization_Studio/topics/COS_intro_features.html.
- [6] Marshall and Swift. Marshall & Swift Equipment Cost Index, 2017. URL <http://www.equipment-cost-index.com/eci/UserContentStart.aspx>. <http://www.equipment-cost-index.com/eci/UserContentStart.aspx>, Online; accessed 30-01-2017.
- [7] European Photovoltaic Industry Association (EPIA). Solar Generation 6. URL <http://www.greenpeace.org/international/en/publications/reports/Solar-Generation-6/>.
- [8] Craig, Cunningham, and Saigo. Facing the Hard Truths about Energy – 2007 Report and 2008 Update, 2008. URL <http://www.npc.org/NPC909/index.html>.
- [9] IEA. IEA - Report, 2017. URL <http://www.iea.org/statistics/statisticssearch/report/?year=2015&country=WORLD&product=Balances>.
- [10] Sophia Haussener. Energy Conversion and Renewable Energy -Solar energy (Lecture slides). Lecture notes, 2017. URL irese.epfl.ch.

Bibliography

- [11] Alternative Fuels Datacenter. Fuel Properties Comparison. URL energy.gov.
- [12] Wikipedia. Fuel flow rates. URL <https://de.wikipedia.org/wiki/Zapfs%3%A4ule>.
- [13] S. Mekhilef, R. Saidur, and A. Safari. A review on solar energy use in industries. *Renewable and Sustainable Energy Reviews*, 15(4):1777–1790, May 2011. ISSN 1364-0321. doi: 10.1016/j.rser.2010.12.018. URL <http://www.sciencedirect.com/science/article/pii/S1364032110004533>.
- [14] María Herrando and Christos N. Markides. Hybrid PV and solar-thermal systems for domestic heat and power provision in the UK: Techno-economic considerations. *Applied Energy*, 161:512–532, January 2016. ISSN 0306-2619. doi: 10.1016/j.apenergy.2015.09.025. URL <http://www.sciencedirect.com/science/article/pii/S0306261915010958>.
- [15] Daniel Chemisana. Building Integrated Concentrating Photovoltaics: A review. *Renewable and Sustainable Energy Reviews*, 15(1):603–611, January 2011. ISSN 1364-0321. doi: 10.1016/j.rser.2010.07.017. URL <http://www.sciencedirect.com/science/article/pii/S1364032110001978>.
- [16] Manuel Romero and Aldo Steinfeld. Concentrating solar thermal power and thermochemical fuels. *Energy & Environmental Science*, 5(11):9234–9245, 2012. doi: 10.1039/C2EE21275G. URL <http://pubs.rsc.org/en/Content/ArticleLanding/2012/EE/C2EE21275G>.
- [17] Ronald R. Gutierrez and Sophia Haussener. Modeling of Concurrent CO₂ and Water Splitting by Practical Photoelectrochemical Devices. *Journal of The Electrochemical Society*, 163(10):H1008–H1018, January 2016. ISSN 0013-4651, 1945-7111. doi: 10.1149/2.0661610jes. URL <http://jes.ecsdl.org/content/163/10/H1008>.
- [18] Soteris A. Kalogirou. Solar thermal collectors and applications. *Progress in Energy and Combustion Science*, 30(3):231–295, January 2004. ISSN 0360-1285. doi: 10.1016/j.peccs.2004.02.001. URL <http://www.sciencedirect.com/science/article/pii/S0360128504000103>.
- [19] International Energy Agency (iea). Statistics (OECD Total), 2015. URL <http://www.iea.org/statistics/statisticssearch/report/?country=OECDTOT&product=balances&year=2015>.
- [20] Benjamin Y. H. Liu and Richard C. Jordan. The interrelationship and characteristic distribution of direct, diffuse and total solar radiation. *Solar Energy*, 4(3):1–19, July 1960. ISSN 0038-092X. doi: 10.1016/0038-092X(60)90062-1. URL <http://www.sciencedirect.com/science/article/pii/0038092X60900621>.
- [21] Richard Perez, Robert Seals, Pierre Ineichen, Ronald Stewart, and David Menicucci. A new simplified version of the perez diffuse irradiance model for tilted surfaces. *Solar Energy*, 39(3):221–231, 1987.
- [22] R. Perez, R. Stewart, C. Arbogast, R. Seals, and J. Scott. An anisotropic hourly diffuse radiation model for sloping surfaces: Description, performance validation, site dependency evaluation. *Solar Energy*, 36(6):481–497, 1986.

- [23] Manuel Collares-Pereira and Ari Rabl. Simple procedure for predicting long term average performance of nonconcentrating and of concentrating solar collectors. *Solar Energy*, 23(3):235–253, January 1979. ISSN 0038-092X. doi: 10.1016/0038-092X(79)90163-4. URL <http://www.sciencedirect.com/science/article/pii/0038092X79901634>.
- [24] M. Collares-Pereira and A. Rabl. Derivation of method for predicting long term average energy delivery of solar collectors. *Solar Energy*, 23(3):223–233, January 1979. ISSN 0038-092X. doi: 10.1016/0038-092X(79)90162-2. URL <http://www.sciencedirect.com/science/article/pii/0038092X79901622>.
- [25] H. Suehrcke and P. G. McCormick. The diffuse fraction of instantaneous solar radiation. *Solar Energy*, 40(5):423–430, January 1988. ISSN 0038-092X. doi: 10.1016/0038-092X(88)90097-7. URL <http://www.sciencedirect.com/science/article/pii/0038092X88900977>.
- [26] John A. Duffie and William A. Beckman. Solar Engineering of Thermal Processes. In *Solar Engineering of Thermal Processes*, pages i–xxvi. Wiley-Blackwell, 4 edition, 2012. ISBN 978-1-118-67160-3. doi: 10.1002/9781118671603.fmatter. URL <https://onlinelibrary.wiley.com/doi/abs/10.1002/9781118671603.fmatter>.
- [27] Hoyt C Hottel and A. Whillier. Evaluation of flat-plate collector performance. In *Transactions of the Conference on the Use of Solar Energy*, pages 74–104. University of Arizona Press, 1955.
- [28] S. A. Klein, J. A. Duffie, and W. A. Beckman. Transient Considerations of Flat-Plate Solar Collectors. *Journal of Engineering for Power*, 96(2):109–113, April 1974. ISSN 0022-0825. doi: 10.1115/1.3445757. URL <http://gasturbinespower.asmedigitalcollection.asme.org/article.aspx?articleid=1418503>.
- [29] E. Skoplaki and J. A. Palyvos. Operating temperature of photovoltaic modules: A survey of pertinent correlations. *Renewable Energy*, 34(1):23–29, January 2009. ISSN 0960-1481. doi: 10.1016/j.renene.2008.04.009. URL <http://www.sciencedirect.com/science/article/pii/S0960148108001353>.
- [30] G. N. Tiwari, R. K. Mishra, and S. C. Solanki. Photovoltaic modules and their applications: A review on thermal modelling. *Applied Energy*, 88(7):2287–2304, July 2011. ISSN 0306-2619. doi: 10.1016/j.apenergy.2011.01.005. URL <http://www.sciencedirect.com/science/article/pii/S0306261911000080>.
- [31] R. Silva, M. Pérez, and A. Fernández-García. Modeling and co-simulation of a parabolic trough solar plant for industrial process heat. *Applied Energy*, 106:287–300, June 2013. ISSN 0306-2619. doi: 10.1016/j.apenergy.2013.01.069. URL <http://www.sciencedirect.com/science/article/pii/S0306261913000809>.

Bibliography

- [32] Max Schmitz, Gianluca Ambrosetti, and Aldo Steinfeld. Optical design of a multi-focus solar dish CPV system based on ellipsoidal mem-brane facets-Solar flux measurements. In *11 th SOLLAB Doctoral Colloquium*, page 25.
- [33] R. Silva, M. Berenguel, M. Pérez, and A. Fernández-Garcia. Thermo-economic design optimization of parabolic trough solar plants for industrial process heat applications with memetic algorithms. *Applied Energy*, 113:603–614, January 2014. ISSN 0306-2619. doi: 10.1016/j.apenergy.2013.08.017. URL <http://www.sciencedirect.com/science/article/pii/S0306261913006521>.
- [34] V. E. Dudley, L. R. Evans, and C. W. Matthews. Test results, Industrial Solar Technology parabolic trough solar collector. Technical Report SAND-94-1117, Sandia National Labs., Albuquerque, NM (United States), November 1995. URL <https://www.osti.gov/biblio/211613>.
- [35] Soteris Kalogirou. The potential of solar industrial process heat applications. *Applied Energy*, 76(4):337–361, December 2003. ISSN 0306-2619. doi: 10.1016/S0306-2619(02)00176-9. URL <http://www.sciencedirect.com/science/article/pii/S0306261902001769>.
- [36] C. Lauterbach, B. Schmitt, and K. Vajen. System analysis of a low-temperature solar process heat system. *Solar Energy*, 101:117–130, March 2014. ISSN 0038-092X. doi: 10.1016/j.solener.2013.12.014. URL <http://www.sciencedirect.com/science/article/pii/S0038092X13005318>.
- [37] J. M. Gordon and A. Rabl. Design, analysis and optimization of solar industrial process heat plants without storage. *Solar Energy*, 28(6):519–530, January 1982. ISSN 0038-092X. doi: 10.1016/0038-092X(82)90323-1. URL <http://www.sciencedirect.com/science/article/pii/0038092X82903231>.
- [38] Ari Rabl. Yearly average performance of the principal solar collector types. *Solar Energy*, 27(3):215–233, January 1981. ISSN 0038-092X. doi: 10.1016/0038-092X(81)90123-7. URL <http://www.sciencedirect.com/science/article/pii/0038092X81901237>.
- [39] Soteris A. Kalogirou. Optimization of solar systems using artificial neural-networks and genetic algorithms. *Applied Energy*, 77(4):383–405, 2004.
- [40] W. A. Beckman, S. A. Klein, and J. A. Duffie. Solar heating design, by the f-chart method. *NASA STI/Recon Technical Report A*, 78, 1977. URL <http://adsabs.harvard.edu/abs/1977STIA...7831071B>.
- [41] S. A. Klein and W. A. Beckman. A general design method for closed-loop solar energy systems. *Solar Energy*, 22(3):269–282, January 1979. ISSN 0038-092X. doi: 10.1016/0038-092X(79)90142-7. URL <http://www.sciencedirect.com/science/article/pii/0038092X79901427>.
- [42] H. Suehrcke and P. G. McCormick. A performance prediction method for solar energy systems. *Solar Energy*, 48(3):169–175, January 1992. ISSN 0038-092X. doi: 10.1016/0038-092X(92)90135-W. URL <http://www.sciencedirect.com/science/article/pii/0038092X9290135W>.

- [43] M. Collares-Pereira, J. M. Gordon, A. Rabl, and Y. Zarmi. Design and optimization of solar industrial hot water systems with storage. *Solar Energy*, 32(1):121–133, January 1984. ISSN 0038-092X. doi: 10.1016/0038-092X(84)90055-0. URL <http://www.sciencedirect.com/science/article/pii/0038092X84900550>.
- [44] I. F. Okafor and G. Akubue. *F-Chart Method for Designing Solar Thermal Water Heating Systems*. September 2012. ISBN 2229-5518.
- [45] Beckman. Welcome | F-Chart Software : Engineering Software, 2018. URL <http://www.fchart.com/>.
- [46] Govind N. Kulkarni, Shireesh B. Kedare, and Santanu Bandyopadhyay. Optimization of solar water heating systems through water replenishment. *Energy Conversion and Management*, 50(3):837–846, 2009.
- [47] Govind N. Kulkarni, Shireesh B. Kedare, and Santanu Bandyopadhyay. Determination of design space and optimization of solar water heating systems. *Solar Energy*, 81(8): 958–968, August 2007. ISSN 0038-092X. doi: 10.1016/j.solener.2006.12.003. URL <http://www.sciencedirect.com/science/article/pii/S0038092X06003112>.
- [48] P. Talebizadeh, M. A. Mehrabian, and M. Abdolzadeh. Prediction of the optimum slope and surface azimuth angles using the Genetic Algorithm. *Energy and Buildings*, 43(11): 2998–3005, November 2011. ISSN 0378-7788. doi: 10.1016/j.enbuild.2011.07.013. URL <http://www.sciencedirect.com/science/article/pii/S0378778811003185>.
- [49] Velimir Čongradac, Marta Prica, Marija Paspalj, Dubravka Bojanić, and Darko Čapko. Algorithm for blinds control based on the optimization of blind tilt angle using a genetic algorithm and fuzzy logic. *Solar Energy*, 86(9):2762–2770, September 2012. ISSN 0038-092X. doi: 10.1016/j.solener.2012.06.016. URL <http://www.sciencedirect.com/science/article/pii/S0038092X12002289>.
- [50] Dan Weinstock and Joseph Appelbaum. Optimal Solar Field Design of Stationary Collectors. *Journal of Solar Energy Engineering*, 126(3):898, 2004. ISSN 01996231. doi: 10.1115/1.1756137. URL <http://SolarEnergyEngineering.asmedigitalcollection.asme.org/article.aspx?articleid=1457085>.
- [51] J. Bany and J. Appelbaum. The effect of shading on the design of a field of solar collectors. *Solar Cells*, 20(3):201–228, April 1987. ISSN 0379-6787. doi: 10.1016/0379-6787(87)90029-9. URL <http://www.sciencedirect.com/science/article/pii/0379678787900299>.
- [52] Moustafa M. Elsayed and Abdullah M. Al-Turki. Calculation of shading factor for a collector field. *Solar Energy*, 47(6):413–424, January 1991. ISSN 0038-092X. doi: 10.1016/0038-092X(91)90109-A. URL <http://www.sciencedirect.com/science/article/pii/0038092X9190109A>.

Bibliography

- [53] Germain Augsburg. Thermo-economic optimisation of large solar tower power plants. 2013. doi: 10.5075/epfl-thesis-5648. URL <https://infoscience.epfl.ch/record/183139>.
- [54] P. Dorato. Optimal temperature control of solar energy systems. *Solar Energy*, 30(2):147–153, January 1983. ISSN 0038-092X. doi: 10.1016/0038-092X(83)90206-2. URL <http://www.sciencedirect.com/science/article/pii/0038092X83902062>.
- [55] M. Niemann, J. Kreuzburg, K. R. Schreitmüller, and L. Leppers. Solar process heat generation using an ETC collector field with external parabolic circle concentrator (PCC) to operate an adsorption refrigeration system. *Solar Energy*, 59(1):67–73, January 1997. ISSN 0038-092X. doi: 10.1016/S0038-092X(96)00092-8. URL <http://www.sciencedirect.com/science/article/pii/S0038092X96000928>.
- [56] Hans Schweiger, João Farinha Mendes, Nikolaus Benz, and Klaus Hennecke. The Potential of Solar Heat in Industrial Processes. A State of the Art Review for Spain and Portugal. page 11, 2000.
- [57] Dirk Pietruschka, Roberto Fedrizzi, Francesco Orioli, Robert Söll, and Reiner Stauss. Demonstration of Three Large Scale Solar Process Heat Applications with Different Solar Thermal Collector Technologies. *Energy Procedia*, 30:755–764, January 2012. ISSN 1876-6102. doi: 10.1016/j.egypro.2012.11.086. URL <http://www.sciencedirect.com/science/article/pii/S1876610212016025>.
- [58] Bastian Schmitt, Christoph Lauterbach, and Klaus Vajen. INVESTIGATION OF SELECTED SOLAR PROCESS HEAT APPLICATIONS REGARDING THEIR TECHNICAL REQUIRMENTS FOR SYSTEM INTEGRATION. page 9, 2012. URL https://www.uni-kassel.de/maschinenbau/fileadmin/datas/fb15/SWC_System_Integration_Schmitt.pdf.
- [59] Hans Schnitzer, Christoph Brunner, and Gernot Gwehenberger. Minimizing greenhouse gas emissions through the application of solar thermal energy in industrial processes. *Journal of Cleaner Production*, 15(13-14):1271–1286, 2007.
- [60] Martin J. Atkins, Michael R. W. Walmsley, and Andrew S. Morrison. Integration of solar thermal for improved energy efficiency in low-temperature-pinch industrial processes. *Energy*, 35(5):1867–1873, 2010.
- [61] Tobias Eiholzer, Donald Olsen, Sebastian Hoffmann, Barbara Sturm, and Beat Wellig. Integration of a solar thermal system in a medium-sized brewery using pinch analysis: Methodology and case study. *Applied Thermal Engineering*, 113:1558–1568, February 2017. ISSN 1359-4311. doi: 10.1016/j.applthermaleng.2016.09.124. URL <http://www.sciencedirect.com/science/article/pii/S1359431116318257>.

- [62] Simon Perry, Jiri Klemes, and Igor Bulatov. Integrating waste and renewable energy to reduce the carbon footprint of locally integrated energy sectors. *Energy*, 33(10):1489–1497, 2008.
- [63] Petar Sabev Varbanov and Jiří Jaromír Klemeš. Integration and management of renewables into Total Sites with variable supply and demand. *Computers & Chemical Engineering*, 35(9): 1815–1826, September 2011. ISSN 0098-1354. doi: 10.1016/j.compchemeng.2011.02.009. URL <http://www.sciencedirect.com/science/article/pii/S0098135411000718>.
- [64] Fabian Bühler, Tuong-Van Nguyen, Brian Elmegaard, and Anish Modi. Process and Economic Optimisation of a Milk Processing Plant with Solar Thermal Energy. In Zdravko Kravanja and Miloš Bogataj, editors, *Computer Aided Chemical Engineering*, volume 38 of 26 *European Symposium on Computer Aided Process Engineering*, pages 1347–1352. Elsevier, January 2016. doi: 10.1016/B978-0-444-63428-3.50229-0. URL <http://www.sciencedirect.com/science/article/pii/B9780444634283502290>.
- [65] Alberto Mian. Optimal design methods applied to solar-assisted hydrothermal gasification plants. 2016. doi: 10.5075/epfl-thesis-6945. URL <https://infoscience.epfl.ch/record/216954>.
- [66] K. Brown, D. Hooker, A. Rabl, S. Stadjuhar, and R. West. End-use matching for solar industrial process heat. Final report. Technical Report SERI/TR-34-091, 5654045, Solar Energy Research Inst., Golden, CO (USA), January 1980. URL <http://www.osti.gov/servlets/purl/5654045/>.
- [67] Andrew C. Beath. Industrial energy usage in Australia and the potential for implementation of solar thermal heat and power. *Energy*, 43(1):261–272, July 2012. ISSN 0360-5442. doi: 10.1016/j.energy.2012.04.031. URL <http://www.sciencedirect.com/science/article/pii/S0360544212003118>.
- [68] C. Lauterbach, B. Schmitt, U. Jordan, and K. Vajen. The potential of solar heat for industrial processes in Germany. *Renewable and Sustainable Energy Reviews*, 16(7):5121 – 5130, 2012. ISSN 1364-0321. doi: <http://dx.doi.org/10.1016/j.rser.2012.04.032>. URL <http://www.sciencedirect.com/science/article/pii/S1364032112003073>.
- [69] Ashish K. Sharma, Chandan Sharma, Subhash C. Mullick, and Tara C. Kandpal. Potential of Solar Energy Utilization for Process Heating in Paper Industry in India: A Preliminary Assessment. *Energy Procedia*, 79:284–289, November 2015. ISSN 1876-6102. doi: 10.1016/j.egypro.2015.11.486. URL <http://www.sciencedirect.com/science/article/pii/S1876610215022183>.
- [70] Ashish K. Sharma, Chandan Sharma, Subhash C. Mullick, and Tara C. Kandpal. Carbon mitigation potential of solar industrial process heating: paper industry in India. *Journal of Cleaner Production*, 112:1683–1691, January 2016. ISSN 0959-6526. doi: 10.1016/j.jclepro.2015.04.093. URL <http://www.sciencedirect.com/science/article/pii/S0959652615004680>.

Bibliography

- [71] Ashish K. Sharma, Chandan Sharma, Subhash C. Mullick, and Tara C. Kandpal. Potential of solar industrial process heating in dairy industry in India and consequent carbon mitigation. *Journal of Cleaner Production*, 140:714–724, January 2017. ISSN 0959-6526. doi: 10.1016/j.jclepro.2016.07.157. URL <http://www.sciencedirect.com/science/article/pii/S0959652616310538>.
- [72] Marco Calderoni, Marcello Aprile, Salvatore Moretta, Aristotelis Aidonis, and Mario Motta. Solar Thermal Plants for Industrial Process Heat in Tunisia: Economic Feasibility Analysis and Ideas for a New Policy. *Energy Procedia*, 30:1390–1400, January 2012. ISSN 1876-6102. doi: 10.1016/j.egypro.2012.11.153. URL <http://www.sciencedirect.com/science/article/pii/S1876610212016694>.
- [73] Steven Meyers, Bastian Schmitt, and Klaus Vajen. Renewable process heat from solar thermal and photovoltaics: The development and application of a universal methodology to determine the more economical technology. *Applied Energy*, 212:1537–1552, February 2018. ISSN 0306-2619. doi: 10.1016/j.apenergy.2017.12.064. URL <http://www.sciencedirect.com/science/article/pii/S0306261917317798>.
- [74] Leonard Kaufman and Peter J Rousseeuw. *Finding groups in data: an introduction to cluster analysis*, volume 344. John Wiley & Sons, 2009.
- [75] François Maréchal and Boris Kalitventzeff. Targeting the integration of multi-period utility systems for site scale process integration. *Applied Thermal Engineering*, 23(14):1763–1784, 2003. ISSN 1359-4311. doi: 10.1016/S1359-4311(03)00142-X. URL <http://www.sciencedirect.com/science/article/pii/S135943110300142X>.
- [76] Kai Chang. parallel-coordinates: A d3-based parallel coordinates plot in canvas, February 2018. URL <https://github.com/syntagmatic/parallel-coordinates>. original-date: 2012-06-01T11:28:26Z.
- [77] K. M. Guthrie. *Data and techniques for preliminary capital cost estimating*. McGraw-Hill, 1969. Open Library ID: OL14799127M.
- [78] Gael D Ulrich. *A guide to chemical engineering process design and economics*. Wiley New York, 1984.
- [79] Richard Turton, Richard C. Bailie, Wallace B. Whiting, Joseph A. Shaeiwitz, and Debangsu Bhattacharyya. *Analysis, Synthesis, and Design of Chemical Processes*. 4th edition, 2012.
- [80] Laurstrasse 10 5201 Brugg 056-462 51 11 Schweizerischer Bauernverband. *Der Schweizer Milchmarkt*. Number 11.02.2016. 2016. URL https://www.google.ch/url?sa=t&rct=j&q=&esrc=s&source=web&cd=4&ved=0ahUKEwj2tIyU4P7KAhUFj3IKHfVrAXYQFgg3MAM&url=http%3A%2F%2Fwww.sbv-usp.ch%2Ffileadmin%2Fsbvuspch%2F07_

- Preise%2Fmilch%2F131204_Milchmarkt_Schweiz_de.pdf&usg=AFQjCNHms5O_sMWsSul8vAhkQhExzhZZxA&sig2=XRjlgnsHE-pwy7ZixT5x2Q&cad=rja). Online; accessed 11-02-2016.
- [81] EUROPEAN COMMISSION. Reference Document on Best Available Techniques in the Food, Drink and Milk Industries. Technical report, EUROPEAN COMMISSION, August 2006. URL http://eippcb.jrc.ec.europa.eu/reference/BREF/fdm_bref_0806.pdf.
- [82] AG Prognos. Energy perspectives 2050. Technical report, Swiss Federal Office of Energy, Bern, September 2012. URL http://www.bfe.admin.ch/themen/00526/00527/06431/index.html?lang=en&dossier_id=06421.
- [83] Aldo Steinfeld. Solar thermochemical production of hydrogen—a review. *Solar Energy*, 78(5):603–615, May 2005. ISSN 0038-092X. doi: 10.1016/j.solener.2003.12.012. URL <http://www.sciencedirect.com/science/article/pii/S0038092X03004663>.
- [84] Sung Moon Ha, Daeho Choi, Minsub Han, and Joon Sik Lee. Optical design of a static solar concentrator using Fresnel lenses. *Journal of Mechanical Science and Technology*, 31(2):949–958, February 2017. ISSN 1738-494X, 1976-3824. doi: 10.1007/s12206-017-0147-8. URL <https://link.springer.com/article/10.1007/s12206-017-0147-8>.
- [85] W. Villasmil, M. Brkic, D. Wullemin, A. Meier, and A. Steinfeld. Pilot Scale Demonstration of a 100-kWth Solar Thermochemical Plant for the Thermal Dissociation of ZnO. *Journal of Solar Energy Engineering*, 136(1):011016–011016–11, November 2013. ISSN 0199-6231. doi: 10.1115/1.4025512. URL <http://dx.doi.org/10.1115/1.4025512>.
- [86] Giv Zanganeh, Roman Bader, Andrea Pedretti, Marco Pedretti, and Aldo Steinfeld. A solar dish concentrator based on ellipsoidal polyester membrane facets. *Solar Energy*, 86(1):40–47, 2012.
- [87] Max Schmitz, Gianluca Ambrosetti, Thomas Cooper, and Aldo Steinfeld. On-sun optical characterization of a solar dish concentrator based on elliptical vacuum membrane facets. *Solar Energy*, 153:732–743, September 2017. ISSN 0038-092X. doi: 10.1016/j.solener.2017.06.009. URL <http://www.sciencedirect.com/science/article/pii/S0038092X17305108>.
- [88] Airlight Energy Holding SA. High concentration photovoltaic thermal, . URL <http://www.airlightenergy.com/high-concentration-photovoltaic-thermal/>.
- [89] IEA. Application of Industrial Heat Pumps: Executive Summary, 2014. URL <http://heatpumpingtechnologies.org/publications/application-of-industrial-heat-pumps-executive-summary/>.
- [90] K. J. Chua, S. K. Chou, and W. M. Yang. Advances in heat pump systems: A review. *Applied Energy*, 87(12):3611–3624, 2010. ISSN 0306-2619. doi: 10.1016/j.apenergy.2010.06.014. URL <http://www.sciencedirect.com/science/article/pii/S030626191000228X>.

Bibliography

- [91] Huijuan Chen, D. Yogi Goswami, and Elias K. Stefanakos. A review of thermodynamic cycles and working fluids for the conversion of low-grade heat. *Renewable and sustainable energy reviews*, 14(9):3059–3067, 2010.
- [92] T. C. Hung, T. Y. Shai, and S. K. Wang. A review of organic rankine cycles (ORCs) for the recovery of low-grade waste heat. *Energy*, 22(7):661–667, July 1997. ISSN 0360-5442. doi: 10.1016/S0360-5442(96)00165-X. URL <http://www.sciencedirect.com/science/article/pii/S036054429600165X>.
- [93] Lon E. Bell. Cooling, heating, generating power, and recovering waste heat with thermoelectric systems. *Science*, 321(5895):1457–1461, 2008.
- [94] H.J. Laue. Annex 35 Final Report - Application of Industrial Heat Pumps, Part 1. Technical report, IEA, 2014. URL <http://heatpumpingtechnologies.org/publications/application-of-industrial-heat-pumps-part-2/>.
- [95] Web of Science [v.5.25.1] - Web of Science Core Collection Home, August 2017. URL https://apps.webofknowledge.com/WOS_GeneralSearch_input.do?product=WOS&search_mode=GeneralSearch&SID=R2JaAJG1qMrpvtvJbFY&preferencesSaved=.
- [96] Philippe Nellissen and Stefan Wolf. Heat pumps in non-domestic applications in Europe: Potential for an energy revolution, May 2015. URL http://www.ehpa.org/fileadmin/red/_EHPA_Archive_Forum/8th_Heat_Pump_Forum_2015/Presentations/Philippe_Nellissen_IHP_potential_EU.pdf.
- [97] Bodo Linnhoff and John R. Flower. Synthesis of heat exchanger networks: I. Systematic generation of energy optimal networks. *AIChE Journal*, 24(4):633–642, July 1978. ISSN 1547-5905. doi: 10.1002/aic.690240411. URL <http://onlinelibrary.wiley.com/doi/10.1002/aic.690240411/abstract>.
- [98] Bodo Linnhoff, David R. Mason, and Ian Wardle. Understanding heat exchanger networks. *Computers & Chemical Engineering*, 3(1–4):295–302, 1979. ISSN 0098-1354. doi: 10.1016/0098-1354(79)80049-6. URL <http://www.sciencedirect.com/science/article/pii/S0098135479800496>.
- [99] Ian C. Kemp. *Pinch Analysis and Process Integration: A User Guide on Process Integration for the Efficient Use of Energy*. Butterworth-Heinemann, April 2011. ISBN 978-0-08-046826-6. Google-Books-ID: gQMxilJQmV4C.
- [100] D. W. Townsend and Bodo Linnhoff. Heat and power networks in process design. Part II: Design procedure for equipment selection and process matching. *AIChE Journal*, 29(5):748–771, September 1983. ISSN 1547-5905. doi: 10.1002/aic.690290509. URL <http://onlinelibrary.wiley.com/doi/10.1002/aic.690290509/abstract>.

- [101] M. R. Shelton and I. E. Grossmann. Optimal synthesis of integrated refrigeration systems I. Mixed-integer programming model. *Computers & Chemical Engineering*, 10(5): 445–459, January 1986. ISSN 0098-1354. doi: 10.1016/0098-1354(86)85014-1. URL <http://www.sciencedirect.com/science/article/pii/0098135486850141>.
- [102] M. R. Shelton and I. E. Grossmann. Optimal synthesis of integrated refrigeration systems II. Implicit enumeration scheme. *Computers & Chemical Engineering*, 10(5):461–477, January 1986. ISSN 0098-1354. doi: 10.1016/0098-1354(86)85015-3. URL <http://www.sciencedirect.com/science/article/pii/0098135486850153>.
- [103] Shankar Vaidyaraman and Costas D. Maranas. Optimal synthesis of refrigeration cycles and selection of refrigerants. *AIChE Journal*, 45(5):997–1017, 1999. ISSN 1547-5905. doi: 10.1002/aic.690450510. URL <http://onlinelibrary.wiley.com/doi/10.1002/aic.690450510/abstract>.
- [104] Cordin Arpagaus, Frederic Bless, Jürg Schiffmann, and Stefan S. Bertsch. Multi-temperature heat pumps: A literature review. *International Journal of Refrigeration*, 69:437–465, September 2016. ISSN 0140-7007. doi: 10.1016/j.ijrefrig.2016.05.014. URL <http://www.sciencedirect.com/science/article/pii/S0140700716301190>.
- [105] Shankar Vaidyaraman and Costas D. Maranas. Synthesis of Mixed Refrigerant Cascade Cycles. *Chemical Engineering Communications*, 189(8):1057–1078, August 2002. ISSN 0098-6445. doi: 10.1080/00986440213475. URL <http://dx.doi.org/10.1080/00986440213475>.
- [106] Frank Del Nogal, Jin-Kuk Kim, Simon Perry, and Robin Smith. Optimal Design of Mixed Refrigerant Cycles. *Industrial & Engineering Chemistry Research*, 47(22):8724–8740, November 2008. ISSN 0888-5885. doi: 10.1021/ie800515u. URL <http://dx.doi.org/10.1021/ie800515u>.
- [107] Chao Fu and Truls Gundersen. A Novel Sensible Heat Pump Scheme for Industrial Heat Recovery. *Industrial & Engineering Chemistry Research*, 55(4):967–977, February 2016. ISSN 0888-5885. doi: 10.1021/acs.iecr.5b02417. URL <http://dx.doi.org/10.1021/acs.iecr.5b02417>.
- [108] *Tehnomont, Solarna Oprema Pula. SKT 100, Tested 2012.* . URL <http://www.tehnomont-solari.hr/>. <http://www.tehnomont-solari.hr/>, Online; accessed: 2016-01-14.
- [109] SPF Institut für Solartechnik. Polysun 1.0, 1992. URL <http://www.velasolaris.com/english/company/about-us.html>.
- [110] Anna S. Wallerand, Angelos Selviaridis, Araz Ashouri, and François Maréchal. Targeting Optimal Design and Operation of Solar Heated Industrial Processes: A MILP Formulation. *Energy Procedia*, 91:668–680, June 2016. ISSN 1876-6102. doi: 10.1016/j.egypro.2016.06.229. URL <http://www.sciencedirect.com/science/article/pii/S1876610216303277>.
- [111] Anna S. Wallerand, Maziar Kermani, Régis Voillat, Ivan Kantor, and François Maréchal. Optimal design of solar-assisted industrial processes considering heat pumping: Case study of a

Bibliography

- dairy. *Renewable Energy*, July 2017. ISSN 0960-1481. doi: 10.1016/j.renene.2017.07.027. URL <http://www.sciencedirect.com/science/article/pii/S0960148117306390>.
- [112] Angelos Selviaridis, Brian R. Burg, Anna S. Wallerand, François Maréchal, and Bruno Michel. Thermo-economic analysis of a trigeneration HCPVT power plant. *CPV conference Proceedings*, 2015.
- [113] Araz Ashouri, Samuel S. Fux, Michael J. Benz, and Lino Guzzella. Optimal design and operation of building services using mixed-integer linear programming techniques. *Energy*, 59(0):365–376, 2013.
- [114] José Antinio Quijera, María González Alriols, and Jalel Labidi. Usage of Solar Energy in an Industrial Process. In *CHEMICAL ENGINEERING TRANSACTIONS*, volume 25, 2011. ISBN 978-88-95608-16-7. doi: 10.3303/CET1125146. URL https://s3.amazonaws.com/academia.edu/documents/46436986/Usage_of_Solar_Energy_in_an_Industrial_P20160613-12337-1fsycty.pdf?AWSAccessKeyId=AKIAIWOWYYGZ2Y53UL3A&Expires=1521381566&Signature=cwQCA2668U6gzfCRG39YADIMUWE%3D&response-content-disposition=inline%3B%20filename%3DUsage_of_solar_energy_in_an_industrial_p.pdf.
- [115] Jose Antonio Quijera, Maria Gonzalez Alriols, and Jalel Labidi. Integration of a solar thermal system in a dairy process. *Renewable Energy*, 36(6):1843–1853, 2011.
- [116] S. A. Klein. Calculation of monthly average insolation on tilted surfaces. *Solar Energy*, 19(4):325–329, January 1977. ISSN 0038-092X. doi: 10.1016/0038-092X(77)90001-9. URL <http://www.sciencedirect.com/science/article/pii/0038092X77900019>.
- [117] Amit Kumar Yadav and S. S. Chandel. Tilt angle optimization to maximize incident solar radiation: A review. *Renewable and Sustainable Energy Reviews*, 23:503–513, July 2013. ISSN 1364-0321. doi: 10.1016/j.rser.2013.02.027. URL <http://www.sciencedirect.com/science/article/pii/S1364032113001299>.
- [118] S. A. Klein, P. I. Cooper, T. L. Freeman, D. M. Beekman, W. A. Beckman, and J. A. Duffie. A method of simulation of solar processes and its application. *Solar Energy*, 17(1):29–37, April 1975. ISSN 0038-092X. doi: 10.1016/0038-092X(75)90014-6. URL <http://www.sciencedirect.com/science/article/pii/0038092X75900146>.
- [119] J. A. Duffie and J. W. Mitchell. f-Chart - Predictions and measurements. *ASME Transactions Journal of Solar Energy and Engineering*, 105:3–9, February 1983. URL <http://adsabs.harvard.edu/abs/1983ATJSE.105....3D>.
- [120] J. A. Clark. An analysis of the technical and economic performance of a parabolic trough concentrator for solar industrial process heat application. *International Journal of Heat and*

- Mass Transfer*, 25(9):1427–1438, September 1982. ISSN 0017-9310. doi: 10.1016/0017-9310(82)90136-3. URL <http://www.sciencedirect.com/science/article/pii/0017931082901363>.
- [121] Sortiris A. Kalogirou and Y. Tripanagnostopoulos. Industrial application of PV/T solar energy systems. *Applied Thermal Engineering*, 27(8–9):1259–1270, 2007.
- [122] Amir Baniassadi, Mahyar Momen, Mehrdad Shirinbakhsh, and Majid Amidpour. Application of R-curve analysis in evaluating the effect of integrating renewable energies in cogeneration systems. *Applied Thermal Engineering*, 93:297–307, January 2016. ISSN 1359-4311. doi: 10.1016/j.applthermaleng.2015.09.101. URL <http://www.sciencedirect.com/science/article/pii/S1359431115010285>.
- [123] Samira Fazlollahi, Stephane Laurent Bungener, Pierre Mandel, Gwenaelle Becker, and Francois Marechal. Multi-objectives, multi-period optimization of district energy systems: I. Selection of typical operating periods. *Computers & Chemical Engineering*, 65:54–66, June 2014. ISSN 0098-1354. doi: 10.1016/j.compchemeng.2014.03.005. URL <http://www.sciencedirect.com/science/article/pii/S0098135414000751>.
- [124] Samira Fazlollahi. Decomposition optimization strategy for the design and operation of district energy systems. 2014. doi: 10.5075/epfl-thesis-6130. URL <https://infoscience.epfl.ch/record/197534>.
- [125] Céline Weber, François Maréchal, and Daniel Favrat. Design and optimization of district energy systems. In Valentin Plesu and Paul Serban Agachi, editor, *Computer Aided Chemical Engineering*, volume 24 of *17th European Symposium on Computer Aided Process Engineering*, pages 1127–1132. Elsevier, 2007. URL <http://www.sciencedirect.com/science/article/pii/S1570794607802124>.
- [126] Fernando Domínguez-Muñoz, José M. Cejudo-López, Antonio Carrillo-Andrés, and Manuel Gallardo-Salazar. Selection of typical demand days for CHP optimization. *Energy and Buildings*, 43(11):3036–3043, November 2011. ISSN 0378-7788. doi: 10.1016/j.enbuild.2011.07.024. URL <http://www.sciencedirect.com/science/article/pii/S037877881100329X>.
- [127] Jakob Moritz Fabian Rager. Urban Energy System Design from the Heat Perspective using mathematical Programming including thermal Storage. 2015. doi: 10.5075/epfl-thesis-6731. URL <https://infoscience.epfl.ch/record/210788>.
- [128] NREL. *National Renewable Energy Laboratory. Renewable Resource Data Center*. Number 11.02.2016. URL http://rredc.nrel.gov/solar/glossary/gloss_g.html, http://rredc.nrel.gov/solar/glossary/gloss_g.html, Online; accessed 11-02-2016.
- [129] B.Y.H. Lui and R.C. Jordan. Daily insolation on surfaces tilted toward the equator. *ASHRAE J.*, 3(10):53–59, 1961.

Bibliography

- [130] Pierre Ineichen, Olivier Guisan, and Richard Perez. Ground-reflected radiation and albedo. *Solar Energy*, 44(4):207–214, 1990.
- [131] Paolo Ambrosetti, Johannes Keller, and Solar Heating. *Das neue Bruttowärmeertragsmodell für verglaste Sonnenkollektoren: Collaborative Programme in energy R, D & D, IEA: being part of the IEA Programme to develop and test solar heating and cooling systems; task III: Performance testing of solar collectors; subtask D: Characterization of the thermal performance of solar collectors*. Eidgenössisches Institut für Reaktorforschung, 1985.
- [132] Airlight Energy Holding SA. Company website, . www.airlightenergy.ch, Online; accessed: 2016-01-14.
- [133] I. J. Hall, R. R. Prairie, H. E. Anderson, and E. C. Boes. Generation of a typical meteorological year. Technical Report SAND-78-1096C; CONF-780639-1, Sandia Labs., Albuquerque, NM (USA), January 1978. URL <https://www.osti.gov/biblio/7013202>.
- [134] Meteonorm7.0. Irradiation data for every place on Earth. 2013.
- [135] SolarGIS. Solar resource maps and GIS data for 180+ countries, 2017. URL <https://solargis.com/maps-and-gis-data/download/>.
- [136] Drury B Crawley, Linda K Lawrie, Frederick C Winkelmann, Walter F Buhl, Y Joe Huang, Curtis O Pedersen, Richard K Strand, Richard J Liesen, Daniel E Fisher, and Michael J Witte. EnergyPlus: creating a new-generation building energy simulation program. *Energy and buildings*, 33(4):319–331, 2001.
- [137] MATLAB. *version 8.6.0. (R2015b)*. The MathWorks Inc., Natick, Massachusetts, 2015.
- [138] Soterios A. Papoulias and Ignacio E. Grossmann. A structural optimization approach in process synthesis—III: Total processing systems. *Computers & Chemical Engineering*, 7(6): 723–734, January 1983. ISSN 0098-1354. doi: 10.1016/0098-1354(83)85024-8. URL <http://www.sciencedirect.com/science/article/pii/0098135483850248>.
- [139] Soterios A. Papoulias and Ignacio E. Grossmann. A structural optimization approach in process synthesis—II: Heat recovery networks. *Computers & Chemical Engineering*, 7(6): 707–721, January 1983. ISSN 0098-1354. doi: 10.1016/0098-1354(83)85023-6. URL <http://www.sciencedirect.com/science/article/pii/0098135483850236>.
- [140] Helen Carla Becker. *Methodology and Thermo-Economic Optimization for Integration of Industrial Heat Pumps*. PhD thesis, 2012.
- [141] Stefano Moret, Emanuela Peduzzi, Leda Gerber, and François Maréchal. Integration of deep geothermal energy and woody biomass conversion pathways in urban systems. *Energy Conversion and Management*, 129:305–318, 2016. ISSN 0196-8904. doi: 10.1016/j.enconman.2016.09.079. URL <http://www.sciencedirect.com/science/article/pii/S0196890416308780>.

- [142] Raffaele Bolliger. *Méthodologie de la synthèse des systèmes énergétiques industriels*. 2010.
- [143] Min-Jung Yoo, Lindsay Lessard, Maziar Kermani, and Francois Marechal. OsmoseLua - An Integrated Approach to Energy Systems Integration with LCIA and GIS. In Kv Gernaey, Jk Husom, and R Gani, editors, *12Th International Symposium On Process Systems Engineering (Pse) And 25Th European Symposium On Computer Aided Process Engineering (Escape), Pt A*, volume 37 of *Computer Aided Chemical Engineering*, pages 587–592, Amsterdam, 2015. Elsevier Science Bv. ISBN 978-0-444-63578-5.
- [144] Angelos Selviaridis. System Modeling and Thermo-Economic Analysis of a High Concentration Photovoltaic Thermal System. Technical report, Ecole Polytechnique Federale de Lausanne, Switzerland, 2014.
- [145] Bastian Schmitt, Christoph Lauterbach, and Klaus Vajen. Investigation of selected solar process heat applications regarding their technical requirements for system integration. In *Proceedings ISES Solar World Congress Kassel*, 2011.
- [146] Christoph Lauterbach, S Javid Rad, Bastian Schmitt, and Klaus Vajen. Feasibility assessment of solar process heat applications. In *Solar World Congress, Kassel*, 2011.
- [147] Bastian Schmitt. Classification of Industrial Heat Consumers for Integration of Solar Heat. *Energy Procedia*, 91:650–660, June 2016. ISSN 1876-6102. doi: 10.1016/j.egypro.2016.06.225. URL <http://www.sciencedirect.com/science/article/pii/S187661021630323X>.
- [148] Holger Müller, Sebastian Brandmayr, and Wilfried Zörner. Development of an Evaluation Methodology for the Potential of Solar-thermal Energy Use in the Food Industry. *Energy Procedia*, 48:1194–1201, January 2014. ISSN 1876-6102. doi: 10.1016/j.egypro.2014.02.135. URL <http://www.sciencedirect.com/science/article/pii/S187661021400397X>.
- [149] Jiri Klemeš, Nan Zhang, Igor Bulatov, and Peter Jansen. *Novel Energy Saving Technologies Assessment by EMINENT Evaluation Tool*, volume 7. 2005.
- [150] Vikas R Dhole and Bodo Linnhoff. Total site targets for fuel, co-generation, emissions, and cooling. *Computers & Chemical Engineering*, 17(Supplement 1):S101–S109, January 1993. ISSN 0098-1354. doi: 10.1016/0098-1354(93)80214-8. URL <http://www.sciencedirect.com/science/article/pii/0098135493802148>.
- [151] José Antonio Quijera, Araceli García, María González Alriols, and Jalel Labidi. Heat integration options based on pinch and exergy analyses of a thermosolar and heat pump in a fish tinning industrial process. *Energy*, 55:23–37, June 2013. ISSN 0360-5442. doi: 10.1016/j.energy.2013.02.025. URL <http://www.sciencedirect.com/science/article/pii/S0360544213001394>.
- [152] José Antonio Quijera and Jalel Labidi. Pinch and exergy based thermosolar integration in a dairy process. *Applied Thermal Engineering*, 50(1):464–474, January 2013. ISSN 1359-4311.

Bibliography

- doi: 10.1016/j.applthermaleng.2012.06.044. URL <http://www.sciencedirect.com/science/article/pii/S1359431112004656>.
- [153] Amir Baniassadi, Mahyar Momen, and Majid Amidpour. A new method for optimization of Solar Heat Integration and solar fraction targeting in low temperature process industries. *Energy*, 90(Part 2):1674–1681, October 2015. ISSN 0360-5442. doi: 10.1016/j.energy.2015.06.128. URL <http://www.sciencedirect.com/science/article/pii/S0360544215008841>.
- [154] Amir Baniassadi, Mahyar Momen, Majid Amidpour, and Omid Pourali. Modeling and design of solar heat integration in process industries with heat storage. *Journal of Cleaner Production*, 170:522–534, January 2018. ISSN 0959-6526. doi: 10.1016/j.jclepro.2017.09.183. URL <http://www.sciencedirect.com/science/article/pii/S0959652617321844>.
- [155] Soterios A. Papoulias and Ignacio E. Grossmann. A structural optimization approach in process synthesis—I: Utility systems. *Computers & Chemical Engineering*, 7(6):695–706, January 1983. ISSN 0098-1354. doi: 10.1016/0098-1354(83)85022-4. URL <http://www.sciencedirect.com/science/article/pii/0098135483850224>.
- [156] Konstantinos Holiastos and Vasilios Manousiouthakis. Minimum hot/cold/electric utility cost for heat exchange networks. *Computers & Chemical Engineering*, 26(1):3–16, January 2002. ISSN 0098-1354. doi: 10.1016/S0098-1354(01)00726-8. URL <http://www.sciencedirect.com/science/article/pii/S0098135401007268>.
- [157] F. Maréchal and B. Kalitventzeff. A tool for optimal synthesis of industrial refrigeration systems. In Rafiqul Gani and Sten Bay Jorgensen, editor, *Computer Aided Chemical Engineering*, volume 9 of *European Symposium on Computer Aided Process Engineering - 1134th European Symposium of the Working Party on Computer Aided Process Engineering*, pages 457–462. Elsevier, 2001. URL <http://www.sciencedirect.com/science/article/pii/S1570794601800717>.
- [158] François Maréchal, Herve Closon, Boris Kalitventzeff, and Sauro Pierucci. A Tool for Optimal Synthesis of Industrial Refrigeration Systems: Application to an Olefins Plant. Technical report, 2002.
- [159] Jian Zhang and Qiang Xu. Cascade refrigeration system synthesis based on exergy analysis. *Computers & Chemical Engineering*, 35(9):1901–1914, September 2011. ISSN 0098-1354. doi: 10.1016/j.compchemeng.2011.02.015. URL <http://www.sciencedirect.com/science/article/pii/S0098135411000779>.
- [160] Meysam Kamalinejad, Majid Amidpour, and S. M. Mousavi Naeynian. Thermodynamic design of a cascade refrigeration system of liquefied natural gas by applying mixed integer non-linear programming. *Chinese Journal of Chemical Engineering*, 23(6):998–1008, June 2015. ISSN 1004-9541. doi: 10.1016/j.cjche.2014.05.023. URL <http://www.sciencedirect.com/science/article/pii/S1004954115000397>.

- [161] Helen Becker, François Maréchal, and Aurelie Vuillermoz. Process integration and opportunities for heat pumps in industrial processes. *International Journal of Thermodynamics*, 14(2): 59–70, 2011.
- [162] Samira Fazlollahi, Gwenaelle Becker, M. Guichard, and François Maréchal. *Multi-objective, multi-period optimization of district energy systems: Networks design*, volume 32. June 2013. ISBN 1570-7946 (ISSN).
- [163] Lua.org. Lua 5.3 Reference Manual, <https://www.lua.org/manual/5.3/>. URL <https://www.lua.org/manual/5.3/>. <https://www.lua.org/manual/5.3/>, Online; accessed 08-12-2016.
- [164] Institut für Solartechnik. Solar Prufung Forschung (SPF), Hochschule für Technik Rapperswil. URL http://www.spf.ch/index.php?id=111&no_cache=1. http://www.spf.ch/index.php?id=111&no_cache=1, Online; accessed 11-02-2016.
- [165] Keymark. *THE Quality Label for Solar Thermal Products in Europe*. The Solar Keymark. CEN Keymark Scheme, December 2016. URL <http://www.estif.org/solarkeymarknew/index.php>. Online; accessed 11-02-2016.
- [166] SunTech. HyPro, STP 290s-20, Monocrystalline silicon. URL <http://de.suntech-power.com/menu/monocrystalline.html>. Accessed: 2016-01-14.
- [167] Anna Sophia Wallerand, Maziar Kermani, Ivan Daniel Kantor, and François Maréchal. General Superstructure Synthesis and Bi-level Solution Strategy for Industrial Heat Pumping. *27th European Symposium on Computer Aided Process Engineering*, (40):1159 – 1164, 2017. doi: 10.1016/B978-0-444-63965-3.50195-1. URL <https://infoscience.epfl.ch/record/232621>.
- [168] International Energy Agency (IEA). *Key World Energy Statistics 2015*. Number 11.02.2016. February 2016. URL <https://www.iea.org/publications/freepublications/publication/key-world-energy-statistics-2015.html>. Online; accessed 11-02-2016.
- [169] Rolf Frischknecht, Niels Jungbluth, Hans-Jörg Althaus, Gabor Doka, Roberto Dones, Thomas Heck, Stefanie Hellweg, Roland Hirschler, Thomas Nemecek, Gerald Rebitzer, and others. The ecoinvent database: Overview and methodological framework (7 pp). *The International Journal of Life Cycle Assessment*, 10(1):3–9, 2005.
- [170] Anna S. Wallerand, Maziar Kermani, Ivan Kantor, and François Maréchal. Optimal heat pump integration in industrial processes. *Applied Energy*, 219:68–92, June 2018. ISSN 0306-2619. doi: 10.1016/j.apenergy.2018.02.114. URL <https://www.sciencedirect.com/science/article/pii/S0306261918302393>.
- [171] Xudong Wang, Yunho Hwang, and Reinhard Radermacher. Two-stage heat pump system with vapor-injected scroll compressor using R410a as a refrigerant. *International Journal of*

Bibliography

- Refrigeration*, 32(6):1442–1451, September 2009. ISSN 0140-7007. doi: 10.1016/j.ijrefrig.2009.03.004. URL <http://www.sciencedirect.com/science/article/pii/S0140700709000814>.
- [172] J. Schiffmann. Integrated Design and Multi-objective Optimization of a Single Stage Heat-Pump Turbocompressor. *Journal of Turbomachinery*, 137(7):071002–071002–9, July 2015. ISSN 0889-504X. doi: 10.1115/1.4029123. URL <http://dx.doi.org/10.1115/1.4029123>.
- [173] F.J. Barnés and C.J. King. Synthesis of cascade refrigeration and liquefaction systems. *Industrial and Engineering Chemistry: Process Design and Development*, 13(4):421–433, 1974. ISSN 0019-7882.
- [174] W.B. Cheng and R.S.H. Mah. Interactive synthesis of cascade refrigeration systems. *Industrial & Engineering Chemistry Process Design and Development*, 19(3):410–420, 1980. ISSN 0196-4305.
- [175] Saidas M. Ranade. New insights on optimal integration of heat pumps in industrial sites. *Heat Recovery Systems and CHP*, 8(3):255–263, January 1988. ISSN 0890-4332. doi: 10.1016/0890-4332(88)90061-0. URL <http://www.sciencedirect.com/science/article/pii/0890433288900610>.
- [176] Michele Zehnder. Efficient air-water heat pumps for high temperature lift residential heating, including oil migration aspects. 2004. doi: 10.5075/epfl-thesis-2998,urn:nbn:ch:bel-epfl-thesis2998-6. URL <https://infoscience.epfl.ch/record/33470>.
- [177] H. Sato, Y. Kimata, Y. Hotta, T. Goto, H. Mizuno, and H. Kobayashi. Development of two-stage compressor for CO₂ heat-pump water heaters. *Mitsubishi Heavy Ind Tech Rev*, 49:92–97, 2012.
- [178] Wilbert F. Stoecker. *Industrial refrigeration handbook*. McGraw-Hill, New York, vol 10 edition, 1998. URL <http://library.wur.nl/WebQuery/clc/977739>.
- [179] Tomoichiro Tamura, Yuuichi Yakumaru, and Fumitoshi Nishiwaki. Experimental study on automotive cooling and heating air conditioning system using CO₂ as a refrigerant. *International Journal of Refrigeration*, 28(8):1302–1307, 2005. ISSN 0140-7007. doi: 10.1016/j.ijrefrig.2005.09.010. URL <http://www.sciencedirect.com/science/article/pii/S0140700705001829>.
- [180] Matej Visek, Cesare Maria Joppolo, Luca Molinaroli, and Andrea Olivani. Advanced sequential dual evaporator domestic refrigerator/freezer: System energy optimization. *International Journal of Refrigeration*, 43:71–79, July 2014. ISSN 0140-7007. doi: 10.1016/j.ijrefrig.2014.03.001. URL <http://www.sciencedirect.com/science/article/pii/S0140700714000486>.
- [181] Chieko Kondou and Shigeru Koyama. Thermodynamic Assessment of High-Temperature Heat Pumps for Heat Recovery. *International Refrigeration and Air Conditioning Conference*, January 2014. URL <http://docs.lib.purdue.edu/iracc/1408>.

- [182] Petter Neksa, Håvard Rekstad, G. Reza Zakeri, and Per Arne Schiefloe. CO₂-heat pump water heater: characteristics, system design and experimental results. *International Journal of Refrigeration*, 21(3):172–179, 1998. ISSN 0140-7007. doi: 10.1016/S0140-7007(98)00017-6. URL <http://www.sciencedirect.com/science/article/pii/S0140700798000176>.
- [183] M. Elakdhar, E. Nehdi, and L. Kairouani. Analysis of a Compression/Ejection Cycle for Domestic Refrigeration. *Industrial & Engineering Chemistry Research*, 46(13):4639–4644, June 2007. ISSN 0888-5885. doi: 10.1021/ie070377e. URL <http://dx.doi.org/10.1021/ie070377e>.
- [184] Hiroshi Oshitani, Yasushi Yamanaka, Hirotsugu Takeuchi, Katsuya Kusano, Makoto Ikegami, Yoshiaki Takano, Naohisa Ishizaka, and Takayuki Sugiura. Vapor compression cycle having ejector. Patent US7254961 B2, August 2007. URL <http://www.google.com/patents/US7254961>.
- [185] Hiroshi Oshitani, Hirotsugu Takeuchi, Etsuhisa Yamada, and Haruyuki Nishijima. Ejector-type refrigerant cycle device. Patent US8186180 B2, May 2012. URL <http://www.google.ch/patents/US8186180>.
- [186] T. R. Colmenares and W. D. Seider. Synthesis of cascade refrigeration systems integrated with chemical processes. *Computers & Chemical Engineering*, 13(3):247–258, 1989. ISSN 0098-1354. doi: 10.1016/0098-1354(89)85002-1. URL <http://www.sciencedirect.com/science/article/pii/0098135489850021>.
- [187] Tao Yang, Yiqing Luo, Yingjie Ma, and Xigang Yuan. Optimal synthesis of compression refrigeration system using a novel MINLP approach. *Chinese Journal of Chemical Engineering*, December 2017. ISSN 1004-9541. doi: 10.1016/j.cjche.2017.10.028. URL <http://www.sciencedirect.com/science/article/pii/S1004954117311011>.
- [188] Chen Danlei, Ma Xue, Luo Yiqing, Ma Yingjie, and Yuan Xigang. Synthesis of refrigeration system based on generalized disjunctive programming model. *Chinese Journal of Chemical Engineering*, November 2017. ISSN 1004-9541. doi: 10.1016/j.cjche.2017.10.017. URL <http://www.sciencedirect.com/science/article/pii/S1004954117311023>.
- [189] B. J. Zhang, Z. L. Zhang, K. Liu, and Q. L. Chen. Network Modeling and Design for Low Grade Heat Recovery, Refrigeration, and Utilization in Industrial Parks. *Industrial & Engineering Chemistry Research*, 55(36):9725–9737, September 2016. ISSN 0888-5885. doi: 10.1021/acs.iecr.6b02033. URL <http://dx.doi.org/10.1021/acs.iecr.6b02033>.
- [190] Gbemi Oluleye, Robin Smith, and Megan Jobson. Modelling and screening heat pump options for the exploitation of low grade waste heat in process sites. *Applied Energy*, 169:267–286, 2016. ISSN 0306-2619. doi: 10.1016/j.apenergy.2016.02.015. URL <http://www.sciencedirect.com/science/article/pii/S0306261916301386>.

Bibliography

- [191] Gbemi Oluleye, Megan Jobson, and Robin Smith. Process integration of waste heat upgrading technologies. *Process Safety and Environmental Protection*, 103, Part B:315–333, September 2016. ISSN 0957-5820. doi: 10.1016/j.psep.2016.02.003. URL <http://www.sciencedirect.com/science/article/pii/S0957582016000306>.
- [192] Ha Dinh, Jian Zhang, and Qiang Xu. Process synthesis for cascade refrigeration system based on exergy analysis. *AIChE Journal*, 61(8):2471–2488, August 2015. ISSN 1547-5905. doi: 10.1002/aic.14843. URL <http://onlinelibrary.wiley.com/doi/10.1002/aic.14843/abstract>.
- [193] Guilian Liu, Hua Zhou, Renjie Shen, and Xiao Feng. A graphical method for integrating work exchange network. *Applied Energy*, 114:588–599, February 2014. ISSN 0306-2619. doi: 10.1016/j.apenergy.2013.10.023. URL <http://www.sciencedirect.com/science/article/pii/S030626191300843X>.
- [194] Mohd Shariq Khan and Moonyong Lee. Design optimization of single mixed refrigerant natural gas liquefaction process using the particle swarm paradigm with nonlinear constraints. *Energy*, 49:146–155, January 2013. ISSN 0360-5442. doi: 10.1016/j.energy.2012.11.028. URL <http://www.sciencedirect.com/science/article/pii/S0360544212008894>.
- [195] Roman Hackl and Simon Harvey. Applying exergy and total site analysis for targeting refrigeration shaft power in industrial clusters. *Energy*, 55:5–14, June 2013. ISSN 0360-5442. doi: 10.1016/j.energy.2013.03.029. URL <http://www.sciencedirect.com/science/article/pii/S036054421300217X>.
- [196] Helen Becker and François Maréchal. Targeting industrial heat pump integration in multi-period problems. In Iftekhar A. Karimi and Rajagopalan Srinivasan, editor, *Computer Aided Chemical Engineering*, volume 31 of *11th International Symposium on Process Systems Engineering*, pages 415–419. Elsevier, 2012. URL <http://www.sciencedirect.com/science/article/pii/B9780444595072500755>.
- [197] M. M. Faruque Hasan, Md. Shamsuzzaman Razib, and I. A. Karimi. Optimization of Compressor Networks in LNG Operations. In Caludio Augusto Oller do Nascimento and Evaristo Chalbaud Biscaia Rita Maria de Brito Alves, editor, *Computer Aided Chemical Engineering*, volume 27 of *10th International Symposium on Process Systems Engineering: Part A*, pages 1767–1772. Elsevier, 2009. doi: 10.1016/S1570-7946(09)70685-6. URL <http://www.sciencedirect.com/science/article/pii/S1570794609706856>.
- [198] Audun Aspelund, David Olsson Berstad, and Truls Gundersen. An Extended Pinch Analysis and Design procedure utilizing pressure based exergy for subambient cooling. *Applied Thermal Engineering*, 27(16):2633–2649, November 2007. ISSN 1359-4311. doi: 10.1016/j.applthermaleng.2007.04.017. URL <http://www.sciencedirect.com/science/article/pii/S1359431107001627>.

- [199] Miguel J. Bagajewicz and Andres F. Barbaro. On the use of heat pumps in total site heat integration. *Computers & Chemical Engineering*, 27(11):1707–1719, November 2003. ISSN 0098-1354. doi: 10.1016/S0098-1354(03)00149-2. URL <http://www.sciencedirect.com/science/article/pii/S0098135403001492>.
- [200] Thomas E Daubert. Physical and thermodynamic properties of pure chemicals: data compilation. *Design Institute for Physacal Property Data (DIPPR)*, 1989.
- [201] Friedrich Kauf. Determination of the optimum high pressure for transcritical CO₂-refrigeration cycles. *International Journal of Thermal Sciences*, 38(4):325–330, April 1999. ISSN 1290-0729. doi: 10.1016/S1290-0729(99)80098-2. URL <http://www.sciencedirect.com/science/article/pii/S1290072999800982>.
- [202] Erik Wallin and Thore Berntsson. Integration of heat pumps in industrial processes. *Heat Recovery Systems and CHP*, 14(3):287–296, May 1994. ISSN 0890-4332. doi: 10.1016/0890-4332(94)90024-8. URL <http://www.sciencedirect.com/science/article/pii/0890433294900248>.
- [203] B. Linnhoff and V. R. Dhole. Shaftwork targets for low-temperature process design. *Chemical Engineering Science*, 47(8):2081–2091, June 1992. ISSN 0009-2509. doi: 10.1016/0009-2509(92)80324-6. URL <http://www.sciencedirect.com/science/article/pii/0009250992803246>.
- [204] Ross E. Swaney. Thermal integration of processes with heat engines and heat pumps. *AIChE Journal*, 35(6):1003–1016, June 1989. ISSN 1547-5905. doi: 10.1002/aic.690350614. URL <http://onlinelibrary.wiley.com/doi/10.1002/aic.690350614/abstract>.
- [205] T. R. Colmenares and W. D. Seider. Heat and power integration of chemical processes. *AIChE Journal*, 33(6):898–915, June 1987. ISSN 1547-5905. doi: 10.1002/aic.690330604. URL <http://onlinelibrary.wiley.com/doi/10.1002/aic.690330604/abstract>.
- [206] Mark R. Shelton and Ignacio E. Grossmann. A shortcut procedure for refrigeration systems. *Computers & Chemical Engineering*, 9(6):615–619, January 1985. ISSN 0098-1354. doi: 10.1016/0098-1354(85)87017-4. URL <http://www.sciencedirect.com/science/article/pii/0098135485870174>.
- [207] B. Linnhoff and E. Hindmarsh. The pinch design method for heat exchanger networks. *Chemical Engineering Science*, 38(5):745–763, January 1983. ISSN 0009-2509. doi: 10.1016/0009-2509(83)80185-7. URL <http://www.sciencedirect.com/science/article/pii/0009250983801857>.
- [208] *CoolProp*. . www.coolprop.org, Online; accessed 11-02-2016.

Bibliography

- [209] E.W. Lemmon, M.L. Huber, and M.O. McLinden. NIST Standard Reference Database 23: Reference Fluid Thermodynamic and Transport Properties-REFPROP. Standard Reference Data Program Version 9.1, National Institute of Standards and Technology, Gaithersburg, 2013.
- [210] Giorgio Soave. Equilibrium constants from a modified Redlich-Kwong equation of state. *Chemical Engineering Science*, 27(6):1197–1203, June 1972. ISSN 0009-2509. doi: 10.1016/0009-2509(72)80096-4. URL <http://www.sciencedirect.com/science/article/pii/0009250972800964>.
- [211] J. Pongo, W. Boras, R. Schacter, K. Hanson, C. Lowe, and J. Forrest. HYSYS-Reference. Technical Report Vol. 1, 2, Hyprotech Ltd., 1996.
- [212] Ding-Yu Peng and Donald B Robinson. A new two-constant equation of state. *Industrial & Engineering Chemistry Fundamentals*, 15(1):59–64, 1976.
- [213] M.N. Dumont and B. Kalitventzeff. BELSIM Vali H users manual. Technical report, Belsim SA, 1995.
- [214] Mehmet Kanoğlu. Exergy analysis of multistage cascade refrigeration cycle used for natural gas liquefaction. *International Journal of Energy Research*, 26(8):763–774, June 2002. ISSN 1099-114X. doi: 10.1002/er.814. URL <http://onlinelibrary.wiley.com/doi/10.1002/er.814/abstract>.
- [215] Gbemi Oluleye, Megan Jobson, Robin Smith, and Simon J. Perry. Evaluating the potential of process sites for waste heat recovery. *Applied Energy*, 161:627–646, January 2016. ISSN 0306-2619. doi: 10.1016/j.apenergy.2015.07.011. URL <http://www.sciencedirect.com/science/article/pii/S0306261915008405>.
- [216] B.M. Adams, L.E. Bauman, W.J. Bohnhoff, K.R. Dalbey, M.S. Ebeida, J.P. Eddy, M.S. Eldred, P.D. Hough, K.T. Hu, J.D. Jakeman, J.A. Stephens, L.P. Swiler, D.M. Vigil, and T.M. Wildey. Dakota, A Multilevel Parallel Object-Oriented Framework for Design Optimization, Parameter Estimation, Uncertainty Quantification, and Sensitivity Analysis: Version 6.0 User Manual. Technical report, July 2014. URL <https://dakota.sandia.gov/documentation.html>.
- [217] J.E. Eddy and K. Lewis. Effective generation of pareto sets using genetic programming. In *Proceedings of ASME Design Engineering Technical Conference*, Pittsburgh, Pennsylvania, 2001.
- [218] DW Townsend and B Linnhoff. Surface area targets for heat exchanger networks. In *ICHEME Annual Research Meeting, Bath, UK*, 1984.
- [219] AM Lincoff, IE Grossmann, and GE Blau. Separation System for Recovery of Ethylene and Light Products from Naphtha-Pyrolysis Gas Stream. *Process Design Case Study*, 1985.
- [220] Maziar Kermani, Anna S. Wallerand, Ivan D. Kantor, and François Maréchal. Generic superstructure synthesis of organic Rankine cycles for waste heat recovery in industrial processes.

- Applied Energy*, 212:1203–1225, February 2018. ISSN 0306-2619. doi: 10.1016/j.apenergy.2017.12.094. URL <http://www.sciencedirect.com/science/article/pii/S0306261917318172>.
- [221] Y. S Chang, M. S Kim, and S. T Ro. Performance and heat transfer characteristics of hydrocarbon refrigerants in a heat pump system. *International Journal of Refrigeration*, 23(3):232–242, May 2000. ISSN 0140-7007. doi: 10.1016/S0140-7007(99)00042-0. URL <http://www.sciencedirect.com/science/article/pii/S0140700799000420>.
- [222] Anna S. Wallerand, Ivan Kantor, Maziar Kermani, and François Maréchal. Method for generic pre-feasibility assessment of industrial energy integration measures: part I. .
- [223] Richard Law, Adam Harvey, and David Reay. Opportunities for low-grade heat recovery in the UK food processing industry. *Applied Thermal Engineering*, 53(2):188–196, 2013. ISSN 1359-4311. doi: 10.1016/j.applthermaleng.2012.03.024. URL <http://www.sciencedirect.com/science/article/pii/S1359431112002086>.
- [224] H. T. Chua, H. K. Toh, A. Malek, K. C. Ng, and K. Srinivasan. A general thermodynamic framework for understanding the behaviour of absorption chillers. *International Journal of Refrigeration*, 23(7):491–507, November 2000. ISSN 0140-7007. doi: 10.1016/S0140-7007(99)00077-8. URL <http://www.sciencedirect.com/science/article/pii/S0140700799000778>.
- [225] Veronika Wilk, Bernd Windholz, Reinhard Jentsch, Thomas Fleckl, Jürgen Fluch, Anna Grubbauer, Christoph Brunner, Daniel Lange, Dietrich Wertz, and Karl Ponweiser. Valorization of industrial waste heat by heat pumps based on case studies of the project EnPro. In *Proceedings of the 12th IEA Heat Pump Conference*, Rotterdam, 2017. IEA Energy Technology Network.
- [226] Sarah Brückner, Selina Liu, Laia Miró, Michael Radspieler, Luisa F. Cabeza, and Eberhard Lävemann. Industrial waste heat recovery technologies: An economic analysis of heat transformation technologies. *Applied Energy*, 151:157–167, August 2015. ISSN 0306-2619. doi: 10.1016/j.apenergy.2015.01.147. URL <http://www.sciencedirect.com/science/article/pii/S0306261915004584>.
- [227] S. Wolf, U. Fah, M. Blesl, A. Voß, and R. Jakobs. Analyse des Potenzials von Industrie - Wärmepumpen in Deutschland. Technical report, Universität Stuttgart, Institut für Energiewirtschaft und Rationelle Energieanwendung (IER), Stuttgart, December 2014. URL http://www.ier.uni-stuttgart.de/publikationen/veroeffentlichungen/forschungsberichte/downloads/141216_Abschlussbericht_FKZ_0327514A.pdf.
- [228] Gondia Sokhna Seck, Gilles Guerassimoff, and Nadia Maïzi. Heat recovery with heat pumps in non-energy intensive industry: A detailed bottom-up model analysis in the French food & drink industry. *Applied Energy*, 111:489–504, November 2013. ISSN 0306-2619. doi: 10.1016/j.apenergy.2013.05.035. URL <http://www.sciencedirect.com/science/article/pii/S0306261913004364>.

Bibliography

- [229] Stefano Moret. Strategic energy planning under uncertainty. 2017. doi: 10.5075/epfl-thesis-7961. URL <https://infoscience.epfl.ch/record/231814>.
- [230] John R. Birge and François Louveaux. *Introduction to Stochastic Programming*. Springer Science & Business Media, June 2011. ISBN 978-1-4614-0237-4. Google-Books-ID: Vp0Bp8kjPxUC.
- [231] Laurence Tock. *Thermo-environomic optimisation of fuel decarbonisation alternative processes for hydrogen and power production*. PhD thesis, STI, Lausanne, 2013.
- [232] EUROSTAT. *Final Energy Consumption EU-28 (based on tonnes oil equivalent)*. Number 05.09.2014. EUROSTAT Statistics, 2012.
- [233] Ronald L. Iman. Latin Hypercube Sampling. In *Wiley StatsRef: Statistics Reference Online*. John Wiley & Sons, Ltd, 2014. ISBN 978-1-118-44511-2. doi: 10.1002/9781118445112.stat03803. URL <http://onlinelibrary.wiley.com/doi/10.1002/9781118445112.stat03803/abstract>.
- [234] Ivan Kantor, Anna S. Wallerand, Maziar Kermani, Hür Bütün, Alessio Santecchia, Raphaël Norbert, Sahar Salame, Hélène Cervo, Sebastian Arias, Franz Wolf, Greet van Eetvelde, and François Maréchal. Thermal profile construction for energy-intensive industrial sectors. In *Proceedings of ECOS 2018*, Portugal, June 2018.
- [235] EUROSTAT. Milk and milk product statistics - Statistics Explained. URL http://ec.europa.eu/eurostat/statistics-explained/index.php/Milk_and_milk_product_statistics.
- [236] Marcel Taal, Igor Bulatov, Jiri Klemes, and Petr Stehlik. Cost estimation and energy price forecasts for economic evaluation of retrofit projects. *Applied Thermal Engineering*, 23(14): 1819–1835, 2003. ISSN 1359-4311. doi: 10.1016/S1359-4311(03)00136-4. URL <http://www.sciencedirect.com/science/article/pii/S1359431103001364>.
- [237] S.G. Hall, S. Ahmad, and R. Smith. Capital cost targets for heat exchanger networks comprising mixed materials of construction, pressure ratings and exchanger types. 14(3):319–335, March 1990. URL <http://www.sciencedirect.com/science/article/pii/0098135490870692>.
- [238] International Energy Agency (iea). *Key World Energy Statistics 2017*. Number 11.02.2017. 2018. URL <https://www.iea.org/publications/freepublications/publication/KeyWorld2017.pdf>. Online; accessed 11-02-2016.
- [239] Wikipedia. List of countries by commercial bank prime lending rate, August 2017. URL https://en.wikipedia.org/w/index.php?title=List_of_countries_by_commercial_bank_prime_lending_rate&oldid=795616870. Page Version ID: 795616870.
- [240] Ecoinvent. ecoinvent 3.4 – ecoinvent. URL <https://www.ecoinvent.org/database/ecoinvent-34/ecoinvent-34.html>.

- [241] eia. Japan's electricity prices rising or stable despite recent fuel cost changes - Today in Energy - U.S. Energy Information Administration (EIA), September 2016. URL <https://www.eia.gov/todayinenergy/detail.php?id=27872>.
- [242] Anna Sophia Wallerand, Maziar Kermani, Ivan Daniel Kantor, and François Maréchal. Online parallel coordinates tool for optimal utility design in the dairy industry. March 2018. URL <https://infoscience.epfl.ch/record/253643>.
- [243] Anna S. Wallerand, Ivan Kantor, Maziar Kermani, and François Maréchal. Method for generic pre-feasibility assessment of industrial energy integration measures: part II. .
- [244] JEAN P. Murray. ALUMINUM PRODUCTION USING HIGH-TEMPERATURE SOLAR PROCESS HEAT. *Solar Energy*, 66(2):133–142, June 1999. ISSN 0038-092X. doi: 10.1016/S0038-092X(99)00011-0. URL <http://www.sciencedirect.com/science/article/pii/S0038092X99000110>.
- [245] B Linnhoff and S Ahmad. Cost optimum heat exchanger networks-1. Minimum energy and capital using simple models for capital cost. *Computers & Chemical Engineering*, 14(7): 729–750, 1990.
- [246] François Maréchal and Boris Kalitventzeff. Process integration: Selection of the optimal utility system. *Computers & Chemical Engineering*, 22, Supplement 1:S149–S156, 1998. ISSN 0098-1354. doi: 10.1016/S0098-1354(98)00049-0. URL <http://www.sciencedirect.com/science/article/pii/S0098135498000490>.
- [247] A Vuillermoz and G Guillotin. Intégration énergétique par analyse du pincement de la fromagerie bel à evron: collecte des données, analyse e préconisations. Technical report, EDF Report H-E26-2010-01532-FR., 2011.
- [248] Solarstrom. go Solar GmbH | Solar Solarzellen Photovoltaik solarstrom. URL <http://www.solarenergy-shop.ch/index.php/de/20-Stueck-Photovoltaik-Modul-Suntech-Mono-BLACK-290-W-Total/c-KAT17/a-P0635>. <http://www.solarenergy-shop.ch/index.php/de/20-Stueck-Photovoltaik-Modul-Suntech-Mono-BLACK-290-W-Total/c-KAT17/a-P0635>, Online; accessed 24-01-2017.
- [249] Linde Group. Refrigerants Environmental Data. Ozone Depletion and Global Warming Potential. URL http://www.linde-gas.com/internet.global.lindegas.global/en/images/Refrigerants%20environmental%20GWPs17_111483.pdf.
- [250] Jo Gwanggon, Amin Kalantarifard, Jang Jihoon, Byeon Eunsong, Jang Yuna, and Yang Gosu. The effects of malodorous substances from Municipal Solid Waste (MSW) to Climate-Change as Greenhouse-Gas: Calculating GWP of Hydrogen Sulfide. Japan, 2015. URL https://www.jstage.jst.go.jp/article/jsmcwm/26/0/26_547/_pdf.

Bibliography

- [251] Kalpesh N. Kothale, Kundlik V. Mali, and S.D. Nimbalkar. Study of R-161 refrigerant as an Alternate Refrigerant to various other refrigerants. In *PRESSCO IJCET Special Issue - 4*, Pune, India, March 2016. MIT College of Engineering. ISBN E - ISSN 2277 – 4106. URL <http://inpressco.com/category/ijcet>.
- [252] Nicholas Cox, Victor Mazur, and Daniel Colbourne. New High Pressure Low-G WP Azeotropic and Near-Azeotropic Refrigerant Blends. Purdue, 2008. URL <http://docs.lib.purdue.edu/iracc/987>.
- [253] Aspen Energy Analyzer. Energy Management Software - Energy Optimization |. URL <http://aspentech.com/products/engineering/aspen-energy-analyzer/>.
- [254] Paul Stadler. Assessment of energy requirements of commercial and industrial facilities in Luxembourg. Technical report, École Polytechnique Fédérale de Lausanne, Lausanne, Switzerland, 2014.
- [255] Samuel Henchoz. Potential of refrigerant based district heating and cooling networks. 2016. doi: 10.5075/epfl-thesis-6935. URL <https://infoscience.epfl.ch/record/217013>.

Anna Sophia Wallerand

Curriculum Vitae

✉ anna.wallerand@gmail.com



Education

- 2013–2018 **PhD Energy**, *École Polytechnique Fédérale de Lausanne (EPFL)*, Switzerland, Integration of solar energy to industrial processes.
Prof. Maréchal, Prof. Haussener
- 2010–2013 **MSc Mechanical Engineering**, *Eidgenössisch Technische Hochschule Zürich (ETHZ)*, Switzerland, GPA 5.3/6.0.
Focus Energy, Flows and Processes; Thesis "High-Temperature Reactor Combined with Thermal Storage for 24/7 Utilization of Concentrated Solar Energy", Professorship of Renewable Energy Carriers (ETHZ) (6.0/6.0)
- 2007–2010 **BSc Mechanical Engineering**, *Eidgenössisch Technische Hochschule Zürich (ETHZ)*, Switzerland.
Thesis "Flame synthesis of dye synthesized solar cells", Particle Technology Laboratory (ETHZ) (6.0/6.0)

Professional Experience

- 2013–2018 **Research and teaching assistant**, *IPese group, EPFL*, Switzerland.
Research on solar integration to industrial processes, including heat pumping, organic Rankine cycles and heat recovery.
Projects:
 - SCCER EIP (Swiss Competence Center for Energy Research - Efficiency in Industrial Processes). Development of methods for improvement of industrial efficiency and environmental impact in particular for plantwide integration (WP4) of heat pumping and solar energy
 - IEA Annex 48: Contribution to the IEA Annex by deriving tools and identifying bottlenecks for wide-scale integration of industrial heat pumpsTeaching:
 - Assistant to master and PhD courses: preparation of exercises, lectures and assistance
 - Supervision of student projects
- 2012–2013 **Intern**, *Airlight Energy Holding SA*, 6710 Biasca, Switzerland, Gianluca Ambrosetti.
Development of a stand-alone software with graphic interface for the forecast of yearly solar plant performance.
- 2010–2011 **Scientific assistance**, *Particle Technology Laboratory (ETHZ)*, Zürich, Switzerland, Antonio Tricoli.
Development, construction, testing, and refinement of dye sensitized photovoltaic cells, involving X-Ray diffraction, UV-visible-near-infrared (UV-vis) spectroscopy, BET surface area measurements.

2008–2009 **Intern**, *ABB Schweiz AG*, Baden, Switzerland, Urs Schneider.
Workshop training on mechatronics and electrics, including milling, turning, drilling, welding, planning, and fabrication of equipment.

Publications

Journals

- Jan 2018 **Applied Energy**, *A.S. Wallerand, M. Kermani, I. Kantor, and F. Maréchal*, Optimal heat pump integration in industrial processes, ISSN 0306-2619. doi: 10.1016/j.apenergy.2018.02.114.
- Feb 2018 **Applied Energy**, *M. Kermani, A.S. Wallerand, I. Kantor, and F. Maréchal*, Generic superstructure synthesis of organic Rankine cycles for waste heat recovery in industrial processes, ISSN 0306-2619. doi: 10.1016/j.apenergy.2017.12.094.
- July 2017 **Renewable Energy**, *A.S. Wallerand, M. Kermani, R. Voillat, I. Kantor, and F. Maréchal*, Optimal design of solar-assisted industrial processes considering heat pumping: Case study of a dairy, ISSN 0960-1481. doi: 10.1016/j.renene.2017.07.
- June 2016 **Energy Procedia**, *A.S. Wallerand, A. Selviaridis, A. Ashouri and F. Maréchal*, Targeting Optimal Design and Operation of Solar Heated Industrial Processes: a MILP formulation, ISSN 1876-6102. doi: <https://doi.org/10.1016/j.egypro.2016.06.229>.
- June 2012 **J. Mater. Chem.**, *A. Tricoli, A.S. Wallerand, M. Righettoni*, Highly porous TiO₂ films for dye sensitized solar cells, doi: 10.1039/C2JM15953H.

Conference proceedings

- Sept 2017 **ESCAPE**, *A.S. Wallerand, M. Kermani, I. Kantor, R. Voillat, and F. Maréchal*, General Superstructure Synthesis and Bi-level Solution Strategy for Industrial Heat Pumping, Computer Aided Chemical Engineering, 27th European Symposium on Computer Aided Process Engineering. doi: 10.1016/B978-0-444-63965-3.50195-1.
- Sept 2017 **ESCAPE**, *M. Kermani, A.S. Wallerand, I. Kantor and F. Maréchal*, A Hybrid Methodology for Combined Interplant Heat, Water, and Power Integration, Computer Aided Chemical Engineering, 27th European Symposium on Computer Aided Process Engineering. doi: 10.1016/B978-0-444-63965-3.50330-5.
- June 13-15, 2015 **CPV-11**, *A. Selviaridis, B. Burg, A.S. Wallerand, F. Maréchal, B. Michel*, Thermo-Economic Analysis of a Trigeneration HCPVT Power Plant, CPV-11 International Conference on Concentrator Photovoltaic Systems, Aix-les-Bains, France.
- June 15-19, 2014 **ECOS**, *A.S. Wallerand, J. Queiroz Albarelli, A. Viana Ensinas, G. Ambrosetti, A. Mian, F. Maréchal*, Multi-objective Optimization of a Solar Assisted 1st and 2nd Generation Sugarcane Ethanol Production Plant, 27th international conference on Efficiency, Cost, Optimisation, Simulation and Environmental Impact of Energy Systems (ECOS).

Languages

Fluent German (mother tongue), English (C1) *Fluent in writing and speaking*
Intermediate French (B1), Italian (A2/B1)